



National Library  
of Canada

Acquisitions and  
Bibliographic Services Branch

395 Wellington Street  
Ottawa, Ontario  
K1A 0N4

Bibliothèque nationale  
du Canada

Direction des acquisitions et  
des services bibliographiques

395, rue Wellington  
Ottawa (Ontario)  
K1A 0N4

*Your file - votre référence*

*Our file - notre référence*

## NOTICE

The quality of this microform is heavily dependent upon the quality of the original thesis submitted for microfilming. Every effort has been made to ensure the highest quality of reproduction possible.

If pages are missing, contact the university which granted the degree.

Some pages may have indistinct print especially if the original pages were typed with a poor typewriter ribbon or if the university sent us an inferior photocopy.

Reproduction in full or in part of this microform is governed by the Canadian Copyright Act, R.S.C. 1970, c. C-30, and subsequent amendments.

## AVIS

La qualité de cette microforme dépend grandement de la qualité de la thèse soumise au microfilmage. Nous avons tout fait pour assurer une qualité supérieure de reproduction.

S'il manque des pages, veuillez communiquer avec l'université qui a conféré le grade.

La qualité d'impression de certaines pages peut laisser à désirer, surtout si les pages originales ont été dactylographiées à l'aide d'un ruban usé ou si l'université nous a fait parvenir une photocopie de qualité inférieure.

La reproduction, même partielle, de cette microforme est soumise à la Loi canadienne sur le droit d'auteur, SRC 1970, c. C-30, et ses amendements subséquents.

# Time-dependent phenomena of excitable cardiac tissue.

by

ARKADY M. KUNYSZ

Department of Physics  
Center for Nonlinear Dynamics  
McGill University  
Montréal, Québec, Canada

March 1996

A thesis submitted to the  
Faculty of Graduate Studies and Research  
in partial fulfillment  
of the requirements for the degree of  
Doctor of Philosophy

©Arkady M. Kunysz, 1996



National Library  
of Canada

Acquisitions and  
Bibliographic Services Branch

395 Wellington Street  
Ottawa, Ontario  
K1A 0N4

Bibliothèque nationale  
du Canada

Direction des acquisitions et  
des services bibliographiques

395, rue Wellington  
Ottawa (Ontario)  
K1A 0N4

*Vous lie - Votre référence*

*Vous lie - Votre référence*

**The author has granted an irrevocable non-exclusive licence allowing the National Library of Canada to reproduce, loan, distribute or sell copies of his/her thesis by any means and in any form or format, making this thesis available to interested persons.**

**L'auteur a accordé une licence irrévocable et non exclusive permettant à la Bibliothèque nationale du Canada de reproduire, prêter, distribuer ou vendre des copies de sa thèse de quelque manière et sous quelque forme que ce soit pour mettre des exemplaires de cette thèse à la disposition des personnes intéressées.**

**The author retains ownership of the copyright in his/her thesis. Neither the thesis nor substantial extracts from it may be printed or otherwise reproduced without his/her permission.**

**L'auteur conserve la propriété du droit d'auteur qui protège sa thèse. Ni la thèse ni des extraits substantiels de celle-ci ne doivent être imprimés ou autrement reproduits sans son autorisation.**

ISBN 0-612-12406-1

**Canada**

*A mes parents, André, Monika.*

*A mes amis.*

*A Francesca.*

*Et à la Vie.*

Candidates have the option of including, as part of the thesis, the text of a paper(s) submitted or to be submitted for publication, or the clearly duplicated text of a published paper(s). These texts must be bound as an integral part of the thesis.

If this option is chosen, **connecting texts that provide logical bridges between the different papers are mandatory.** The thesis must be written in such a way that it is more than a mere collection of manuscripts; in other words, results of a series of papers must be integrated.

The thesis must still conform to all other requirements of the "Guidelines for Thesis Preparation". **The thesis must include:** A Table of Contents, an abstract in English and French, an introduction which clearly states the rationale and objectives of the study, a comprehensive review of the literature, a final conclusion and summary, and a thorough bibliography or reference list.

Additional material must be provided where appropriate (e.g. in appendices) and in sufficient detail to allow a clear and precise judgment to be made of the importance and originality of the research reported in the thesis.

In the case of manuscripts co-authored by the candidate and others, **the candidate is required to make an explicit statement in the thesis as to who contributed to such work and to what extent.** Supervisors must attest to the accuracy of such statements at the doctoral oral defense. Since the task of the examiners is made more difficult in these cases, it is in the candidate's interest to make perfectly clear the responsibilities of all the authors of the co-authored papers. **Under no circumstances can a co-author of any component of such a thesis serve as an examiner for that thesis.**

## Abstract

The effects of electrical stimulation protocols on the spontaneous activity of multicellular experimental cardiac preparations are examined. Particular attention is drawn to the contribution of stimulation history to the dynamics observed under different experimental protocols. The experimental study focuses on phase resetting, periodic stimulation and fixed delay stimulation of embryonic chick heart cell aggregates. In addition, similar experiments are carried out on rabbit atrioventricular cell clusters to draw a comparison between the dynamics in rapid and slow inward current cardiac preparations. Three classes of models of the rhythmic behaviour are considered. The Shrier-Clay ionic model of electrical activity in spontaneously beating embryonic chick heart cell aggregates is used to model the response of this preparation to various stimulation protocols. A modified version of this model, which includes a simplified sodium pump term, is developed to account for the effects of stimulation history on the response of embryonic chick heart cell aggregates to sustained external stimulation. Simple nonlinear models expressed in terms of difference equations are considered to describe phase resetting behaviour, phase locking, and the effects of stimulation history on the dynamics during stimulation. A simplified model of a relaxation oscillator is also proposed that incorporates a time dependent term. These different classes of models offer complementary approaches to the understanding of the contribution of stimulation history to the development of complex dynamics in excitable systems. This work shows the importance of the interaction between time dependent phenomena and the intrinsic properties of excitable cardiac tissue to the rhythms observed in many experimental and clinical contexts. The limitations of the current experimental and theoretical approaches are discussed and their relevance to the modeling of biological systems is examined.

## Résumé

Cette étude porte sur l'influence de différents protocoles de stimulation électrique sur l'activité spontanée de préparations multicellulaires de tissu cardiaque excitable, avec emphase sur la contribution de la stimulation passée aux rythmes observés. L'étude expérimentale comporte les protocoles suivants: réajustement de phase ("phase resetting"), stimulation périodique et stimulation à délai fixe. Les expériences ont été effectuées sur des agrégats de cellules de coeur d'embryon de poulet ainsi que des préparations multicellulaires prélevées du noeud atrio-ventriculaire du lapin, afin de comparer les dynamiques observées dans des cellules possédant des mécanismes ioniques d'activation différents. Trois types de modèles théoriques sont présentés. Le modèle ionique de Shrier-Clay, décrivant l'activité électrique d'agrégats de cellules cardiaques d'embryon de poulet, est utilisé pour modéliser les effets de divers protocoles de stimulation électrique sur l'activité rythmique de cette préparation. Une version modifiée de ce modèle comprend une description simplifiée de la pompe sodium potassium. Cette dernière variante permet de modéliser l'influence des effets de la stimulation passée sur la réponse rythmique à divers protocoles expérimentaux de stimulation électrique. Des modèles non-linéaires sont aussi développés afin de décrire les phénomènes expérimentaux. Ces modèles, présentés sous forme d'équations différentielles ordinaires ou d'équations à différences complètent les résultats obtenus par simulation numérique des modèles ioniques décrits ci-haut. Ces formulations théoriques complémentaires permettent de mieux cerner les principaux phénomènes responsables de l'interaction dynamique entre les effets de la stimulation passée et les propriétés d'excitabilité intrinsèques de ces préparations de tissu cardiaque. Cette étude démontre qu'un nombre grandissant de rythmes expérimentaux et cliniques peuvent être interprétés en fonction de l'influence de la stimulation passée sur l'excitabilité du tissu cardiaque. Ce document contient aussi une discussion portant sur les limitations des modèles théoriques proposés ainsi que sur leur applicabilité à d'autres systèmes biologiques.

## Acknowledgments

I wish to thank professor Leon Glass for his guidance, insight, friendly advice and patience through the years I have spent under his supervision. His fondness of the rhythms and dynamics of Nature has been a great source of motivation and interest that goes beyond the completion of this project.

I also express my gratitude to professor Alvin Shrier, my co-supervisor, for his endless support, encouragement, energy and understanding. The complicity and trust he shares with his students make his laboratory a special interdisciplinary place where dynamic scientific research and good atmosphere naturally combine.

I extend my thanks to other members of the Center for Nonlinear Dynamics, professors Michael Mackey, Michael Guevara, John Outerbridge and Danny Kaplan for stimulating conversations, advice and computer help, and to Candace Taylor for secretarial assistance in sometimes scary situations.

My deepest thanks go to my fellow co-workers and friends Andrew Munk, Gil Bub and Adam Sherman with whom I have shared many enthrilling discussions, late stressful nights, efficient collaborations and hours of laughs behind the gun metal blue doors. In particular, I am indebted to Adam Sherman for providing excellent software support during the experimental part of this work, and to Cedric Gordon and Lin Kebang for technical assistance. I also thank Kosta Vassilakos, Caroline Haurie, Misha Rosenberg, Harald Henschke, Raffi Adjemian, Jafar Shenasa, Kevin Kwaku and Frank for their friendship and humour.

Finally, very special thanks to my friends Ninnis, Zen and Afefskaya, to Katioucha, Olivia, Mami, Toki, Webby and Sol, Lomic, Saki, Anna-Maria, Gilles, the H Ensemble, the NAZ, Sufia, Lilian, Sam, V, Hamid, Olivier, Anne, Bruno<sup>2</sup>, Barbie, Annie and Sophie to whom I partly owe my sanity and so many great moments of life. Dziękuję to my parents for their endless support. And merci to you Francesca, for your smile, your care and infinite patience, your encouragement and these innumerable things that make life beautiful.

# Contents

Abstract	i
Résumé	ii
Acknowledgments	iii
Table of Contents	vii
List of Figures	x
List of Tables	xi
Contributions to original knowledge	xii
Contributions to publications	xv
<b>1 Introduction</b>	<b>1</b>
1.1 Excitable media . . . . .	2
1.1.1 A few classical examples . . . . .	2
1.1.2 Excitable media in physiology . . . . .	4
1.1.3 The heart as an excitable medium . . . . .	5
1.1.4 Cardiac rhythms . . . . .	6
1.1.5 Overdrive suppression: definition and mechanisms . . . . .	7
1.1.6 Towards modeling excitable media . . . . .	9
1.2 Ionic models of excitable heart tissue . . . . .	9
1.2.1 Simplified model of ionic fluxes across membranes . . . . .	10
1.2.2 A step further: the GHK approximation . . . . .	11
1.2.3 The Hodgkin and Huxley (or H+H) formalism . . . . .	12
1.2.4 A few models of ionic activity . . . . .	15
1.2.5 Simplified models of excitability . . . . .	17
1.3 Nonlinear dynamics . . . . .	17
1.3.1 Fundamentals . . . . .	18

1.3.2	Stability in differential equations . . . . .	20
1.3.3	Finite difference equations . . . . .	20
1.3.4	Simple models of biological oscillators . . . . .	23
1.4	The final word . . . . .	25
<b>2</b>	<b>Methodology</b>	<b>27</b>
2.1	Culturing techniques . . . . .	27
2.1.1	Embryonic chick heart cell aggregates . . . . .	27
2.1.2	Preparation of AV nodal cell clusters . . . . .	28
2.2	Electrophysiology . . . . .	29
2.3	Data Analysis . . . . .	30
<b>3</b>	<b>Ionic mechanisms and nonlinear dynamics of chick heart cell aggregates</b>	<b>32</b>
3.1	Foreword . . . . .	32
3.2	Rationale for using embryonic chick heart cell aggregates rather than single cells . . . . .	34
3.3	Experimental observations . . . . .	34
3.3.1	Phase resetting . . . . .	34
3.3.2	Phase locking . . . . .	38
3.4	Theoretical results based on a model of ion currents . . . . .	41
3.4.1	Ionic model . . . . .	41
3.4.2	Control electrophysiological results . . . . .	44
3.4.3	Phase resetting . . . . .	45
3.4.4	Phase locking . . . . .	50
3.4.5	Limitations of the ionic model . . . . .	57
3.4.6	Comparison with other preparations . . . . .	59
3.5	Nonlinear dynamics . . . . .	60
3.5.1	Iteration of the phase resetting curve . . . . .	61
3.5.2	Period doubling bifurcations and chaotic dynamics . . . . .	62
3.5.3	Phase locking zones . . . . .	67
3.5.4	Universality . . . . .	69
3.6	Conclusions . . . . .	73
3.7	Appendix: detailed description of the Shrier-Clay ionic model . . . . .	74

<b>4</b>	<b>Overdrive suppression of spontaneously beating chick heart cell aggregates: Experiment and theory</b>	<b>78</b>
4.1	Foreword . . . . .	78
4.2	Experimental protocols . . . . .	79
4.2.1	Overdrive suppression for different numbers of stimuli . . . . .	79
4.2.2	Overdrive suppression at different frequencies . . . . .	80
4.3	Theoretical model . . . . .	80
4.4	Results . . . . .	82
4.4.1	Overdrive suppression at fixed stimulation frequency for different numbers of stimuli and different stimulus intensities . . . . .	82
4.4.2	Overdrive suppression at different frequencies . . . . .	88
4.5	Discussion . . . . .	91
4.6	Appendix . . . . .	96
4.6.1	The theoretical model . . . . .	96
4.6.2	Analysis of the theoretical model . . . . .	98
<b>5</b>	<b>Overdrive suppression and phase resetting in a model for p - oxysmal tachycardias</b>	<b>105</b>
5.1	Foreword . . . . .	105
5.2	Experimental protocols . . . . .	106
5.2.1	Fixed delay stimulation . . . . .	106
5.2.2	Phase resetting . . . . .	107
5.2.3	Overdrive suppression . . . . .	107
5.3	Theoretical modeling . . . . .	107
5.4	Experimental results . . . . .	109
5.4.1	Fixed delay stimulation . . . . .	109
5.4.2	Phase resetting . . . . .	115
5.4.3	Overdrive suppression . . . . .	115
5.5	A nonlinear theoretical model . . . . .	117
5.5.1	Interaction between excitability and history dependent effects . . . . .	117
5.5.2	Ionic model . . . . .	121
5.6	Discussion . . . . .	125
5.6.1	Limitations of the ionic model . . . . .	128
5.6.2	Reentry . . . . .	130
5.7	Appendix A: description of the modified ionic model . . . . .	132

5.8	Appendix B: setting of parameters in nonlinear model . . . . .	134
<b>6</b>	<b>Phase resetting and dynamics in isolated atrioventricular nodal cell clusters</b>	<b>139</b>
6.1	Foreword . . . . .	139
6.2	Experimental protocols . . . . .	140
6.2.1	Phase resetting . . . . .	141
6.2.2	Overdrive suppression . . . . .	141
6.2.3	Periodic stimulation . . . . .	141
6.3	Iteration of phase resetting curves (PRC's) . . . . .	141
6.4	Results . . . . .	143
6.4.1	Phase resetting . . . . .	143
6.4.2	Overdrive suppression . . . . .	149
6.4.3	Periodic stimulation . . . . .	150
6.4.4	Conclusions . . . . .	153
	<b>Conclusions</b>	<b>157</b>

# List of Figures

2.1	Schematic view of experimental setup . . . . .	31
3.1	Phase resetting of spontaneously beating embryonic chick heart cell aggregates. Protocol and definitions. . . . .	36
3.2	Experimental examples of phase resetting with different stimulus intensities. . . . .	37
3.3	Experimental traces of 1:1 phase locking, with different stimulation frequencies. . . . .	39
3.4	Experimentally observed rhythms intermediate to 1:1 and 2:1 phase locking. . . . .	40
3.5	Experimentally observed rhythms intermediate to 1:1 and 1:2 phase locking. . . . .	42
3.6	Ion currents underlying the action potential and pacemaker activity in the Shrier and Clay model. . . . .	46
3.7	Comparison of experimental control activity with numerical simulations of the Shrier-Clay ionic model. . . . .	47
3.8	Phase resetting in the Shrier-Clay ionic model of electrical activity. . . . .	48
3.9	Phase resetting curves. Comparison between experimental data and the results of numerical simulations of the Shrier-Clay ionic model. . . . .	49
3.10	Ionic mechanisms of phase delay and advance in the Shrier and Clay model. . . . .	51
3.11	Phase locking of the Shrier and Clay model in 1:1 patterns. . . . .	53
3.12	Rhythms intermediate to 1:1 and 2:1 phase locking in the Shrier and Clay model. . . . .	54
3.13	Rhythms intermediate to 1:1 and 1:2 phase locking in the Shrier and Clay model. . . . .	55
3.14	Phase locking as a function of the cycle time between pulses ( $\theta = T_s/T_0$ ). . . . .	56
3.15	Ionic basis of 5:4 entrainment in the Shrier and Clay model as described in the text. . . . .	58
3.16	Experimental and numerically simulated (Shrier-Clay ionic model) phase resetting and phase transition curves. . . . .	63

3.17	Determination of phase locking from the phase transition curve. . . . .	64
3.18	Period doubling dynamics. Experimental and numerical simulations of Shrier-Clay ionic model. . . . .	66
3.19	Aperiodic rhythms obtained from an experimental preparation and from the ionic model. . . . .	68
3.20	Phase locking zones. Experimental and from iteration of phase transition curves as numerically obtained from the Shrier-Clay ionic model. . . . .	70
3.21	Regions of chaotic dynamics predicted from iteration of the phase response curve of the ionic model. . . . .	71
4.1	Tracings of membrane voltage showing overdrive suppression following increasing numbers of stimuli of fixed frequency. Experiment and theory.	83
4.2	Numerical simulations of the model showing the relationship between overdrive suppression and the level of $Z$ . . . . .	85
4.3	Composite picture of overdrive suppression as a function of stimulation time for 2 different atrial aggregates and numerical simulations of theoretical model. . . . .	86
4.4	Experimental recordings showing the dependence of overdrive suppression on action potential frequency. . . . .	87
4.5	Dependence of overdrive suppression (1:1 entrainment) upon stimulation frequency. . . . .	89
4.6	1:1 periodic stimulation at a rate slower than the intrinsic frequency (experiment). . . . .	90
4.7	Duration of the first beat following overdrive stimulation in a single aggregate at 2 different stimulation intensities for 50 stimuli, and for 5 different aggregates as a function of stimulus period. . . . .	92
4.8	Dependence of overdrive suppression upon action potential frequency. Comparison between experimental data and model simulations. . . . .	93
4.9	Geometrical illustration of theoretical model. . . . .	99
4.10	Setting of parameters in theoretical model. . . . .	103
5.1	Description of phase resetting and overdrive suppression protocols. . . . .	108
5.2	Rhythms during fixed delay stimulation of embryonic chick heart cell aggregates. Dependence upon the value of the delay. . . . .	111
5.3	Number of action potential per sequence as a function of the delay. . . . .	113

5.4	Irregular rhythms during fixed delay stimulation. . . . .	114
5.5	Results of phase resetting and overdrive suppression experiments in embryonic chick heart cell aggregates. . . . .	116
5.6	Interaction between overdrive suppression and the excitability of the preparation: qualitative model for the dynamics during fixed delay stimulation. . . . .	119
5.7	Numerical simulations of nonlinear model. Fixed delay stimulation for different delay values. . . . .	122
5.8	Phase resetting and overdrive suppression in the modified Shrier-Clay ionic model. . . . .	124
5.9	Numerical simulations of the modified Shrier-Clay ionic model during fixed delay stimulation for different delays. . . . .	126
5.10	Ionic mechanisms contributing to the complex rhythms during fixed delay stimulation of the modified Shrier-Clay ionic model. . . . .	131
5.11	Setting of parameters in nonlinear model. . . . .	138
6.1	Phase resetting of embryonic chick heart cell aggregates and of AV nodal cell clusters. . . . .	145
6.2	Phase resetting curves in AV nodal cell clusters. . . . .	147
6.3	Comparison of single stimulus and long term history dependent effects in embryonic chick heart cell aggregates and AV nodal cell clusters. . . . .	148
6.4	Phase locking zones for periodically stimulated AV nodal cell clusters. . . . .	152
6.5	Complex rhythms during periodic stimulation of AV nodal cell clusters. Contribution of changes in action potential morphology. . . . .	154

# List of Tables

3.1	Membrane current components for the Shrier and Clay model of ionic currents in atrial chick heart cells. . . . .	76
4.1	Summary of the parameters used in the numerical simulations. . . . .	102

## Contributions to original knowledge

This thesis studies the importance of stimulation history in the development of complex dynamics during the application of various stimulation protocols to model experimental preparations of pacemaking cardiac tissue.

In Chapter 1, I present an introduction to the experimental and theoretical aspects of excitable systems with special reference to the heart. In particular, this chapter contains an introduction to the various types of cardiac dynamics observed both experimentally and clinically, a definition of overdrive suppression, as well as a summary of the theoretical methods used to model the dynamical behaviour of excitable systems, including ionic modeling, relaxation oscillators and difference equations.

Chapter 2 contains an outline of the experimental methods. Tissue preparation techniques are discussed followed by a description of the experimental setup.

Chapter 3 consists of a review of our present understanding of the effects of electrical stimulation on spontaneously oscillating embryonic chick heart cell aggregates, without consideration of stimulation history dependent phenomena. The experimental study focuses on phase resetting and periodic stimulation. The experimental observations are compared with the results obtained by numerical simulation of an ionic model of electrical activity of embryonic chick heart cell aggregates and by iteration of a simple nonlinear model expressed in terms of difference equations. The ionic mechanisms underlying the development of complex dynamics are discussed and the limitations of the ionic model emphasized. I provide an analysis of the results obtained by iteration of the nonlinear model that helps gain insight into the mathematical structure of the dynamics considered. Issues of universality are also discussed. This chapter emphasizes the complementarity of both approaches in the understanding of biological dynamics that could be improved by including stimulation history dependent effects.

In Chapter 4, I carry out an extensive study of the qualitative aspects of overdrive suppression in embryonic chick heart cell aggregates using three sets of experimental protocols: 1) stimulation at a fixed frequency varying the number of stimuli, 2) stimulation at different frequencies, 3) stimulation with different intensities. A mathematical model is developed, based on a system of nonlinear ordinary differential equations, to account for the experimental observations. The main idea of the model is that overdrive suppression arises as a result of a hyperpolarizing current that is

induced by action potentials. This work shows that the frequency of action potentials is the major determinant of overdrive suppression. Consequently, during periodic pacing of spontaneous oscillators at different rates, the fastest frequency where 1:1 entrainment can be maintained is associated with maximal overdrive suppression.

Chapter 5 is devoted to an experimental and theoretical analysis of the rhythms arising during fixed delay stimulation of embryonic chick heart cell aggregates. During fixed delay stimulation, bursts of rapid activity interspersed with prolonged pauses are typically observed for a wide range of delays. Cessation of stimulation is followed by overdrive suppression. I use a simple nonlinear model, based on the interaction between excitability and overdrive suppression, to describe these dynamics. A modified version of the Shrier-Clay ionic model of electrical activity is also presented, that includes a simplified sodium pump term. I show that the complex patterns during fixed delay stimulation arise due to delicate interactions between overdrive suppression and phase resetting which can be described in terms of the underlying ionic mechanisms. Since this preparation is an experimental model of a reentry tachycardia, these results may provide a basis for understanding incessant tachycardias in the intact heart.

Finally, in Chapter 6, I present a dynamical investigation of spontaneously active cell clusters from the rabbit atrioventricular node. The goal of this study is to better characterize the phase resetting and the rhythms during periodic stimulation of this slow inward current system. Phase resetting curves of both strong, weak as well as discontinuous types are obtained by applying single current pulses of different intensities and latencies following every ten action potentials. Graded responses are elicited in a wide range of stimulus phases and amplitudes. A single premature stimulus causes a transient prolongation of the cycle length. Sustained periodic stimulation, at rates faster than the intrinsic beat rate, results in various N:M (stimulus frequency:action potential frequency) entrainment rhythms as well as periodic or irregular changes in action potential morphology. The changes in action potential characteristics are evaluated by computing the area under the action potential trace and above a fixed threshold (-45 mV). I show that the variations in action potential morphology play a major role in the onset of complicated dynamics observed in this experimental preparation. In this context, the prediction of entrainment rhythms using techniques based on the iteration of phase resetting curves (PRC's) are inadequate since the PRC does not carry information directly related

to the changes in action potential morphology. This study demonstrates the need to consider graded events which, though not propagated, have important implications in the understanding of dynamical diseases of the heart.

## Contributions to publications

The following is a statement of the contributions of the author to the material presented in this thesis. Chapters 3, 4 and 6 are based on recently published material. The text of Chapter 5, pending minor modifications, is awaiting submission. The author's contributions to these chapters are:

Chapter 3: Based on the text of **Ionic Mechanisms and Nonlinear Dynamics of Embryonic Chick Heart Cell Aggregates**, by V. C. Kowtha, A. Kunysz, J. R. Clay, A. Shrier and L. Glass. This review publication has appeared in *Progress in Biophysics & Molecular Biology*, **61(3):255-281**, 1994 (reproduced with kind permission from Elsevier Science Ltd, The Boulevard, Langford Lane, Kidlington OX5 1GB, UK). The author of the thesis:

- Performed most of the experiments in Dr. Shrier's laboratory.
- Wrote the computer programs to perform the iteration of the phase resetting curves, and carried out all the simulations related to nonlinear dynamics.
- Assisted in revising the ionic model, writing the manuscript, and producing some of the figures.

Chapter 4: based on the text of **Overdrive Suppression of Spontaneously Beating chick Heart Cell Aggregates: Experiment and Theory** by A. Kunysz, L. Glass and A. Shrier, *Am. J. Physiol.*, **269:H1153-H1164**, 1995 (reproduced with kind permission from The American Physiological Society, 9650 Rockville Pike, Bethesda, MD 20814, USA). This manuscript contains the most extensive study of the qualitative aspects of overdrive suppression in embryonic chick heart cell aggregates. A simple model for overdrive suppression is also presented. The author:

- Performed all the experiments in Dr. Shrier's laboratory.
- Developed the theoretical model under Dr. Glass' supervision.
- Entirely wrote the original manuscript and produced all the figures.

Chapter 5: based on a manuscript in preparation. This chapter contains the first study of the dynamics during fixed delay stimulation of embryonic chick heart cell aggregates. Two theoretical models are developed and the results of numerical simulations are compared with experimental data. The ionic model is a modified version of the Shrier-Clay ionic model of electrical activity, that now contains a sodium pump term. The nonlinear model captures the interaction between phase

resetting and history dependent effects that underlies the complex dynamics observed experimentally. This study may have implications in the understanding of reentrant tachycardias. The author:

- Performed all the experiments in Dr. Shrier's laboratory.
- Analyzed the experimental data.
- Developed the nonlinear model and incorporated a sodium pump term in the Shrier-Clay ionic model of activity.
- Produced all the figures.
- Entirely wrote the text of Chapter 5.

Chapter 6: based on the text of **Phase Resetting and Dynamics in Isolated Atrioventricular Nodal Cell Clusters** by A. Kunysz, A. Munk and A. Shrier, *Chaos*, 5(1):184-192, 1995 (reproduced with kind permission from The American Institute of Physics, 500 Sunnyside B'vd., Woodbury, NY 11797, USA). The experimental study was independently initiated by the two first authors (A. Munk is a Ph.D. student in the Department of Physiology). In this publication, the authors demonstrate the influence of changing action potential morphology upon the complexity of the dynamics during periodic stimulation. A comparison is also drawn between overdrive suppression in AV nodal cell clusters and embryonic chick heart cell aggregates. The relevance of this work to "dynamical diseases" is discussed. The author:

- Performed all the experiments (with A. Munk) in Dr. Shrier's laboratory.
- Was responsible for the analysis of the data and the nonlinear aspects of this work.
- Entirely wrote the manuscript.

# Chapter 1

## Introduction

Recent advances in mathematics and computer modeling have triggered a rapid expansion in the field of nonlinear dynamics. Today, we have heard of the “butterfly effect” and have been confronted with the sheer beauty of a Mandelbrot set. A fractal dimension was attributed to clouds and raindrops, while planets were caught in chaotic motion. We have also heard of the “universal” laws of chaotic systems. The striking fact is that nonlinear systems can be found everywhere.

The proper function of physiological systems relies on a constant exchange and processing of information. In the body, this is achieved *via* the transmission of electrical or chemical signals. The ability to propagate information relies on an essential property of many physiological systems: excitability or the possibility of a large transient excursion of a state variable in response to suprathreshold input (see below). Since excitability necessarily implies nonlinear dynamical properties, one may say that nonlinearity is essential to life. The incessant beating of the heart is probably the most remarkable example of the necessary presence of nonlinear systems in life. Since heart disease is a primary cause of mortality in most industrialized countries, there is a very good rationale for conducting extensive experimental and theoretical studies of such excitable biological systems.

Embryonic chick heart cell aggregates are one of the model experimental preparations used in the study of the mechanisms underlying the cardiac rhythm as well as of rhythmogenesis and dynamical behaviour in excitable biological tissue. Under suitable experimental conditions, the aggregates beat spontaneously with a regular rhythm. Because they are devoid of neural and hormonal inputs, virtually isopotential, and can be made quiescent at will, embryonic chick heart cell aggregates are particularly attractive as a model of excitable biological tissue. Moreover, previous

electrophysiological studies have yielded a wealth of experimental data that provided a good understanding of the mechanisms underlying electrical activity in this preparation [19, 31, 34, 50, 55, 125, 157, 158, 159, 164]. Periodically stimulated embryonic chick heart cell aggregates offered the earliest example of chaotic behaviour in an excitable biological system [154, 78]. In order to account for the various rhythms observed experimentally, simplified models were developed that were later adapted to other biological systems (for review, see Reference [70]). Although these models are rather successful at predicting most of the experimental rhythms, their description does not account for the stimulation history dependent effects that underly the evolution of rhythms observed both clinically and experimentally. As a result, we need new theoretical approaches to improve our understanding of excitability in biological systems. The following sections of this Chapter provide a brief survey of some of the properties of excitable media and of the techniques used in the theoretical modeling of excitation.

## 1.1 Excitable media

Excitable media are ubiquitous in nature. An excitable medium is best defined by its *threshold* behaviour which is a manifestation of the intrinsic nonlinearity of this class of systems. The threshold behaviour is directly related to the notion of external stimulation of the system. By external stimulation, I mean the application of an electric impulse, the addition of a fixed quantity of a chemical reagent or perhaps a mechanical input. Provided that the amplitude of the stimulation exceeds a certain threshold, an excitable medium previously in its resting state reacts by a large change in the variable(s) describing the state of the system. On the contrary, a perturbation lower or even slightly lower than threshold will induce a minimum departure from the initial condition. The excitation phase is transient; the excitable medium quickly returns to its original state. The return to the initial state is followed by an episode of refractoriness to further external stimuli (refractory period). The presence of this refractory period is an essential feature of excitable systems.

### 1.1.1 A few classical examples

An excitable medium is generally thought to be a collection of spatially distributed excitable elements which interact with their neighbours according to the laws of dif-

fusion. It is understood that excitable media contain an energy source which allow them to excite under stimulation. This excitation then propagates to neighbouring elements: we have spread of excitation. The characteristics of the excitation phase (such as duration, rate and morphology of response) reflect the nature of the intrinsic mechanisms underlying excitability. In response to stimulation, an originally homogeneous excitable medium is capable of organization. This structuring may appear in both time and space. For example, a front (or traveling wave) of excitation may propagate from the stimulation front throughout the entire medium. Provided that certain conditions are met, an excitable medium may have the self-exciting property. Sustained self-excitation can also occur as the wave of excitation catches its own tail (reentry). The study of excitable media and of the conditions under which these different patterns of organization occur is of increasing practical and theoretical interest. In particular, the search for criteria which guarantee stability of specific excitation patterns has attracted considerable attention (for review see [188]).

The Belousov-Zhabotinsky (B-Z) reaction is one of the celebrated examples of an "autowave process" occurring in an excitable medium. An autowave process is a wave phenomenon in which the choice of an initial condition has no other consequence than the onset of one of several possible stable regimes. In the B-Z reaction, bromate oxidizes citric acid in the presence of cerium (as a catalyst). For suitably chosen initial concentration of the reagents, Belousov [10, 11] observed sustained oscillations in the colour of the solution, due to periodic changes in cerium concentration. Stimulation (by mechanically stopping the propagation front) of the circular wave can result in the formation of a spiral pattern of excitation [179, 187]. As we shall discuss later, there is evidence that similar phenomena take place in biological tissue. For other initial conditions (different chemical concentrations of the reagents), these oscillations are absent [179]. However, the medium is still excitable: a small perturbation in the form of contact with a hot iron wire may result in the propagation of a single wave of excitation [180].

In the previous example, we have dealt with an initially homogeneous and continuous medium. Similar behaviour can also occur if one discretises the excitable medium. In the experimental context, the best example is offered by the study of Nagumo et al, in 1963 [135]. In their experiment, a two-dimensional grid of iron wires was immersed in a bath containing nitric acid. Their results (published only 15 years later), clearly indicate some level of organization within the bath, with the

apparition of spiral waves. Spiral waves as well as other patterns of spatio-temporal organization were also observed in numerical simulations of cellular automata with heterogeneously distributed refractory times [130] as well as models of nerve networks [54]. In this case, we are clearly dealing with a system in which time and space are discrete. The state of each element of the system depends upon the previous states of neighbouring elements.

We have mentioned the ubiquity of excitable media. Although they are perhaps most easily observed in chemical systems and computer models, it is in the biological sciences that they may have the most importance. Life (at least our notion of it) is based on the exchange of information. In a string of RNA, special sequences (codons) mark the beginning and the end of a code that may be specific to the production of a given protein. Chemical messengers are used to trigger the onset of various organic reactions. The propagation of nerve impulses determines our ability to perform physical tasks and to perceive the world. Cardiac function relies on the intrinsic excitable property of the cardiac tissue. However, many physiological systems are of uttermost complexity. It is in this context that experiments carried out on chemical, electrical or numerical systems can be useful at providing a better understanding of the importance of excitable media in biological systems.

### 1.1.2 Excitable media in physiology

Excitable systems are common in physiological systems. Excitable behaviour is found in neurons [90, 58], pancreatic cells [25], intestinal cells [151], and heart tissue [92, 96, 182]. When describing physiological systems, the action potential (AP), recorded as a change in the cellular transmembrane potential  $V_m$ , is a manifestation of the large change in the state variable(s) associated with excitation. Excitable physiological media can be either quiescent or autonomously oscillating. Electrical coupling between the cells guarantees the spread of the excitation to neighbouring excitable tissue, provided that successive excitations do not occur at intervals shorter than the *refractory time*. The presence of the refractory time has serious consequences on the spatio-temporal organization of physiological excitable tissue. In a one dimensional excitable medium, it ensures unidirectional propagation of the original impulse. During sustained electrical stimulation, the propagation of excitation can be blocked (partially or entirely) if the period between successive stimuli is too short. This may result in the onset of complex rhythmic patterns, which are

of particular importance in the study of the heart. These rhythms will be further described in another part of this Chapter and in Chapter 3.

### 1.1.3 The heart as an excitable medium

The heart is a complex anatomical structure, possessing four distinct hydrodynamical chambers. The pumping cycle of the heart can be divided into the contraction of the atria (with filling of the ventricles) and the much more forceful contraction of the ventricles (recirculation of blood). When isolated from the rest of the body, the heart is capable of sustaining spontaneous activity. All the cardiac cells are excitable and some groups of cells can sustain spontaneous electrical activity. In the healthy heart, the basic cardiac rhythm originates from a small group of spontaneously oscillating or *pacemaker* cells located in the SA node. The activity of the other groups of slowly beating spontaneous cells (subsidiary pacemakers) is normally entrained (suppressed) by the faster sinus rhythm [173]. These latent pacemakers (for example the AV node) can assume dominating pacemaker function if the SA node fails to produce the basic rhythm or if an interruption in the propagation of the sinus rhythm occurs [173]. The atrio-ventricular (AV) node forms the only anatomical (and excitable) link between the atria and the ventricles. The lower electrical coupling between AV nodal cells is the mechanism that, by delaying the propagation of the electrical impulse to the ventricles, ensures the proper filling of the latter before contraction occurs. The rapidly conducting Purkinje fibers complete the spread of activity to the ventricles. The heart is therefore a strongly heterogeneous three-dimensional excitable medium. There is strong spatial specialization within the cells that constitute the myocardium. In addition, the heart rhythm is subject to neuronal and hormonal inputs that adapt cardiac output to the changing needs of life.

In relation to the specialization of individual cells, the action potential characteristics change with anatomical location. Most cardiac action potentials are of long duration. Action potentials of ventricular cells last for 200 to 400 ms, in strong contrast to typical 5 ms AP's recorded in the nervous system and in skeletal muscle [138]. This difference can be explained in terms of the different functions of the action potential in these different types of excitable tissue. In skeletal muscle, the action potential is a simple trigger for contractility. In the heart, the action potential partly overlaps with the period of contraction, therefore controlling the length of the contractile phase. This was confirmed in experiments in which the action potential

duration was artificially prolonged by the injection of electrical current [132]. There is a direct relationship between action potential duration and the length of contraction of cardiac muscle. Other action potential characteristics vary as well. Ventricular cells are characterized by very fast depolarization phases ( $(\frac{dV}{dt})_{max}$ , maximum upstroke velocity of the action potential), with typical maximum values around 400 V/s and almost ideal “one or none” responses to excitation [78]. In pacemaker cells (SA and AV nodal), the onset of the action potential is much slower. Because many types of cells are found within the small nodal regions,  $(\frac{dV}{dt})_{max}$  values are typically between 4 and 30 V/s [97, 162, 128]. In addition, these groups of cells often show “graded” or incomplete responses to stimulation [97, 162]. These experimental observations reflect the differences in the nature of the mechanisms underlying the onset of excitation. Some of the implications of the graded responses of AV nodal cells to stimulation will be discussed in Chapter 6.

#### 1.1.4 Cardiac rhythms

Cardiac rhythms have attracted a great deal of attention since cardiac malfunction is often associated with abnormal and complex cardiac dynamics. In the healthy heart, the cardiac rhythm is entirely synchronized to the beating of the pacemaker cells of the SA node [16]: there is 1:1 entrainment between the sinus rhythm and the rest of the myocardium. More complex rhythms may arise in a variety of pathological situations. In this short section, I review some of these most important dynamical behaviours.

Most dysrhythmias are characterized by a loss of 1:1 entrainment with the sinus rhythm (some of the exceptions include sinus bradycardia or tachycardia and first degree AV block). This loss of 1:1 entrainment generally appears as a consequence of two possible factors: 1) a block of conduction of the electrical impulse; 2) a competition between rhythms due to the emergence of a subsidiary pacemaker or to the appearance of a reentrant circuit. The resulting new rhythm can be either periodic or irregular. The loss of 1:1 entrainment was first reported at the end of the XIXth century in the context of sustained external stimulation of animal hearts [62]. At high stimulation rates, some of the stimuli did not induce a contraction of the cardiac muscle. Instead, the response of the cardiac muscle to external electrical seemed to follow a variety of N:1 entrainment patterns. Subsequent experiments [64] indicated that similar patterns could be obtained at normal heart rates by artificially (sur-

gically) disrupting the normal conduction of cardiac electrical impulses. In these series of experiments,  $N:1$  and  $N:M$  patterns were observed as well. Further experimental investigations also led to the discovery of  $2N:2M$  as well as chaotic types of entrainment [117, 91]. Similar rhythmic patterns can also be found in other types of physiological tissue subject to external forcing, such as nervous fibers [53] or the respiratory system [145, 146, 142].

The rhythms described above are often observed in the clinical context. In particular,  $2:1$  and  $4:1$  rhythms of entrainment appear in many common forms of atrioventricular block. Wenckebach rhythms [82], characterized by an increasing PR interval (time interval between the P and the R waves in the electrocardiogram) that finally leads to the skipping of a ventricular contraction are also found in many rhythmic disturbances of heart function.  $2N:2M$  rhythms can be observed during episodes of atrioventricular block associated with atrial flutter [117]. Such  $2N:2M$  patterns can appear as oscillations in the time between successive activations or as alternations in action potential morphologies. Irregular entrainment rhythms occur in some of the most lethal cardiac dysrhythmias such as ventricular fibrillation. Interestingly, although such irregular patterns were first experimentally observed 150 years ago, their aperiodicity was for long attributed to the lack of control of experimental conditions. Finally, paroxysmal ventricular tachycardia is a pathological condition characterized by often seemingly irregular "bursting" behaviour [140, 166].

This description of cardiac rhythms was oriented towards the characterization of *stable* entrainment patterns. However, the *evolution of rhythms* between different patterns of entrainment is a common experimental and clinical observation. In heart tissue, the mechanisms underlying such evolutions of rhythms also play an important role in maintaining proper heart function. In particular "overdrive suppression" plays an important role in maintaining the domination of the sinus rhythm over latent pacemakers.

### 1.1.5 Overdrive suppression: definition and mechanisms

Overdrive suppression is an important cardiac phenomenon that defines the relationship between the pacemakers of the heart [173]. Overdrive suppression has been defined as a transient suppression of the intrinsic rhythm (prolongation in spontaneous cycle length) due to stimulation at rate higher than the spontaneous frequency [173, 174]. In the heart, the activity of the latent pacemakers (such as the AV

node, or slowly beating Purkinje fibers) is normally suppressed by the faster sinus rhythm. However, since overdrive suppression is a transient phenomenon (normally maintained by the incessant sinus rhythm), the subsidiary pacemakers can assume dominant pacemaker function if the sinus rhythm is disrupted. Initial reports of overdrive suppression were given by Gaskell [63] who first described its possible function in his study of the tortoise heart, and by Erlanger and Cushny [53, 42]. Nowadays, numerous studies of overdrive suppression in various types of cardiac tissue are available. In the clinical context, overdrive suppression is used as a test for proper sinus node function (sinus node test) [101]

The experimental studies of overdrive suppression have focused on both the qualitative aspects and the mechanisms. In 1966, Killip first reported that the magnitude of overdrive suppression was dependent upon the duration and the rate of the drive (actually the action potential frequency) [104]. Since overdrive suppression is a function of drive duration, the intrinsic properties of excitable tissue gradually change during sustained stimulation. Although the effects of a prolongation in the spontaneous cycle length on the excitability of cardiac tissue are still not well understood, this phenomenon undoubtedly plays a major role in the evolution of rhythms during sustained periodic stimulation [186]. For example, the progressive lengthening of the cycle length during rapid drive may cause a gradual decrease in excitability that result in an evolution of the original rhythm (say 2:1) towards higher degree of block (say 3:1). However, since overdrive suppression is a function of action potential frequency, overdrive suppression can decrease in the 3:1 regime. The original excitability is then partly restored and the initial 2:1 rhythm can potentially reappear, with a subsequent oscillation between the two regimes. Because overdrive suppression may strongly influence the dynamical behaviour during periodic stimulation, the incorporation of such time-dependent effects into theoretical models of excitable tissue is of prime importance. Some possible ways to achieve that goal are discussed in Chapters 4 and 5.

The primary mechanism of overdrive suppression is a decrease in the slope of diastolic depolarization (i.e. the slow depolarization towards threshold) [173]. Such an effect could occur as the result of the increase (decrease) in the conductance of a hyperpolarizing (depolarizing) current. Experimental evidence suggests that many ionic mechanisms can underly overdrive suppression. In Purkinje fibers, overdrive suppression can be induced by an increase in extracellular potassium concentrations

[1, 174]. A possible role of calcium ions has also been suggested [106, 134]. However, many reports indicate that the activation of the sodium-potassium pump due to increased accumulation of intracellular sodium ions or extracellular potassium ions (or both) during fast drive is a major factor in the development of overdrive suppression [41, 143]. Finally, neural and hormonal factors can also play a role [175]. A more detailed discussion on the subject can be found in Reference [173] and in Chapter 4.

### 1.1.6 Towards modeling excitable media

The quantitative description of excitable media (e.g. threshold behaviour) is often independent of the very mechanisms that underly excitability in a particular system. In the same fashion, we can often describe the oscillation of a periodic system without possessing detailed knowledge of the underlying physical phenomena. A similar quantitative approach can be used in the mathematical modeling of excitable phenomena. It often brings the advantage of a simpler theoretical formalism than the descriptive approach, in terms of the detailed underlying processes. In reality, both approaches are complementary and equally interesting. The modeling of the heart offers a good example. The cardiac rhythm that appears on the electrocardiogram (ECG) is a global manifestation of the intrinsic properties of the excitable cardiac tissue. Since the heart contains millions of excitable cells, we are considering a statistical or macroscopic property of the heart. The biophysicist or physiologist who studies the ionic mechanisms of excitability works on the cellular level. Each cell contains thousands of individual ionic channels. Thus, the cellular level corresponds to the mesoscopic scale. The microscopic scale is reached in the studies of ion pores, of sub-cellular structures, and in the recent advances in molecular biology.

## 1.2 Ionic models of excitable heart tissue

The excitability of biological tissue is due to ion (charge) movement. The transmembrane potential  $V_m$  of an excitable cell is a function of the chemical gradients and of the ionic fluxes across the membrane. The cells possess active transport mechanisms that maintain suitable ionic gradients across the membrane. In this section, we summarize the theoretical basis of transmembrane ionic fluxes. We also present some of the most current ionic models of electrical activity, with special reference to the heart.

### 1.2.1 Simplified model of ionic fluxes across membranes

Most of the charge movement across cellular membranes is due to sodium ( $\text{Na}^+$ ), potassium ( $\text{K}^+$ ), calcium ( $\text{Ca}^{2+}$ ) and chloride ions ( $\text{Cl}^-$ ). The particular electrochemical gradients are different for each ion and can vary from one cell type to another. The most important fact is that sodium and potassium gradients run in opposite directions. The electrochemical potential, for a given ion species, is equal to the algebraic sum of the concentration gradient moving ions out of the cells and of the electrical force due to the presence of a negative intracellular potential. At equilibrium, an expression for the electrochemical potential can be derived using Boltzmann's equation. The result is the well known Nernst equation [136]

$$E_r = \frac{kT}{zF} \ln \frac{[X_o]}{[X_i]} \quad (1.1)$$

where  $E_r$  is the Nernst potential,  $k$  is Boltzmann's constant,  $T$  the absolute temperature,  $z$  the valence of the given ion,  $F$  the Faraday constant,  $[X_o]$  and  $[X_i]$  the respective extracellular and intracellular concentrations of the ion species  $X$ . Typical physiological values for the Nernst potential vary from  $\approx -100$  mV for potassium,  $\approx -40$  mV for chloride,  $\approx +40$  mV for sodium and  $\approx +130$  mV for calcium ions. These values are just rough estimates, since the ionic concentrations depend upon numerous factors.

On the average, the inner side of the membrane is charged negatively with respect to the extracellular space. For a given membrane potential  $V_m$ , the flow of ions  $X$  across the membrane is proportional to the potential difference with respect to the equilibrium potential  $E_x$  (this potential difference is often referred to as the "driving force"). The ionic current  $i_X$  (for the ion  $X$ ) is then

$$i_X = g_X(V_m - E_X) \quad (1.2)$$

where  $g_X$  is the membrane conductance to ions  $X$  and  $V_m$  the transmembrane potential. Indeed,  $g_X$  can itself be a function of the number and the properties (such as gating) of the ionic channels conducting ion  $X$ . The total transmembrane current carried by ion  $X$  when *all* the channels are open and independent of the gating mechanism is usually written as:

$$\bar{i}_X = \bar{g}_X(V_m - E_X) \quad (1.3)$$

where  $\bar{g}_X$  is now the maximum channel conductance. This equation is just Ohm's law. The effect of this current is to move the transmembrane potential towards the equilibrium potential of ion  $X$ . The transmembrane potential  $V_m$  is generally more positive than  $E_K \approx -100mV$ . By convention, the outward currents due to  $K^+$  ions are positive. Conversely, sodium and calcium currents are inward and negative.

### 1.2.2 A step further: the GHK approximation

The cell membrane is a thin lipid bilayer permeable to ions. In the GHK approximation [71, 89], there is no assumption concerning the presence of specialized *ionic channels*. The derivation of the GHK equation relies on several fundamental assumptions: 1) permeant ions partition instantaneously (from the solution) into a homogeneous membrane of thickness  $l$ ; 2) there are no interactions between individual ions; 3) there is a constant electric field throughout the membrane (constant field approximation). In addition, the membrane is assumed to have a specific permeability for each ion species: the GHK equation describes the total current of *each ion* separately.

The total ionic flow (current) for each ion species is the sum of a diffusive component and of the current due to the presence of a constant electric field throughout the membrane. The density of the total current for ion  $X$  can be written as

$$I_X = -z_X D_X F k T \frac{d[X]}{dx} - F z_X^2 D_X [X] \frac{dV}{dx} \quad (1.4)$$

where  $z_X$  is the valence of ion  $X$ ,  $D_X$  the diffusion coefficient of  $X$  inside the membrane,  $[X]$  is the concentration of ion  $X$ , and  $V$  is the electrical potential at a distance  $x$  from the outer part of the membrane. By diffusion-solubility theory, the membrane permeability to ion  $X$ ,  $P_X$ , is related to  $D_X$  by

$$P_X = \frac{D_X \beta_X}{l} \quad (1.5)$$

where  $\beta_X$  is the water-membrane partition coefficient for ion  $X$  [88].

By integrating equation (equation) across the membrane of thickness  $l$ , one obtains the GHK current equation

$$I_X = P_X z_X^2 \frac{V F^2}{k T} \frac{[X]_i - [X]_o \exp\left(\frac{-z_X F V}{k T}\right)}{1 - \exp\left(\frac{-z_X F V}{k T}\right)}. \quad (1.6)$$

At dynamical equilibrium, the total current in a homogeneous portion of the membrane must vanish. An expression for the corresponding membrane potential (equilibrium rest potential  $E_r$ ) can be obtained using the equation above,

$$E_r = \frac{kT}{F} \ln \frac{\Sigma^+ P_{X_i} [X_i]_o + \Sigma^- P_{X_i} [X_i]_i}{\Sigma^+ P_{X_i} [X_i]_i + \Sigma^- P_{X_i} [X_i]_o} \quad (1.7)$$

where  $\Sigma^+$  ( $\Sigma^-$ ) denotes summation over cations (anions) and the subscript  $i$  indicates that we consider all the different ions  $X_i$ . This equation is the GHK voltage equation, used for studies of membrane permeability to ions and the description of sodium and potassium ionic currents in excitable cells. In particular, the GHK equations account for the *rectification* (marked departure from Ohm's law) observed for certain classes of channels. However, the Hodgkin-Huxley formalism [90] (discussed below) is the most useful theoretical model of ionic currents.

### 1.2.3 The Hodgkin and Huxley (or H+H) formalism

For the biophysicist, the names of Cole, Marmont, Hodgkin and Huxley are associated with some of the most important studies in the field of ionic channels. In 1949, Cole and Marmont designed the voltage clamp technique [38, 124]. The cellular transmembrane potential changes due to ionic fluxes across the membrane. These ionic fluxes are themselves a function of membrane potential. Therefore, adequate control of the transmembrane potential is a prime requirement in the study of the properties of ionic channels and fluxes. The voltage clamp technique was designed to achieve that goal. In the original experiments by Cole and Marmont, the membrane potential across an area of the membrane of the giant squid axon was kept constant by inserting a long wire electrode inside the axoplasm. This had the effect of shorting the resistance of the axoplasm and allowed uniform polarization of the nerve fibre. Variants of the original technique, including single or double microelectrode and sucrose-gap methods represent some of the main experimental tools used in modern biophysics [138, 88].

Three years later (in 1952), the voltage clamp was successfully used by Hodgkin and Huxley [90] to produce the first study of voltage sensitive conductances in the cell membrane of the giant squid axon. For the first time, distinct ionic currents were identified and, using the experimental data, a model describing the kinetics of these ionic currents was proposed.

The cell membrane is a lipid bilayer that acts as a capacitor. The ionic fluxes occur through *ionic channels* determined by conformational characteristics of specialized proteins contained in the membrane. The membrane contains several different populations of ionic channels each of which determines the properties of a membrane current (for example, the conductance of the channel). Because the conformation of the proteins changes with transmembrane potential, so does the conductance of ionic channels: this is the voltage gating property. It is generally believed that the opening and closing of ionic channels is governed by a stochastic voltage-dependent process (alternative deterministic hypotheses were also proposed: see for example References [119, 120]). When considering the statistical properties of large numbers of individual ionic channels (i.e. a membrane current) the *macroscopic* properties of the ionic current can generally be described by deterministic functions of the membrane potential. Classically, there are two types of gates. The opening of both the *activation* and the *inactivation* gates is necessary for the ionic channel to be open. A channel closes by *inactivation* when the ionic flux is interrupted by the closing of the inactivation gate. A channel is said to *deactivate* when it stops to conduct due to the closing of the activation gate. On the macroscopic scale (large population of channels: a membrane current), a membrane current deactivates (inactivates) when a significant portion of the ionic channels is deactivated (inactivated). Although most of the gates are voltage-sensitive, ligand binding mediated and ion sensitive gating mechanisms have also been reported [88].

In the Hodgkin-Huxley description of ionic currents, the membrane of the cell is modeled as a parallel RC circuit. The capacitance of the membrane  $C_m$  is constant and the membrane resistance  $R_m$  is a function of the sum of the conductances of all the ionic channels at a given time. In their first series of experiments, Hodgkin and Huxley identified three distinct currents:  $I_{Na}$  a rapidly activating and inactivating inward sodium current;  $I_K$  an outward current carried by potassium ions and characterized by delayed activation; and  $I_L$  described as a time-independent "leakage" current. Assuming that the membrane is isopotential (*space-clamped*), the change in transmembrane potential due to the membrane currents is described by

$$C_m \frac{dV_m}{dt} = -(I_{Na} + I_K + I_L + I_{applied}) \quad (1.8)$$

where  $I_{applied}$  is the stimulation current,  $C_m$  is expressed in  $\mu F/cm^2$  and all currents are given in terms of current densities.

Although the H+H formalism was derived before ionic channels were discovered, the dynamics of gating were described in a fashion that is analogous to the statistical properties of a population of ionic channels. The H+H description of gating relies on the assumption that one or several gates (charged "particles" bound to the membrane) close or open the ionic channel in response to changes in membrane voltage, and following first order kinetics. Consider one of the gates and let  $n$  denote the probability that the gate is in a position that opens the channel. Then  $1 - n$  is the probability that the gate (channel) is closed. The voltage and time dependent changes in  $n$  are described by

$$1 - n \xrightleftharpoons[\beta_n]{\alpha_n} n, \quad (1.9)$$

where  $\alpha_n$  is the voltage dependent rate constant describing the transition between the closed and the open state, and  $\beta_n$  the transition rate from the open to the closed state.

This reaction can be described by the ordinary differential equation

$$\frac{dn}{dt} = \alpha_n(1 - n) - \beta_n n. \quad (1.10)$$

By making the substitutions

$$\tau_n = \frac{1}{\alpha_n + \beta_n}$$

and

$$n_\infty = \frac{\alpha_n}{\alpha_n + \beta_n},$$

where  $n_\infty$  is the steady state value of  $n$  for a given transmembrane potential, one obtains the other common form of this equation

$$\frac{dn}{dt} = \frac{n_\infty - n}{\tau_n}. \quad (1.11)$$

The membrane current due to ion  $X$  can now be written

$$I_X = n\bar{g}_X(V_m - E_X). \quad (1.12)$$

In many cases, several gating "particles" are needed to properly describe the kinetics of a given membrane current. This is for instance the case for the fast sodium current for which the classical description assumes the existence of three activation gates and a single inactivating one (normally referred to as  $m$  and  $h$ ) [88].

The mathematical description of membrane currents proposed by Hodgkin and Huxley led to the development of many other ionic models of excitable tissue. In

particular, the original model developed for the giant squid axon was successfully adapted to describe the ionics of excitation of cardiac tissue. In the process, with increasing amounts of data obtained from voltage clamp experiments, many other ionic currents were discovered leading to a much more complex presentation of the theoretical models.

#### 1.2.4 A few models of ionic activity

The action potential of cardiac cells is typically 30 to 100 times longer than in nerve tissue [138]. In some specialized groups of cells (nodal cells), the upstroke of the action potential is also much slower than in ventricular or nerve cells [128]. Some cells are spontaneously active while others are quiescent. These differences in action potential characteristics have led to the development of numerous ionic models highly specific to the type of tissue under consideration. In cardiac cells, calcium currents play an important role. Calcium currents are partly responsible for the considerable duration of the action potential [88]. They underly the slow upstroke of the action potential in pacemaker cells, and play a significant role in regulating the contractility of cardiac muscle [88]. Numerous other currents were also discovered and incorporated into existing ionic models. As a result, the Beeler-Reuter model, which describes the electrical activity of mammalian ventricular muscle, is eight-dimensional and contains the description of five separate currents [9]. The original H+H model was only four-dimensional [90]. The MNT (McAllister, Noble and Tsien) ionic model of Purkinje fibre tissue has ten dimensions and describes seven currents [122]. Another model developed for Purkinje fibers by DiFrancesco and Noble has over a hundred parameters and is 14-dimensional [48]. In chapter 3, I review a high dimensional ionic model of activity, the Shrier-Clay model for embryonic chick heart cell aggregates. The main rationale for developing such complicated theoretical models is the assumption that the inclusion of *all* the ionic components and a detailed description of their kinetics is needed to achieve an accurate simulation of cardiac action potentials. Such models can then be used to perform computer experiments which allow very good control of the experimental parameters (often hard to achieve in complex physiological systems). In combination with pharmacological research, they have proved to be a useful tool in designing new therapeutic approaches for the treatment of disease.

The increasing complexity of ionic models raises a number of questions. One of

them concerns the significance of the enormous number of parameters included in these theoretical descriptions. In a model containing hundreds of parameters, the role of each parameter is hard to evaluate. The high dimensionality of the ionic models also forbids (in most cases and for most people) a good intuitive understanding of the important parameters of the system as well as analytical analysis. Because the usefulness of such models relies heavily on numerical simulations, special care must also be taken in the choice of the algorithms used for integration. To summarize, these complex models often show a certain lack of transparency.

The situation may worsen as new electrophysiological data prompts biophysicists to include new or modified components. For example, excitable (and other) cells possess active transport mechanisms that are responsible for maintaining suitable ionic gradients across the membrane [88, 15]. Many of these pumps or co-transporters perform their task by exchanging ions across the membrane. Depending on the stoichiometric ratio of the exchange, some of these mechanisms are known to be electrogenic: they hyperpolarize the membrane *via* extrusion of excess positive ions. The sodium-potassium pump is perhaps the best example of an electrogenic mechanism [15, 165]. Its primary function is to maintain the sodium gradient across the membrane by exchanging sodium ions from the intracellular space for potassium ions of extracellular origin. Experimental data indicates that a 3:2 ( $\text{Na}^+:\text{K}^+$ ) stoichiometry is typical of this exchange [165]. Because the sodium-potassium pump can be activated by high stimulation rates, it may produce a significant hyperpolarizing effect that may influence the excitability of the cell. Since this may in turn affect the dynamical behaviour under stimulation, such components must be (and sometimes are, for example, see References [48, 178]) included in ionic models. An attempt to incorporate a simplified model of the sodium pump in the Shrier-Clay ionic model is described in Chapter 5.

Most descriptions of ionic mechanisms assume constant ionic gradients across the membrane. However, it is well known that rapid stimulation may result in important changes in intracellular (and extracellular if the extracellular space is constrained) ionic concentrations. Moreover, recent studies indicate the presence of subcellular structures that amount to a compartmentalization of the intracellular space available to calcium ions [88]. There is no *a priori* reason to reject the possibility that similar structures exist for other ions [112]. Such compartmentalization could affect the driving force for that ion species, and could have important consequences on the

response of cells to excitation.

### 1.2.5 Simplified models of excitability

The classical way of deriving simplified models of excitability is to reduce the dimensionality of the original descriptive theoretical model. For example, the time scale of activation of the fast sodium channel is an order of magnitude shorter than time scales involved in the kinetics of the other currents. In a first order approximation, this fast kinetic process can therefore be omitted. This approach was followed by Gul'ko et al. [83] in reducing a model of activity of Purkinje fibres to a three-dimensional model of excitability. The authors chose the remaining parameters to best reproduce the characteristics of action potentials provided by electrophysiological experiments. The resulting simplified model preserves the excitation properties inherent in the Hodgkin-Huxley model and in the original equations. However, further simplification of this model, based on asymptotic techniques, was necessary to carry out analytical work [109]. In many cases where such a simplification was attempted, the characteristics of the action potentials generated by the simpler model were in good agreement (within 10 %) with the results of the original model. Some of these models will be described in the next section.

## 1.3 Nonlinear dynamics

Nonlinearity is essential to excitable phenomena. The description of the voltage-dependence of the gating of ionic channels in the Hodgkin-Huxley description reflects this nonlinearity. The heart oscillation is itself a nonlinear phenomenon, that can either be described by capturing the qualitative properties of the oscillation or by describing the mechanisms underlying its excitability. The expansion of the field of nonlinear dynamics has found numerous applications in biology, electrophysiology, in experimental studies (methods in signal and data processing) and in theoretical modeling of excitable phenomena (see References [70, 181]). The methods of nonlinear dynamics have been successfully used to develop simplified theoretical paradigms describing the phase-resetting of circadian clocks [181], the dynamical aspects of erythropoiesis [70], population dynamics and excitability (and conduction) in cardiac tissue [70, 78, 75]. The main feature of these simplified models is that they preserve the complex dynamical properties characteristic of the original systems.

These mathematical models appear in the form of difference equations or as simple systems of differential equations.

### 1.3.1 Fundamentals

The dynamical behaviour of a system can be described by a trajectory in phase space (defined in terms of the state variables of the system). The trajectory describes the dynamical evolution of the system with respect to time. In this description, time can be a continuum or be discretised. The motion of a point in the phase space of a system is generally constrained. *Attractors* are regions of phase space which attract nearby trajectories. The nature of the attractor determines the dynamical behaviour of the system (in terms of periodicity). In a dynamical system, the nature of the attractor (and the qualitative dynamics of the system) can change dramatically in response to small alteration in one of the parameters of the system: this event is called a *bifurcation*. Attractors can be found in any number of dimensions. The maximum dimension of the attractor is the number of degrees of freedom of the system.

Attractors which underly periodic behaviour are either closed trajectories in phase space or discrete points. Point attractors describe steady state behaviour: they are *stable fixed points*. For example, the resting state of excitable tissue is affiliated with the presence of a stable fixed point. Stable limit cycles are attractors which describe periodic behaviour<sup>1</sup>. Stability implies that outlying trajectories asymptotically converge to the attractor. The periodic behaviour of spontaneously active or externally stimulated excitable tissue can be the manifestation of an underlying stable limit cycle. Attractors that are unstable repel arbitrary close trajectories unless the trajectory coincides with the attractor (exactly on the unstable orbit or the unstable fixed point). Toroidal n-dimensional attractors in phase space are associated with aperiodic trajectories. Irregular motion can be *quasiperiodic* or *chaotic*. Quasiperiodic motion is represented by a trajectory that densely connects all the points of the attractor in a homogeneous manner and that does not cross the same point twice. Given two arbitrarily close initial conditions, the evolution of one of the trajectories can be predicted at any time if sufficient knowledge of the evolution of the other trajectory is available.

---

<sup>1</sup>The concept of limit cycle was first introduced by Poincaré in 1881 as a closed curve in the phase space of a system of ordinary differential equations.

Chaos appears as irregular dynamics occurring in a deterministic system in which trajectories remain in an invariant region of phase space while arbitrarily close initial conditions yield diverging (in the sense of predictability) trajectories (on average, this divergence is exponential). This sensitivity to initial conditions is the most common of the definitions of chaotic regimes [73]. Attractors corresponding to chaotic motion are *strange attractors*. Their "strangeness" comes from their generally complex shapes. On a strange attractor, the density of trajectories is not homogeneous as in quasiperiodic motion. Strange attractors are *self-similar* and *scale invariant*. By scale invariance I mean that the geometrical organization of the trajectories on the attractor is the same on all size scales. Self-similarity implies that a given trajectory looks the same on all size scales. Structures possessing both properties are said to be *fractal* and are objects of non-integer dimension [123].

Deterministic chaos has been related to many examples of aperiodic behaviour found in biological systems and excitable tissue. The experimental data describing the dynamical behaviour of a system is normally collected in the form of a time series. In order to ascertain the chaotic nature of an irregular time series, careful tests have to be conducted. The computation of the Lyapunov exponents is the simplest technique available. The sign of the Lyapunov exponents is a test of the exponential divergence (or convergence) of nearby trajectories in phase space. Each dimension in phase space is associated with a Lyapunov exponent. A Lyapunov exponent is positive if the trajectories diverge in terms of the corresponding variable. Conversely, a negative Lyapunov exponent is associated with converging trajectories. If an attractor exists and if the largest Lyapunov exponent is positive, the system is chaotic [183]. A zero Lyapunov exponent may indicate the presence of quasiperiodic motion. Zero Lyapunov exponents may also arise when a bifurcation (change in the qualitative dynamics of the system) occurs. For simple theoretical models of dynamical systems, the Lyapunov exponents can often be computed analytically or numerically. However, special care must be taken before interpreting the results of tests designed to conclude on the chaotic nature of the dynamics. For example, chaotic time series are characterized by broad-band spectra. However, this does not imply that *all* time series possessing broad-band spectra are chaotic. An interesting example can be found in references [137, 72].

### 1.3.2 Stability in differential equations

The analysis of stability in systems of nonlinear ordinary differential equations is based on the linearisation of the systems in the neighbourhood of their fixed points (or steady states, see above). Consider the system

$$\frac{dx_i}{dt} = f_i(x), i = 1, \dots, N, \quad (1.13)$$

where  $f_i$  are differentiable functions. At the steady state ,

$$\frac{dx_i^*}{dt} = 0, i = 1, \dots, N, \quad (1.14)$$

In the vicinity of the steady state, the dynamics are described by:

$$\frac{dx}{dt} = A(x - x^*), \quad (1.15)$$

where the matrix  $A$  has elements

$$a_{ij} = \left. \frac{\partial f_i}{\partial x_j} \right|_{x^*}. \quad (1.16)$$

The eigenvalues of  $A$  computed by evaluating  $\det(A - \lambda I) = 0$  (where  $I$  is the identity matrix) characterize the qualitative dynamical behaviour in the vicinity of  $x^*$ . The steady state is *asymptotically stable* (i.e. asymptotically approached as  $t \rightarrow \infty$ ) if *all* the eigenvalues are negative. The steady state is *unstable* if at least one of the eigenvalues has positive real part. The fixed point is *neutrally stable* when the real part of the largest of the eigenvalues vanishes. A Hopf bifurcation occurs when the real part of two complex eigenvalues vanishes. A supercritical Hopf bifurcation is associated with soft excitation; the amplitude of the oscillation is a smooth function of the parameter of the system. Conversely, subcritical Hopf bifurcations are linked to hard excitation and the transition is abrupt; a large amplitude oscillation appears. Both types of excitation are found in excitable biological systems. A review of bifurcation theory in systems of nonlinear ordinary equations can be found in Reference [86].

### 1.3.3 Finite difference equations

Finite difference equations have interesting properties. Even one or two dimensional finite difference equations are capable of displaying the most complex dynamics. Of

course, that is not to say that simpler dynamics can not be found. This richness in the dynamics is particularly striking when a comparison with systems of ordinary differential equations is drawn. In one-dimensional ordinary differential equations the requirement that trajectories be continuous forbids the observation of oscillating or chaotic dynamical behaviour. Finite difference equations can be obtained from systems of ordinary differential equations by considering the return of a cross section of the flow unto itself (the Poincaré map). Finite difference equations are of the form

$$x_i(t+1) = f_i(x_i(t)), i = 1, \dots, N. \quad (1.17)$$

where  $f_i$  is a nonlinear function and  $x_i(t)$  denotes the value of element  $x_i$  at time  $t$ . Provided that an initial condition  $x_i(0)$  is given, the evolution of the system can be obtained by simple iteration of the finite difference equation. For reasons of clarity,  $x_i(t+n)$  will be now referred to as  $x_{t+n}$ . Finite difference equations can be linearized in the vicinity of a fixed point using methods analogous to those described in the previous section. The steady state  $x^*$ , defined by  $x^*(t+1) = x^*(t)$  is *stable* if all the eigenvalues of the Jacobian are located inside the unit circle. Conversely, the steady state is *unstable* if at least one of the eigenvalues lies outside of the unit circle. If two complex eigenvalues simultaneously cross the unit circle, we have a Hopf bifurcation. Let us now consider the one-dimensional case.

Any one-dimensional finite difference equation can be written in the form

$$x_{t+1} = f(x_t) \quad (1.18)$$

where  $f$  is a nonlinear function. The stability of a steady state  $x^*$  is guaranteed if  $|\left(\frac{\partial f}{\partial x}\right)_{x^*}| < 1$ . If this is not the case, the steady state is unstable. Let  $x_0$  denote the initial condition. There is a periodic orbit of period  $n$  if  $x_{t+n}^* = x_t^*$  and  $x_{t+j}^* \neq x_t^*$ , for  $1 \leq j < n$ . The stability of the orbit will be determined by the absolute value of  $\xi$  defined as

$$\xi = \frac{df^n(x^*)}{dx} \Big|_{x^*} = \prod_{i=1}^n \left(\frac{\partial f}{\partial x}\right) \Big|_{x^*} \quad (1.19)$$

where  $f^n$  is the  $n$ th composition of  $f$  with itself. When  $|\xi| > 1$ , the orbit is unstable. The stability criterion is that  $|\xi| < 1$ . When  $|\xi| = 1$ , a bifurcation arises the nature of which is determined by the sign of  $\xi$ . When  $\xi = 1$  there is a tangent bifurcation. A period-doubling bifurcation (with the dynamical consequences that the name indicates) is found when  $\xi = -1$ . This type of bifurcations is of particular

interest since a sequence of period-doubling bifurcations is one of the "routes to chaos" [52].

Two types of one-dimensional finite difference equations (or maps) are of particular interest. Maps characterized by a single hump on the unit interval have been studied extensively. A review of the general results can be found in [47]. More appealing to us are *circle maps* that map the unit circle unto itself. In particular, circle maps arise in the context of periodic forcing of biological oscillators. A general form for circle maps is

$$\phi_{t+1} = f(\phi_t) \pmod{1}, \quad (1.20)$$

where  $f$  is some (not necessarily continuous or nonlinear) function and  $\phi$  some point of the unit circle. For continuous circle maps, the *topological degree* describes the number of times  $\phi_{t+1}$  goes around the unit circle when  $\phi_t$  goes around once. The rotation number  $\rho$  defined as

$$\rho = \lim_{n \rightarrow \infty} \sup \frac{1}{N} \sum_{i=1}^N \Delta \phi_i, \quad (1.21)$$

where  $N$  is the total number of iterations and  $\Delta \phi_i = \phi_{t+i+1} - \phi_{t+1}$ , is often used to obtain partial information about the qualitative dynamical regime. In particular, the rotation number is rational for periodic orbits. The Lyapunov number  $\lambda$ , defined as

$$\lambda = \lim_{n \rightarrow \infty} \frac{1}{N} \sum_{i=1}^N \ln |f'(\phi_i)|, \quad (1.22)$$

where  $f'(\phi_i)$  is the first derivative of  $f$  evaluated at successive iterates  $\phi_i$  can be used to test for chaotic dynamics. The Lyapunov number is positive for chaos, negative for periodic orbits and zero for quasiperiodicity [87].

Periodic stimulation of biological oscillators can often be described by circle maps. At low stimulus intensities, these circle maps are found to be invertible (one to one). For invertible circle maps, theoretical studies predict the existence of an Arnold tongue structure [4, 70] in the amplitude versus period of stimulation bifurcation diagram. The infinite number of N:M patterns of entrainment found in the bifurcation diagram obey simple ordering rules, as described by the Farey tree. The Arnold structure disappears at higher amplitudes of stimulation. Chaotic dynamics as well as bistability (with the same stimulation parameters two different dynamical regimes can be observed with different choices of initial conditions) can be found in

non-invertible circle maps. Such maps are of special interest to the modeling of cardiac excitation since many types of typical dynamical behaviour resemble strongly experimentally observed cardiac rhythms. A thorough treatment of circle maps can be found in Reference [47].

### 1.3.4 Simple models of biological oscillators

The landmark study by van der Pol and van der Mark [170] was the first attempt to model the heartbeat as an electrical phenomenon. Their simple electrical model of the heart consisted of three coupled oscillating components representing the SA node, the atrium and the ventricle. The circuit was so designed that the "SA node" could entrain the "atrium" which could affect the "ventricle" but not vice-versa. With this simple circuit (perhaps not that simple for the time) the authors were able to reproduce many of the cardiac rhythms including different types of heart block and bistability. The success of this approach led to a multiplication of electrical models of the heart. Van der Pol also proposed a simple differential equation to model nonlinear oscillations. Its variants as well as the original equation have been of great importance in development of applied mathematics. The original periodically forced equation was

$$\frac{d^2u}{dt^2} - \epsilon(1 - u^2)\frac{du}{dt} + u = B \cos(\omega t), \quad (1.23)$$

where  $B$  is the amplitude of the forcing. When  $B = 0$  a stable limit cycle oscillation is found. Different entrainment regions are found as  $B$  and  $\omega$  are varied. Although bistability was known to be present in this equation, aperiodic dynamics were also observed [115, 116]. In order to better describe the dynamics of excitability, the two-dimensional form of the van der Pol relaxation oscillator was independently modified by FitzHugh and Nagumo [57, 58]. The FitzHugh-Nagumo equations can be written as

$$\begin{aligned} \frac{dE}{dt} &= E - \frac{E^3}{3} - g + I_{stim} \\ \frac{dg}{dt} &= \epsilon(E + a - bg) \end{aligned} \quad (1.24)$$

where  $E$  is the membrane potential and  $g$  approximates a slow current (when  $\epsilon \ll 1$ ) and  $I_{stim}$  is the applied stimulus current. The computation of the nullclines (defined by  $\frac{dE}{dt} = 0$  and  $\frac{dg}{dt} = 0$ ) is helpful to give insight into the dynamics of the system. The major feature here is that one of the nullclines is a cubic function. Although this

model is unable to reproduce the *detailed* characteristics of the nerve fibre or cardiac tissue it successfully encompasses many essential characteristics of excitable tissue including threshold behaviour, a form of artificially induced bursting behaviour and the existence of absolute and relative refractory periods. A further simplification can be achieved by approximating the cubic nullcline by a piecewise linear function. One such study was carried out by Krinsky *et al.* [108]. We use a similar method in chapter 4. Although some of the detailed aspects of excitability are missing, such simplified models are very useful since this simplicity allows the use of analytical tools.

The Poincaré oscillator is another prototypical model of biological oscillations that is under intensive scrutiny [78]. This very simple two-dimensional system of ordinary differential equations is written in polar coordinates as

$$\begin{aligned}\frac{d\phi}{dt} &= 2\pi \pmod{2\pi} \\ \frac{dr}{dt} &= ar(1-r),\end{aligned}\tag{1.25}$$

where  $\phi$  is the phase of the oscillation,  $r$  the radial coordinate and  $a$  some positive real number. These equations possess a limit cycle that lies exactly on the unit circle. This limit cycle is globally attracting for all initial condition except the origin. The parameter  $a$  sets the rate at which a perturbation away from the limit cycle relaxes back to the limit cycle. In most theoretical studies, the relaxation is assumed to be instantaneous: this corresponds to the limiting case  $a \rightarrow \infty$ . In this case, the effect of a stimulus is to simply reset the phase of the oscillation. The assumption about instantaneous relaxation to the limit cycle allows analytical computation of the so-called phase transition curve. It also underlies the theoretical computation of entrainment rhythms during periodic stimulation using iterative techniques based on the response to a single stimulus of a given amplitude (phase resetting). This theoretical method will be discussed in more detail in Chapter 3. Because of their considerable success and simplicity, iterative techniques have also been considered in the development of theoretical models of AV nodal conduction and rhythms and of the propagation of electrical impulses in the heart [78, 75, 82, 184, 26].

The integrate-and-fire model of excitation is another example of significant importance. In this class of theoretical models, the activity rises towards a fixed threshold and is then reset to zero. The first studies of integrate-and-fire models go back to the late 1930's. These simple models display a rich dynamical structure.

The applications of integrate-and-fire models range from the modeling of circadian rhythms to theoretical approaches of respiration [146, 6].

In general, the prediction of experimentally observed patterns of entrainment based on iterative techniques relies on the strong assumption of instantaneous relaxation to the original limit cycle. Although many of the theoretical predictions are in good agreement with experimental evidence, the underlying assumption is unrealistic, as confirmed by numerous electrophysiological experiments. In particular, it lacks the inclusion of time-dependent effects that can play a major role in the generation and propagation of electrical impulses in excitable biological tissue. An example of such an effect is overdrive suppression which has been discussed in a previous section of this chapter. Although overdrive suppression is normally specific to cardiac tissue, other analogous time-dependent effects take place in other biological systems, *via* ionic accumulation processes or due to the slow kinetics of some transmembrane currents. Recently, there has been an increasing interest in modeling such phenomena since their influence on the dynamical behaviour is now ascertained but poorly understood. Two models of overdrive suppression in embryonic chick heart cell aggregates are presented in Chapters 4 and 5. Another issue of interest is the possible role of changes in action potential morphology (rather than the timing of successive activations) in the onset of rhythms of great complexity. Since many of the iterative techniques presently used to predict entrainment rhythms do not describe changes in action potential morphology, the development of new theoretical methods may be necessary in the future. This issue is further discussed in Chapter 6.

## 1.4 The final word

After this overview of some of the properties and dynamical behaviours of excitable systems and of their theoretical descriptions (with special reference to the heart), it is perhaps time to ask specific questions. The previous discussion of the influence of the time-dependent processes on the dynamical behaviour of excitable systems suggests many possibilities for further research. In particular, few mathematical models of excitation exist which incorporate a description of time-dependent phenomena. Since the quantitative aspect of such time-dependent phenomena may be preparation specific, the mathematical description of these effects must be based on carefully collected experimental data. In this sense, embryonic chick heart cell aggregates rep-

resent an excellent experimental preparation to carry out both the experimental and the theoretical study. Chapter 2 contains a detailed description of the experimental setup and of the experimental methods used throughout this study. A review of the present understanding of the generation of rhythms in embryonic chick heart cell aggregates is given in Chapter 3. This Chapter also contains the description of the most recent ionic model of this preparation as well as a discussion of the results that can be obtained (in the context of periodic stimulation) by applying some of the iterative nonlinear techniques briefly presented in the Introduction. A detailed study of overdrive suppression in embryonic chick heart cell aggregates, combined with a simplified theoretical model of this effect, is presented in Chapter 4. Chapter 5 examines the rhythms that arise with fixed delay stimulation (with respect to the upstroke of the action potential) of spontaneously beating chick heart cell aggregates. The dynamics are discussed and compared with the results of numerical simulations of a simplified nonlinear iterative model and of a modified ionic model which contains a simple sodium-potassium pump component. The contributions of phase resetting and overdrive suppression to the dynamics during fixed delay stimulation are emphasized and explained in terms of ionic mechanisms. Finally, in Chapter 6, I present the results of a study of the dynamics during periodic stimulation in AV nodal cell clusters, and a comparison is drawn with Chapters 3 and 4. The main goal of Chapter 6 is to illustrate the influence of changes in action potential morphology on the complexity of the dynamics and the inadequacy of theoretical methods based on the iteration of phase resetting curves to predict the experimental rhythms. Each Chapter also contains a discussion of the relevance of the results to the clinical, physiological and mathematical disciplines.

# Chapter 2

## Methodology

This chapter summarizes the materials and methods used in the experimental studies presented in the subsequent chapters. Whenever necessary, additional descriptions of the experimental procedures are also included in each chapter of this manuscript.

### 2.1 Culturing techniques

#### 2.1.1 Embryonic chick heart cell aggregates

Aggregates were prepared using techniques described previously [43, 44, 45, 75]. White Leghorn chick embryos were incubated for 7 days at 37°C and a relative humidity of 85%. They were then decapitated and their hearts were excised. Atrias and ventricles were isolated, fragmented and then dissociated into single cells in a DNase and trypsin containing medium [43]. The resulting cell suspension was filtered through a 12.0  $\mu\text{m}$  diameter pore size filter and centrifuged for 15 minutes at 170 g. The cells were resuspended and aliquoted into 25 ml Erlenmeyer flasks containing 3 ml of maintenance medium at densities of  $5 \times 10^5$  to  $7 \times 10^5$  cells per flask. The flasks were then gassed with a mixture containing 5%  $\text{CO}_2$ , 10%  $\text{O}_2$ , 85%  $\text{N}_2$ , sealed with a silicone rubber stopper and placed on a gyratory table (70 revolutions/minute and 37°C temperature) to allow the formation of spherical aggregates.

The dissociation medium contained  $5.25 \times 10^{-5}$  g/ml crystalline lyophilized trypsin (Worthington Biochemical, 245 U/mg) and  $5 \times 10^{-6}$  g/ml deoxyribonuclease I (Worthington Biochemical,  $9.1 \times 10^4$  U/mg) in a  $\text{Ca}^{2+}$  and  $\text{Mg}^{2+}$  -free, phosphate buffered, balanced salt solution with following concentrations: NaCl 116.0 mM, KCl 5.4 mM,  $\text{NaH}_2\text{PO}_4$  0.44mM,  $\text{NaHPO}_4$  0.95 mM, dextrose 5.6 mM. A pH of 7.3 was

obtained by adding either 1M HCl or 1M NaOH. The maintenance medium contained 20% medium 199 (Grand Island Biological (GIBCO)), 4% fetal bovine serum (GIBCO) and 2% horse serum (Kansas City Biological) in a bicarbonate buffered, balanced salt solution. Final concentrations were (approximately): NaCl 116.0 mM, KCl 1.3 mM, CaCl<sub>2</sub> 1.8 mM, MgSO<sub>4</sub> 0.8 mM, NaH<sub>2</sub>PO<sub>4</sub> 0.9 mM, NaHCO<sub>3</sub> 20.0 mM, MgSO<sub>4</sub> 0.8 mM, dextrose 5.5 mM. Gentamicin sulfate (Schering, Garamyacin, 10 mg/ml) was added to a final concentration of  $5 \times 10^{-5}$  g/ml. The enzyme-inactivating medium was similar to the maintenance medium except for: fetal bovine serum 0%, horse serum 10%, and KCl 4mM (approximately). All solutions were filtered with a 0.22  $\mu$ m-diameter pore size, sterile filter.

After 48 to 96 hours in culture, the aggregates were transferred to a circular (35 mm x 10 mm) plastic tissue culture dish (Corning). A thin layer of mineral oil (KLEAROL (Witco)) was poured on top of the medium to prevent evaporation. The bathing medium was gassed from above with a mixture of 5% CO<sub>2</sub>, 10% O<sub>2</sub> and 85% N<sub>2</sub>. Temperature was maintained at about  $36 \pm 1^\circ\text{C}$ . The bicarbonate buffer maintained the medium at a pH of 7.2 to 7.3. Under such conditions more than 95% of the aggregates show spontaneous rhythmic activity. Most of the aggregates studied had a diameter of about 175  $\mu$ m and contained approximately 1500 to 2000 cells.

### 2.1.2 Preparation of AV nodal cell clusters

New Zealand White rabbits (1.5-2.5 kg) were anaesthetised with an intramuscular injection containing Ketamine (75 mg/kg weight) and Xylazine (5 mg/kg weight). Heparin (300 I.U./kg, sodium salt) was injected intravenously to prevent blood coagulation. A mid-line thoracotomy was then performed and the heart was quickly removed. The aorta was cannulated to perfuse the coronary artery (Langendorff perfusion) with normal oxygenated Tyrode solution at 37°C for 2-3 minutes until the remaining blood was washed out. The perfusate was replaced with oxygenated Ca<sup>2+</sup>-free Tyrode solution for approximately 10 minutes. The perfusate was switched to Ca<sup>2+</sup>-free solution (100ml) containing 495 units/ml collagenase (Sigma Type IX) and 0.4 units/ml protease (Sigma Type XIV), which was recirculated using a peristaltic pump. The perfusion was continued for 20 to 25 minutes, after which time

the atria and atrioventricular septum were cut away from the ventricles and placed in a dissection chamber containing  $\text{Ca}^{2+}$ -free oxygenated Tyrode solution. The atrioventricular node was identified from its anatomical location [128]. A small piece of nodal tissue ( $2 \times 3 \text{ mm}^2$ ) was carefully dissected from the underlying muscle using vascular scissors. The piece of tissue was cut into fine pieces and allowed to stir in the collagenase-protease solution at  $37^\circ\text{C}$ . Elastase, 100 units/ml. (Sigma Type IV) was then added to this solution. Microaliquots were taken until single atrioventricular cells were observed. At this stage, the cells were placed into a recording chamber mounted on the stage of an inverted microscope (Zeiss Axiovert, Oberkochen, Germany) and the cells were allowed to settle on the glass base for 5 minutes. The chamber was then perfused with oxygenated  $\text{Ca}^{2+}$ -free solution for 5-10 minutes at a rate of 2 ml/min. The solution was then gradually changed to normal oxygenated Tyrode solution. Experiments were carried out at a temperatures of  $35^\circ\text{C} \pm 0.5^\circ\text{C}$ .

The normal oxygenated Tyrode solution contained (in mM): NaCl, 121.0;  $\text{NaHCO}_3$ , 15.0; KCl, 5.0;  $\text{CaCl}_2$ , 2.2;  $\text{MgCl}_2$ , 1.0;  $\text{NaH}_2\text{PO}_4$ , 1.0; glucose, 5.5 and the pH was adjusted to 7.2-7.4 by titrating with 4 M-NaOH solution. The  $\text{Ca}^{2+}$ -free Tyrode was made by replacing  $\text{CaCl}_2$  2.2 mM with  $\text{CaCl}_2$  0.15 mM.

## 2.2 Electrophysiology

A schematic view of the experimental setup is shown in Figure 2.1. Electrical activity was recorded using borosilicate microelectrodes filled with 3M KCl (typical microelectrode resistance: 40 to 60  $\text{M}\Omega$ ). The transmembrane potential was recorded using an amplifier with negative capacitance compensation, to the nearest quarter of a millivolt. The bathing medium was kept at virtual ground by coupling to a current to voltage converter (10-100 mV/nA) through an agar salt bridge and a chlorided silver wire. Current pulses were injected into the aggregate *via* the same microelectrode used for recording the transmembrane potential. Currents were measured to the nearest nA. Pulses of current were generated by a microcomputer based stimulation program (Alembic Software). The duration of the current pulses was 20 msec. Voltage and injected current waveforms were monitored on a digital oscilloscope (Tektronix 5110) and recorded on an FM instrumentation recorder (Hewlett-Packard, model

3964A, 3dB frequency response at 3 ips for DC to 1250 Hz) at a tape speed of 3.75 ips for subsequent offline analysis.

## 2.3 Data Analysis

Offline analysis was carried out on the digital oscilloscope and by an automated computer system. Magnetic tapes were played back at 15 ips, and the voltage waveform was sampled at 1 KHz by an IBM compatible 386 computer through an A/D interface (Omega). Interbeat intervals were calculated from the digitized waveform by a pattern recognition program (Alembic Software, Montreal, Canada). Computer programs were written (FORTRAN) to carry out further analysis of the interbeat intervals. Figures of experimental traces were printed on a laser printer (HP Laserjet III and IV) through graphing packages (Grapher, CorelDraw).

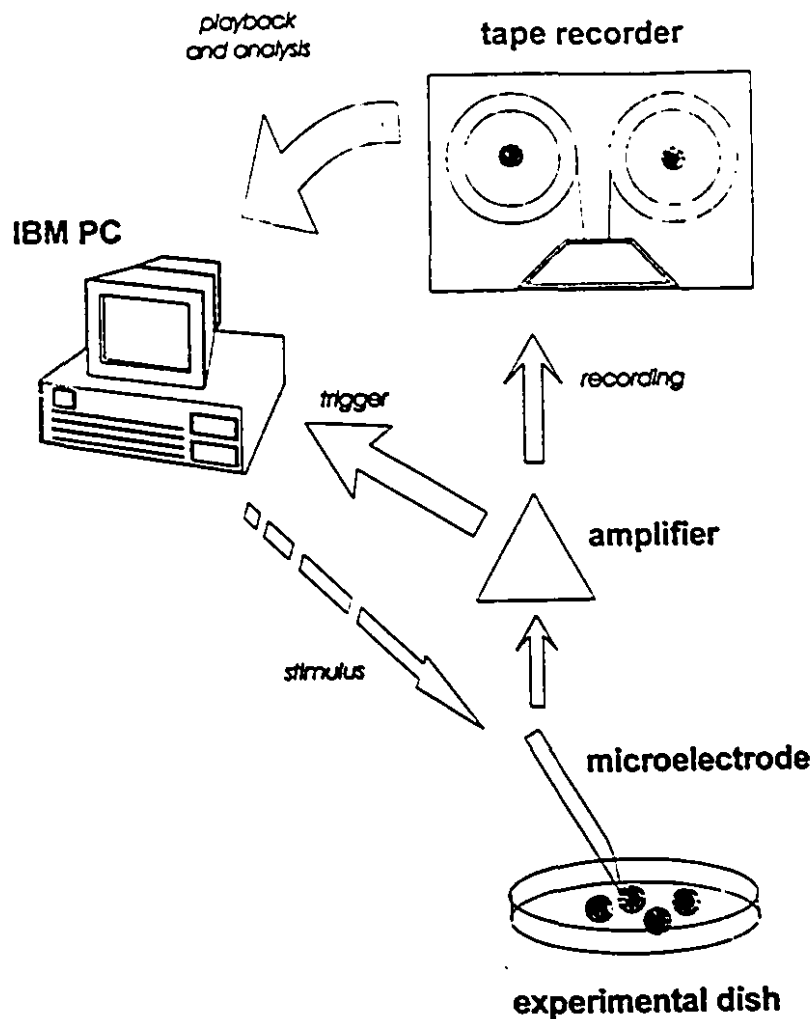


Figure 2.1: Schematic view of experimental setup. Aggregates in the experimental dish are impaled using a micromanipulator (Leitz, Germany), with a glass microelectrode filled with 3 mM KCl. This microelectrode is used to both measure the transmembrane potential and electrically stimulate the preparation. The electrical signal is stored on magnetic tape for subsequent off-line analysis and may also be used to provide a trigger for stimulation during phase resetting or fixed delay protocols. The parameters of the experimental protocols are remotely controlled by a stimulator program (Alembic Software, Montreal, Canada) on a 386 PC computer.

## Chapter 3

# Ionic mechanisms and nonlinear dynamics of chick heart cell aggregates

### 3.1 Foreword

The naturally occurring rhythm of biological oscillators can be altered by the application of single or periodic stimuli [144, 141, 181, 70]. A single stimulus generally alters the timing of subsequent beats thereby resetting the phase of the rhythm while producing only transient effects upon the intrinsic rhythmicity of the oscillator. Periodic stimuli can have more profound effects, including a variety of regular and irregular rhythms. Experimental studies concerning the effects of single and periodic stimuli have been carried out in many different preparations, including the effects of light stimuli on endogenous circadian rhythms [148]; the effects of afferent input on respiratory rhythmogenesis [28, 145, 142]; and the effects of electrical stimulation in the heart, where this approach has been used to investigate the origins of complex cardiac arrhythmias [152, 171, 94]. A remarkable aspect of this body of work is that important qualitative similarities exist between the dynamics in all of these systems despite the broad differences in the physiological preparations studied and the stimuli employed.

Over the past decade our group has been exploring cardiac dynamics using an experimental model system, the chick heart cell aggregate. This preparation has proven to be very useful for such studies, more so than single, isolated cells (see below), because it is a relatively stable oscillator with a spontaneous period of oscillation that is sufficiently short to allow extensive, systematic analyses over a time

span of hours. Consequently, we have been able to investigate delicate regions of phase resetting and the evolution of complex rhythms to an extent not previously possible. The main experimental findings concerning the effects of brief duration current pulses have also been observed in many other preparations. Thus, this system may serve as a paradigmatic preparation concerning the effects of single and periodic stimulation on the timing of spontaneous oscillators. Since the heart cell aggregate is well space clamped, it is suitable for voltage clamp analysis of the ionic currents underlying spontaneous activity [29, 125]. We have conducted such studies to determine the main current components in this system and have evaluated their role in pacemaker activity and repolarization [159, 19]. This information can be used to elucidate the ion current mechanisms underlying specific aspects of dynamic behavior such as the response of the system to a single current pulse [32, 35, 161]. This approach, which is similar to that originally used by Hodgkin and Huxley [90] for the squid giant axon and by McAllister, et al., [122] and DiFrancesco and Noble [48] for cardiac preparations, has the considerable advantage that the dynamics generated by the model can be firmly tied down to specific ionic mechanisms, thereby facilitating the examination of critical, practical questions such as the role of drugs that block certain channels, the effects of changes in the ionic composition of the bathing medium, or the effects of electrical perturbation. However, ionic models tend to be complex, which makes general principles governing the dynamics of these systems difficult to formulate. An alternative approach involves nonlinear mathematics, that is, the analysis of the changes in the qualitative properties of the solutions of generalized, finite difference equations with applied stimuli, or perturbations [181, 70]. The form of the equations used can be relatively simple and need only describe the response of the system to perturbations without reference to specific mechanisms. The resulting analysis can provide a mathematical description of the dynamics of any given system, including rhythms associated with chaotic dynamics, but offers no information concerning ionic mechanisms.

In this chapter we summarize research that integrates these two complementary approaches for the analysis of biological dynamics, focusing mainly on research from our group concerning the effects of current pulse perturbations on spontaneously beating, embryonic chick heart cell aggregates.

## 3.2 Rationale for using embryonic chick heart cell aggregates rather than single cells

At this point most cardiac electrophysiologists may well be wondering why we have used aggregates in this study, or more correctly, re-aggregates, rather than single cells, especially since we obtain a single cell suspension during our tissue culture preparation, as noted above. The main reason is that aggregates appear to be superior models for the intact embryonic heart compared to single, isolated embryonic chick cardiac cells. For example, the threshold for the action potential in single cells is typically -40 to -20 mV, rather than -60 mV found in intact myocardial tissue, and the maximum diastolic potential, MDP, is typically -70 rather than -90 mV [34]. Other investigators, in particular the Emory group, have reported similar action potential waveforms from single cells [55, 127]. Moreover, single cells usually beat irregularly, at best, which means they do not provide a stable model for a cardiac oscillator [30]. The reason for the discrepancy in MDP appears to be that single cells lack the  $I_{K_r}$  repolarization current described below. Paradoxically, the absence of  $I_{K_r}$ , which is an outward current component, may also explain the relative lack of autonomous activity in single cells, because this current repolarizes the membrane potential to -90 mV, i.e., well below threshold, which removes inactivation of inward currents, most notably  $I_{Na}$ . In the absence of  $I_{K_r}$  these preparations tend to rest at potentials where inward currents are inactivated. We do not at present understand the reasons underlying the differences in ion currents between single cells and aggregates. Our strategy has been to continue to use aggregate preparations because they have properties which more accurately reflect those of the intact heart, and because they are good model oscillators.

## 3.3 Experimental observations

### 3.3.1 Phase resetting

An example of phase resetting is shown in Fig. 3.1. This figure also illustrates the terminology used throughout this study. The control cycle length, that is, the interbeat interval ( $T_0$ ), was determined for each preparation from the average of ten

successive beats. The effects of single pulses on the subsequent timing of action potentials was determined as a function of the phase  $\phi = t_s/T_0$  of the stimulus. The cycle was scanned with a single stimulus delivered each 10 spontaneous beats incrementing the value of  $t_s$  in 5 msec steps. The perturbed cycle length,  $T(\phi)$ , is the time from the upstroke of the action potential (AP) before the stimulus to the upstroke of the AP after the stimulus. The plot of the normalized perturbed cycle length  $PRC(\phi) = T(\phi)/T_0$  as a function  $\phi$  is the phase response curve (PRC).

The example of phase resetting in Fig. 3.1 corresponds to a 40 nA current pulse 20 msec in duration which was applied close to the time of occurrence of maximum diastolic potential in the control cycle. The pulse produced approximately a 40% prolongation of the time of occurrence of the subsequent action potential without significant effect on the subsequent spontaneous activity. In other words, the electrical activity several beats after the current pulse is indistinguishable from the activity prior to the pulse, except that the phase of the activity has been shifted or reset. Further examples of phase resetting are illustrated in Fig. 3.2. Each column in Fig. 3.2 consists of a control record (top trace) and four records below each control which demonstrate the effects of different current pulse amplitudes on phase resetting at various different points in the unperturbed cycle. The lowest current amplitude (8 nA) produced a modest effect on the timing of the subsequent beat, primarily a phase advance, especially as the time of the pulse relative to MDP of the previous action potential was increased. The transition from little effect of this pulse amplitude on phase resetting (top record underneath the control in the 8 nA panel) to a clearly observable phase advance (second and third records in this panel) was a continuous, gradual function of the time in the unperturbed cycle at which the current pulse was applied. Larger current pulses (16 and 32 nA) produced a significant phase delay when the pulse was applied close to the time of occurrence of MDP. The maximal phase delay with 32 nA pulse was approximately 35%. These larger pulses also produced a more marked phase advance at later times in the unperturbed cycle compared to the 8 nA pulses. Moreover the transition from phase delay to phase advance become increasingly more abrupt as the current amplitude was increased, so much so that it appeared to be discontinuous function of time of application of the pulse for 48 nA. Further results of this nature are given in references [75, 35].

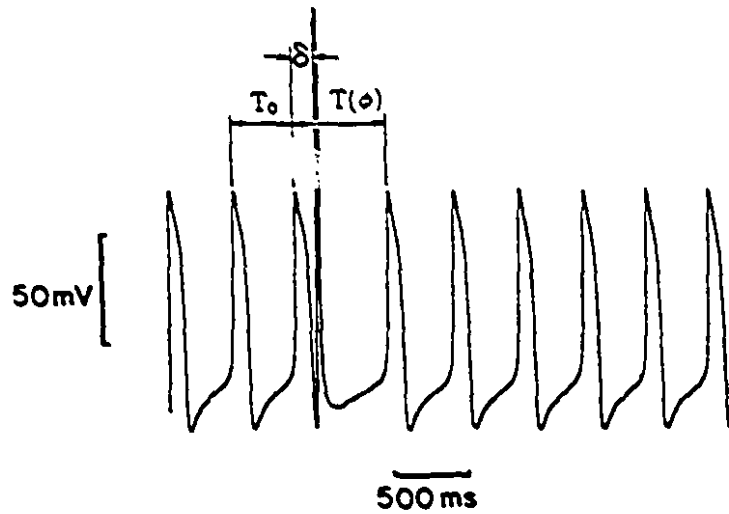


Figure 3.1: Phase resetting of the rhythmic, spontaneous activity of an embryonic chick heart cell aggregate. This experiment illustrates a phase delay induced by a 40 nA current pulse 20 msec in duration (same duration used for all results in this study) applied close to the time of occurrence of maximum diastolic potential (MDP). The terminology used throughout this review is also illustrated here. The control, unperturbed cycle length is  $T_0$ ; the time of pulse injection relative to the preceding action potential is  $t_s$ ; and the perturbed cycle length induced by the current pulse is  $T(\phi) = T_0 PRC(\phi)$ , where  $\phi = t_s/T_0$ . From Reference [34].

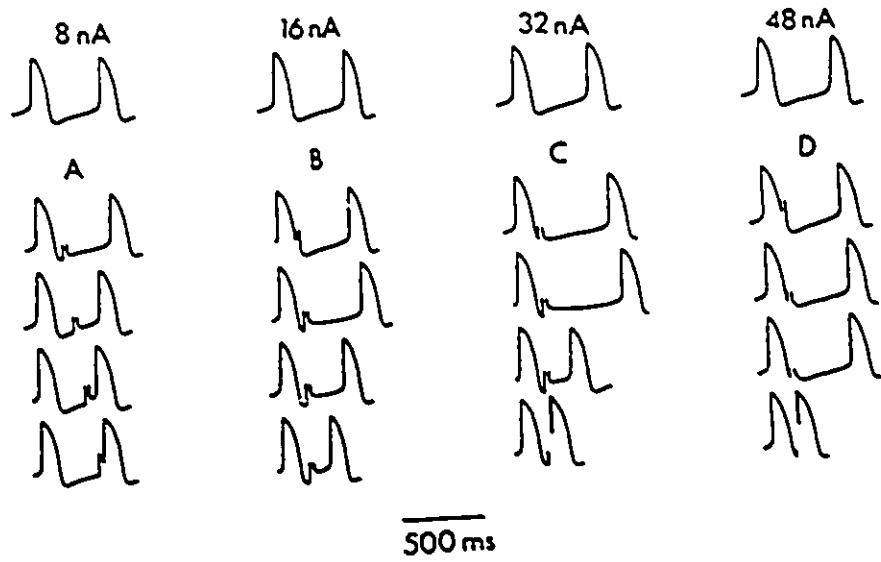


Figure 3.2: Phase resetting for current pulses having amplitudes ( $i_{pulse}$ ) of 8, 16, 32, and 48 nA for panels A, B, C and D, respectively. The pulses were applied at the times indicated by the stimulus artifacts. The record at the top of each panel is the control cycle.

### 3.3.2 Phase locking

The heart cell aggregates in this study were also stimulated with periodic trains of action potentials of the same amplitudes ( $i_{pulse}$ ) as used in the phase resetting experiments. The cycle length,  $T_s$ , of the stimulus train was varied between  $0.3 T_0$  and  $1.8 T_0$ . The stimulus trains consisted of 50-100 stimuli so that the length of each of these runs was typically between 10 seconds and 2 minutes ( $T_0$  was between 300 msec and 700 msec) with a rest interval of 30 to 45 seconds between each run.

These preparations can be locked to the frequency of periodic current pulses provided that the stimulation frequency does not differ too much from the intrinsic frequency [95, 75, 67, 80], a result which is referred to as 1:1 entrainment. An example of 1:1 entrainment with various cycle lengths is illustrated in Fig. 3.3. The control  $T_0$  for this preparation was 640 msec (Fig. 3.3A). A 1:1 entrainment pattern was observed for cycle lengths greater than the intrinsic  $T_0$  with 48 nA current pulses, as illustrated in Fig. 3.3B for  $T_s = 850$  msec. The pulses intrinsically locked at times shortly after MDP of each AP, which is where maximum prolongation occurred. Fig. 3.3B illustrates approximately the greatest degree of slowing of the beat rate which we were able to achieve. A 1:1 pattern was also observed with  $T_s \approx T_0$ , as illustrated in Fig. 3.3C with  $T_s = 690$  msec. Similarly, 1:1 patterns were obtained with  $T_s$  considerably less than  $T_0$ , as illustrated in Fig. 3.3D for  $T_s = 440$  msec.

Patterns more complex than 1:1 entrainment occur when the stimulation frequency differs sufficiently from the intrinsic frequency. The periodic rhythms that are observed under these conditions are usually classified by the ratio N:M where N is the number of imposed stimuli and M the number of cycles in a repeating sequence. For stimulation frequencies sufficiently greater than the intrinsic frequency N:M rhythms occur with  $N > M$ , as shown in Fig. 3.4. For example the third panel in Fig. 3.4 illustrates a 5:4 rhythm, that is, the preparation essentially skipped a beat every fifth pulse when  $T_s$  was set as 200 msec. During the establishment of these rhythms a transient phase often occurs in which an evolution of rhythms takes place before a stable rhythm is established [186]. The stable rhythms shown in Fig. 3.4, represent N:M patterns observed after all transients had disappeared.

With stimulation frequencies sufficiently less than the intrinsic frequency N:M rhythms occur with  $N < M$ . The results were obtained from the same preparation as in Fig. 3.4. The 1:2 entrainment result in Fig. 3.5 and the control above this trace

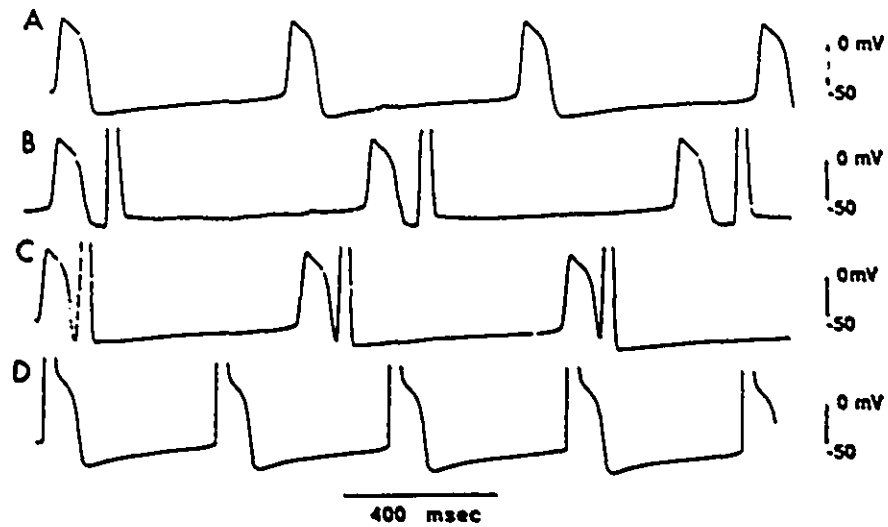


Figure 3.3: Phase locking (1:1 entrainment) with  $i_{pulse} = 48$  nA. A. Control spontaneous activity ( $T_0 = 640$  msec). B. Entrainment in a 1:1 pattern with  $T_s$ , the cycle length of the pulses, significantly greater than  $T_0$  ( $T_s = 850$  msec). C-D. Entrainment with  $T_s = 690$  and  $440$  msec respectively. Times of current pulse application in B-D are indicated by the stimulus artifacts.

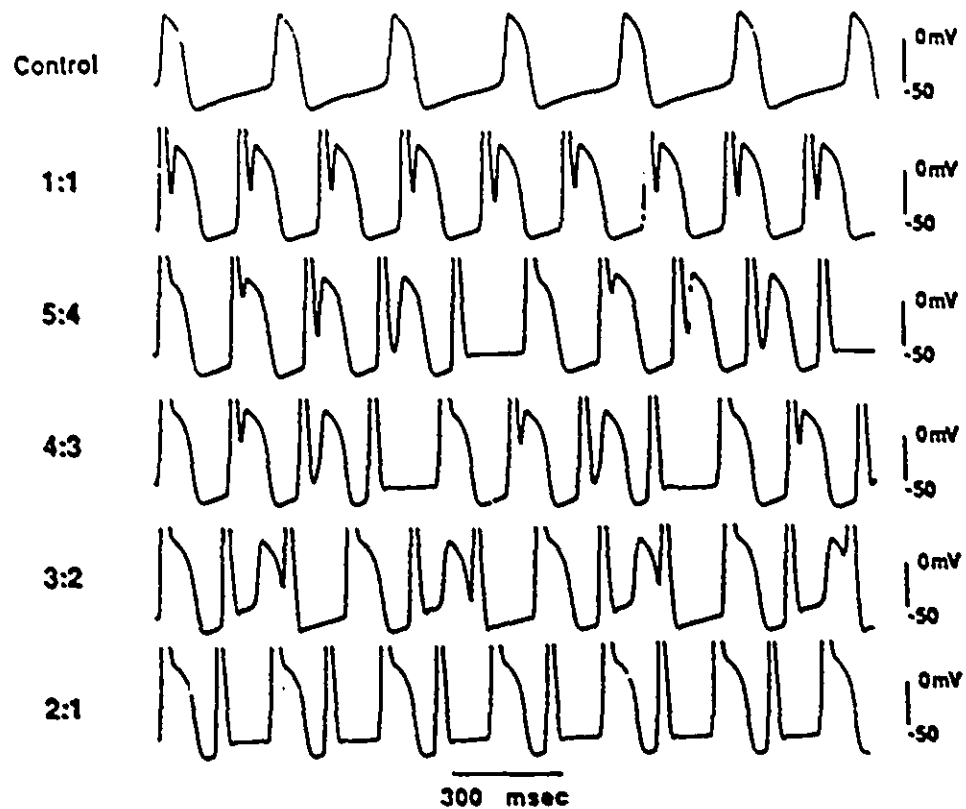


Figure 3.4: Experimentally observed rhythms intermediate to 1:1 and 2:1 phase locking. Top panel illustrates control spontaneous activity from a preparation different from that illustrated in Fig. 1 ( $T_0 = 300$  msec). Shown below the control trace are 1:1, 5:4, 4:3, 3:2, and 2:1 phase locking for  $i_{pulse} = 25$  nA, and  $T_s = 220, 200, 190, 180,$  and  $160$  msec, respectively. From Reference [34].

were obtained from a different aggregate. In addition to N:M patterns, aperiodic rhythms are occasionally observed in heart cell aggregates, particularly in transition from one regular rhythm to another [75]. We defer a discussion of these results to section 3.5.

## 3.4 Theoretical results based on a model of ion currents

### 3.4.1 Ionic model

Our model of ion currents in embryonic chick atrial heart cell aggregates is a revised version of the Shrier and Clay ionic model such as previously described [159, 35]. The parameters of the model are given in detail in Table 3.1. The model consists of 5 components based on voltage clamp results from our group and from others: namely  $I_{Na}$ , the fast inward sodium ion current which underlies the rapid upstroke phase of the action potential;  $I_{Ca}$ , the calcium ion current which underlies the latter part of the upstroke and which is also primarily responsible for maintaining membrane depolarization during the plateau phase of the action potential;  $I_{K_s}$  (referred to as  $I_{x2}$  in reference [159]), the primary time dependent outward current which initiates repolarization as  $I_{Ca}$  is inactivated during the plateau;  $I_{K_r}$  (referred to as  $I_{x1}$  in reference [159]), the primary time dependent outward current underlying the fastest phase of repolarization; and  $I_b$ , the background current, which appears to consist of three subcomponents;  $I_{b1}$ , a net inward, time independent current (the pacemaker component) which depolarizes the membrane potential to threshold of  $I_{Na}$ , and two components which inwardly rectify, termed  $I_{b2}$  and  $I_{b3}$  [35]. These preparations do have the classical pacemaker current,  $I_f$  [49], but only at relatively negative potentials, i.e., below -90 mV [19]. Our simulations suggest that this current is not a significant factor for pacemaking in atrial cells, whereas it is significant in ventricular heart cell aggregates [19]. The component underlying pacemaking in atrial cells is  $I_{b1}$ , a net inward, time independent current whose ion constituents are as yet, unknown. A time independent background current has recently been described in mammalian sino-atrial nodal cells [85]. In the numerical simulation, the control cycle length of the spontaneous beating was adjusted by changing the magnitude of  $I_{b1}$ .

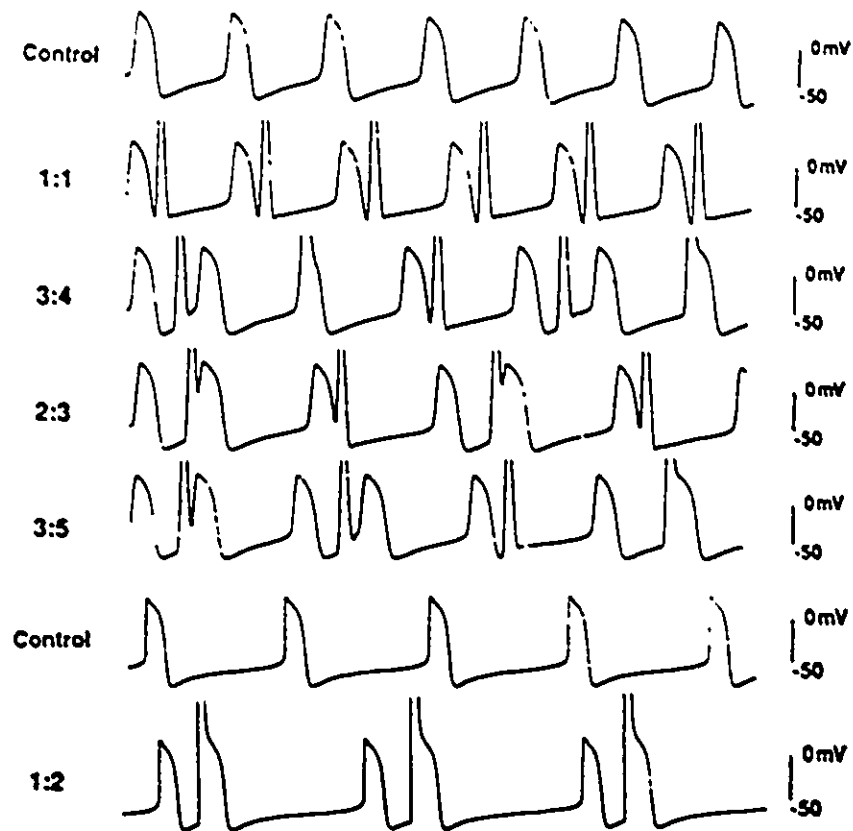


Figure 3.5: Experimentally observed rhythms intermediate to 1:1 and 1:2 phase locking. Top panel illustrates control spontaneous activity from the same preparation as in Fig. 3.4. The four traces below the control illustrate 1:1, 3:4, 2:3, and 3:5 phase locking for  $T_s = 330, 375, 430,$  and  $495$  msec, respectively, with  $i_{pulse} = 25$  nA. The bottom two panels illustrate control spontaneous activity and 1:2 phase locking from another preparation with control cycle length  $T_0 = 500$  msec. From Reference [34].

Our model of  $I_{Na}$  was taken without modification from reference [50]. Our  $I_{Ca}$  model was developed by us based on the observations of this current by [98]. This component is the  $I_{Ca,L}$  current [8]. Embryonic chick myocardial cells have little of the  $I_{Ca,T}$  calcium ion current component [110]. The  $I_{K_s}$  and  $I_{K_r}$  components of the model are based on measurements of these currents from atrial heart cell aggregates and from single atrial cells [159, 34]. The  $I_{K_s}$  component is qualitatively similar to the classical delayed rectifier potassium ion channel in nerve [33] except that the activation range is between -20 and +20 mV, as compared to -60 to 0 mV in nerve, and the kinetics of this current are substantially slower in heart than in nerve. The  $I_{K_s}$  kinetics from single cells as measured with the patch clamp technique are similar to our  $I_{K_s}$  measurements from aggregates [34]. We have observed the  $I_{K_r}$  component only in aggregates, not in single cells for reasons which have not yet been elucidated [34]. Our model of this component is based on the measurements of [159]. The  $I_{K_r}$  current might usefully be referred to as an inward rectifier with a gate. Its open channel current-voltage relation inwardly rectifies, similar to  $I_{K1}$  possibly because of "instantaneous" blockade by intracellular  $Mg^{2+}$ , which is known to be the mechanism underlying the inward rectification of  $I_{K1}$  [169]. The  $I_{K_r}$  component also has a clear time dependent gate having kinetics which are similar to those of  $I_{K_s}$  except that the maximum  $I_{K_r}$  time constant (1 sec) occurs at -35 mV, whereas the maximum time constant for  $I_{K_s}$  (also  $\approx$  1 sec) occurs at 0 mV. The  $I_{K_r}$  activation range is between -50 and -25 mV (a relatively narrow range). Moreover,  $I_{K_r}$  has an N shaped open channel current-voltage relation with a peak outward current at  $\approx$  -65 mV and with a current reversal at  $E_K$ , the potassium ion equilibrium potential. However, the channel is essentially closed in the steady state for -40 mV, because the gate is closed. It also passes little current for  $V > 0$ , because of inward rectification of the open channel. Consequently,  $I_{K_r}$  contributes very little to the steady state current voltage relation. This component is primarily a transient current which can, nevertheless, contribute significantly during the action potential, as described below.

The other feature of the model which is particularly worthy of note is the mechanism of inactivation of  $I_{Ca,L}$ . This component does inactivate with membrane potential, i.e., the classical mechanism of inactivation. However, it inactivates during the action potential primarily because of the inward, calcium ion current dependent mechanism of inactivation reported originally [102, 113]. Our model of  $I_{Ca,L}$  was designed with these results in mind, in particular the "crossover" effect reported by

[113], which we have also observed in embryonic chick myocardial cells (A. Kristof et al., unpublished observations). That is, an increase of  $\text{Ca}_0^{2+}$  from 1.8 to 5 mM produces a significant increase in inward  $I_{Ca}$  elicited by a voltage clamp step to 0 mV. It also produces a significant increase in the rate of inactivation of  $I_{Ca}$ , so much so that the records in 1.8 and 5 mM  $\text{Ca}_0^{2+}$  “crossover” when superimposed. Our model mimics this effect. To the best of our knowledge, it is the only cardiac membrane model which does so. This inactivation process is especially significant in elucidating electrical activity which we have observed with sub-maximal doses of tetrodotoxin (TTX). For example,  $5 \times 10^{-8}\text{M}$  TTX does not abolish spontaneous activity in these preparations, but it does substantially reduce the upstroke velocity (i.e.,  $\dot{V}_{Max}$ ) so much so that the upstroke phase is almost completely attributable to  $I_{Ca}$  [161]. Consequently the  $I_{Ca}$  amplitude during the upstroke is actually a good deal larger than in control, simply because the upstroke phase is slower, thereby allowing more time for activation of this current to take place. Paradoxically, the action potential duration under these conditions is reduced, which would appear to contradict conventional reasoning concerning the effects of an increase in  $I_{Ca}$ . To our surprise, our model mimicked this effect because the increase in  $I_{Ca}$  also caused a marked increase in the calcium ion current dependent inactivation process which reduced the duration of action potential relative to control [161]. In other words, this result provides a physiological correlate to the “crossover” effect of [113].

### 3.4.2 Control electrophysiological results

An action potential predicted by the ionic model is shown in the top panel of Fig. 3.6 with the underlying ion currents illustrated below this waveform. The respective roles of  $I_{K_s}$  and  $I_{K_r}$  are, once again, worthy of comment. The  $I_{K_s}$  component along with  $I_{b2}$  and  $I_{b3}$  provide the mechanism of repolarization during the plateau. However, these components are sufficient to repolarize the membrane potential only to about -50 mV, as illustrated by the simulation in Fig. 17C of Reference [159] in which the  $I_{K_r}$  component was deleted from the ionic model. The  $I_{K_r}$  component underlies repolarization between -90 and -50 mV. This channel is opened relatively rapidly during the plateau phase of the action potential, but it does not contribute to repolarization during this phase because of its inward rectification. As the membrane repolarizes from the plateau, the instantaneous N-shaped current voltage relation of

$I_{Kr}$  comes in to play. At the foot of the action potential, i.e., MDP, and during the first 100 msec or so after MDP, the  $I_{Kr}$  channels close, thereby allowing  $I_{b1}$  to depolarize the membrane to threshold of  $I_{Na}$ .

A comparison of the ionic model with control electrical activity is shown in Fig. 3.7. The model compares favorably with experiment, even to the extent that the action potential of the model is essentially the same as the experimental action potential waveform, except that the plateau phase is slightly more rectangular in the model as compared to experiment (see Fig. 2 in Reference [35]).

### 3.4.3 Phase resetting

Examples of phase resetting from the ionic model are illustrated in Fig. 3.8 for conditions which correspond to the experimental results in Fig. 3.2. The ionic model closely mimics these results including the apparent discontinuity in timing of a phase advance and phase delay with large current pulses. These effects are further amplified by the phase resetting curves in Fig. 3.9 from an experimental preparation (left hand panel) and from the model (right hand panel). The arrows in the bottom three results in the left hand panel (experiment) and in the bottom right hand panel (model) illustrate the apparent discontinuity in phase resetting as a function of the time of pulse application in the unperturbed cardiac cycle which occurs for relatively large pulse amplitudes. This result, which is beyond the scope of this review, is discussed in considerable detail in Reference [35].

The ionic mechanism of phase resetting is primarily attributable to the  $I_{Kr}$  and  $I_{Na}$  components, as illustrated in Fig. 3.10 in which a 40 nA pulse was used close to the transition between a phase advance and phase delay in the PRC. The respective time courses of  $I_{Kr}$  and of  $I_{Na}$  are shown below the voltage wave forms in each example. The dashed lines illustrate the behavior of these currents in control, results which are also shown in Fig. 3.6. The effect of a current pulse on  $I_{Kr}$  in the model applied shortly after the time of occurrence of the MDP is to effectively increase the amplitude of this component. The important point here is that a significant fraction of  $I_{Kr}$  channels remain open for 100-150 msec following MDP. The effect of a relatively large depolarizing current pulse in this phase of the unperturbed cycle is to quickly move the membrane potential away from  $E_K$ , thereby increasing the driving force for the residual  $I_{Kr}$  channels. (The inward rectification of  $I_{Kr}$  discussed

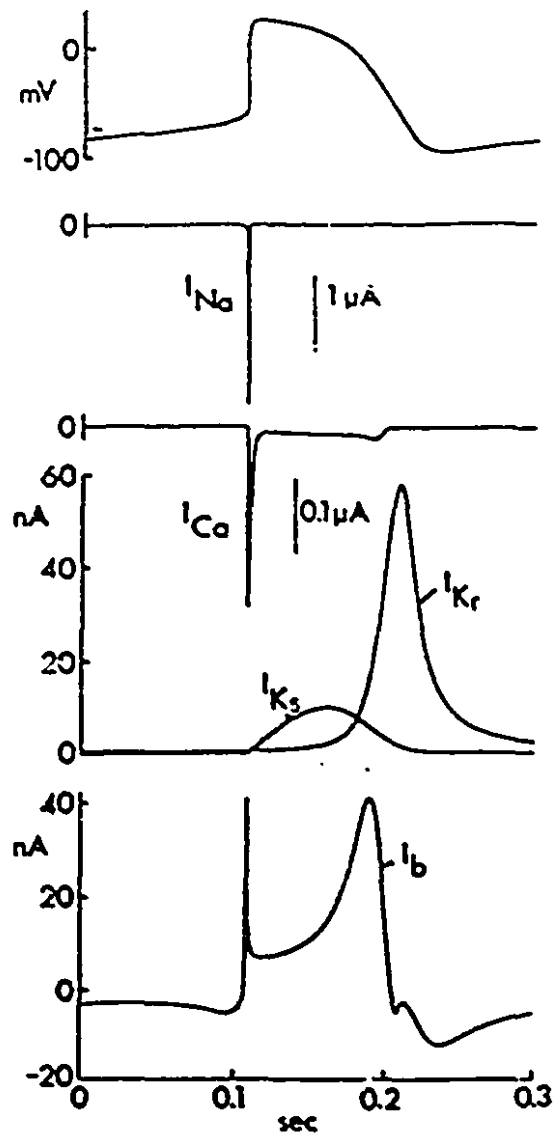


Figure 3.6: Ion currents underlying the action potential and pacemaker activity in the Shrier and Clay model, as described in the text. From Reference [34].

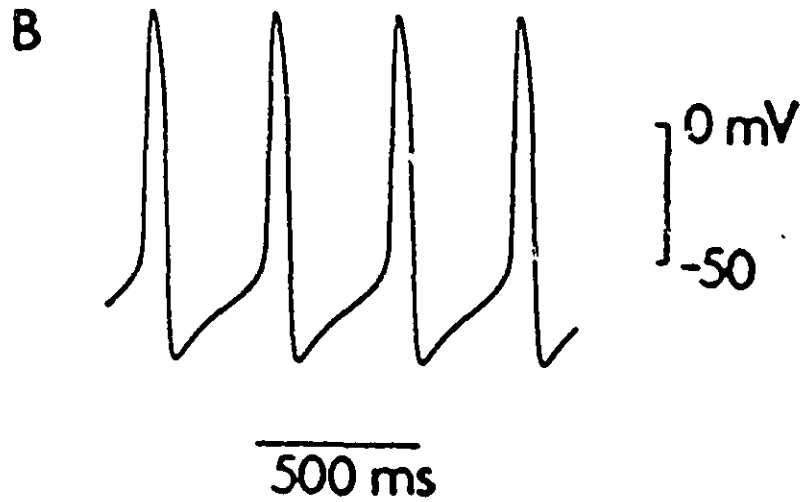
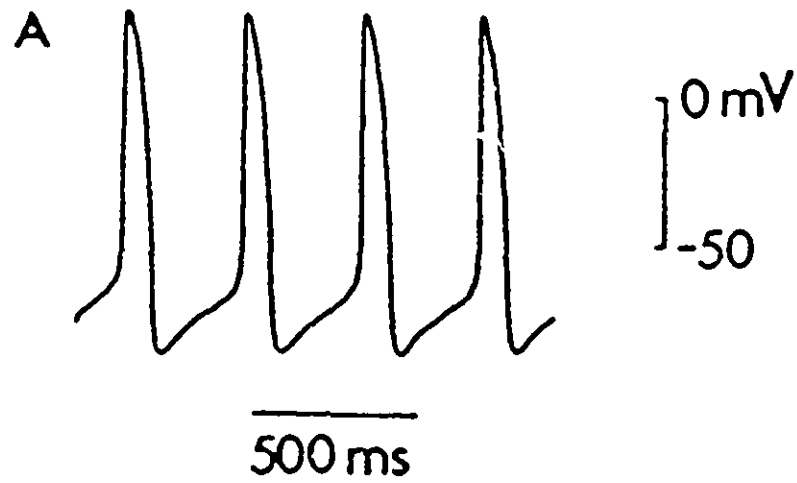


Figure 3.7: A. Experimentally observed waveform in control conditions. B. Predictions of the Shrier and Clay model. We note here that the amplitude of the  $I_{b1}$  component of the model has been adjusted throughout this study so that the model closely matches the various control interbeat intervals ( $T_0$ ) observed experimentally.

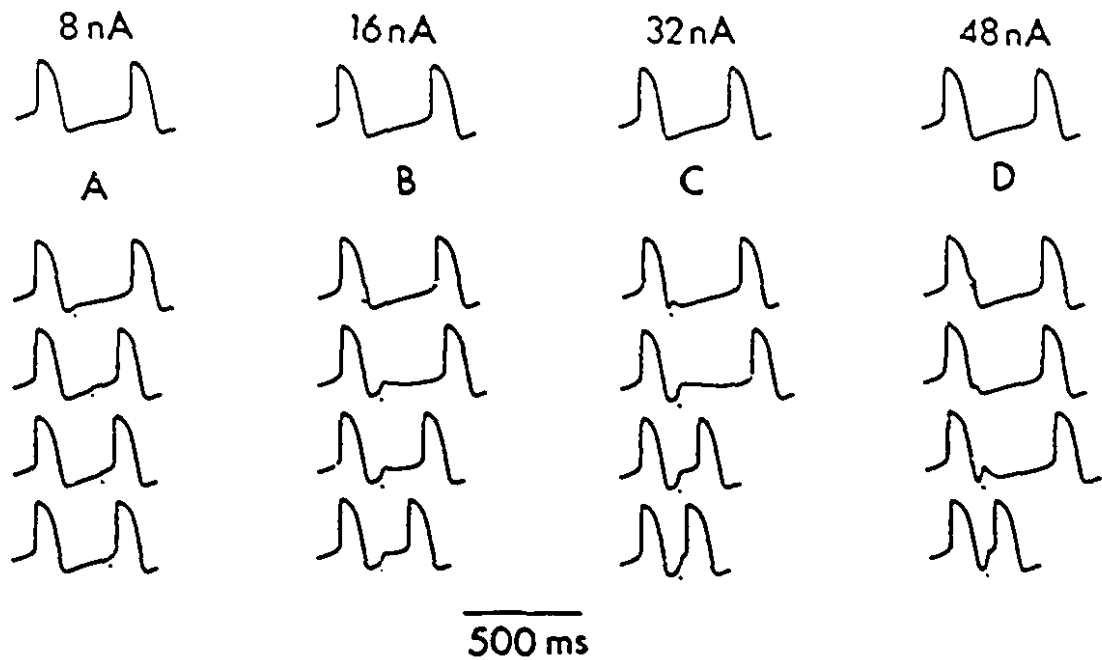


Figure 3.8: Phase resetting of the model for conditions similar to those shown for the experimental result in Fig. 3.2. The horizontal bars under each each record in panels A through D represents the time at which the pulse was applied in the model. A similar representation is used for the timing of current pulses in subsequent simulations. The current pulse amplitudes in the model here and in subsequent simulations were, in general, the same as the current pulse amplitudes used experimentally with appropriate scaling for the size of the aggregate. That is, the model was designed for a  $200\ \mu\text{m}$  diameter aggregate [34]. The current pulse used in the model to simulate a result from a different size aggregate (usually smaller) was scaled according the cube of the diameter [29]. However, this procedure was not always followed. In some instances a current pulse amplitude was used which gave the best agreement between theory and experiment for a particular phase resetting curve of the preparation in question. The relative current pulse amplitudes used to simulate other PRC's from that preparation were then scaled according to the experimental amplitudes. From Reference [34].

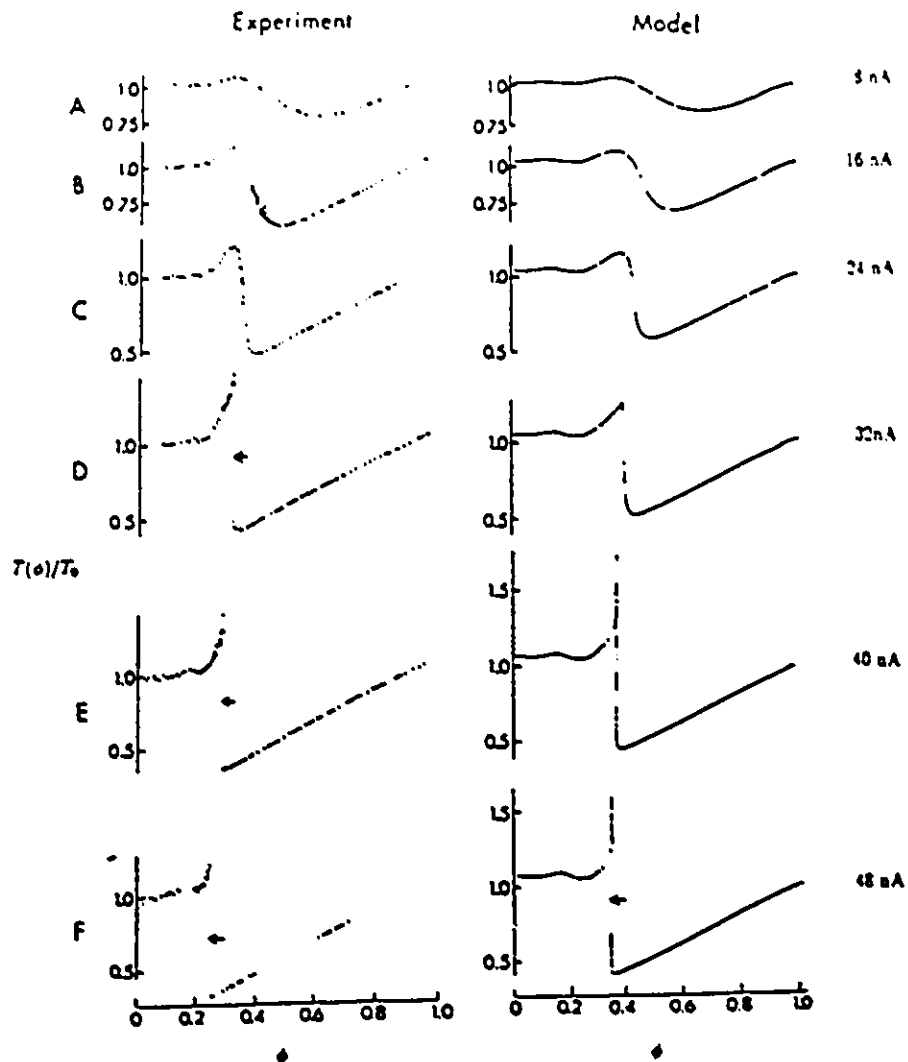


Figure 3.9: Phase resetting curves (PRC's) for current pulse amplitudes given in the far right margin. Experimental results are illustrated in the left panel. The corresponding results from the model are illustrated in the right hand panel. The vertical axes ( $PRC(\phi)$ ) represent the perturbed cycle length,  $T(\phi)$ , normalized relative to the unperturbed cycle length,  $T_0$ . These terms are defined in Fig. 3.1. The horizontal axes represent the phase in the cycle,  $\phi$ , at which the pulse was delivered. The arrows indicate apparent discontinuities in the PRC's, an issue which is discussed in detail in Reference [34].

above does not come into play for potentials below threshold, i.e.,  $V = -60$  mV). Moreover, the  $I_{K_r}$  time constant is significantly greater at  $-60$  mV (250 msec), as compared to  $-90$  mV (50 msec), so that the residual  $I_{K_r}$  channels deactivate slower than in control. The current pulse also produces premature activation of  $I_{Na}$ , but this effect is overcome by the increase of  $I_{K_r}$ , which leads to a significant phase delay. However, the interplay between  $I_{Na}$  and  $I_{K_r}$  during, and at the end of relatively large amplitude current pulses, such as 40 nA, is so delicate that when these pulses are applied 1 msec later, a significant phase advance occurs in the model as shown in the right hand panel. The slightly later time of pulse application permits a slightly greater deactivation of  $I_{K_r}$  to take place. Consequently, the current pulse depolarizes the membrane potential ever so slightly closer to threshold of  $I_{Na}$  than in the left hand panel. The combination of a reduction in amplitude of  $I_{K_r}$  and an increase in  $I_{Na}$  allows the premature activation of  $I_{Na}$  to dominate in this instance and when the current pulse is applied at later times in the unperturbed cycle. In other words, the abrupt transition between phase delay and phase advance illustrated in Fig. 3.10 is, in essence, a threshold phenomenon, which is known to be a steep function of pulse parameters [56].

#### 3.4.4 Phase locking

The simulations generated by the ionic model corresponding to the experimental results in Figs. 3.3-3.5 are shown, respectively, in Figs. 3.11-3.13. Fig. 3.11 illustrates the simulated electrical activity for 1:1 entrainment. A 1:1 rhythm with  $T_s > T_0$  could be obtained for  $T_s$  up to 30% greater than  $T_0$  (Fig. 3.11B). Phase locking with a 1:1 rhythm is also shown in Fig. 3.11C and Fig. 3.11D, for  $T_s \approx T_0$  and  $T_s < T_0$ , respectively. More complicated entrainment patterns occur in the model, as in the experimental preparation, when the stimulation frequency differs sufficiently from the intrinsic rhythm. These results are shown in Figs. 3.12 and 3.13. The details of the simulation protocols are given in the respective figure legends. The phase locking behavior of the ionic model is fundamentally the same as that of the aggregate preparation. This observation applies both to the qualitative appearance of the various N:M rhythms and to the general ranges of stimulation. The close approximation of theory to experiment is further shown in Fig. 3.14, which illustrates the transition from 2:1 to 1:2 entrainment in the form of a "devil's staircase" in which the N:M

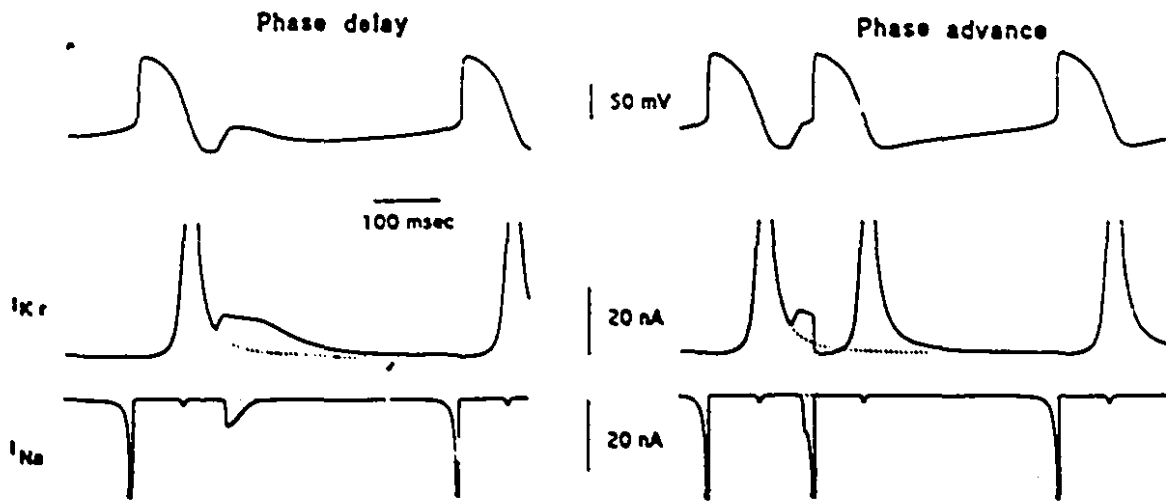


Figure 3.10: Ionic mechanisms of phase delay and advance in the Shrier and Clay model, as described in the text. A 40 nA current pulse was applied in the model shortly after MDP, as indicated in the voltage waveform in each panel. The time of the pulse in the right hand panel was 1 msec later than in the left hand panel.  $I_{Kr}$  and  $I_{Na}$  components are shown below the voltage waveform in each panel. The dashed lines illustrate the behavior of these components in the absence of a current pulse.

rhythms are plotted as a function of the period of the stimulation.

The ionic mechanism of entrainment follows closely from the analysis of phase resetting given above. Phase locking in a 1:1 entrainment rhythm with  $T_s < T_0$  is attributable to premature activation of  $I_{Na}$ . The result in Fig. 3.11B in which 1:1 entrainment occurs with  $T_s > T_0$  is attributable to the properties of  $I_{Kr}$ , as described above in the analysis of phase delays. As noted above, the interplay between  $I_{Kr}$  and  $I_{Na}$  leading to a phase delay is a rather delicate phenomenon, whereas premature activation of  $I_{Na}$  is relatively robust. Consequently, the latter result, that is 1:1 entrainment with  $T_s < T_0$ , occurs over a broader range of stimulus parameters than does 1:1 entrainment with  $T_s > T_0$ .

Entrainment patterns more complicated than 1:1 occur when the timing and amplitude of the current pulses relative to the unperturbed interbeat interval is such that neither premature activation of  $I_{Na}$  nor resetting of  $I_{Kr}$  dominates after each pulse. This result is illustrated for 5:4 entrainment in Fig. 3.15. For the sake of clarity, the vertical axes in the bottom two panels of Fig. 3.15 have been amplified to illustrate the behavior of the underlying  $I_{Na}$  and  $I_{Kr}$  components. The arrow labeled a in the middle panel of Fig. 3.15 points out the increase of  $I_{Kr}$  described above, which occurs during and immediately after the first current pulse in this simulation as the membrane potential is depolarized away from  $E_K$ . The  $I_{Na}$  component is also increased (as noted above and by the arrow labeled a in the bottom panel of Fig. 3.15), because the membrane potential is depolarized close to threshold of this current near the end of the current pulse. In this particular instance, the effect of the pulse on  $I_{Na}$  is the dominant factor, resulting, subsequently in an action potential. (The small "blips" of  $I_{Na}$ , arrows labeled f in the bottom panel, represent the slight reactivation of  $I_{Na}$  which occurs during repolarization of the AP. This effect is also shown in Fig. 3.10). The  $I_{Kr}$  component is rapidly diminished to  $\approx 0$  during the upstroke phase of the action potential, because of the marked inward rectification of this component, as described above. The  $I_{Kr}$  amplitude once again increases during repolarization, an effect which was also described above. The timing of the next pulse in the current pulse sequence is such that it occurs slightly earlier relative to MDP than the previous pulse. Consequently, the effect of this pulse on  $I_{Kr}$  (arrow b in the middle panel of Fig. 3.15) is slightly greater than with the previous pulse, because  $I_{Kr}$  has had less time to deactivate. However, the  $I_{Na}$  component still dominates (arrow b in bottom panel of Fig. 3.15), as it does in the succeeding pulse (arrow c

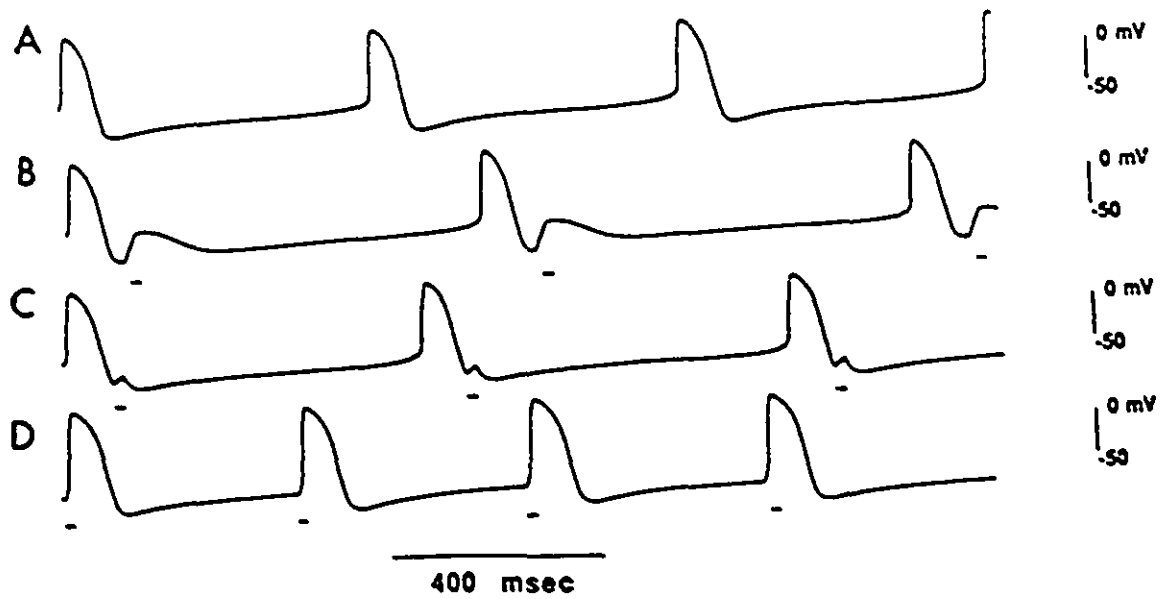


Figure 3.11: Phase locking of the Shrier and Clay model in 1:1 patterns. A. Spontaneous activity in the model with  $I_{b1}$  adjusted to give  $T_0 = 600$  msec. B-D. Entrainment in 1:1 patterns with  $T_s = 800, 680$  and  $400$  msec, respectively. These results are to be compared with the experimental results in Fig. 3.3.

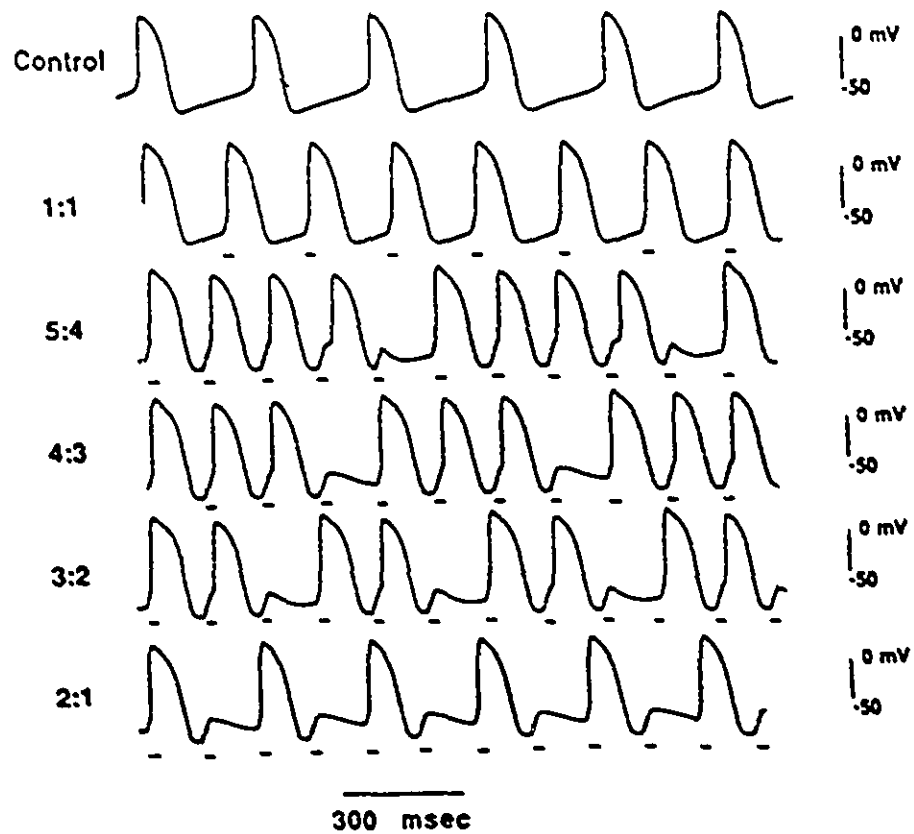


Figure 3.12: Rhythms intermediate to 1:1 and 2:1 phase locking in the Shrier and Clay model. The  $I_{b1}$  parameter was adjusted so that  $T_0 = 300$  msec. These results were obtained with  $i_{pulse} = 25$  nA and  $T_s = 200, 184, 178, 160$  and  $150$  msec, respectively. These results are to be compared with the corresponding experimental results in Fig. 3.4.

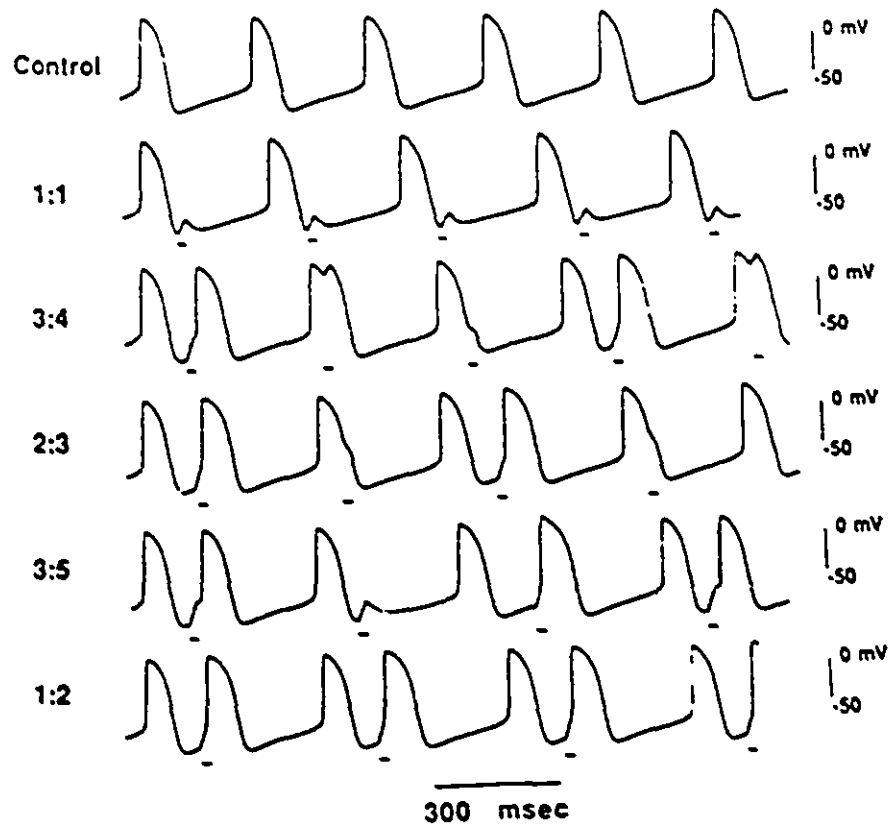


Figure 3.13: Rhythms intermediate to 1:1 and 1:2 phase locking in the Shrier and Clay model with  $T_s = 330, 375, 430, 470,$  and  $495$  msec, respectively, and with  $T_0 = 300$  msec. These results are to be compared with the corresponding experimental results in Fig. 3.5.

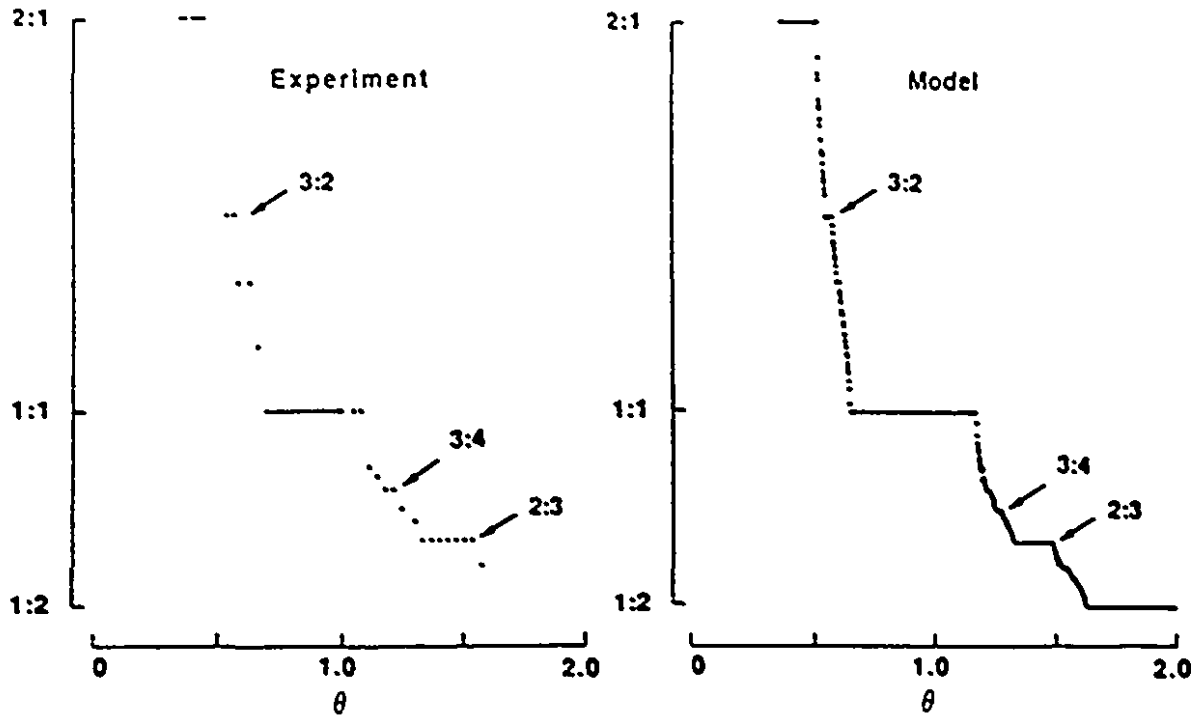


Figure 3.14: Phase locking as a function of the cycle time between pulses ( $\theta = T_s/T_0$ ). The left hand panel illustrates various phase locking regimes for the preparation illustrated in Fig. 3.3 and the first five panels in Fig. 3.4 ( $T_0 = 300$  msec) with  $i_{pulse} = 25$  nA. The right hand panel illustrates the various phase locking regimes of the Shrier and Clay model with  $i_{pulse} = 24$  nA. These results are sometimes referred to as a "devil's staircase".

in the middle and bottom panels of Fig. 3.15), although it does so less compellingly with each pulse in the a-d pulse sequence, because  $I_{Kr}$  has successively less time to deactivate, and each pulse depolarizes the membrane potential slightly less close to threshold of  $I_{Na}$  throughout the sequence. Consequently, the  $I_{Kr}$  component is dominant during and after pulse d (middle and bottom panels of Fig. 3.15), which effectively causes the model to skip a beat. The subsequent pulse (labeled e in Fig. 3.15) elicits an AP due to activation of  $I_{Na}$ . The  $I_{Kr}$  component does not produce an inhibiting effect in this case, because it is largely deactivated at the beginning of the pulse.

### 3.4.5 Limitations of the ionic model

The success of the Shrier and Clay ionic model in describing the experimental results given above leads to an important question, namely, why is the model so successful, and where do its limitations become more apparent. The success of this ionic model appears to lie primarily in its description of  $I_{Na}$  and  $I_{Kr}$ . The model of  $I_{Na}$  of Ebihara and Jones [50], which we completely borrowed in formulating the Shrier and Clay model, may well be the most successful description of  $I_{Na}$  for any cardiac membrane preparation. Our model of  $I_{Kr}$ , described in Reference [159], also appears to be successful. When either of these currents is reduced or blocked altogether, discrepancies between the numerical simulations of the ionic model and the corresponding voltage changes of the aggregate preparation become apparent. For example, the effects of submaximal doses of TTX [161] are well described (qualitatively) by the model with appropriate reductions in  $I_{Na}$  amplitude, but significant quantitative discrepancies are apparent, such as in the current pulse annihilation experiment described in Fig. 6 of Reference [161]. Similarly, when  $I_{Kr}$  is blocked by either risitolid or E-4031, the model is qualitatively consistent with experiment, especially for submaximal doses of these compounds, but it does not describe the excitatory after depolarizations (EAD's) which we observe when  $I_{Kr}$  is completely blocked (A. Shrier, unpublished results). These and other discrepancies appear to be due in part to inadequacies of our model of  $I_{Ca}$ . Our description of this component does successfully mimic the "crossover" effect of Lee, et al. [113], as noted above, but it does not successfully mimic some of the long term inactivation properties of this current elucidated with two pulse protocol voltage clamp experiments [99]. A further shortcoming of our

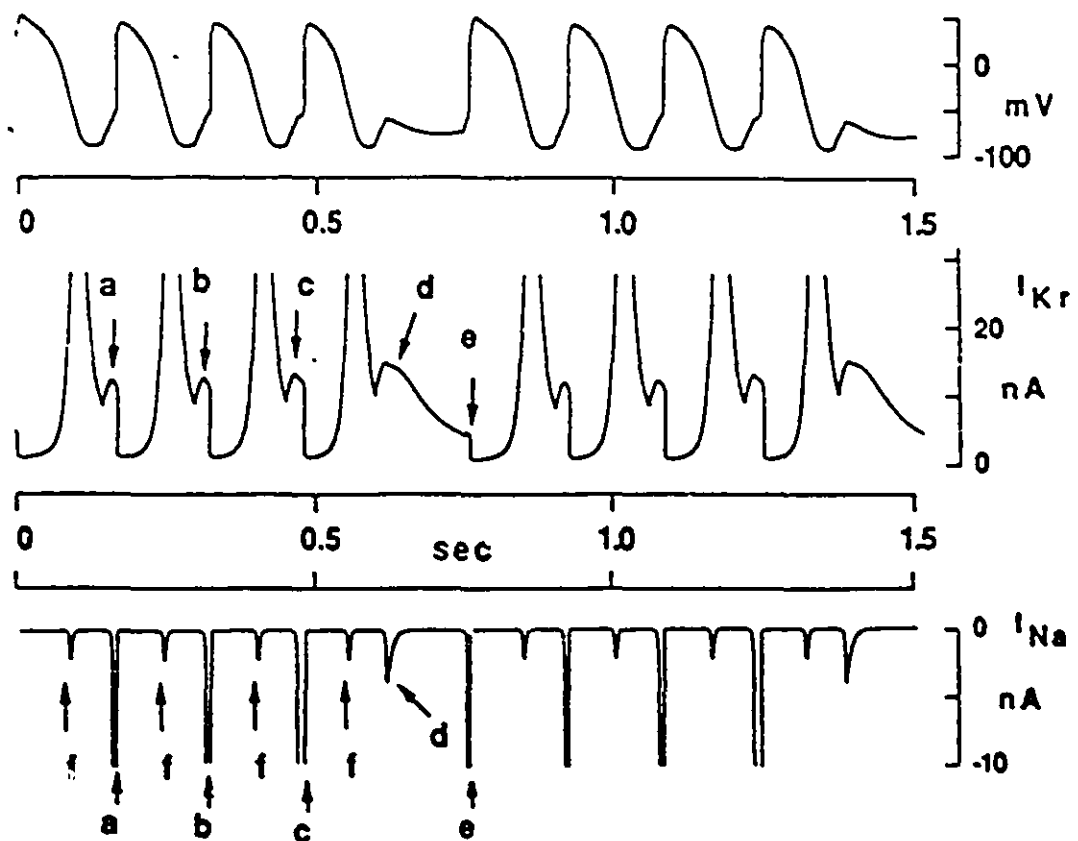


Figure 3.15: Ionic basis of 5:4 entrainment in the Shrier and Clay model as described in the text. The bottom two panels illustrate the behavior of  $I_{Kr}$  and  $I_{Na}$  in this pattern.

ionic model is the lack of various exchanger currents which have been reported in the heart, such as the sodium calcium exchanger. The model also lacks the sodium potassium pump current. We deliberately excluded these components in our original formulation of the model. Our goal was a minimal ionic model which successfully mimicked the action potential and pacemaker waveforms. The surprise of this analysis is how well the model also mimics most of the dynamics shown above, although the model clearly is deficient especially in its lack of the sodium ion pump current, because heart cell aggregates do exhibit a clear overdrive suppression [172, 186] which is a hallmark of the pump current [172, 61, 143]. Incorporation of this component into our model in a realistic fashion, is not, in our view, a straightforward process. DiFrancesco and Noble [48] have assumed in their model of electrical activity in cardiac Purkinje fibers that accumulation of potassium ions in the extracellular spaces during activity is an important mechanism controlling the amplitude of the pump current. However, potassium ion accumulation is not, in our view, a significant factor in heart cell aggregates, a view shared by Stimers, et al. [164] in their investigation of the pump current in aggregates. Nevertheless, regardless of mechanism, the pump current may play an important role in the dynamics of these preparations (see below), and it must, necessarily, be incorporated into our ionic model.

### 3.4.6 Comparison with other preparations

The value of the analysis given here for cardiac preparations other than chick atrial heart cells depends, to an extent, on how representative the various ion current components in the chick heart are of cardiac ion currents in other species. The  $I_{Na}$  component in the chick, which the above analysis indicates is a prominent player in phase locking, appears to be representative of  $I_{Na}$  in other preparations. For example,  $I_{Na}$  measurements from single cells dissociated from rat heart, rabbit cardiac Purkinje fibers, and human heart are largely similar to the  $I_{Na}$  results from embryonic chick heart cells [20, 37, 50, 21]. Consequently, the mechanism of 1:1 phase locking at beat rates greater than that of the intrinsic rhythm is likely to be the same in mammalian preparations as it is in avian preparations, i.e., premature activation of  $I_{Na}$  over a relatively broad range of pulse parameters.

Potassium ion currents in the heart, unlike  $I_{Na}$  and  $I_{Ca}$ , are remarkable more for intraspecies differences than for similarities. For example, rabbit ventricular myo-

cytes have a significant transient outward potassium ion current,  $I_{K_s}$  [65], whereas guinea-pig and chick myocytes do not ([156], and A. Shrier, unpublished observations). The latter two preparations do have a significant  $I_{K_s}$  component [126, 7, 34], although  $I_{K_s}$  does not appear to be a significant factor in phase locking other than helping to set the duration of the plateau phase of the AP.

The dominant repolarization current in chick myocytes is the  $I_{K_r}$  component [159], which has also been observed in guinea pig and in cat cardiac myocytes [156, 59]. The avian measurements of  $I_{K_r}$  are remarkably similar to those in mammalian cells concerning the rectification and voltage activation range of this component, but they differ concerning kinetics. The  $I_{K_r}$  kinetics in the chick are similar to those of  $I_{K_s}$  (but with a different voltage range), whereas they are significantly faster than those of  $I_{K_s}$  in mammalian cells, hence the label  $I_{K_r}$ , where "r" refers to "rapid" [156], although in our preparations "r" might more appropriately refer to "repolarization" [159]. In any case, this comparison suggests that the role of  $I_{K_r}$  in phase resetting and phase locking in mammalian cells could well be different from that of avian cells. Nevertheless, all excitable cells, whether quiescent or autonomous, will show a transition from 1:1 to 2:1 phase locking as the current pulse frequency is increased, because of refractoriness. The specific nature of the (potassium) ion current underlying the refractory behavior would appear to be preparation specific.

### 3.5 Nonlinear dynamics

The above results provide an analysis of the dynamics of the heart cell aggregates and an evaluation of the role of the underlying ionic currents. However, this analysis does not readily explain the complex sequence of patterns observed as stimulation parameters are changed, including phenomena such as period doublings and irregular dynamics.

Insights into these complexities can be gained by applying techniques from the field of nonlinear mathematics [75, 67, 70, 184, 81]. This approach also provides the framework for addressing other questions arising from the experimental data. These questions include: What is the connection between the phase resetting properties and dynamics during periodic stimulation? How can we predict complex rhythms that are found as stimulus amplitude and frequency vary? Why are the results obtained

from heart cell aggregates similar to results in other systems in which the underlying mechanisms of rhythmogenesis are certainly different? We address these questions in the following section by applying the techniques from nonlinear dynamics to the Shrier and Clay ionic model of the heart cell aggregate. This blending of theoretical techniques is an attempt to establish links between ionic mechanisms and nonlinear dynamics.

### 3.5.1 Iteration of the phase resetting curve

The effects of periodic stimulation can be computed from phase response curves (PRC's, such as those in Fig. 3.9), provided that the stimulation does not change the intrinsic properties of the oscillator and that the time interval between the stimuli is sufficiently long [141, 75, 67, 184]. The basic idea here is that a single stimulus leads to an instantaneous phase resetting from one point of the cardiac cycle to a second point on the cycle. The theoretical formulation of this process is carried out in terms of finite difference equations [70]. Calling the phase of the  $i$ th current pulse  $\phi_i$ , we have,

$$\phi_i = f(\phi_{i-1}, \theta) = 1 + \phi_{i-1} - \frac{T(\phi_{i-1})}{T_0} + \theta \quad 0 \leq \phi < 1 \pmod{1}, \quad (3.1)$$

where  $\theta = T_s/T_0$ ,  $T_s$  is the cycle length of the stimulus train, and  $\frac{T(\phi_{i-1})}{T_0}$  is the phase response curve as determined from single pulse experiments. Assuming that  $\phi_0$  is the phase of the unperturbed spontaneous cycle at which the initial current pulse of a train of periodic pulses is applied, Equation (3.1) can be numerically iterated to determine the dynamics.

The manner in which Equation (3.1) is implemented is illustrated in Fig. 3.16 and 3.17. Typical PRC's from a 150  $\mu\text{m}$  diameter aggregate are shown in Fig. 3.16A and 3.16B, for current pulse amplitudes 26 nA and 55 nA, respectively. The corresponding model results are given in Fig. 3.16C and 3.16D, respectively. The results in Fig. 3.16C and 3.16D have been transformed according to Equation (3.1) in Fig. 3.16E and 3.16F, respectively, with  $\theta = 0$ . Note that  $T(\phi)/T_0$  is approximately equal to  $\phi$  in Fig. 3.16C for  $\phi > 0.4$  and similarly in Fig. 3.16D for  $\phi > 0.3$ . Equation (3.1) gives  $\phi_i \approx 1$  for these conditions, as shown in Fig. 3.16E and 3.16F. The results in Fig. 3.16C and 3.16D have been transformed according to Equation (3.1) with  $\theta$

= 0.33 in Fig. 3.16G and 3.16H. In other words, the plots in Fig. 3.16E and 3.16F are shifted along the y axis (modulo 1) as the frequency of the externally applied current pulse train is altered. We hereafter refer to plots such as those in Fig. 3.16G and 3.16H as phase transition curves (PTC's).

Results similar to those in Fig. 3.16G and 3.16H are the basis for the determination of the dynamics using the iterative procedure illustrated in Fig. 3.17. The experimental recording in the top of the left panel in Fig. 3.17 is an example of 2:3 phase locking with 24 nA current pulses applied at a relative frequency of  $\theta = 1.2$ . The transient pattern which occurred before stable 2:3 phase locking was achieved is shown here. The PRC transformed according to Equation (3.1) for these conditions is shown below the experimental recording. The initial current pulse of the current pulse train was applied to the preparation at  $\phi_0 = 0.85$ . All subsequent phases at which the current pulses occur relative to the activity of the preparation can be determined by iteration. For example,  $\phi_1 = 0.38$ ,  $\phi_2 = 0.7$ ,  $\phi_3 = 0.35$ ,  $\phi_4 = .62$ ,  $\phi_5 = .32$ ,  $\phi_6 = .55$ , and  $\phi_7 = .3$ , as shown in Fig. 3.17 by the horizontal and vertical lines superimposed upon the phase transition curve. All subsequent results alternate between the latter two values, i.e., 0.55 and 0.3. The corresponding analysis in the model is shown in the right hand panel of Fig. 3.17. We note that a stable 2:3 phase locking pattern is achieved in the model much more rapidly than in the experimental result, for reasons that we do not as yet fully understand. One clear practical advantage of the approach of Figs. 3.16 and 3.17 is that regions of parameter space for which a particular type of phase resetting occurs, such as 2:3, can be predicted from the PRC rather than using direct integration of the full ionic model which can be a laborious procedure.

### 3.5.2 Period doubling bifurcations and chaotic dynamics

One of the important observations of nonlinear dynamics is that systems that are described by nonlinear functions, such as those in Equation (3.1), can display complex rhythms in which there is aperiodic behavior, and in which two initial conditions that lie close to one another have different dynamics as time proceeds. A formal definition for chaotic dynamics can be provided by the Lyapunov exponent,  $\lambda$ , which is defined

$$\lambda = \lim_{N \rightarrow \infty} \frac{1}{N} \sum_{i=1}^N \ln |f'(\phi_i, \theta)|, \quad (3.2)$$

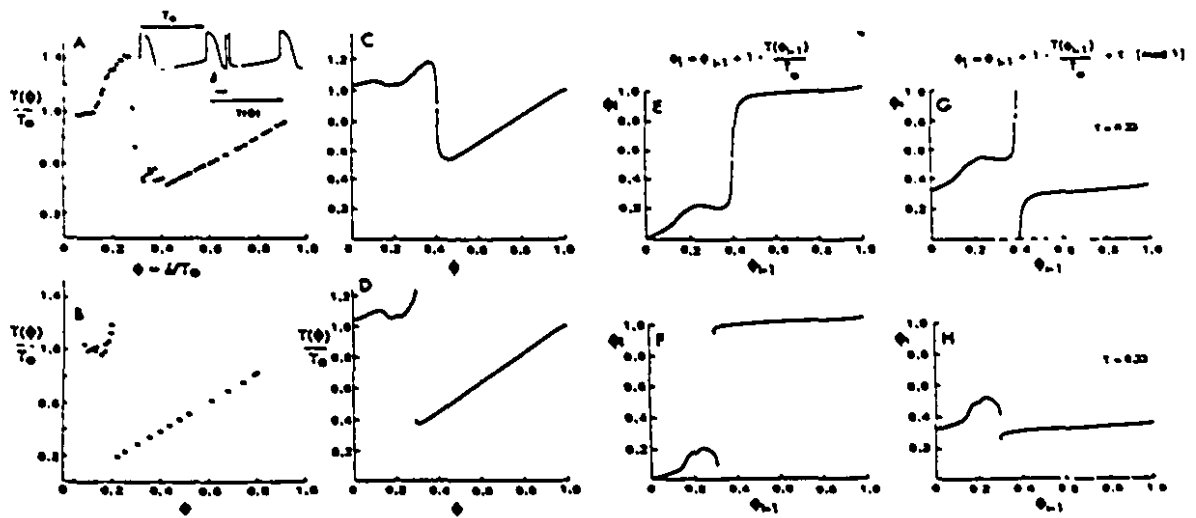


Figure 3.16: A-B. Experimentally observed phase response curves (PRC's) for moderate and relatively large amplitude pulses ( $i_{pulse} = 26$  and  $55$  nA for A and B, respectively). The trace above panel A illustrates the manner in which the PRC was determined as in Fig. 3.1. C-D. PRC's from the Shrier and Clay ionic model ( $i_{pulse} = 26$  nA and  $55$  nA for C and D, respectively, with  $I_{b1}$  adjusted to give  $\tau_c = 365$  msec). E-F. Phase transition curves as determined from respective PRC's in C and D using Equation (3.1) in the text with  $\theta = 0$ . G-H. PTC's from E-F with  $\theta = 0.33$ . These results are the same as in E-F, modulo 1, following an upward shift along the y axis by 0.33.

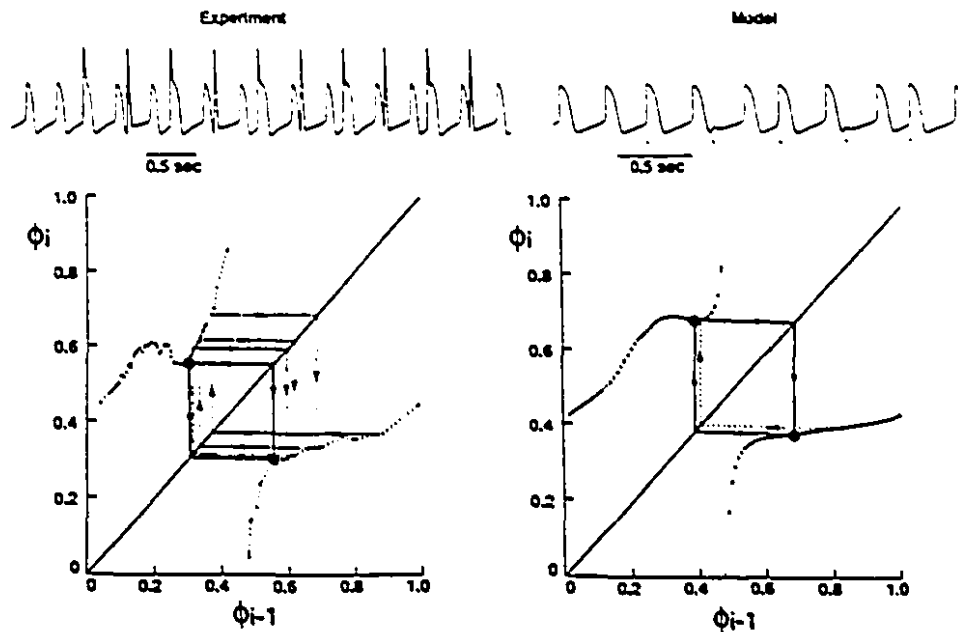


Figure 3.17: Determination of phase locking from the phase transition curve. Left hand panel: The experimental recording illustrates the effects of the first ten pulses of a current pulse train with  $T_s = 430$  msec,  $i_{pulse} = 25$  nA for a preparation with  $T_0 = 300$  msec ( $\theta = 430/300 = 1.44$ ). This activity is consistent with 2:3 phase locking following an initial transient during the first six pulses. The relative time in the unperturbed cycle at which the first pulse was applied was 0.85. The phases at which subsequent pulses occur can be determined from this point and the phase transition curve for these conditions, which is shown below the recording. The horizontal and vertical lines demonstrate the iterative procedure described in the text, as the activity locks on to the 2:3 pattern. Right hand panel: The trace in the upper part of the panel illustrates the effect of the first five pulses of a current pulse train on the Shrier and Clay ionic model ( $T_0 = 300$  msec,  $i_{pulse} = 25$  nA and  $T_s = 420$  msec). The times of occurrence of the pulses are indicated by the horizontal bars below the trace. The bottom part of the panel illustrates the old phase new phase diagram for  $i_{pulse} = 25$  nA and  $\theta = 1.41$  along with the corresponding iteration, as described in the text. Note that the transient in the model which occurs before stable 2:3 phase locking is achieved is significantly less than in the experimental result. The solid symbols in both panels are the phase space representation of the steady state 2:3 rhythm.

where  $N$  is the total number of iterations and  $f'(\phi_i, \theta)$  is the first derivative of the function  $f$  evaluated at successive phases  $\phi_i$ . A positive Lyapunov number reflects divergence of two nearby initial conditions and is taken as a definition for chaos [183, 70, 184]. The Lyapunov number was estimated by taking the summation over 420 iterates following a transient of 400 iterations.

Chaotic dynamics are often established following characteristic changes in the dynamics, technically called bifurcations, that arise as a consequence of changes in the parameters of stimulation. One well studied phenomena is period doubling bifurcations, in which the period of an oscillation doubles. This result was first documented in a biological system by Guevara et al. [75], using periodically stimulated heart cells aggregates with relatively large amplitude current pulses applied at stimulation frequencies which were a bit less than the intrinsic frequency of the preparation. An example of a period doubling bifurcation is illustrated by the 2:2 rhythm in the top panel of Fig. 3.18. In this record a current pulse was injected either immediately after the MDP of an action potential, or during the initial part of the plateau phase of the action potential. Even more complex patterns occur with  $N=M=2n$ , with  $n>1$ , such as the 4:4 pattern illustrated in the second panel of Fig. 3.18. The 2:2 and 4:4 rhythms during periodic stimulation of heart cell aggregates here are similar to the rhythms observed by Guevara et al. [75] and typify the period doubling route to chaotic dynamics [69, 70]. Numerical integration of the Shrier and Clay ionic model displays similar rhythms, as illustrated in the bottom half of Fig. 3.18. The current pulse amplitude in the simulations was 43 nA. Only very slight changes in the frequency of the pulse train were needed to obtain these results ( $T_s=455, 460$  and  $467$  msec for the 1:1, 2:2 and 4:4 results respectively).

Examples of chaotic dynamics are illustrated, from experimental data (left) and from numerical integration of the revised version of the Shrier and Clay ionic model (right) are illustrated in the top panels of Fig. 3.19. The phase transition curves for the conditions of these results are closer in appearance to Fig. 3.16H than Fig. 3.16G. In particular, they have roughly parabolic shapes for  $\phi_i < 0.3$ , as illustrated in Fig. 3.19 (open symbols). The relative phases of each of the current pulses in the chaotic rhythms in Fig. 3.19 are shown by the closed symbols. These points lie approximately on a continuous curve coincident with the parabolic portion of the PTC. Since iteration of the PTC gives chaotic dynamics using Equation (3.1), this supports our interpretation that this rhythm is chaotic. However, numerical integ-

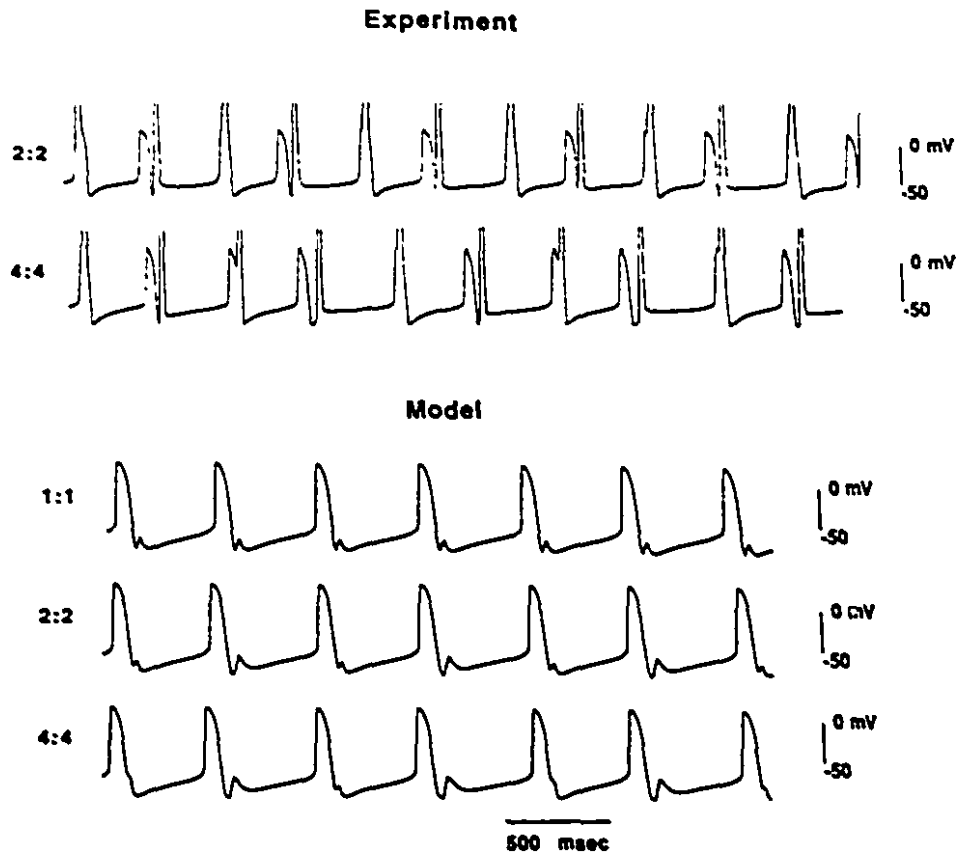


Figure 3.18: Period doubling rhythms. The top two panels illustrate 2:2 and 4:4 rhythms from two different aggregates with  $i_{pulse} = 43$  and  $48$  nA, respectively. In the 2:2 result  $T_0 = 303$  msec and  $T_s = 342$  msec and in the 4:4 result  $T_0 = 321$  and  $T_s = 386$  msec. The model results correspond to  $i_{pulse} = 43$  nA, and  $T_s = 455, 460,$  and  $467$  msec for 1:1, 2:2 and 4:4 rhythms, respectively, with  $T_0 = 435$  msec.

ration of the Shrier and Clay ionic model did not appear to give chaotic dynamics. The simulation record shown in the top part of Fig. 3.19 represents a 10 second record of irregular dynamics which was bounded, both before and after, by regular dynamics obtained without a change in stimulus parameters. The relative difficulty of finding chaotic dynamics from numerical integration of the full "revised" Shrier and Clay equations presumably reflects the narrow range of parameter values for which these dynamics are observed, and the numerical difficulties associated with searching phase space over a fine range of parameter values. It is important to recognize that the experimental system always contains small amounts of "membrane noise" that would act to destroy regular rhythms with long periodicities, as well as other factors such as the  $\text{Na}^+/\text{K}^+$  pump that might help introduce additional beat to beat variability in the deterministic model. Further numerical studies are needed to assess the importance of these factors. Finally, we note that other ionic models for spontaneously oscillating and periodically forced excitable biological systems display chaotic dynamics over limited stimulation ranges, for example, see References [77, 25, 70, 176], and references therein.

### 3.5.3 Phase locking zones

We have observed experimental results over a broad range of pulse intensities and frequencies. The experimental data can be conveniently summarized in a two-dimensional representation where the abscissa gives the normalized period of the stimulation and the ordinate gives the amplitude of the current pulse. The summary of the results is represented by the various symbols in Fig. 3.20 which were obtained by a visual inspection of the corresponding records generated by the ionic model. This approach requires extensive computations at each combination of stimulation parameters chosen. Another method for computing phase locking zones is to iterate Equation (3.1), as discussed above and as shown in previous studies [67, 81, 184]. The results of the computation are represented by the solid lines which demarcate the boundaries between phase locking zones. The largest zone is the 1:1 entrainment zone. It occurs when the stimulation period is approximately equal to the intrinsic frequency of the aggregate, but it also extends at higher amplitude stimulation to stimulation periods that are up to 30% of the intrinsic period. The 2:1 and 2:3 zones occur for stimulation periods approximately 0.5 and 1.5 times the intrinsic period.

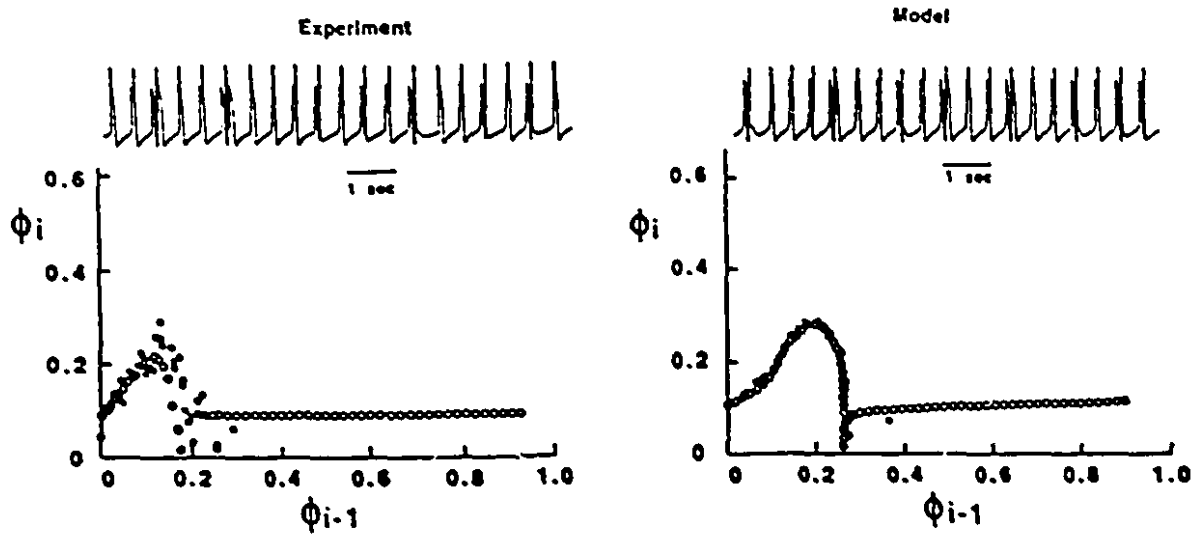


Figure 3.19: Aperiodic rhythms obtained from an experimental preparation (left panel) and from the ionic model (right panel), as described in the text. For the experimental result,  $T_0 = 450$  msec,  $T_s = 490$  msec, and  $i_{pulse} = 43$  nA. Model parameters were the same except for  $T_s$ , which was 497 msec. The upper panels show the electrical activity of the experimental preparation and the model. Lower panels show the old phase-new phase representation of the aperiodic activity, represented by the solid symbols. The phase transition curves are represented in both panels by the open symbols.

In comparison with the 1:1 zone, the 2:1 and 2:3 zones occur over narrower regions of stimulation parameter space. Finally, between the 2:1 and 1:1 zones there are  $N:M$  rhythms with  $N>M$  and evolving rhythms. Between the 1:1 and 2:3 zones there are  $N:M$  rhythms with  $N<M$ , period-doubled rhythms such as the 2:2 and 4:4 rhythms, and chaotic rhythms. In general, the rhythms obtained by iterating Equation (3.1) are in good accord with the experimental results. However, a more extensive and detailed analysis of the rhythms generated by the full ionic model has yet to be undertaken.

The regions of the parameter space displaying chaotic dynamics are shown in Fig. 3.21. The shaded areas in this figure correspond to regions of parameter space in which iteration of Equation (3.1) yields a positive Lyapunov number. However, as mentioned above, the simulation in Fig. 3.13 is the only result from numerical integration of the Shrier and Clay equations that appeared to be chaotic. The difficulty we had in finding chaos in the full ionic model may be attributable to the extremely fine structure of the dynamics in the shaded areas in Fig. 3.21. In fact, computations using the PTC of the model indicate that chaotic rhythms occur in narrow bands interspersed among complex, although non-chaotic, higher order rhythms. To address this point in detail one would need to extensively evaluate the PTC for stimuli in these regions, which is beyond the scope of studies conducted to date.

### 3.5.4 Universality

The preceding sections describe experimental determination of phase resetting and phase locking of chick heart cell aggregates, and develops theoretical models for the analysis of these results in the context of ionic models based on voltage clamp data and nonlinear finite difference equations. There is in general good agreement between the theoretical models and the experimental data. In this section we discuss the relevance of this work to experimental and theoretical studies of other spontaneously oscillating biological preparations.

A property common to many different systems is that their behaviour changes from simple to irregular as some external parameter is varied. What is notable is that these behaviours vary in a fashion which is independent of a particular function. Rather, there are a large class of nonlinear functions which generate stable cycles in one parameter range and then as the parameter is changed there are period

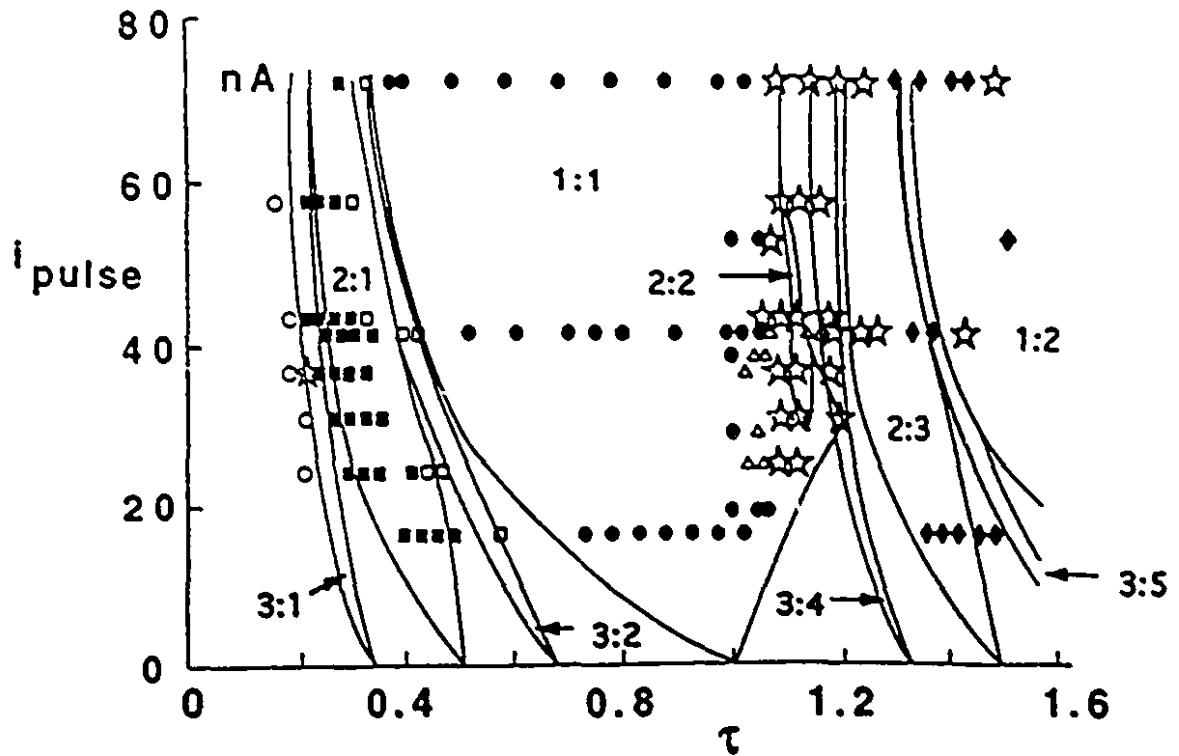


Figure 3.20: Phase locking zones. The various symbols illustrate different phase locked rhythms, as determined from visual inspection of experimental recordings from seven different aggregates. These results have been normalized according to the configuration of the PRC, so that they all correspond to a  $200 \mu\text{m}$  diameter aggregate. The symbols represent 3:1 ( $\circ$ ); 2:1 ( $\square$ ); 3:2 ( $\sqcup$ ); 1:1 ( $\bullet$ ); 2:2 ( $\triangle$ ); 2:3 ( $\diamond$ ); and irregular rhythms ( $\star$ ), respectively. The boundaries of various zones in the ionic model (as indicated by the hand drawn lines) were determined from the PTC's using the iterative approach described in the text and in Fig. 3.16. The  $I_{b1}$  component in the Shrier and Clay ionic model was set so that  $T_0 = 366$  msec.

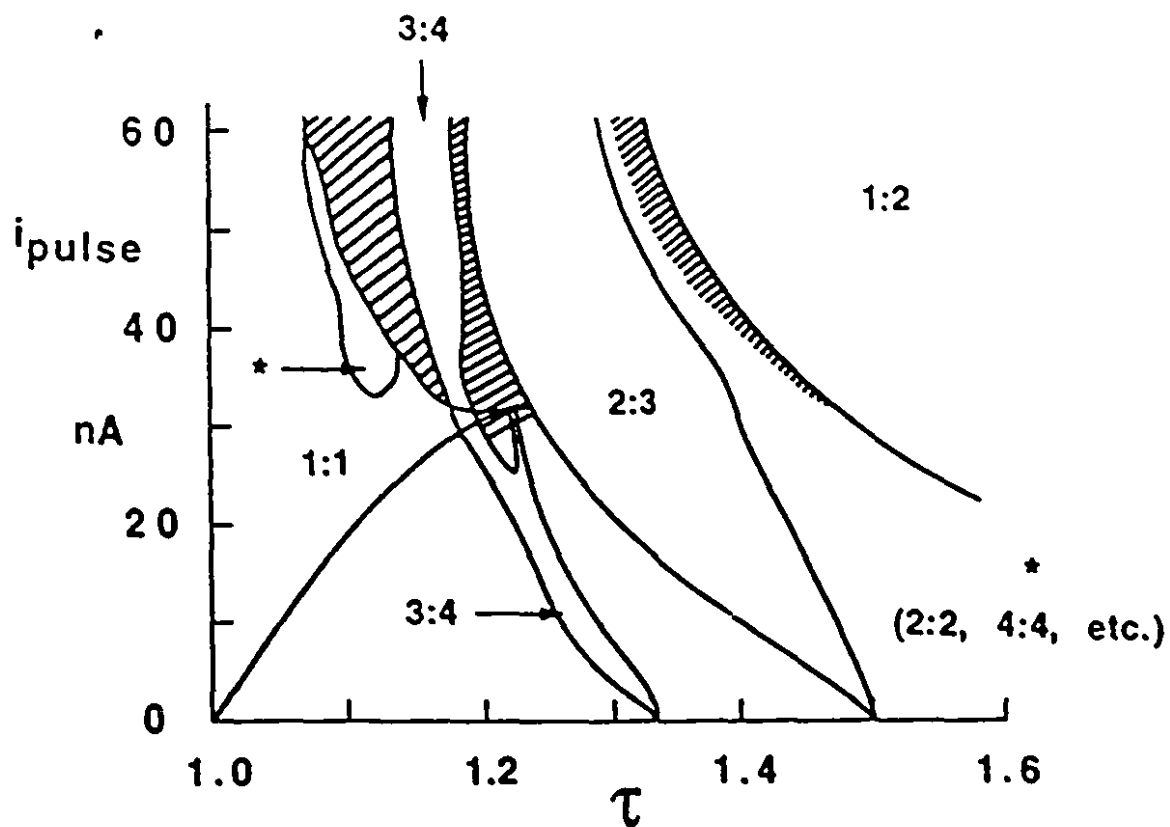


Figure 3.21: Regions of chaotic dynamics predicted from iteration of the phase response curve of the ionic model. A portion of the plot in Fig. 3.20 is shown with the  $N:M$  zones as indicated. The shaded regions correspond to regions where a mixture of complex and chaotic (positive Lyapunov number) rhythms were found.

doublings and chaotic dynamics. Indeed, in a variety of systems, including the heart cell aggregates, there are characteristics of the different iterated maps that behave in a "universal" fashion. In this context the results of these studies on the heart cell aggregates may serve as a model of the dynamics observed in other cardiac preparations and biological oscillators in general.

The various rhythms that we have observed in heart cell aggregates and in our model of this system bear a striking resemblance to rhythms observed in other experiments involving periodic stimulation of cardiac tissue [26, 3]. Moreover, analogous rhythms have been observed in cardiac arrhythmias in the human heart, such as second degree heart block, that arise as the parameters of electrical stimulation are varied [160]. Furthermore, similar types of rhythms are also observed in other physiological systems as well as in abstract theoretical models [70, 76].

From a mathematical perspective, the reason for the similarities in dynamics between different systems are well understood. Briefly, dynamical systems that are described by one-dimensional finite difference equations, Equation (3.1), have a limited repertoire of possible behaviors. In the current case, the nonlinear function  $f$  is derived from the PRC. Provided the PRC satisfies certain mathematical properties, then one can make strong statements concerning the effects of periodic stimulation on the system. For example, if the stimulus strength is sufficiently weak, we know that if we observe  $N : M$  phase locking for some value of stimulus period  $\theta_1$  and  $N' : M'$  phase locking for stimulus period  $\theta_2$ , then there exists an intermediate stimulation period  $\theta$ , with  $\theta_1 < \theta < \theta_2$ , which gives a locking ratio  $N + N' : M + M'$ . This observation gives insight into the ordering of the locking zones for low values of the stimulus intensity. The other important mathematical insight into the current results arises from the parabolic shape of regions of the PTC for moderate to relatively large amplitude stimuli. The appearance of this geometry will give rise to period doubling bifurcations and chaotic dynamics, regardless of the specific mechanisms. Despite these results, a detailed understanding of the complete global organization of the phase locking zones for all stimulus amplitudes and intensities remains a difficult problem, currently the subject of research in mathematics.

Nevertheless, the "universal" appearance of similar rhythms in such a wide variety of different systems has important implications for the interpretation of the current results. Based on the observation of the rhythms alone, one cannot conclude that some particular theoretical model is validated by the experiments. On the contrary,

a very broad range of different theoretical models will all give a rough approximation to the observed results. Thus, simple models with parabolic PTC's may therefore provide a convenient way to characterize results from complex systems, and may have predictive power concerning the ordering of the dynamics and the range of stimulus parameters required. However, the different theoretical models will differ in subtle, but nevertheless important features such as the shapes and quantitative boundaries of the different zones.

### 3.6 Conclusions

The various rhythms that are observed in heart cell aggregates described above can be reasonably well explained in terms of ionic mechanisms as well as of nonlinear mathematics. The results of this work may be generalized to other excitable cells, independent of the detailed ionic mechanisms, because of similarities in the underlying nonlinear mathematics. Therefore, we believe that the chick heart cell aggregate, and its responses to electrical stimulation, give broadly applicable insights into dynamics arising from the stimulation of other biological oscillators.

The current analysis makes certain important simplifications that will need modification in future studies. The weakest step in what we have sketched out is the assumption that the stimulation does not change the properties of the oscillation. This assumption is not well satisfied during stimulation at rapid pacing rates. Following the cessation of rapid pacing, the intrinsic rhythm of the heart cell aggregate slows, a phenomenon that is known as overdrive suppression. Overdrive suppression is observed in diverse cardiac preparations, and is frequently observed in humans following the tachycardia. Previous work on the chick heart cell aggregates has begun to characterize overdrive suppression and to explore the consequences of overdrive suppression on the dynamics of the heart cell aggregates. A further investigation of the qualitative aspects of this phenomenon is also presented in Chapter 4. For example, during periodic stimulation at rapid pacing rates there is often an evolution of rhythms such that higher grades of block occur before the stable rhythm is established [186]. Modifications in the simple finite difference Equation (3.1) have been proposed to account for these effects, but the mathematical structure of the resulting equations is more complicated (it is a 2 dimensional nonlinear finite difference

equation) and it is not as well understood. These effects may be associated with activation of the  $\text{Na}^+/\text{K}^+$  pump and  $\text{Na}^+/\text{Ca}^{2+}$  exchanger, transient inhomogeneities of cations in the extracellular space and intracellular space, or some combination of these effects. In order to account for the time dependent effects associated with rapid stimulation, modifications in the ionic model will have to be implemented. Chapter 5 is partly devoted to the development of such a modified ionic model.

The response of the heart cell aggregates to electrical stimulation is relevant for the interpretation of cardiac arrhythmias. For example, parasystole [95, 177] and atrioventricular heart block [160] display many similarities to the rhythms in the heart cell aggregate preparation. Indeed, the experimental results on heart cell aggregates directly motivated the clinical observations reported in Reference [160]. Moreover, the knowledge obtained from heart cell aggregates may help provide a basis for understanding the phase resetting and phase locking of ventricular tachycardia observed in a clinical context during the diagnosis and control of ventricular arrhythmias [100]. The ionic mechanisms underlying these arrhythmias are still not well known. Since pharmacological interventions affect ionic channels directly, an understanding of the ionic mechanisms in this model preparation may have long range implications for therapy.

An additional direction for future research involves investigating the molecular biology of the ionic currents. The dynamics in chick heart cell aggregates display subtle reproducible differences depending on the age of the embryo at the time of culturing, the part of the heart from which the culture is derived, and the composition of the growth medium. Understanding the molecular basis of these changes, and associating them with the observed dynamics during different stimulation protocols provides a challenge for the future.

### 3.7 Appendix: detailed description of the Shrier-Clay ionic model

In this Appendix we present the details of the modified version of the Shrier and Clay ionic model for atrial chick heart cell aggregates used in the theoretical part of the present work. The current components are explicitly given in Table 3.1. Numerical simulations were implemented with a variable time step Euler iteration technique

[131] for the membrane voltage and a Rush and Larsen [155] iteration method for the gating parameters.

Table 3.1: Membrane current components for the Shrier and Clay model of ionic currents in atrial chick heart cells.

**Sodium ion current:**

$$I_{Na} = 328m^3(t)h(t)(V - 40).$$

$$\dot{m}(t) = -(\alpha_m + \beta_m)m(t) + \alpha_m;$$

$$\dot{h}(t) = -(\alpha_h + \beta_h)h(t) + \alpha_h;$$

$$\alpha_m = 320(V + 47.13)/(1 - \exp(-0.1(V + 47.13))) \text{ s}^{-1};$$

$$\beta_m = 80 \exp(-V/11) \text{ s}^{-1};$$

$$\alpha_h = 135 \exp(-(V + 80)/6.8) \text{ s}^{-1};$$

$$\beta_h = 3560 \exp(0.079V) + 3.1 \times 10^8 \exp(0.35(V + 3)) \text{ s}^{-1}; \quad \text{when } V < -40mV \text{ and}$$

$$\alpha_h = 0$$

$$\tau_h = (\alpha_h + \beta_h)^{-1} = 0.00013(\exp(-(V + 10.66)/11.1) + 1) \text{ , s} \quad \text{otherwise.}$$

**Delayed rectifier potassium current:**

$$I_{Ks} = 1.4n(t)(V + 100).$$

$$\dot{n}(t) = -(\alpha_n + \beta_n)n(t) + \alpha_n;$$

$$\alpha_n = 0.08(V - 15)/(1 - \exp(-0.08(V - 15))) \text{ s}^{-1};$$

$$\beta_n = 0.156 \exp(-0.055(V - 15)) \text{ s}^{-1}.$$

**Primary repolarization current:**

$$I_{Kr} = I_0s(t).$$

$$\dot{s}(t) = -(\alpha_s + \beta_s)s(t) + \alpha_s;$$

$$\alpha_s = 18.4 \exp(0.12(V + 12)) \text{ s}^{-1};$$

$$\beta_s = 0.0288 \exp(-0.09(V + 12)) \text{ s}^{-1};$$

$$I_0 = 850y^2(145p_{Kr} - 1.3r_{Kr})/(1 + y + 52.8y^2),$$

$$\text{with } y = 1.3r_{Kr}/(145p_{Kr}),$$

$$r_{Kr} = (1 + \exp(V/25))^{-1}, \text{ and } p_{Kr} = 1 - r_{Kr}.$$

**Background current:**

$$I_{b_1} + I_{b_2} + I_{b_3}, \text{ where}$$

$$I_{b_1} = 0.123(V - 40),$$

$$I_{b_2} = 409.5y_1^3(145p_{Kr} - 1.5r_{Kr})/(1 + y_1 + y_1^2 + 1.5y_1^3),$$

$$I_{b_3} = 1.476|V + 65|y_2^2(145p_{Kr} - 10.7r_{Kr})/(1 + y_2 + 9y_2^2),$$

$$y_1 = 1.5r_{Kr}/(145p_{Kr}), \quad y_2 = 10.7r_{Kr}/(145p_{Kr}).$$

**Calcium ion current:**

$$I_{Ca} = 20d(t)f(t)(g(t))(V - 40).$$

$$\dot{d}(t) = -(\alpha_d + \beta_d)d(t) + \alpha_d;$$

$$\dot{f}(t) = -(\alpha_f + \beta_f)f(t) + \alpha_f;$$

$$\alpha_d = 2600 \exp(-0.02V)/(\exp(-0.15V) + 1) \text{ s}^{-1};$$

$$\beta_d = 1780 \exp(-0.17(V + 39))/(\exp(-0.072(V + 39)) + 1) \text{ s}^{-1};$$

$$\alpha_f = 0.025 \exp(-0.1V) \text{ s}^{-1};$$

$$\beta_f = 0.25V/(1 - \exp(-0.2V)) \text{ s}^{-1};$$

$$\dot{g} = -g[Ca_i]/(5 \times 10^{-8}) + (1 - g)/(0.025(1 + \exp(0.10(V + 50)))), \text{ where}$$

$[Ca_i]$  is the internal calcium ion concentration (mol/liter), with

$$\dot{[Ca_i]} = -13 \times 10^{-6} I_{Ca} + 80(10^{-7} - [Ca_i]).$$

## Chapter 4

# Overdrive suppression of spontaneously beating chick heart cell aggregates: Experiment and theory

### 4.1 Foreword

Single or sustained periodic stimulation can affect the properties of pacemaker cardiac tissue. In particular, rapid stimulation at a rate faster than the intrinsic frequency of the preparation will often lead to a transient slowing of the spontaneous rhythm. This effect is called “overdrive suppression” [173]. Overdrive suppression has been observed in cardiac tissues derived from many species [174, 172, 173, 74, 36, 66, 143, 106, 134, 41, 101, 149]. Vassalle demonstrated that an important mechanism underlying overdrive suppression in dog and sheep Purkinje fibers is the activation of an electrogenic Na/K pump [172]. Although subsequent studies have confirmed the role of the electrogenic Na/K pump [143, 118, 36, 61, 41, 173], other ionic mechanisms including extracellular potassium accumulation [106, 172], and intracellular calcium accumulation [134, 74] play a role in the overdrive suppression.

Recently, we characterized overdrive suppression in spontaneously beating chick heart cell aggregates [186]. We studied the kinetics of buildup and decay of the overdrive suppression following stimulation at constant frequency, and demonstrated the role of overdrive suppression in the evolution of rhythms during periodic stimulation. The current paper extends this work by considering the effects of stimulation frequency, amplitude, and duration of pacing on overdrive suppression. Although we

are interested in the detailed ionic mechanisms of the heart cell aggregates [105], we believe that development of simplified theoretical models can play a complementary role to the ionic models by providing easily understandable equations demonstrating the main phenomena. In the current paper we propose a system of nonlinear ordinary differential equations to model the cardiac oscillator based on the van der Pol equation [170, 57]. This oscillator equation is modified by implementing an additional equation to account for overdrive suppression based on the hypothesis that rapid stimulation induces an electrogenic outward current [172, 173]. We assume that each action potential induces an outward current that decays slowly during diastole. At rapid stimulation rates there is inadequate time between action potentials for the outward current to return to control levels leading to an increased outward current and lower spontaneous frequency. The outward current plays a role during control activity as well as during electrical stimulation. The experimental results concerning the buildup and decay of overdrive suppression found in the current work are in good agreement with the simulations of the theoretical model.

## 4.2 Experimental protocols

Experiments were carried out in 20 preparations. 15 focused on overdrive at different frequencies, 5 on overdrive suppression for different numbers of stimuli. The electrical activity of the aggregate was recorded in the absence of external stimulation for five to ten minutes. Aggregates displaying marked (more than 5%) variability in the IBI were discarded.

### 4.2.1 Overdrive suppression for different numbers of stimuli

The aggregates were stimulated with increasing numbers of stimuli. Successive trains of 1,2,4,6,8,10,15,25,50 and 100 stimuli were delivered, separated by rest periods of approximately 30 seconds. The period of stimulation was typically of about  $0.6 T_0$  ( $T_0$  is the control cycle length of the preparation) and in all cases there was 1:1 entrainment between the stimulator and the preparation. All measured time intervals were normalized to the control cycle length defined as the average of the 5 cycle lengths preceding the drive. The post-drive cycle length was evaluated as

a function of stimulation duration. The subsequent decay of overdrive was plotted on the same time scale. In some instances, the protocol was repeated for several different amplitudes of stimulation to investigate the relationship between overdrive suppression and the intensity of the stimulus.

## 4.2.2 Overdrive suppression at different frequencies

Trains of 50 or 100 stimuli were delivered at different stimulation periods ( $T_s$ ) with a rest of 30 seconds between successive trains to allow the cycle time to return to control. The period of stimulation was automatically decremented. Different stimulation strengths were also used to investigate the relationship between overdrive suppression and the intensity of the stimulus as well as the entrainment rhythms. The measured time intervals were normalized following the procedure described in the previous protocol.

## 4.3 Theoretical model

Since the pioneering work of van der Pol and van der Mark [170], simple systems of ordinary differential equations (ODE's) have been used to model qualitative features of biological oscillators [70, 181, 57]. We have chosen a piecewise linear approximation to the van der Pol equations that contains a stable oscillating solution, *a limit cycle*, to represent the cardiac cycle. For technical details concerning the mathematics, see the Appendix.

The theoretical model is designed to capture the important qualitative properties of overdrive suppression in a schematic fashion. The main assumption of this work is that *overdrive suppression arises as a consequence of a hyperpolarizing (outward) current that is induced by action potentials*. Although we imagine that this current is associated with the transport of positive ions from the intracellular space to the extracellular space during the cycle, we develop the theoretical model in a general way that is consistent with a number of different ionic mechanisms. Therefore, the present simplified theoretical model can provide a complementary approach to traditional ionic modeling and represents an important step in our understanding of overdrive suppression.

In order to carry out this task, the equations for the cardiac oscillator are modified to include a history dependent hyperpolarizing current. The prolongation of the intrinsic cycle length following rapid stimulation is primarily due to a decrease in the slope of diastolic depolarization and, to a lesser extent, to changes in action potential duration, maximum diastolic and threshold potentials [186].

The differential equations that we adopt for the periodically stimulated cardiac cells are

$$\begin{aligned}\frac{dV}{dt} &= \frac{1}{\epsilon}(y - f(V)), \\ \frac{dy}{dt} &= \alpha(V) - \beta \frac{Z}{Z+k}, \\ \frac{dZ}{dt} &= -\gamma \frac{Z}{Z+k} + \Delta Z \delta(t - t_{AP}),\end{aligned}\tag{4.1}$$

where  $V(t)$  corresponds to the experimentally observed transmembrane voltage,  $y$  controls the timing of the phases of the action potential, and  $Z$  is the variable associated with the history dependent hyperpolarizing current. The properties of the oscillation in the absence of  $Z$  are determined by the piecewise linear functions  $f(V)$  and  $\alpha(V)$  (see Appendix). Finally  $\epsilon, \beta, \gamma, \Delta Z$  are positive constants,  $\delta$  is the Dirac delta function and  $t_{AP}$  represents the time of upstroke of the action potential.

The physical interpretation of this equation is as follows. If we first fix  $Z = 0$  there will be a stable oscillation of  $V$  and  $y$ . For  $0 < \epsilon \ll 1$ , the oscillation is similar to a cardiac action potential with periodic rapid increases in  $V$  that we associate with the successive onsets of the action potential. Now consider what happens when  $Z$  is allowed to vary. The onset of the action potential leads to an instantaneous increment,  $\Delta Z$ , of the factor  $Z$ . Meanwhile, during the entire cycle, the level of  $Z$  is reduced following some  $Z$ -dependent rate. There is an associated term,  $-\beta \frac{Z}{Z+k}$ , influencing the dynamics of  $y$  in the second equation. This term prolongs the duration of the depolarizing (pacemaker) phase of the cardiac cycle, and to a lesser extent, decreases the duration of the plateau of the action potential. Therefore, the removal of  $Z$  can be associated with a hyperpolarizing current, where the magnitude of the current is proportional to  $\frac{Z}{Z+k}$ . The Appendix gives further details.

Numerical simulations were carried out by integrating Equation (4.1) using a fourth order Runge-Kutta method. In order to eliminate transients, initial conditions were chosen to lie on the limit cycle. The parameters of Equation (4.1) were adjusted for each aggregate studied using the method described in the Appendix.

## 4.4 Results

### 4.4.1 Overdrive suppression at fixed stimulation frequency for different numbers of stimuli and different stimulus intensities

In this protocol the aggregates were stimulated for several different durations maintaining a constant stimulation frequency. Figure 4.1 shows a typical experiment from an aggregate with a basic cycle length  $T_0$  of 520 msec stimulated at a stimulation period of 300 msec ( $\approx 0.58 T_0$ ). Initiation of the drive is generally followed by a transient depolarization which may reflect changes in ionic gradients across the membrane. A hyperpolarization (increase in maximum diastolic potential) can sometimes be observed during the longer (1 min. at 3 Hz) drives in spontaneously beating embryonic chick heart cell aggregates [143], but was not clearly present in our experiments. After 4 (top panel), 15 (middle panel), and 50 (bottom panel) stimuli, the first interbeat interval following the drive,  $T'$ , was prolonged by 20%, 70% and 160%, respectively, over control.

The results of periodic stimulation for the same number of stimuli and the same stimulus periods in the theoretical model are shown in the right hand side of Figure 4.1. The degree of post-drive suppression of activity is roughly comparable to what is observed in the experimental system. However, because the time-dependent process described in Equation 1 does not influence the geometry of the limit cycle, no drive induced hyperpolarization in MDP (maximum diastolic potential) is found in the theoretical results (see Appendix).

Figure 4.2 illustrates how overdrive suppression is induced in the theoretical model during periodic stimulation (1, 4, 15 stimuli) at a rate faster than control. In each of the 3 panels, the top trace shows  $V(t)$ . The corresponding changes in the level of  $Z$  are presented in the bottom trace. The control cycle length is 500 msec and the stimulus period 300 msec. The upstroke phase of the action potential is associated with a significant increase ( $\approx 30\%$ ) in the level of  $Z$ . Under control conditions (prior to stimulation), the same quantity of cations  $Z$  is removed by the electrogenic mechanism active during the entire cycle. During periodic stimulation, increased action potential frequency results in accumulation of  $Z$  which stimulates the electrogenic mechanism hence reducing the slope of diastolic depolarization. As

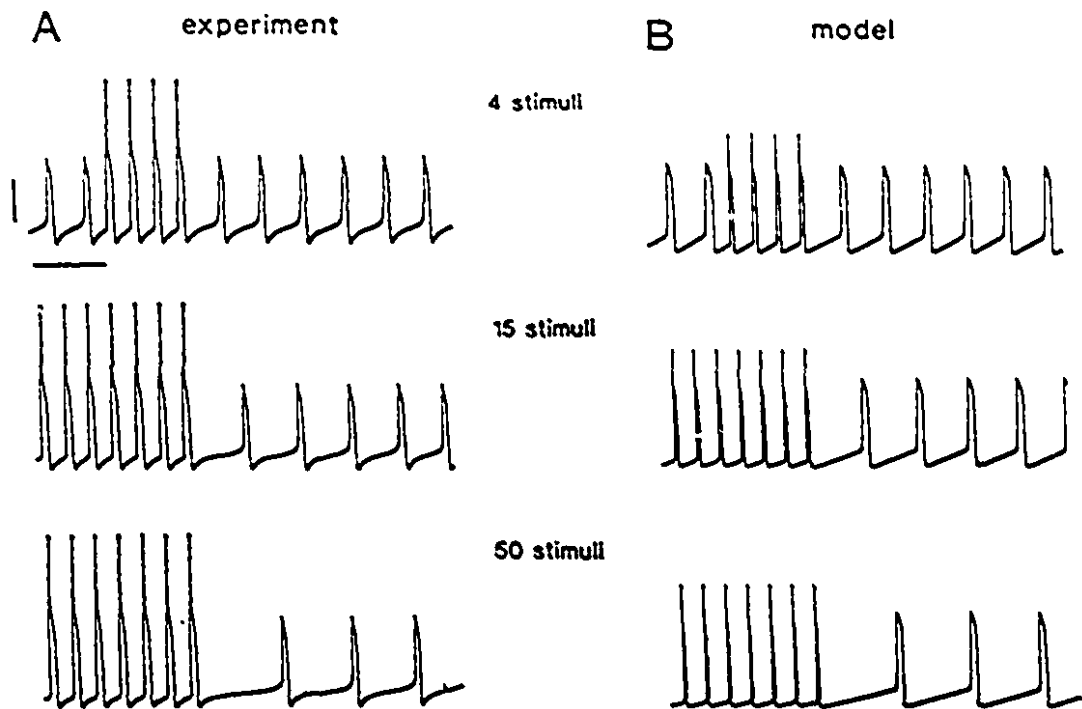


Figure 4.1: Tracings of membrane voltage showing overdrive suppression following increasing numbers of stimuli of fixed frequency. Stimulation of an atrial aggregate (aggregate AK 71) with a basic cycle length of 470 msec for several different durations maintaining a constant stimulation period of 280 msec ( $.65 T_0$ ): 4 (top panel), 15 (middle panel), and 50 (bottom panel) stimuli results in increasing post-drive suppression of automaticity (overdrive suppression). The pulse amplitude was 40 nA and the stimulus duration was 20 msec (in all experimental traces). The stimulus artefacts appear as the off-scale deflections. The left hand panels show the experiments and the right hand panels show the simulations. The values of the parameters used in this simulation (and for all other protocols and aggregates as well) can be found in Table 4.1. In all the figures, the vertical calibration bar indicates 50 mV and the horizontal calibration bar shows 1 sec. The top of the vertical calibration bar indicates zero potential.

in Figure 4.1, the apparent decrease in action potential duration during overdrive in the model is due to the geometry of the limit cycle (see Appendix). Following cessation of stimulation, the level of  $Z$  decays due to the increased extrusion *via* the hyperpolarizing current and to the slow down of spontaneous activity (overdrive suppression). After 15 stimuli, the two-fold increase in the level of  $Z$  is associated with a 50% lengthening of the cycle length. Six seconds after cessation of stimulation the level of  $Z$  is only 10% above normal and control activity has almost resumed.

A composite picture of overdrive suppression, expressed as  $T'/T_0$  versus stimulation time is shown in Figure 4.3 for 2 different atrial aggregates stimulated with respectively  $T_s=300$  and 310 msec. The post-drive pause developed slowly with the number of stimuli applied. As the number of stimuli applied increased even further, the post-drive prolongation sometimes shows a tendency to saturate [186]. The right hand panel of Figure 4.3 shows the results of simulation. There is good agreement between the numerical simulation and experimental data concerning the magnitude of the overdrive effect and its dependence on the number of stimuli applied. In the numerical simulation however, the decay rate of overdrive suppression is initially too slow and then becomes too fast.

During sustained periodic stimulation at a fixed frequency, the observed entrainment pattern is often a function of the stimulus intensity [75, 79, 186, 105]. For example, as the amplitude of the stimulus is varied while the period of stimulation is maintained constant, different types of N:M locking between the stimulator and the preparation can be observed. The tracings shown in Figure 4.4 were obtained by maintaining a constant period of stimulation ( $T_s=145$  msec), but with the stimulation intensities of  $\approx 18$  nA in panel A,  $\approx 28$  nA in panel B, and  $\approx 40$  nA in panel C. As the stimulation intensity increases there are different coupling patterns between the stimulus and the aggregate with 2:1 locking in panel A, 3:2 locking in panel B, and 1:1 locking in panel C. The changes in the locking ratio are associated with changes in overdrive suppression. Following stimulation leading to 1:1 phase locking, the post-drive prolongation reached 340% over control but this was reduced to 120% over control following 3:2 locking and 70% over control following the 2:1 locking. Similar results were obtained in 6 other preparations. This demonstrates that it is the frequency of the action potentials, rather than the period of stimulation which is most critical in determining the magnitude of overdrive suppression.

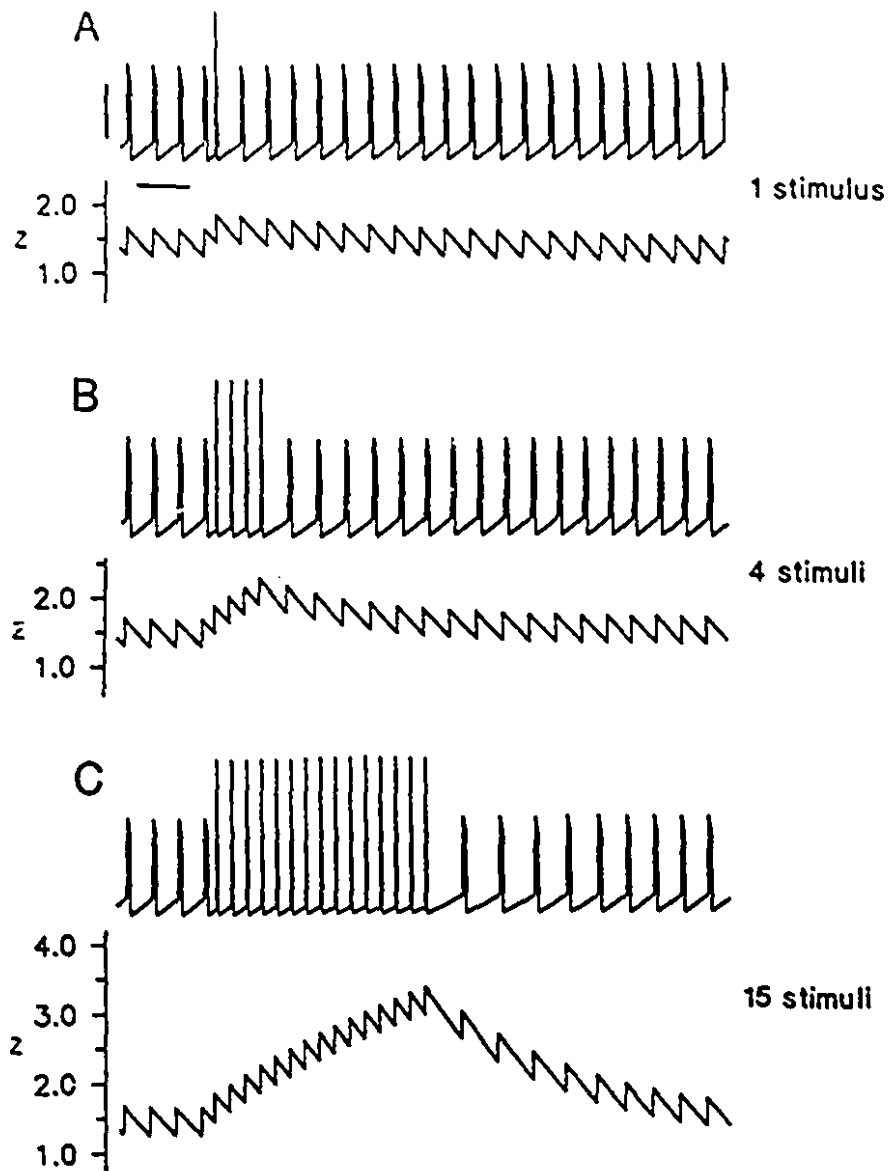


Figure 4.2: Numerical simulations of the model showing the relationship between overdrive suppression and the level of  $Z$ . The parameters in the model were adjusted to obtain a control cycle length of 500 msec. Trains of 1, 4 and 15 stimuli (top to bottom,  $T_s = 300$  msec) were applied (1:1 entrainment) and the resulting tracings for  $V(t)$  and  $Z(t)$  (in units of  $k$ ) are presented in each panel. Under control conditions the level of  $Z$  varies by  $\approx 30\%$  within the cycle. Overdrive suppression is due to an increased magnitude of the  $Z$ -sensitive electrogenic current because high action potential frequency during periodic stimulation causes accumulation of  $Z$ . This overdrive suppression decays subsequently and within 10 to 15 seconds control activity is restored.

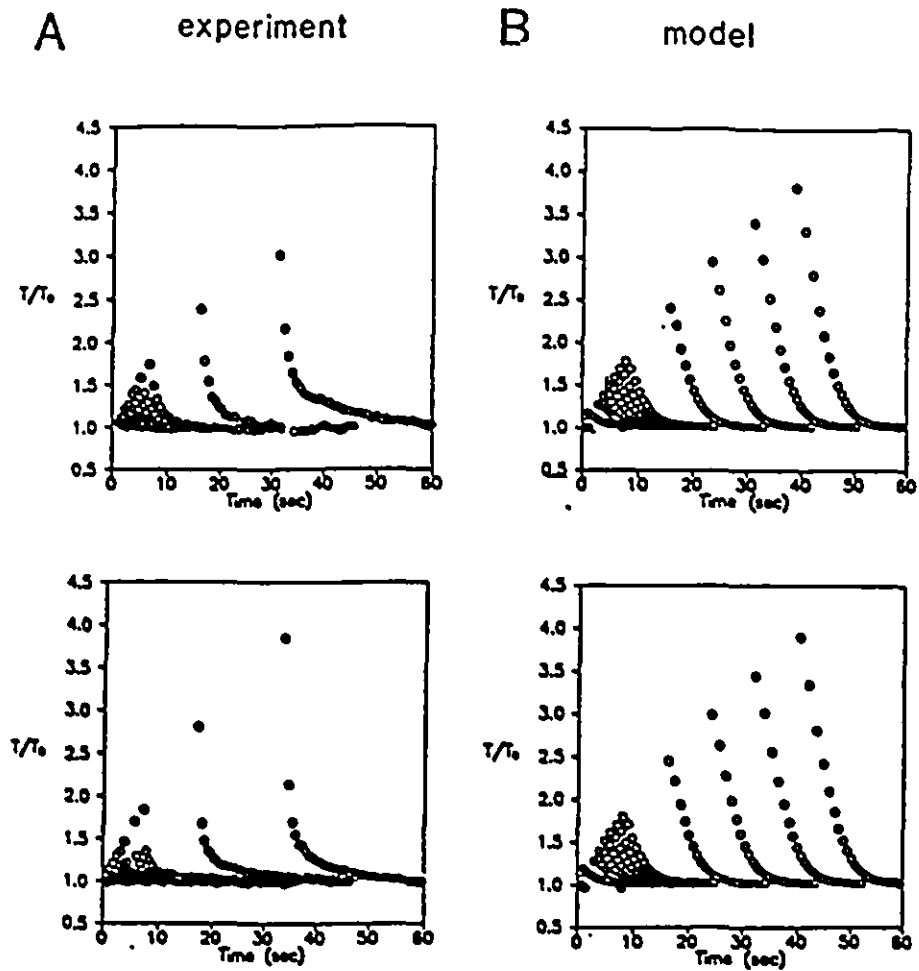


Figure 4.3: A composite picture of overdrive suppression as a function of stimulation time for 2 different atrial aggregates (AK 61 and AK 71) stimulated with  $T_s = 310$  msec and  $T_s = 300$  ms, respectively. The interbeat intervals following the drive, normalized to the control cycle length ( $T'/T_0$ ), are shown for increasing stimulus train durations. Following the drive, the first cycle length is the longest and normal activity is restored after 10 to 30 seconds. The left hand panels show the experiments and the right hand panels show the simulations.

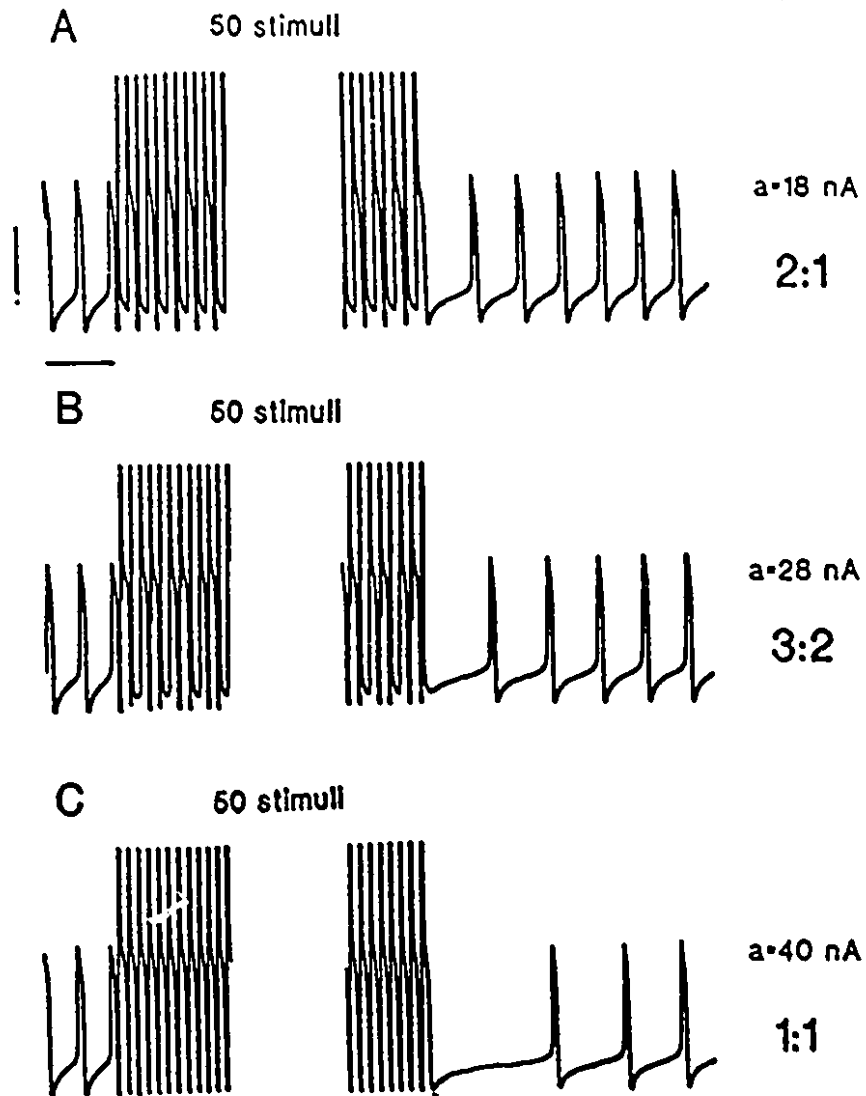


Figure 4.4: Recordings showing the dependence of overdrive suppression on action potential frequency. An atrial aggregate of diameter  $180 \mu\text{m}$  and control cycle length  $470 \text{ msec}$  (aggregate AK71) was stimulated with trains of 50 pulses of fixed period ( $T_s = 145 \text{ msec}$ ), but different stimulus intensities. In panels A to C respectively: A 2:1 locking, pulse amplitude  $\approx 18 \text{ nA}$ ; B 3:2 locking, stimulus intensity  $\approx 28 \text{ nA}$ ; C 1:1 locking, stimulus amplitude  $\approx 40 \text{ nA}$ . For a fixed rate of pacing, overdrive suppression is directly proportional to action potential frequency. For clarity, not all the pulses are shown.

#### 4.4.2 Overdrive suppression at different frequencies

During periodic stimulation, different coupling rhythms between the stimulus and the preparation can be observed by either changing stimulation intensity or stimulation frequency [75, 79, 186, 105]. In the range of 1:1 entrainment during periodic stimulation with  $T_s < T_0$ , there is overdrive suppression, where the increase in the magnitude of the slowing of the intrinsic rate is inversely proportional to the period of stimulation  $T_s$ . This is illustrated in Figure 4.5 which shows three tracings recorded from a 180  $\mu\text{m}$ , 7-day old atrial aggregate with control cycle length of 520 msec. The aggregate was stimulated for 50 stimuli at three different periods of stimulation: 145, 250 and 355 msec. In all three cases, there was stable 1:1 entrainment between the stimulator and the aggregate. After the drive, the first interbeat interval was prolonged by respectively 300%, 140% and 40% over control. Thus, the post-drive prolongation following a fixed number of stimuli increases as the period of stimulation decreases, provided there is a maintained constant rhythm.

An interesting property of the experimental preparation is that it can be entrained in 1:1 fashion to periodic depolarizing stimuli with  $T_s > T_0$ . However, this effect is much more difficult to observe than the 1:1 entrainment with  $T_s < T_0$  and could be measured in 4 preparations only, as illustrated in Figure 4.6. In these cases, following cessation of stimulation, the intrinsic rate is slightly elevated, an effect that has been called underdrive acceleration [173]. The importance of this effect is that it indicates a contribution of an electrogenic hyperpolarizing current even during control conditions, which is consistent with the theoretical model.

As the stimulation frequency increases, maintaining the stimulation intensity fixed, there is typically a critical stimulation frequency that sets the fastest rate at which 1:1 entrainment can be maintained [79, 186, 105]. In the 1:1 entrainment zone, the length of the first beat following the drive is inversely proportional to the period of pacing. At faster stimulation frequencies there are N:M rhythms with  $N > M$ , such as were shown in Figure 4.4 where the magnitude of the overdrive effect decreases as a consequence of the dropped beats. In all the preparations studied, this "peaking" phenomenon was related to sudden changes in action potential frequency resulting from the transition from N:M to N':M' phase locking with  $\frac{N'}{M'} \geq \frac{N}{M}$ . This is illustrated in panels A and B of Figure 4.7 which show the duration of the first beat following overdrive stimulation in a single aggregate at 2 different stim-

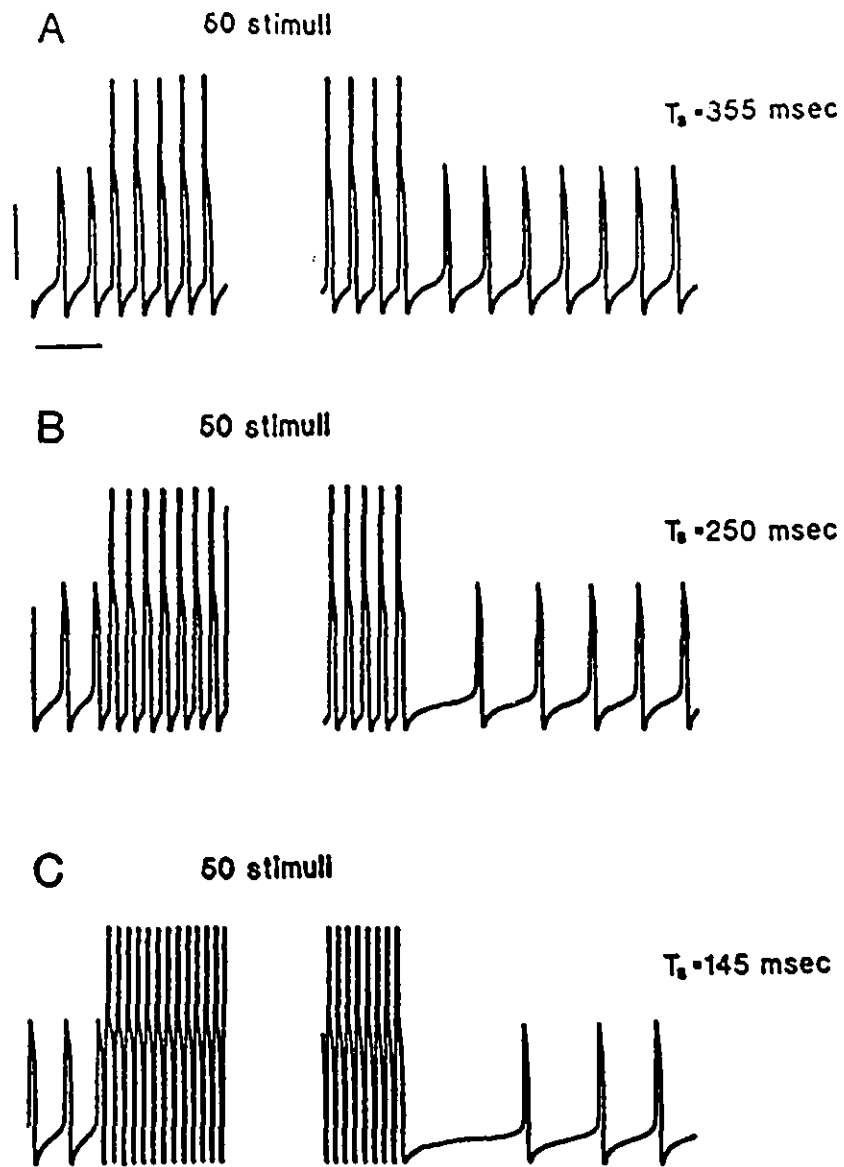


Figure 4.5: Dependence of overdrive suppression (1:1 entrainment) upon stimulation frequency. Tracings from a 180  $\mu\text{m}$ , 7-day old atrial aggregate with control cycle length of 470 msec (AK 71, same as in Figure 6). The aggregate was stimulated for 50 stimuli at three different periods of stimulation: 145, 250 and 355 msec, during which 1:1 locking was maintained during the stimulation. The pulse amplitude was fixed at  $\approx 40$  nA. The post-drive prolongation increases with the shorter periods of stimulation (higher action potential frequencies).

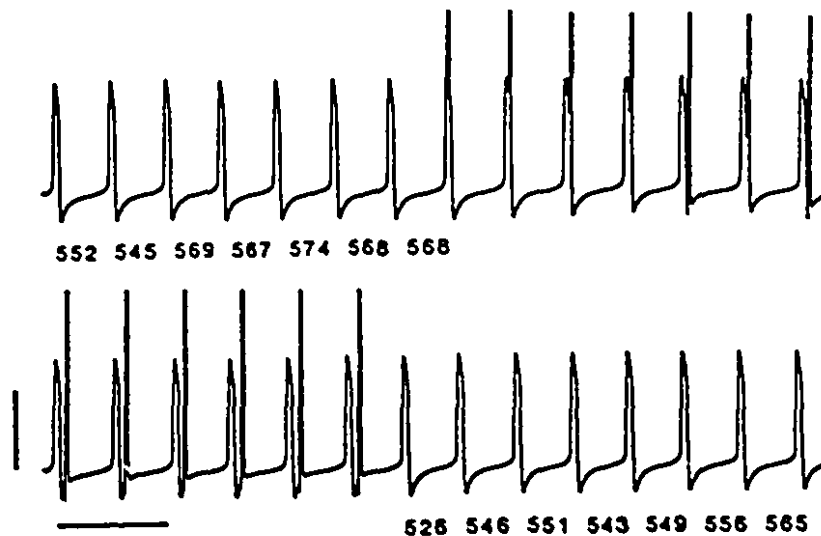


Figure 4.6: Periodic stimulation at a rate slower than the intrinsic frequency, but maintaining 1:1 locking, in a  $150\ \mu\text{m}$  atrial aggregate (AK 61) with a control cycle length of 560 msec. The top trace shows a sample of control activity prior to stimulation. In the bottom recording, the aggregate is stimulated in a 1:1 fashion using  $\approx 20\ \text{nA}$  pulses. The timing of the pulses is indicated by the off-scale vertical deflections. The stimulation period was 580 msec. The length of the successive interbeat intervals (in msec) after the pulse train is indicated below the experimental trace. Following the termination of stimulation there is a slight acceleration of the intrinsic rhythm, or underdrive acceleration (here about 6%), with a slow recovery to control. This effect shows that the electrogenic mechanism is active even under control conditions, which is in agreement with the theoretical model.

ulation intensities for 50 stimuli. At the higher stimulation intensity (right panel), the 1:1 entrainment was maintained for shorter stimulation periods ( $T_s/T_0 = 0.3$ ), whereas with the weaker stimulation intensity (left panel), the 1:1 entrainment was maintained until  $T_s/T_0 = 0.45$ . Panel C shows data in the same format superimposed for six different aggregates, including panels A and B, using different stimulus amplitudes. For each aggregate, the post-drive prolongation and the period of stimulation have been normalized to the respective control cycle length. For stimulation periods where 1:1 entrainment was found for all 6 aggregates, overdrive suppression, scaled to the intrinsic cycle length, was approximately the same independent of the preparation and the stimulus strength.

Figure 4.8 shows a composite picture of the first post overdrive cycle length following 50 stimuli as a function of the period of the stimulation, for 5 different aggregates (filled symbols), superimposed on the theoretical simulation (solid line). The measured time intervals are normalized to the control cycle length of the preparation. The parameters used in the numerical simulation were set for each aggregate according to the procedure described in the Appendix. The values used in the numerical simulation are presented in Table 4.1. In all 5 aggregates there is a similar dependence of overdrive suppression on the period of stimulation (scaled to intrinsic cycle length). This behavior is consistent with the numerical simulation of the theoretical model.

## 4.5 Discussion

In this study we have documented the effects of stimulation history on the overdrive suppression of spontaneous activity of chick atrial heart cell aggregates. The magnitude of overdrive suppression is, for a given entrainment pattern, proportional to the duration of the stimulation and inversely proportional to the period of stimulation. These findings are consistent with previous observations in chick heart cell aggregates [143, 186] as well as studies in a number of different preparations including Purkinje fibers in sheep [172, 173] and dog [172, 173, 66], sinoatrial node in rabbits [149, 150, 134], guinea pigs [74], and humans [101]. In chick heart cell aggregates and other preparations, very fast pacing may lead to a partial block of activity [79, 186]. Under such circumstances, for a fixed number of stimuli, overdrive

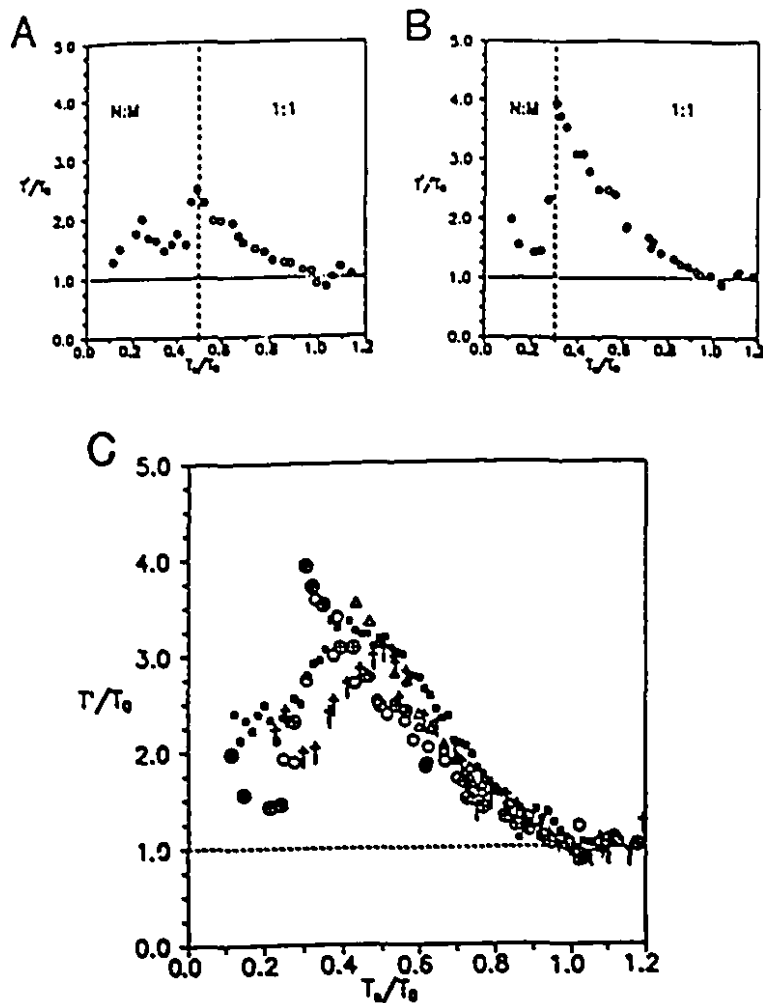


Figure 4.7: The duration of the first beat following overdrive stimulation in a single aggregate (panels A and B, aggregate AK 71) at 2 different stimulation intensities for 50 stimuli, and for 5 different aggregates (panel C), as a function of stimulus period. In panels A and B: at the higher stimulation intensity (right panel), the 1:1 entrainment was maintained for shorter stimulation periods ( $T_s/T_0 = 0.3$ ), whereas with the weaker stimulation intensity (panel A), the 1:1 entrainment was maintained until  $T_s/T_0 = 0.45$ . Panel C shows a composition of data from 5 different aggregates (AK34: crosses, AK36: closed squares, AK70: open triangles, AK71: crossed circles, AK78: open squares), with the post-drive prolongation and the period of stimulation normalized to the respective control cycle lengths. In the 1:1 entrainment region, the magnitude of overdrive suppression is not a function of amplitude of stimulation and is approximately the same for all preparations. The decrease in overdrive suppression observed at high stimulation frequencies corresponds to increasing degrees of block (lower action potential frequency) during stimulation.

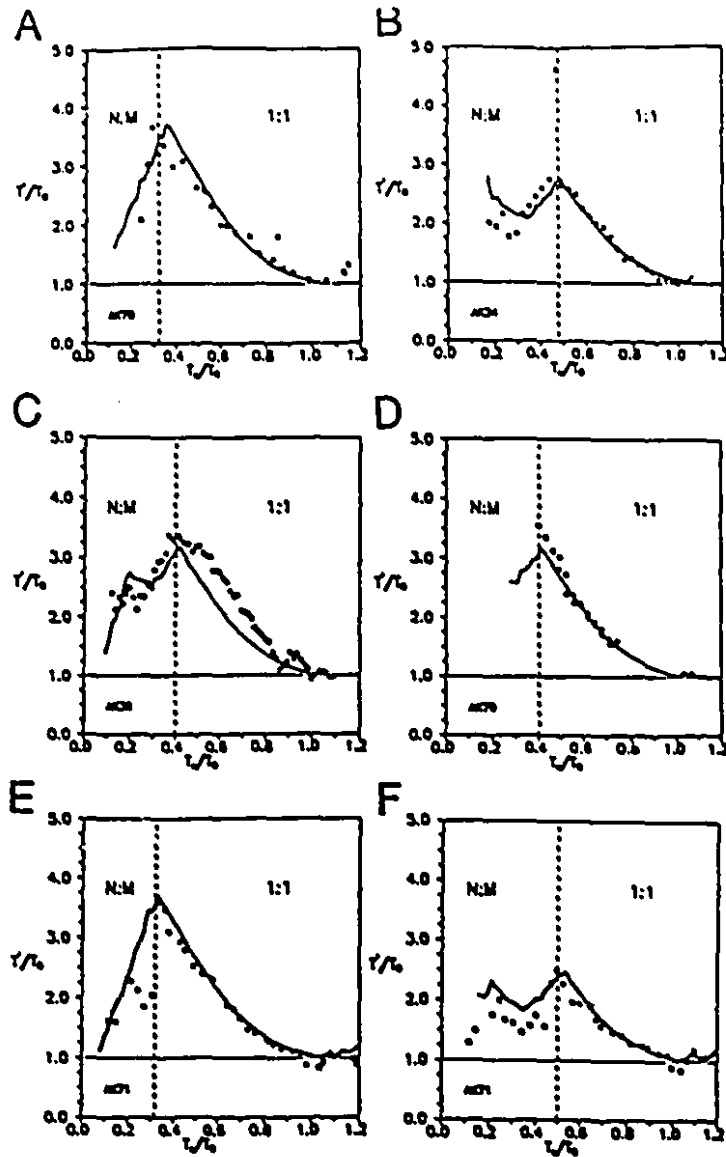


Figure 4.8: Composite picture of the first cycle length following 50 stimuli as a function of the period of the stimulation, for 5 different aggregates (filled symbols), superimposed on the theoretical simulation (solid line). The data shown in panels E and F was obtained from the same aggregate using two different stimulus amplitudes. The values of the parameters used in the simulations for each aggregate can be found in Table 4.1 using the identification code in the lower corner of each panel.

suppression decreases with increasing degree of block (i.e. lower action potential frequency). This is in agreement with the idea that the frequency of action potentials is the major determinant of the post-drive prolongation in the cycle length [172, 173].

The development of the theoretical model was motivated by a desire to present a relatively clear mathematical picture based on physiologically plausible assumptions and in reasonable agreement with qualitative experimental evidence. The formulation adopted in this paper offers several advantages: 1) the model is based on a two-dimensional approximation to the cardiac oscillator which is not preparation specific and may therefore be applicable to a wide class of biological systems; and 2) this comparatively simple model can represent a useful step towards the integration of an overdrive inducing mechanism in a high-dimensional ionic model since it captures most of the qualitative aspects of overdrive suppression in this preparation. Such a fully developed ionic model may be necessary to overcome some of the limitations imposed by the low-dimensional nature of the present formulation. For example, the apparent shortening of the action potential during overdrive (Figure 4.1) is due to the simple geometry of the strongly attracting limit cycle. In the model, the action potential corresponds to the downward branch of the limit cycle (see Appendix). Shorter action potentials arise when a strong stimulus is applied early during phase 4 causing the trajectory to join the downward branch of the limit cycle towards the end of the action potential. In view of this, given the relative simplicity of the theoretical model presented in this chapter, we believe that our assumptions concerning the major role of changes in slope of phase 4 in overdrive suppression in this preparation represent a valuable step towards understanding the determinants of overdrive suppression.

Another limitation of the model is its inadequacy in reproducing the experimentally observed phase-resetting behavior. The details of the phase-resetting depend on a complex interplay of several ionic currents [105] which are not expressed in the present model. Numerous ionic models exist which incorporate electrogenic currents [178] and can provide a platform for studying overdrive suppression. However, these models are often preparation specific, and are generally not very transparent. Thus, the present formalism provides a complementary approach to the modeling of cardiac activity simpler than traditional ionic models.

Overdrive suppression has been related to several mechanisms such as the stimulation of the sodium-potassium pump *via* an increased level of internal sodium

[143, 118, 36, 61, 41, 172, 173], accumulation of potassium outside the cells [106, 172], augmented uptake of calcium [134, 74], and the release of neuromediators [175]. In embryonic chick heart cells, overdrive suppression was found to be reduced by ouabain, an extracellular blocker of the Na/K pump [143, 118]. Since the Na/K pump plays a major role in overdrive suppression in chick heart cell aggregates, it is tempting to believe that, for this preparation, the theoretical model is a crude approximation to the mechanisms underlying the influx (fast sodium current) and the active transport (sodium pump) of sodium ions. A connection can be made between the model and the induction of overdrive suppression by assuming that the influx of cations  $Z$  which enters the cell during the upstroke phase of the action potential represents the influx of sodium ions. In order to maintain a constant beat-to-beat level of intracellular  $Z$ , this same quantity of ions  $Z$  is extruded *via* some  $Z$ -sensitive (Michaelis-Menten kinetics) electrogenic mechanism active during the entire cycle. Increased entry of cations  $Z$  during fast pacing (higher AP frequency) activates the electrogenic mechanism which in turn slows down diastolic depolarization, transiently suppressing automatic activity. Following the drive, the intracellular level of  $Z$  is gradually restored and the cycle length returns to control. After a fixed number of stimuli, the post-drive prolongation is longer for faster stimulation rates. Thus, the theoretical model is consistent with a wide body experimental results that has been accumulated over the past 25 years [172, 173, 101].

However, the theoretical model offers possibilities for other types of kinetic behaviors. For example, it appears that overdrive suppression generally saturates following stimulation of long duration [172, 74]. However, in the theoretical model whether or not the overdrive suppression saturates depends on the parameters for the kinetics of the inflow and extrusion of  $Z$ , as well as the frequency of stimulation. When very high frequency stimulation is applied, the influx of cations  $Z$  may exceed the extrusion capacity of the fully activated electrogenic mechanism. Under these conditions, provided that 1:1 entrainment can be maintained, the theoretical model predicts that post-drive prolongation would not saturate, and that there could be very long prolongations until activity resumed. This could be of potential clinical relevance in the setting of prolonged supraventricular tachycardia.

In order to be able to account for the overdrive suppression following a single premature AP, we must assume a very significant variation (up to 30%) in the level of  $Z$  during the cycle. The present theoretical model does not incorporate any

assumptions concerning the structure and the geometry of the intracellular space. Consequently, one may suppose that the large changes in the level of  $Z$  remain confined to a partition of the intracellular space which is available to the  $Z$ -sensitive electrogenic mechanism. In fact, in order to properly describe the sodium-calcium exchange in excitable cells, several authors suggest a hypothetical compartmentalization of the intracellular space available to incoming sodium ions [112, 22]. Although the existence of this “fuzzy space” remains unproven, it offers a possible explanation for the large changes in the level of  $Z$  we must assume in the theoretical model.

The current study may have implications in the study of rhythms observed in other systems. For example, sustained periodic stimulation at fast frequencies may induce “fatigue” in the AV node [13] and changes in the Purkinje fiber conduction properties [66], sometimes leading to a complex evolution of rhythms [167]. In patients undergoing the sinus node recovery test, an unusually long post-drive suppression of activity is often associated with sick sinus syndrome [101]. During this clinical test, as the frequency of the stimulation is increased, the post-drive pause reaches a maximum then diminishes [101]. The present study suggests that this “peaking” phenomenon may be related to changes in action potential frequency during periodic stimulation. However, the actual mechanisms responsible for overdrive suppression in the sino-atrial node may be very different from those in the atrial aggregates and there may be rate-dependent contributions from changes in neurohumoral factors [175], as well as changes in sinoatrial conduction during overdrive.

## 4.6 Appendix

### 4.6.1 The theoretical model

In the Appendix we provide technical details on the properties of the differential equation used to model the cardiac oscillator. The two-dimensional system of ordinary differential equations that is used to model the action potential in the absence of the hyperpolarizing current is based on a modified version of the van der Pol equation [170, 57], and is given by

$$\begin{aligned}\frac{dV}{dt} &= \frac{1}{\epsilon}(y - f(V)), \\ \frac{dy}{dt} &= \alpha(V),\end{aligned}\tag{4.2}$$

where  $f(V)$  and  $\alpha(V)$  are piecewise linear functions of  $V$ , and  $\epsilon$  is a positive constant. For  $0 < \epsilon \ll 1$ , this equation is taken as a prototypical example of a limit cycle oscillation with fast relaxation to the limit cycle. The parameters and functions in the equation were selected so that  $V(t)$  corresponds roughly to the experimentally observed transmembrane voltage. For the heart cell aggregates, we assume that

$$\begin{aligned} \frac{V}{20} + 4 & , \quad V \leq -60, \\ f(V) = -\frac{V}{80} + \frac{1}{4} & , \quad -60 < V < 20, \\ \frac{V}{20} - 1 & , \quad V \geq 20. \end{aligned}$$

and  $\alpha$  is a piecewise constant function of  $V$  such that

$$\alpha(V) = \begin{cases} \alpha_4 & , \quad V < 0, \\ -\alpha_{APD} & , \quad V \geq 0, \end{cases}$$

where  $\alpha_4$  and  $\alpha_{APD}$  are positive constants related to the duration of phase 4 (diastolic depolarization) and the action potential duration, respectively (see below).

A representation of the limit cycle in the  $V - y$  plane, *phase plane*, is shown in Figure 4.9A. The phase plane is divided into several regions corresponding to the phases of the cardiac cycle: the upstroke (Region I), the plateau of the action potential (Region II), and the repolarization (Region III), diastolic depolarization (Region IV). The solid line represents the  $V$  nullcline, *i.e.* the set of points such that  $\frac{dV}{dt} = 0$ . The dotted line shows the trajectory of a phase point as it travels on the limit cycle. Provided  $0 < \epsilon \ll 1$ , (we will assume in what follows that  $\epsilon = 25000^{-1}$ ) the cycle can be divided into 2 phases, the action potential and phase 4. The durations of the action potential,  $t_{APD}$ , and phase 4,  $t_4$ , and can be found by direct integration of equation 2. The duration of phase 4 is the length of time for  $y$  to increase from 0 to 1. Since  $dy/dt = 1/\alpha_4$  during phase 4, we immediately find

$$t_4 = \frac{1}{\alpha_4}.$$

Similarly,

$$t_{APD} = \frac{1}{\alpha_{APD}}.$$

The relationship between  $\alpha_4$ ,  $\alpha_{APD}$  and the  $V$  variable is summarized in Panel B of Figure 4.9. An example of an action potential generated by this equation is shown

in Figure 4.9C. In numerical simulations, the model is driven by periodically adding a positive (depolarizing stimulus) constant to the  $V$  variable. Since the limit cycle is strongly attracting, high amplitude stimulation at an early phase of the cycle may elicit a premature action potential with shortened duration (see Figures 4.1 and 4.2). Although this is inconsistent with experimentally measured behaviour, it is observed that changes in action potential duration play a negligible role in overdrive suppression in this preparation [186].

In the presence of the hyperpolarizing current associated with  $Z$  the dynamics are given by Equation (4.1) in the text which is repeated here for completeness, with the substitution  $g(Z) = \frac{Z}{Z+k}$

$$\begin{aligned}\frac{dV}{dt} &= \frac{1}{\epsilon}(y - f(V)), \\ \frac{dy}{dt} &= \alpha(V) - \beta g(Z), \\ \frac{dZ}{dt} &= -\gamma g(Z) + \Delta Z \delta(t - t_{AP}),\end{aligned}\tag{4.3}$$

where  $\beta$ ,  $\gamma$ , and  $\Delta Z$  are positive constants, and  $t_{AP}$  is the time of the onset of the action potential. We assume that the removal of  $Z$  follows Michaelis-Menten kinetics so that  $g(Z) = \frac{Z}{Z+k}$ , where  $k$  is a parameter that sets the scale of  $Z$ . As before, simulation of stimulation is carried out by adding a positive (depolarizing) constant to the  $V$  variable. We associate the start of the action potential with the time when the trajectory crosses the line  $f(V) = -\frac{V}{80} + \frac{1}{4}$  while  $V$  increases.

#### 4.6.2 Analysis of the theoretical model

For each aggregate it is necessary to specify 6 parameters:  $\alpha_4, \alpha_{APD}, \beta, \gamma, \Delta Z, k$ . We briefly give our strategy for determining the values of these parameters, and then give the details.

One of the experimental findings is that the slope of phase 4 following overdrive suppression may be quite small but is never negative. In the context of the theoretical model this means that  $\beta = \alpha_4$ , so that with maximum overdrive the slope of phase 4 approaches 0. The parameter  $k$  is used to set the scale of  $Z$ , so it is arbitrary. In the computations we will express the concentrations of  $Z$  in units of  $k$ . The parameters  $\alpha_4, \alpha_{APD}$  are related to the duration of phase 4 and the action potential duration,

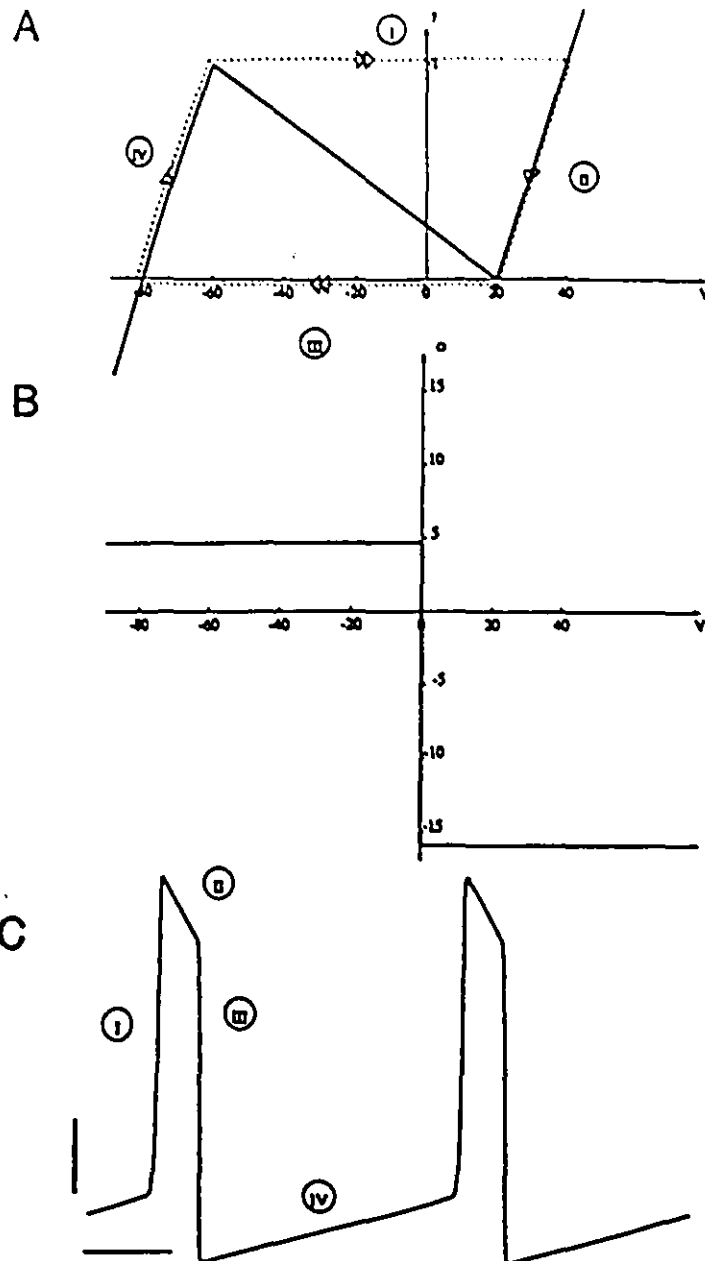


Figure 4.9: The geometry of the functions  $f(V)$  and  $\alpha(V)$  in equation (4.3) assuming that  $Z$  is fixed at 0, and  $\epsilon \ll 1$ . The  $V - y$  phase plane is shown in panel A. The solid line is the nullcline (i.e. the set of points such that  $\frac{dV}{dt} = 0$ ) and corresponds to the function  $f(V)$  in the text. The dashed line is an approximate sketch of the limit cycle, with various regions associated with the phases of the action potential. In panel B: a geometrical representation of the discontinuous function  $\alpha(V)$ . In regions II and IV of the phase plane the value of  $\alpha(V)$  is directly proportional to  $\frac{dV}{dt}$ . Panel C shows the result of the corresponding simulation of  $V(t)$ . The different phases of the action potential are indicated. Exceptionally, in this figure, the horizontal calibration bar indicates 100 msec and the vertical calibration bar shows 20 mV.

respectively, using relations we give below, and are computed from measured values of these phases of the action potential appropriately modified by the effects of the overdrive term under control conditions. This only leaves 2 parameters,  $\gamma$  and  $\Delta Z$ . We derive expressions that relate these 2 parameters to the cycle length at control ( $T_0$ ), the cycle length that is found in the cycle following a cycle induced by a stimulus delivered at phase  $\phi$  during phase 4 ( $T'(\phi)$ ), and the mean value of  $Z$  during a control cycle, ( $\bar{Z}_0$ ).

For the computations that follow, in which it is necessary to compute the duration of various phases of the cycle, it is convenient to approximate the function  $g(Z)$  by its mean value during a cycle. The justification for this approximation is based on the power series expansion around the mean value  $\bar{Z}$  during the cycle. We find that

$$g(Z) = \frac{\bar{Z}}{Z+k} + \frac{k}{(Z+k)^2}(Z-\bar{Z}) + \dots$$

Comparison of the magnitudes of the first terms shows that the first order term is at least ten times smaller than the zeroth order term as long as  $|Z - \bar{Z}|$  is less than  $0.4 k$ . Under control conditions or following a single premature AP, the changes in the level of  $Z$  are at most of the order of  $0.5 k$  for all the aggregates studied (see Table 4.1 and Figure 4.2 in text). During the cycle, we can therefore approximate the function  $g(Z(t))$  by

$$g(\bar{Z}) = \frac{\bar{Z}}{\bar{Z}+k}. \quad (4.4)$$

The duration of phase 4 (diastolic depolarization),  $t_4$ , can be calculated from the above equations. The duration of phase 4 is determined by the integral

$$1 = \int_0^{t_4} dy = \int_0^{t_4} ds(\alpha_4 - \alpha_4 g(Z(s))).$$

Since at the end of phase 4 we have  $y(t)=1$ , the duration of phase 4 can be approximated

$$t_4 = \frac{1}{\alpha_4 - \alpha_4 g(\bar{Z})}. \quad (4.5)$$

A similar expression can also be obtained for the action potential duration

$$APD = \frac{1}{\alpha_{APD} + \alpha_4 g(\bar{Z})}. \quad (4.6)$$

The expressions for the effects of overdrive stimulation of the heart cell aggregates are in qualitative agreement with experimental observations, the duration of phase

4 increases while the action potential duration decreases. However, since  $\alpha_{APD}$  is approximately twice the magnitude of  $\alpha_4$  (see Table 1), the effect of overdrive on the action potential duration (after the drive) is small compared to the effect on the duration of phase 4. Consequently, to facilitate computations, in the estimation of parameters we will assume that the action potential duration is constant so that under control conditions, the cycle length is

$$T_0 = APD + \frac{1}{\alpha_4 - \alpha_4 g(Z_0)}. \quad (4.7)$$

We now consider the effect of a single stimulus on the cycle length delivered at a phase  $\phi$  during phase 4 of a control cycle that induces an action potential. The period of the cycle following the stimulus is  $T'$  and the mean value of  $Z$  during the cycle is  $\bar{Z}$ . Since the resulting perturbation in the cycle length is small (experimentally measured: about 7% on average for  $\phi = 0.5$ ), we obtain (see Figure 4.2A in text)

$$\bar{Z} = \bar{Z}_0 + \Delta Z(1 - \phi). \quad (4.8)$$

From equation (4.5) we now find

$$\frac{T' - APD}{T_0 - APD} = \frac{\alpha_4 - \alpha_4 g(\bar{Z}_0)}{\alpha_4 - \alpha_4 g(\bar{Z})} = \frac{\bar{Z} + k}{Z_0 + k}. \quad (4.9)$$

Substituting for  $\bar{Z}$  from equation (4.8) into equation (4.9), and solving for  $\Delta Z$ , we find,

$$\Delta Z = \left( \frac{T' - APD}{T_0 - APD} - 1 \right) \left( \frac{\bar{Z}_0 + k}{1 - \phi} \right). \quad (4.10)$$

Under control conditions, the influx of cations,  $\Delta Z$  that enter during the action potential must balance the ions removed by the electrogenic pump. Consequently, from equation (4.3) we find

$$\gamma g(\bar{Z}_0) T_0 = \Delta Z. \quad (4.11)$$

Approximating  $g(\bar{Z}_0)$  from equation (4) and solving for  $\gamma$  we obtain

$$\gamma = \frac{\Delta Z (\bar{Z}_0 + k)}{Z_0 T_0}. \quad (4.12)$$

To summarize the procedure used to set the parameters: we first use Equation (4.5) to obtain  $\alpha_4$  from the experimentally measured duration of phase 4 (at control),  $t_4 = T_0 - APD$ . Equation (4.6) and the experimentally measured APD are then used to compute  $\alpha_{APD}$  as a function of  $\bar{Z}_0$ . In the next step, by means of Equation

Table 4.1: Summary of the parameters used in the numerical simulations.

aggregate	$T_0$ , APD (msec)	$T'(\phi = 0.5)/T_0$	$\alpha_4, \alpha_{APD}$ ( $\text{sec}^{-1}$ )	$\Delta Z$ ( $k$ )	$\gamma$ ( $k.\text{sec}^{-1}$ )	stim. amplitude
AK71	520, 80	1.07	5.68, 9.09	0.41	1.33	90 and 100
AK78	620, 85	1.08	4.67, 8.96	0.46	1.25	100
AK70	620, 100	1.07	4.81, 7.11	0.42	1.12	97
AK34	470, 65	1.07	6.17, 11.68	0.41	1.44	93
AK36	640, 100	1.07	4.63, 7.22	0.41	1.08	97
AK61	540, 80	1.07	5.43, 9.24	0.41	1.27	120

(4.10), we compute  $\Delta Z$  from the perturbed cycle length following a premature AP elicited at phase  $\phi$ . Finally we calculate  $\gamma$  using the steady state condition (4.12). Therefore, both the degree of post-drive prolongation and the rate of the subsequent decay to control cycle length are controlled by a single parameter ( $T'$ ) determined from single pulse experiments which suggests that the kinetics of dissipation of overdrive suppression are mainly governed by a steady state condition for beat to beat variations in the level of  $Z$  (Equation (4.11)).

All of the above parameters are a function of  $\bar{Z}_0$ . Since we have no direct way of measuring  $\bar{Z}_0$  for each aggregate, we used the following method. A complete set of parameters was calculated for several values of  $\bar{Z}_0$ . For each value of  $\bar{Z}_0$ , the model was simulated to obtain a graph of overdrive suppression at different frequencies of stimulation. The resulting family of curves was superimposed on the corresponding experimental data as shown in Figure 4.10. For  $\bar{Z}_0$  between 1.25  $k$  and 1.75  $k$ , there is good agreement between numerical simulation and experiment. Since qualitative aspects of overdrive suppression at different frequencies (in the 1:1 entrainment zone) are similar in all preparations (Figure 4.7), an average value of  $\bar{Z}_0 = 1.50 k$  was assumed for all the experiments considered.

Finally, the amplitude of the stimulus employed in the numerical simulation was adjusted by matching the range of the 1:1 entrainment zone in the numerical simulation with the corresponding experimental results.

The values of the different parameters are summarized in Table 4.1.

The simple geometry of the limit cycle and the mode of action of the time-dependent component which affects the  $y$  variable but not  $V$  (Equation 4.1) is re-

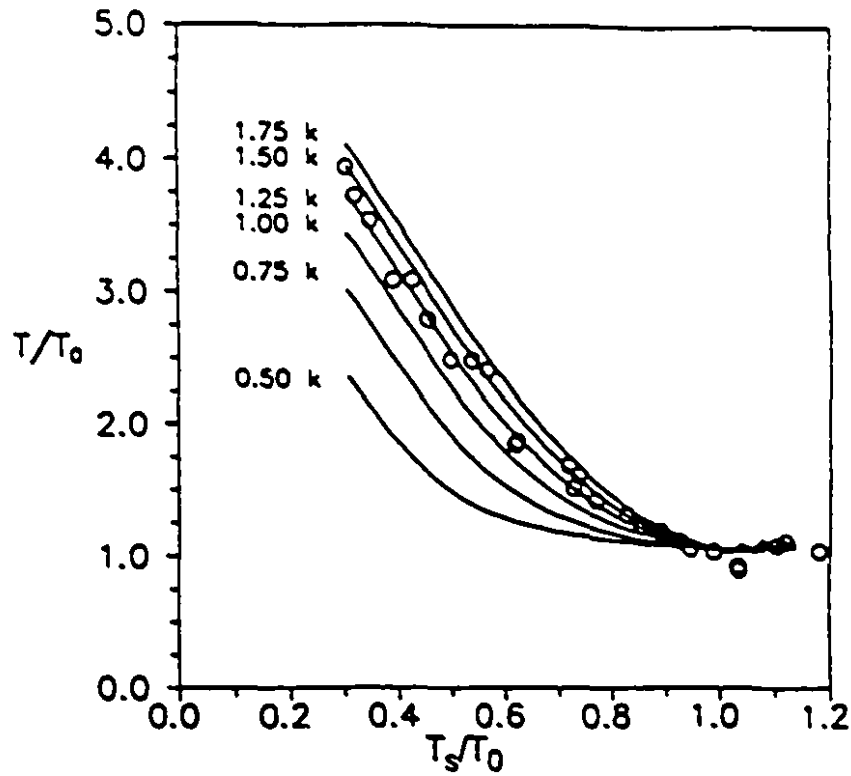


Figure 4.10: Figure showing the procedure to determine the value of the parameter  $\bar{Z}_0$  (average control level of  $Z$ ). The open circles show typical experimental data for overdrive suppression at different periods of stimulation (aggregate AK71), normalized to the control cycle length. The results of the corresponding simulation using 6 different values of  $\bar{Z}_0$  (as indicated in the left part of the figure, in units of  $k$ ) are shown as the solid lines. For  $\bar{Z}_0$  between  $1.25 k$  and  $1.75 k$ , there is good agreement with the experimental data. The average value of  $\bar{Z}_0 = 1.50 k$  was therefore retained.

sponsible for the lack of effect of the hyperpolarizing current on MDP in the numerical simulations. Indeed, such a hyperpolarization of MDP is sometimes observed during prolonged (longer than 1 min. at 3Hz) overdrive in spontaneously beating embryonic chick heart cell aggregates [143] and may contribute to the post-drive pause. Because of the short (typically less than 30 sec) duration of the drives used in our experimental protocols as well as the low value of membrane resistance at MDP, only a small effect of overdrive on MDP would be expected. This may explain the apparent lack of hyperpolarization of MDP observed in our overdrive protocols. In the context of the present theoretical model, such overdrive induced changes in MDP could potentially be incorporated by letting the geometry of the limit cycle itself be influenced by increased action potential frequency. However, in view of the small magnitude of hyperpolarization observed in our experiments, such modifications are not warranted at the present time.

## Chapter 5

# Overdrive suppression and phase resetting in a model for paroxysmal tachycardias

### 5.1 Foreword

Tachycardias are a leading cause of patient mortality and morbidity. A comparatively infrequent, but nevertheless important class of arrhythmias are incessant or repetitive paroxysmal tachycardias. [140] Such tachycardias can be supraventricular [18, 107, 39] or ventricular [40, 114], and are characterized by their sudden onset and offset. At least two mechanisms might underly the generation of these arrhythmias. The tachycardia could be set by the rhythm of rapidly bursting spontaneous cells. Alternatively, the arrhythmia can be due to physiological properties of the tissue composing the reentrant pathways (circuits followed by the reentrant excitation), as proposed for some supraventricular tachycardias [107]. In the current paper, we examine an experimental model for paroxysmal tachycardias generated by a reentry mechanism that reproduces many of the qualitative features of these arrhythmias. We develop a simple nonlinear model, based on the interaction between overdrive suppression and the excitability of the preparation, described in terms of difference equations. We also propose a modified version of the Shrier-Clay ionic model of electrical activity that includes a simplified sodium pump term. The results of the computer simulations are in good accord with experimental findings.

The experimental model consists of spontaneously beating aggregates of embryonic chick atrial heart cells. Under the experimental conditions, this preparation

beats with a regular rhythm [75, 78, 79, 105, 111]. The reentry loop is modeled by introducing an artificial electronic delay after which the pacemaker receives a stimulus. This fixed delay and the intensity of the stimulus can be experimentally modified. This preparation is similar to experimental models of atrial pathways in which atria are stimulated at a fixed delay following ventricular activation [163, 153, 13, 166]. In the current case, the stimuli shift the membrane potential thereby influencing the ionic mechanisms of the preparation. A previous publication from our group [185] contained preliminary observations that rhythms consisting of bursts of excitation could be observed for certain values of the delay. However, this effect was not studied systematically and a detailed mechanism for the bursting behavior was not proposed.

In the present manuscript, we characterize the dynamics observed for a variety of different delays. We show that in order to understand these rhythms it is necessary to understand the interactions between two different phenomena: the phase resetting of the spontaneous oscillations [79, 105] and the development of overdrive suppression during fast drive [186, 111]. The complex bursting patterns that are observed emerge naturally from a consideration of the interplay of these factors.

## 5.2 Experimental protocols

Experiments were carried out on 10 different preparations. During each experiment, three different protocols were executed:

### 5.2.1 Fixed delay stimulation

20 msec depolarizing current pulses were delivered at a fixed time delay following the upstroke of every action potential. The duration of the protocol was between 90 and 300 seconds. After a rest period of 30 seconds to allow the cycle length to return to control, the protocol was repeated at increasingly shorter delays and for several different amplitudes of the stimulus.

### 5.2.2 Phase resetting

The phase resetting curve, PRC, describes the perturbation in the cycle length due to a single depolarizing stimuli as a function of the phase of the stimuli. Call the intrinsic period of the oscillator  $T_0$ . The coupling interval of a stimulus,  $t_s$ , is the time interval from the start of the preceding action potential to the stimulus. The phase of the stimulus,  $\phi$  is defined by  $\phi = \frac{t_s}{T_0}$ , see Figure 5.1A. Note that the upstroke of the action potential is defined to have zero phase. For a given amplitude of stimulation, the PRC is obtained by applying single depolarizing stimuli of 20 msec duration at increasing coupling intervals after the last upstroke of an action potential, every 10 action potentials. The perturbed cycle length is the time interval from the upstroke of the last spontaneous AP before the stimulus to the upstroke of the first AP after the current pulse. The PRC is a plot of the perturbed cycle length, normalized to control, as a function of the phase  $\phi$ .

### 5.2.3 Overdrive suppression

The aggregates were stimulated using different drive durations. Trains of 2,4,6,8,15,30,50 and 100 stimuli were applied, separated by time intervals of approximately 30 seconds to allow the cycle length to return to control. The period of the stimulation was about 60% of the control cycle length and 1:1 entrainment between the stimulator and the preparation was always maintained. A representative voltage trace obtained during overdrive stimulation is shown in Fig 5.1B to illustrate this procedure. Spontaneous AP's appear on the left, followed by a train of 50 depolarizing stimuli (for clarity, not all are shown). Cessation of stimulation was followed by a transient decrease of the intrinsic frequency of the preparation: the first interbeat interval following the drive was 170 % of  $T_0$ . The intrinsic cycle length following the stimulation is denoted by  $T'$  which gradually returns to  $T_0$ . An experiment is represented by plotting the normalized interbeat intervals  $\frac{T'}{T_0}$  as a function of time on a single graph.

## 5.3 Theoretical modeling

Two different types of theoretical model were employed in this work. The first is a simplified nonlinear dynamical model similar to models used previously in related

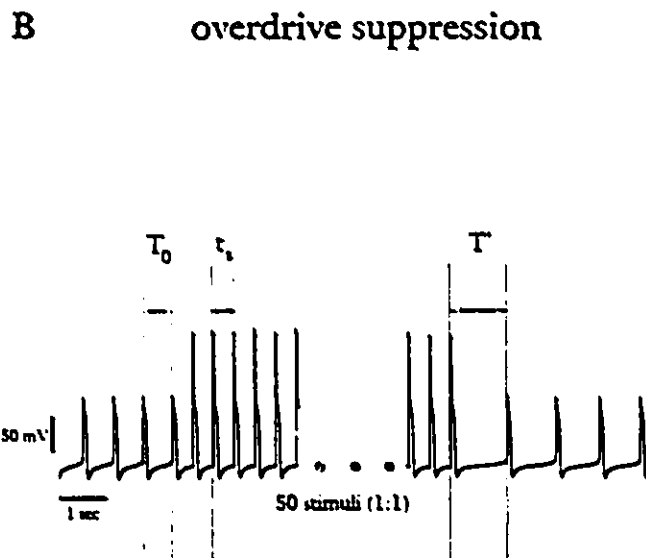
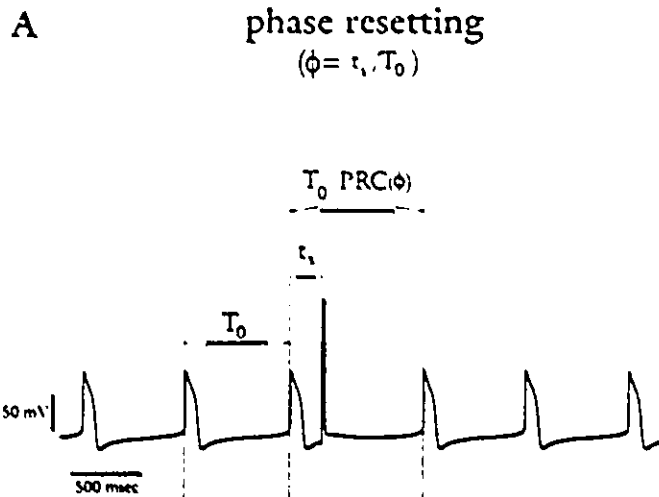


Figure 5.1: Phase resetting and overdrive suppression protocols in embryonic chick heart cell aggregates. Panel A: illustration of phase resetting protocol. Single depolarizing stimuli are injected every 10 spontaneous AP's, for increasing values of  $\tau_s$ . The perturbed cycle length normalized to control ( $T_0$ ) is measured as a function of the phase  $\phi = \frac{\tau_s}{T_0}$ . Panel B: Overdrive suppression. The spontaneously beating aggregate is periodically stimulated at a rapid rate ( $0.6 T_0$ ), in 1:1 entrainment. A transient decrease in the intrinsic firing frequency (overdrive suppression) is observed at the end of the drive.

contexts [26, 111, 186]. This model accounts in a qualitative way for the interaction of overdrive and phase resetting in the context of fixed delay stimulation. Although this style of theoretical model gives insight into the dynamics, it is not adequate to deal with the ionic mechanisms. The nonlinear model is presented in the results section.

In order to account for the ionic mechanisms in this system, we employ the Shrier-Clay ionic model for embryonic chick atrial heart cell aggregates [105]. The ionic model needs to be modified to account for overdrive suppression by including a simplified electrogenic sodium pump term. The present model consists of 6 components, namely:  $I_{Na}$ , the fast inward sodium current responsible for the rapid upstroke of the action potential;  $I_{Ca}$ , the calcium current responsible for the final part of the upstroke and (primarily) for keeping membrane depolarization throughout the plateau phase of the action potential;  $I_{Ks}$ , the time dependent outward current which underlies the initial repolarization at the end of the plateau phase of the action potential;  $I_{Kr}$ , the time dependent inwardly rectifying outward current involved in the later phase of repolarization;  $I_b$ , a three-component background current which underlies depolarization during phase 4 of the cardiac cycle; and  $I_p$ , a simplified hyperpolarizing voltage independent sodium pump term, with a 3:2 ( $Na^+ : K^+$ ) stoichiometry, which depends on the internal sodium concentration following Michaelis-Menten kinetics and is responsible for overdrive suppression. Further details concerning the kinetics of the first five components and the applicability of the original ionic model to experimental work can be found in Reference [105]. The details of the modified ionic model are given in Appendix A.

## 5.4 Experimental results

### 5.4.1 Fixed delay stimulation

During fixed delay stimulation, current pulses are injected at a constant time interval following each action potential. Figure 5.2 illustrates typical behavior observed during fixed delay stimulation for several values of the delay  $\delta$ . The data was obtained from a 120  $\mu\text{m}$  embryonic chick heart cell aggregate (control cycle length  $T_0 = 760$  msec); the stimulus intensity was 24 nA. In each panel of Figure 5.2, we show: (a)

a 12 second representative voltage trace showing the typical rhythm found for that value of the delay (left panels, the stimuli appear as the off-scale deflections); (b) a graph of the evolution of the interbeat intervals before, during and after stimulation, the beginning and the end of the drive are indicated by solid arrows (right panels, the dashed horizontal line corresponds to the control cycle length). The length of the delay decreases from A to F. For the longest delays (A to D) series of premature action potentials are interrupted by prolonged cycles ("bursting behavior"). The average number of action potentials per burst as well as the duration of the pauses separating the sequences decrease as the delay is shortened. In Panel A (delay = 400 msec), there is a sequence of 45 premature action potentials before failure of excitation occurs. This pattern roughly repeats itself, as shown in the graph on the right (IBI vs time), during the latter part of the protocol. During each bursting sequence, the interbeat intervals are shortest at the beginning of the sequence, then gradually increase until the sequence ends. In some instances, an oscillation in the interbeat intervals is observed before loss of entrainment. The first sequence at the beginning of the drive is usually the longest. Its termination is often associated with the emergence of a relatively stable bursting pattern. Cessation of stimulation is followed by a marked prolongation in the intrinsic cycle length (overdrive suppression [173], i.e. a transient decrease in the intrinsic firing rate following sustained stimulation at a frequency faster than control). The duration of the first interbeat interval after the drive is comparable to the length of the pause separating successive burst sequences towards the end of the drive. In panel A, the first cycle length following the drive is about 280% of the control cycle length.

The number of action potentials (AP's) per burst sequence is directly proportional to the delay. Accordingly, for delays somewhat longer than 410 msec, 1:1 entrainment could be maintained without occasional failed excitations (not shown). At a delay of 410 msec, the typical number of action potentials per sequence was 20 to 35 (apart from the much longer initial sequence). At a delay of 360 msec (Panel B), 6 to 10 AP's per burst can be seen. In Panel C (delay = 310 msec), there are only 4 to 6 AP's per burst. Finally, in Panel D, the bursting sequences are short (2 to 4 AP's). Although the frequency of stimulation during bursting is now higher, the post-drive pause is shorter, due to lower average action potential frequency [111]. At intermediate delays, other bursting sequences can indeed be found.

In Panel E (delay of 220 sec), there are doublets of action potentials as well as

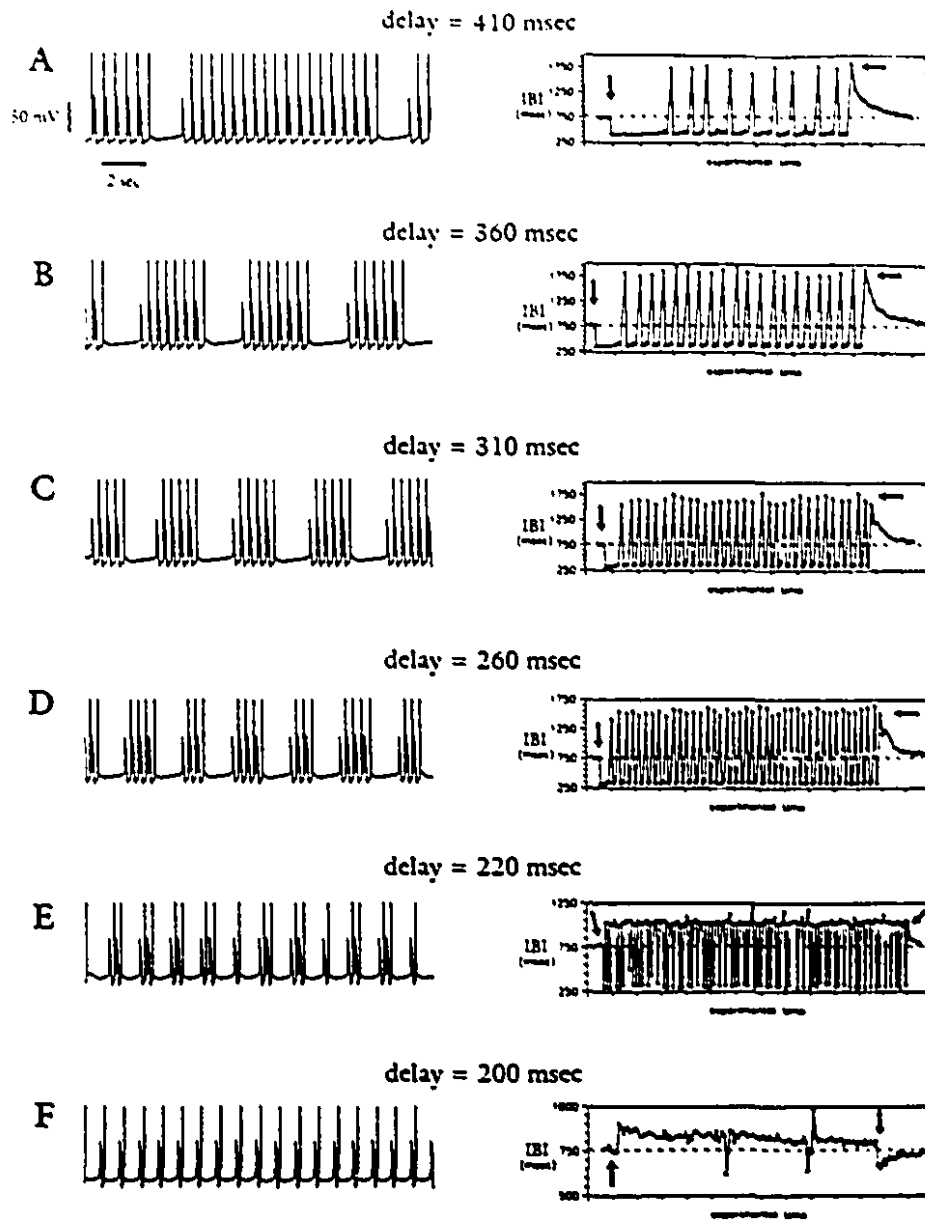


Figure 5.2: Fixed delay stimulation in a 180  $\mu\text{m}$  embryonic chick heart cell aggregate, for several values of the delay. In each panel, left: 12 seconds voltage trace; right: graph of the interbeat intervals as a function of time, corresponding to the entire protocol. The ticks on the horizontal axis are 10 seconds apart. The dashed line corresponds to control cycle length (760 msec). The arrows indicate the beginning and the end of the protocol. The stimuli appear as the off-scale deflections. Stimulus amplitude: 24 nA.

delayed action potentials. For this value of the delay, stimuli fall close to the refractory period of the preparation resulting in either delayed or premature AP's. In Panel F, the delay is too short (200 msec) for the stimuli to consistently evoke premature action potentials; almost all the AP's are delayed. As the drive progresses, the interbeat intervals decrease. In addition, following cessation of stimulation there is a progressive increase in the cycle length back to the control levels (underdrive acceleration). We show later that a single unified mechanism can account for underdrive acceleration as well as overdrive suppression.

The dependence of the number of action potentials per burst upon the time delay is summarized in Figure 5.3. In this figure,  $n$  (symbol) is the number of AP's in the initial (transient) burst while  $m$  is calculated as the average number of AP's per sequence during the last 30 seconds of the protocol. We assume that  $m$  approximates the number of AP's per burst under steady state overdrive conditions.  $n$  and  $m$  are increasing functions of the delay. 1:1 entrainment is found for delays greater than 460 msec ( $n$  and  $m$  are infinite). In general,  $m$  is significantly smaller than  $n$ . These experimentally measured values of  $n$  and  $m$  as a function of the delay can be used to help set the parameters in the nonlinear theoretical model (see below and Appendix B).

Fixed delay stimulation often results in the onset of irregular rhythms. In particular, the number of AP's per burst can vary considerably throughout the fixed delay protocol. For example, in Figure 5.2D, sequences of 2 to 4 AP's are intermixed. A more striking example of an irregular rhythm is illustrated in Figure 5.4, for a 150  $\mu\text{m}$  aggregate ( $T_0 = 580$  msec) with a delay of 180 msec. The stimulus amplitude was 30 nA. A 64 seconds voltage trace is shown in Panel A (each segment corresponds to 16 seconds). 6 spontaneous AP's appear at the beginning of the trace. Immediately following the onset of fixed delay stimulation, short bursts alternate with pairs of slightly delayed AP's. Subsequently, delayed action potentials predominate (end of second and beginning of third segments) until a pattern analogous to the beginning of the trace reemerges. The irregularity of the rhythm is even more apparent in Panel B, which shows the evolution of the interbeat intervals during the drive. Slight overdrive suppression is observed at the end of the drive. Other irregular traces (as well as rhythms similar to those described in the previous figure) were found in all the aggregates in this study at several stimulus intensities.

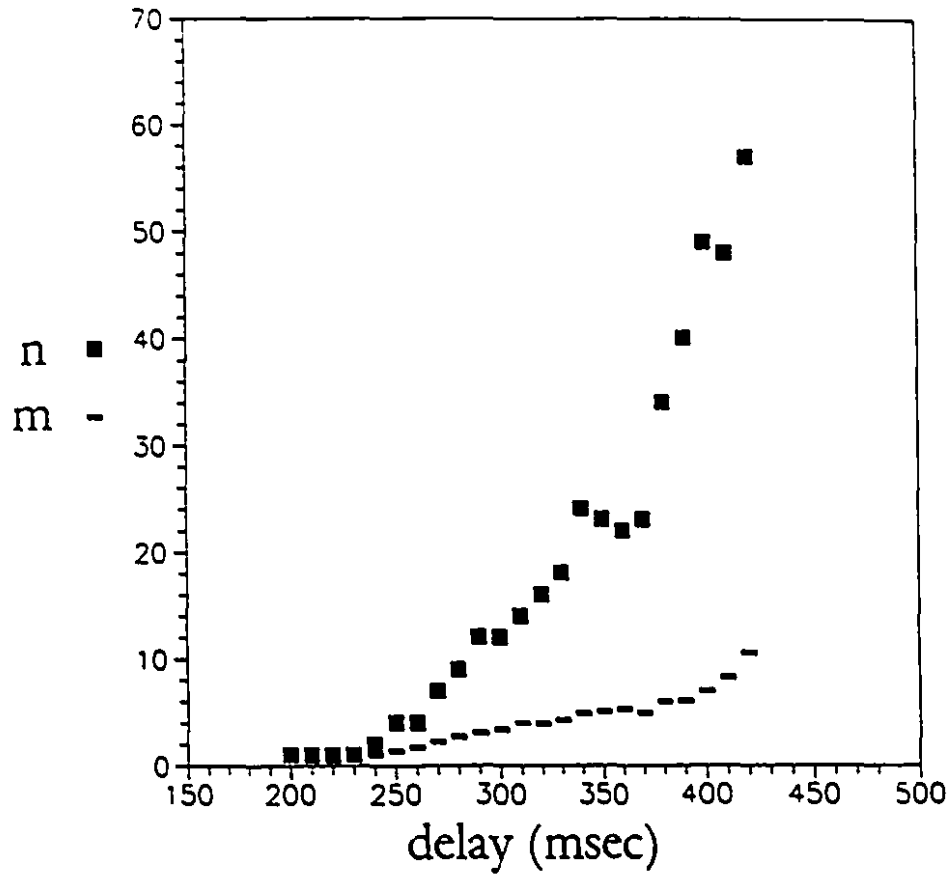


Figure 5.3: Dependence of the number of AP's in the initial sequence ( $n$ , symbol) and under steady-state overdrive conditions ( $m$ , symbol, average over 30 last seconds of protocol) upon the delay, for the data presented in Figure 6.2.

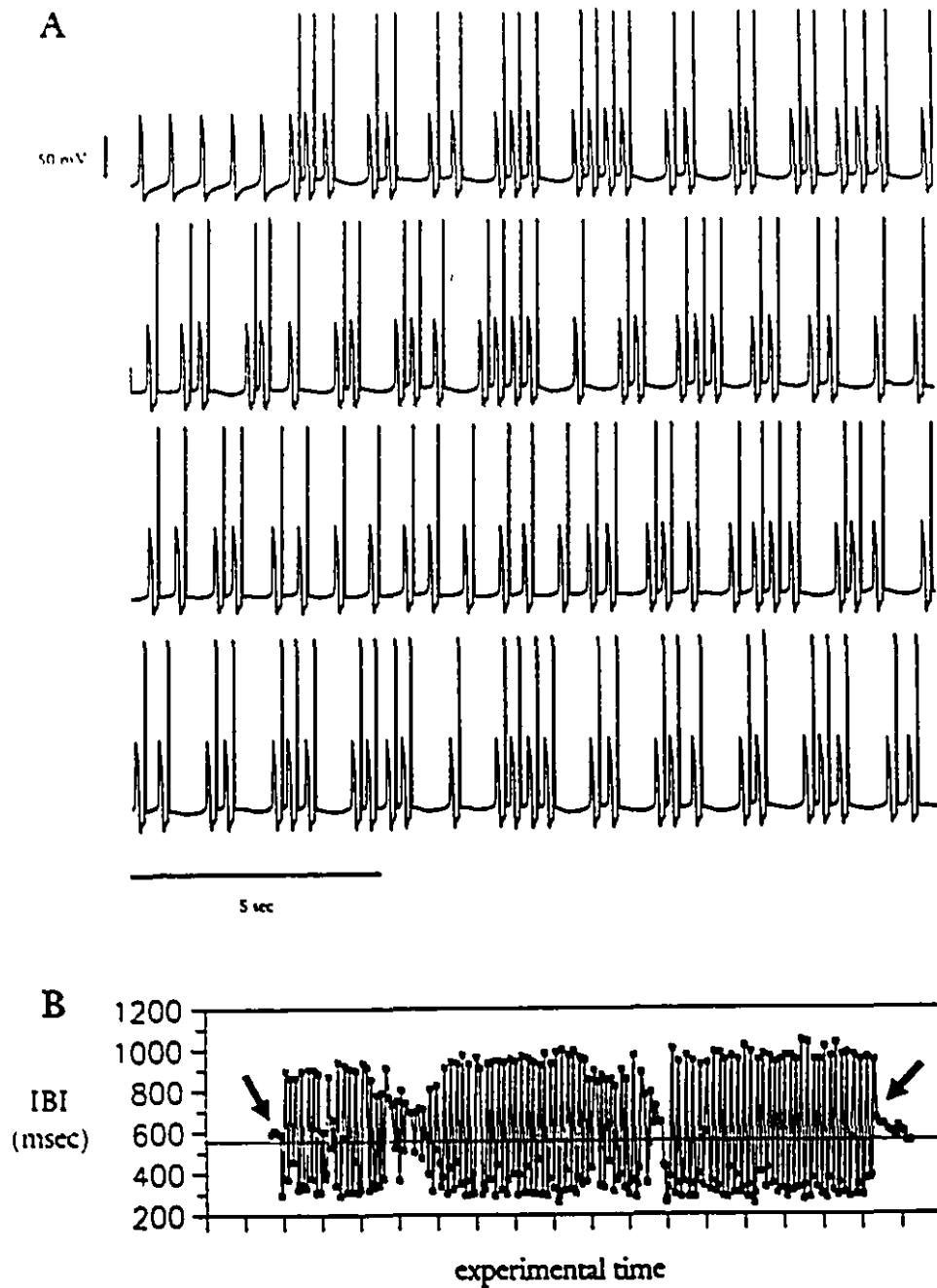


Figure 5.4: Irregular rhythms during fixed delay stimulation. The aggregate was  $150 \mu\text{m}$  in diameter ( $T_0 = 580 \text{ msec}$ , stimulus amplitude =  $30 \text{ nA}$ ). Panel A: 64 second voltage trace presented in 4 segments, during fixed delay stimulation. The delay was  $180 \text{ msec}$ . 6 spontaneous AP's appear at the beginning of the trace. The stimuli appear as the off-scale deflections. Note the irregular rhythm. Panel B: evolution of the interbeat intervals versus time throughout the entire protocol. The ticks on the horizontal axis are 10 seconds apart.

### 5.4.2 Phase resetting

The response of biological oscillators to an isolated stimulus depends upon the phase at which the stimulus was injected and the intensity of the stimulus [181, 70, 184, 78, 79]. The results in these experiments were similar to those in previous studies. Since the PRC is essential in interpretation of the rhythms during fixed delay stimulation we show a representative tracing.

Figure 5.5A shows a PRC obtained for the same aggregate as in Figures 5.1 and 5.2 and for the same stimulus intensity of 24 nA. Stimuli delivered at early phases delayed the onset of the next spontaneous AP so that  $PRC(\phi) > 1$ . Stimuli injected at later phases induced premature excitation and  $PRC(\phi) < 1$ . We identify the critical phase,  $\phi_c$ , as the phase that separates the regions of advance and delay of the action potential. In any given preparation, the critical phase decreases as stimulus amplitude increases.

### 5.4.3 Overdrive suppression

Overdrive suppression [173] is the transient prolongation in the intrinsic cycle length as a result of stimulation at a rate faster than control. Previous extensive studies of this phenomenon in embryonic chick heart cell aggregates have shown that the magnitude of overdrive suppression depends upon the number of stimuli applied as well as the action potential frequency during the drive [186, 111]. Since overdrive suppression plays a major role in the evolution of rhythms during fixed delay protocols, it was characterized in each preparation. Results of an overdrive stimulation experiment for the same aggregate and stimulation intensity as in Figure 5.2 are shown in Figure 5.5B. We plot  $\frac{T'}{T_0}$  for trains of 2,4,6,8,10,30,50 and 100 stimuli. Following the drive, the cycle length gradually returned to control. After 30 seconds of rest, the preparation had fully recovered from overdrive. The first interbeat interval following the drive was directly proportional to the duration of stimulation. Following 20 stimuli, it was prolonged by approximately 60%. After 100 stimuli, there was a 2.5-fold increase in cycle length. These experimental findings agree well with previous studies in the same preparation [186, 111].

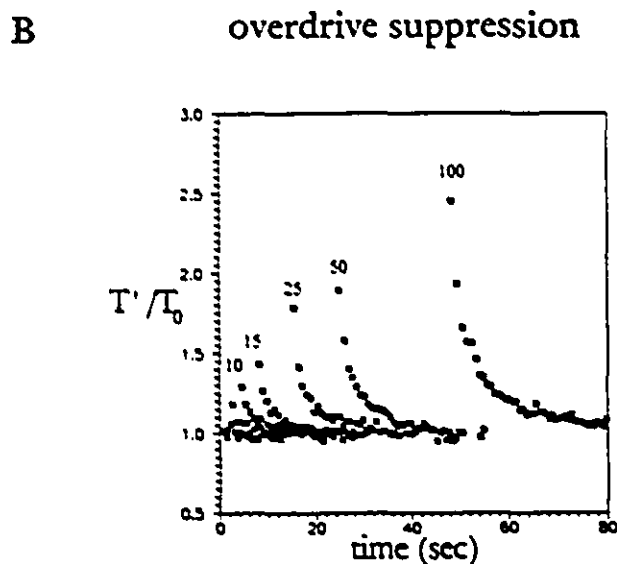
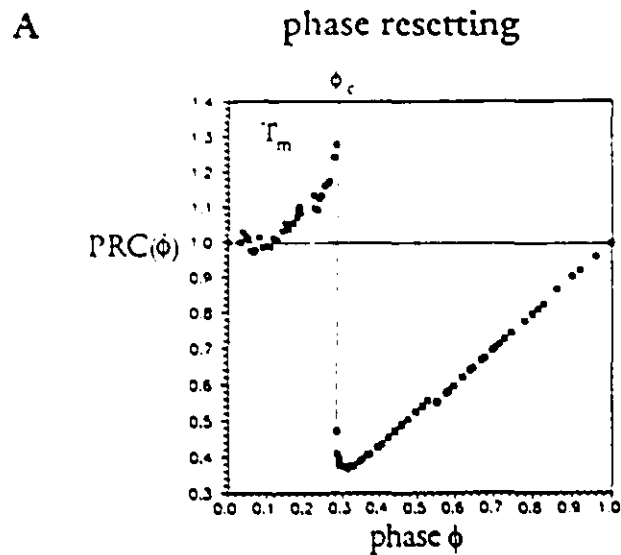


Figure 5.5: Phase resetting and overdrive suppression in embryonic chick heart cell aggregates (same aggregate as in Figures 5.1 and 5.2). The phase resetting curve ( $PRC(\phi)$ ) is shown in Panel A (amplitude=24 nA). Stimuli injected earlier than the critical phase  $\phi_c$  delay the onset of the next spontaneous AP. Premature excitation occurs when  $\phi > \phi_c$ . Panel B: build-up of overdrive suppression. The panel shows the time course of the normalized cycle length following stimulation (at  $0.6 T_0$ , 1:1 entrainment, see Fig. 5.1B) of increasing duration. The first interbeat after the drive is the longest and increases with the duration of the drive. The subsequent decay in cycle length follows an exponential time course (time constant  $\approx 15$  sec).

## 5.5 A nonlinear theoretical model

The excitability of cardiac tissue is often described as a function of the time elapsed since the previous activation. For example, extensive studies from our group [79, 78, 70, 184] assumed that during periodic stimulation, the effect of a single stimulus depended solely on the phase of the stimulus. The current experiment was designed specifically to study a situation in which that hypothesis breaks down.

During fixed delay stimulation, all the stimuli are delivered at the same coupling interval following the previous action potential. Based on the earlier work we would expect that the effect of all the stimuli would be identical. However, subsequent studies from our group [186, 111] documented that the definition of phase based simply on the coupling interval needs to be modified in circumstances in which the intrinsic cycle length changes due to stimulation history. We now develop a theory that can account in a qualitative way for the experimental data of Figures 5.2 and 5.4. In particular, we propose a nonlinear model to account the way in which stimulation history modulates the excitability of the preparation and in this fashion we account for the experimentally observed evolution of rhythms and bursting behaviour (Figures 5.2 and 5.4).

### 5.5.1 Interaction between excitability and history dependent effects

During the course of stimulation with fixed delay, there is a successive train of action potentials. We denote the successive interbeat intervals between actions potentials as  $IBI_1, IBI_2, IBI_3, \dots$ . As a consequence of the stimulation, the intrinsic cycle length (as modified by stimulation history) will in general vary from its control value,  $T_0$ . We denote the successive values of the intrinsic cycle length by  $T'_1, T'_2, T'_3, \dots$ . For example, as shown during the analysis of overdrive suppression, a consequence of a rapid burst of action potentials is to increase the intrinsic cycle length to a value greater than  $T_0$ .

The nonlinear model relies on the assumption that *the phase of the stimulus must be rescaled to the instantaneous value of intrinsic cycle length*. The dynamical effects

of premature stimulation can thus be predicted based on the PRC if we define an effective phase,  $\phi'_i$ ,

$$\phi'_i = \frac{\delta}{T'_i}. \quad (5.1)$$

The consequences of this assumption can be understood by consideration of Figure 5.6. The phase resetting curve is the same as in Figure 5.5A. The topmost horizontal line indicates the control cycle length. The vertical line corresponds to the critical phase  $\phi_c$ , the smallest phase where a single stimulus can elicit a premature action potential. Let  $\phi_0$  denote the effective phase of the first stimulus during the fixed delay protocol. Since there is no prior stimulation history,  $\phi_0 = \frac{\delta}{T_0}$ . In Figure 5.6, we choose  $\phi_0 = 0.4$ . During the stimulation, the preparation is initially entrained in a 1:1 fashion, causing a gradual build-up of overdrive suppression which slowly decreases the effective phase  $\phi'$ , as indicated by the arrow. Failure of excitation occurs at beat  $i$  if  $\phi'_i \leq \phi_c$ . If the stimulus does not initiate an action potential, there is a prolonged interbeat interval. The cycle length of the prolonged interval will be the sum of  $T'_i$  and a term associated with the resetting of the oscillation. This in turn will lead to a decrease in the intrinsic cycle length. Consequently, there will be an increase in  $\phi'_{i+1}$  initiating another bursting sequence. Thus the bursting is associated with the modulation of the effective phase, as a consequence of the slow buildup and rapid decrease of the overdrive suppression.

Based on the above qualitative description, we develop a nonlinear model. The basic equation is

$$\begin{aligned} IBI_{i+1} &= T'_i + PRC(\phi'_i)T_0 - T_0, \text{ if } \phi'_i < \phi_c, \\ IBI_{i+1} &= \max\{\delta, PRC(\phi'_i)T_0\}, \text{ if } \phi'_i > \phi_c, \end{aligned} \quad (5.2)$$

In this equation we make the assumption that the PRC is not rescaled, but only the phase of the stimulus so that the phase resetting makes a small additive effect to the prolongation of the cycle length following failure of the stimulus to elicit an action potential. Finally, the second equation ensures that no premature action potential is evoked before the stimulus is injected.

In order to implement the above equations, it is necessary to determine the history dependent intrinsic cycle length,  $T'_i$  to rescale the phase using Equation 5.1.

The approach taken to incorporate the history dependence of the intrinsic cycle length is similar to that of Zeng et al. [186]. The main assumptions are: 1) the

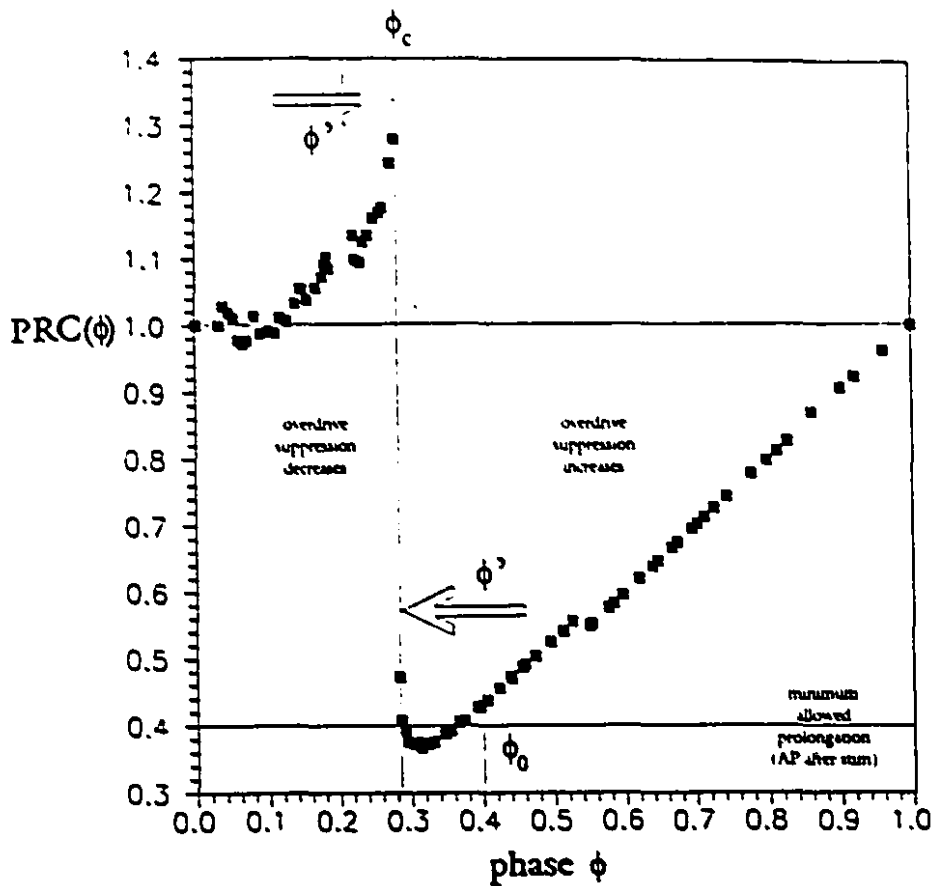


Figure 5.6: Interaction between overdrive suppression and the excitability of the preparation: qualitative model for the dynamics during fixed delay stimulation. To predict the rhythms based on the PRC, the effective phase  $\phi' = \frac{\delta}{T}$  is used in lieu of  $\phi$ . Same PRC as in Figure 5.3.  $\phi'$  decreases (increases) with overdrive suppression (underdrive acceleration). Loss of entrainment (premature AP) occurs when  $\phi'$  is less (greater) than  $\phi_c$ . The resulting change in overdrive levels re-initiates the original rhythm. Premature AP's can not be elicited prior to stimulation.

intrinsic cycle length can be written as  $T'_i = (1 + S_i)T_0$  where  $S_i$  represents the history-dependent effects ( $S > 0$  corresponds to overdrive suppression whereas  $S < 0$  corresponds to underdrive acceleration); 2) each action potential contributes to  $S$  by an amount that depends on the preceding interbeat interval; 3)  $S$  is a superposition (sum) of the contributions from individual action potentials; 4) each contribution to  $S$  decays exponentially with time constant  $\tau$ . Letting  $i$  and  $i + 1$  denote successive beat to beat values of  $S$ , we can write

$$S_{i+1} = S_i \exp(-IBI_{i+1}/\tau) + \varepsilon \left(1 - \frac{IBI_{i+1}}{T_0}\right), \quad (5.3)$$

where  $\varepsilon$  is the maximum change (normalized to the control interbeat interval) in cycle length due to a single premature action potential (in the theoretical limit of a premature AP elicited immediately after the preceding spontaneous AP [111]).

To summarize, given an initial phase  $\phi_0 = \frac{\delta}{T_0}$ , we find  $IBI_1$  using Equation 5.2. We then find  $S_1$  and  $T'_1$  by means of Equation 5.3 (and using  $S_0 = 0$ ). Equation 5.1 now serves to compute  $\phi'_1$  and we may proceed to subsequent iterates. Appendix A describes the methods used to set the parameters of the model.

The results of the numerical simulations of the nonlinear model are shown in Figure 5.7, using the same format as in Figure 5.1 and the following set of parameters:  $\varepsilon = .065$ ,  $\tau = 20$  sec. For 6 values of the delay, each panel contains a simulated 20 second voltage trace resulting from iteration of Equations (5.1-5.3) (left) as well as a graph showing the evolution of the interbeat intervals throughout and after fixed delay stimulation (right). In the left hand panels, each spike is an action potential. The values of the delay were chosen to closely reproduce the experimentally observed dynamics. In general, the rhythms depicted in this figure are similar to the experimental observations presented in Figure 5.2. When  $\delta = 410$  msec, an initial transient of 42 premature AP's is followed by sequences containing 9 to 15 action potentials, interspersed with long pauses (up to 210 % of  $T_0$ ). Cessation of stimulation (arrow) is followed by a marked transient prolongation in the cycle length. This effect decays within 30 seconds. In some instances, an oscillation in the cycle length precedes the interruption of a bursting sequence. In Panel B, an initial irregular transient is followed by periodic sequences of 7 action potentials. The rhythm appears irregular in Panel C, with an alternation of sequences of 3 to 4 action potentials. In D, doublets and triplets are interspersed in a slightly irregular fashion. For a delay of

230 msec, the dynamics are characterized by an irregular pattern of delayed AP's interspersed with doublets. In Panel F (delay = 190 msec), delayed action potentials predominate over occasional premature excitations, following a long initial sequence of delayed activations (which terminates due to time-dependent shortening of the intrinsic cycle length). Underdrive acceleration (faster intrinsic rhythm, 85 % of control cycle length) is found at the end of the drive. The values of the delay used in this figure are within 10 % of the experimental time delays.

### 5.5.2 Ionic model

One of the hallmarks of experimental data obtained during fixed delay protocols is the presence of very long pauses between successive bursts of action potentials. In many cases, following a burst of 8 to 10 AP's, the duration of such pause may well equal 4 or 5 times the control cycle length. Termination of the protocol is also followed by a transient prolongation of the intrinsic cycle length that is of the same magnitude. Previous studies have shown that ouabain, a blocker of the sodium potassium pump (in micromolar concentrations), markedly reduced overdrive suppression in this preparation [143]. We have therefore modified the latest version of the Shrier-Clay ionic model of electrical activity for embryonic chick heart cell aggregates to include a simplified sodium pump term. A detailed description of this new component can be found in the Appendix B. The original Shrier-Clay ionic model of electrical activity is reviewed in Reference [105].

The Shrier-Clay ionic model reproduced the electrical activity and the excitability properties of small, rapidly beating aggregates, (BCL  $\approx$  380 msec). Since the addition of the sodium pump term increased the intrinsic cycle length by 30% (BCL=520 msec), the maximum amplitude of the background current was adjusted [105] to restore the original rate of firing as well as the adequate phase resetting behavior. A 10 second voltage trace of spontaneous activity is shown in the top, left panel of Figure 5.8. The control cycle length is 380 msec. A phase resetting curve obtained with 33 nA stimuli is shown in the top right panel. The amplitude of the stimulus was chosen to closely match the shape of the experimental PRC in Figure 5.5A. The values for the critical phase  $\phi_c$  and the maximum prolongation  $T_m$  are in close agreement with experimental data. A short study of overdrive suppression in the modified

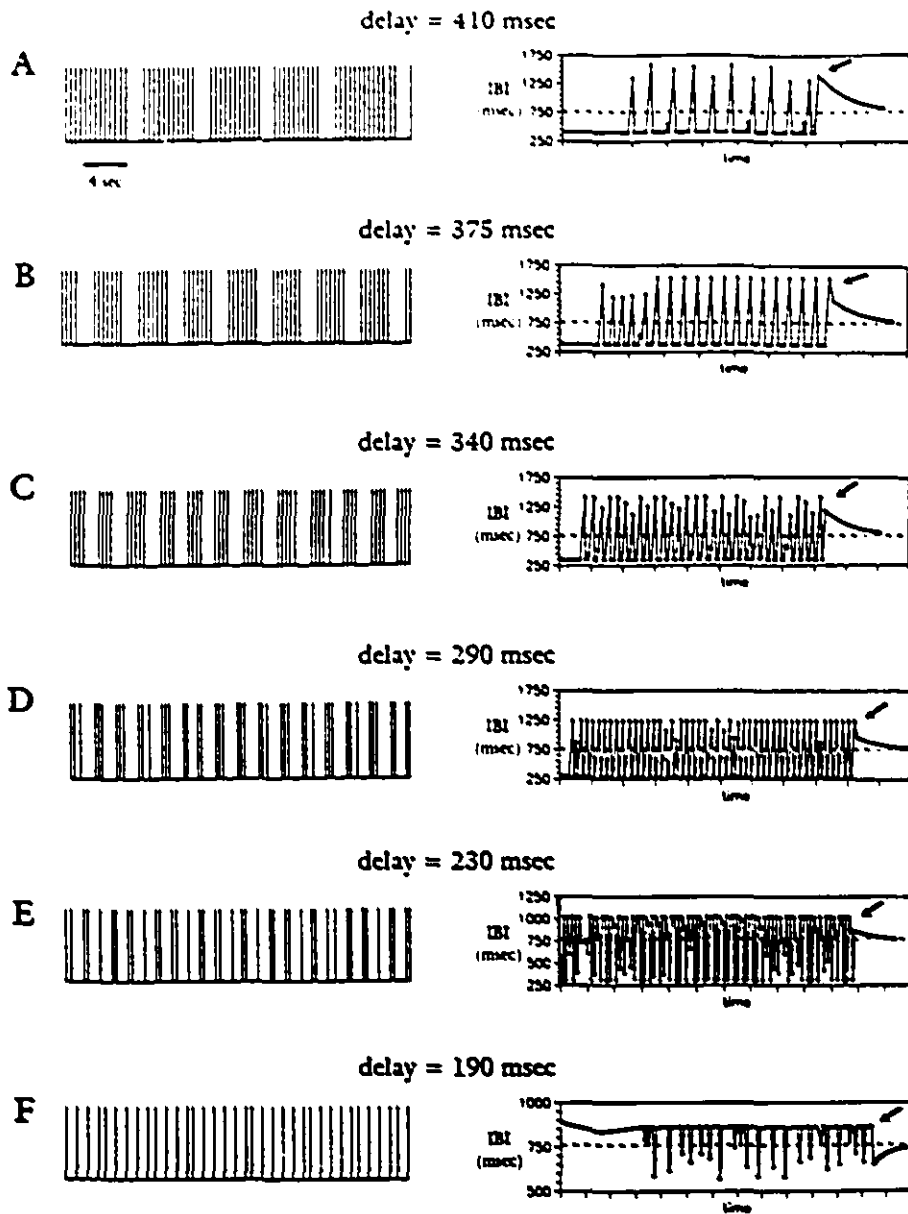
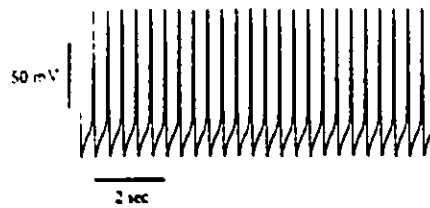


Figure 5.7: Numerical simulations of nonlinear model using parameters described in text. Fixed delay stimulation for different delay values. Left hand panels show simulated voltage traces (20 sec, spikes are AP's). The evolution of the interbeat intervals (IBI) is shown on the right. The dashed line indicates control cycle length. The arrow marks the end of stimulation. Compare with the experimental data of Figure 5.2.

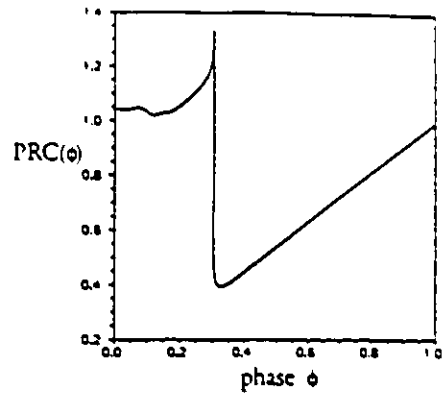
ionic model is presented in the bottom part of the figure. A 10 second voltage trace illustrating overdrive suppression after 50 periodic stimuli (stimulus period  $\approx .55 T_0$ , 1:1 entrainment) is shown in Panel a. The first cycle length following the drive is 160 % of control cycle length. The slow decay of overdrive suppression appears clearly in this figure. Panel b illustrates the build-up of the internal levels of sodium during and after the rapid periodic drive. The average beat to beat concentration of internal sodium under control conditions was set to be 15 mMol/L. The upstroke phase of the action potentials is associated with a rapid increase in  $[Na_i]$  (by  $\approx 3$  mM) that is primarily due to entry of sodium ions through the fast sodium channels. The extrusion of sodium ions by the sodium potassium pump during the cycle is responsible for maintaining the steady state average sodium levels. The increased action potential frequency during rapid stimulation (1:1 entrainment) results in a marked build-up of the internal sodium levels and a corresponding potentiation of the sodium pump current. When the drive terminates, the enhanced pump activity causes a gradual decrease of the internal sodium levels while markedly prolonging the intrinsic cycle length by virtue of its electrogenic nature. Panel c shows a study of the build-up of overdrive suppression as a function of the number of stimuli applied ( $T_s = .55T_0$ ). The format of this panel is identical to Figure 5.5B. There is good agreement with experimental data.

The results presented in Figure 5.9 were obtained by numerical integration of the modified ionic model described in the present paper. The format of the figure is identical to that of Figures 5.2 and 5.7. In Panel A (delay of 133 msec), there is a stable reentrant (1:1) pattern followed by marked overdrive (about 350 % of control cycle length) after stimulation has ceased. This overdrive suppression decays within 30 seconds. As in Figure 5.2, bursting behavior is observed with most of the delays (panels B to E), and the number of action potentials per burst decreases as the delay becomes shorter. In Panels B to D, bursting patterns almost identical to the corresponding panels of Figure 5.2 can be seen. In particular, long sequences of AP's (bursts) are associated with prolonged inter-burst pauses. However, these patterns occur for a range of delays that is much narrower than in the experimental context. This suggests, in the present simplified formulation, the build-up of overdrive suppression during rapid firing does not properly influence the excitability of the model aggregate. For some delays, a growing oscillation in the interbeat intervals is observed before the sequence terminates. When normalized to the control

spontaneous activity



phase resetting



overdrive suppression

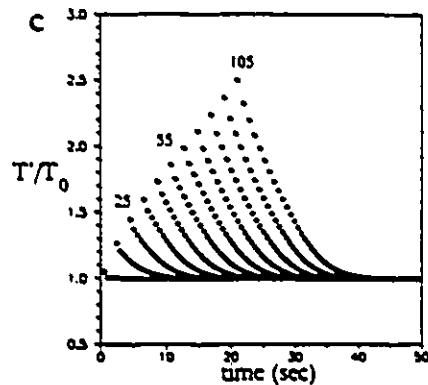
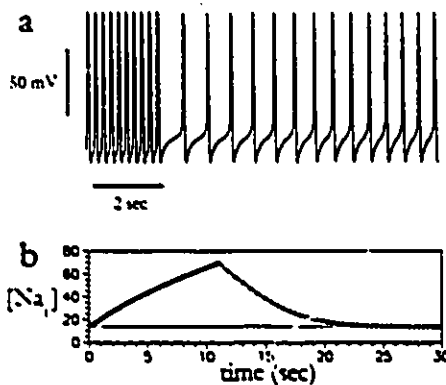


Figure 5.8: Phase resetting and overdrive suppression in the modified Shrier-Clay ionic model. Top left panel: spontaneous activity. The cycle length is 380 msec. Top right panel: phase resetting curve (stimulus amplitude = 33 nA). Compare with Figure 5.5A. Bottom: overdrive suppression in modified ionic model. Panel a: 10 second voltage trace showing overdrive after 50 stimuli ( $T_s \approx .55 T_0$ , 1:1 entrainment). The build-up (decay) of internal sodium levels during (following) rapid stimulation is shown in panel b. Panel c: build-up of overdrive suppression as a function of the number of stimuli applied (same stimulation frequency). Compare with Figure 5.5B.

cycle length (380 msec), the length of the post-drive prolongation is comparable with experimental measurements. This overdrive suppression is closely related to the internal sodium levels that increase strongly during long bursting sequences. During the stimulation protocol, the internal sodium concentration increases until the corresponding cycle length is too long for the entrainment to be maintained. As for the previous panels, the data presented in Panels E and F resembles strongly the experimental observations. At a delay of 122.5 msec (Panel E), sequences of 3 AP's are interspersed with episodes of delayed activations. For a slightly shorter delay, no premature AP's are evoked. Slight underdrive acceleration is observed following the drive, that is related to the decreased intracellular sodium levels due to lower action potential frequency during the drive.

## 5.6 Discussion

We have shown that fixed delay stimulation can result in a surprising variety of rhythms that arise as a result of a complex interplay between overdrive suppression and the excitation properties of the preparation as described by the phase resetting curve. Because fixed delay stimulation can be viewed as a simplified model of a reentrant loop, this study has implications in clinical investigations of arrhythmias, in mathematical modeling of cardiac rhythmogenesis and in basic electrophysiology. In the remainder of this section, we discuss some of the limitations as well as the implications of the present study to our present understanding of the mechanisms of cardiac activity and pathology. We also comment on the validity of the models presented in this chapter and provide further details concerning our understanding of the rhythms that arise during fixed delay stimulation.

Overdrive suppression has been studied in a variety of cardiac tissues, derived from many species [174, 173, 143, 63, 134, 74]. Despite this wide body of data, few attempts have been made to understand the influence of overdrive suppression on the phase resetting properties of cardiac tissue. In a recent publication from our group [186], a simple iterative model was proposed in which the PRC (both the perturbed cycle length and the phase) was scaled according to the overdriven cycle length. Although the model was successful at reproducing some of the experimental data, the very mechanism in which overdrive modulates phase resetting is

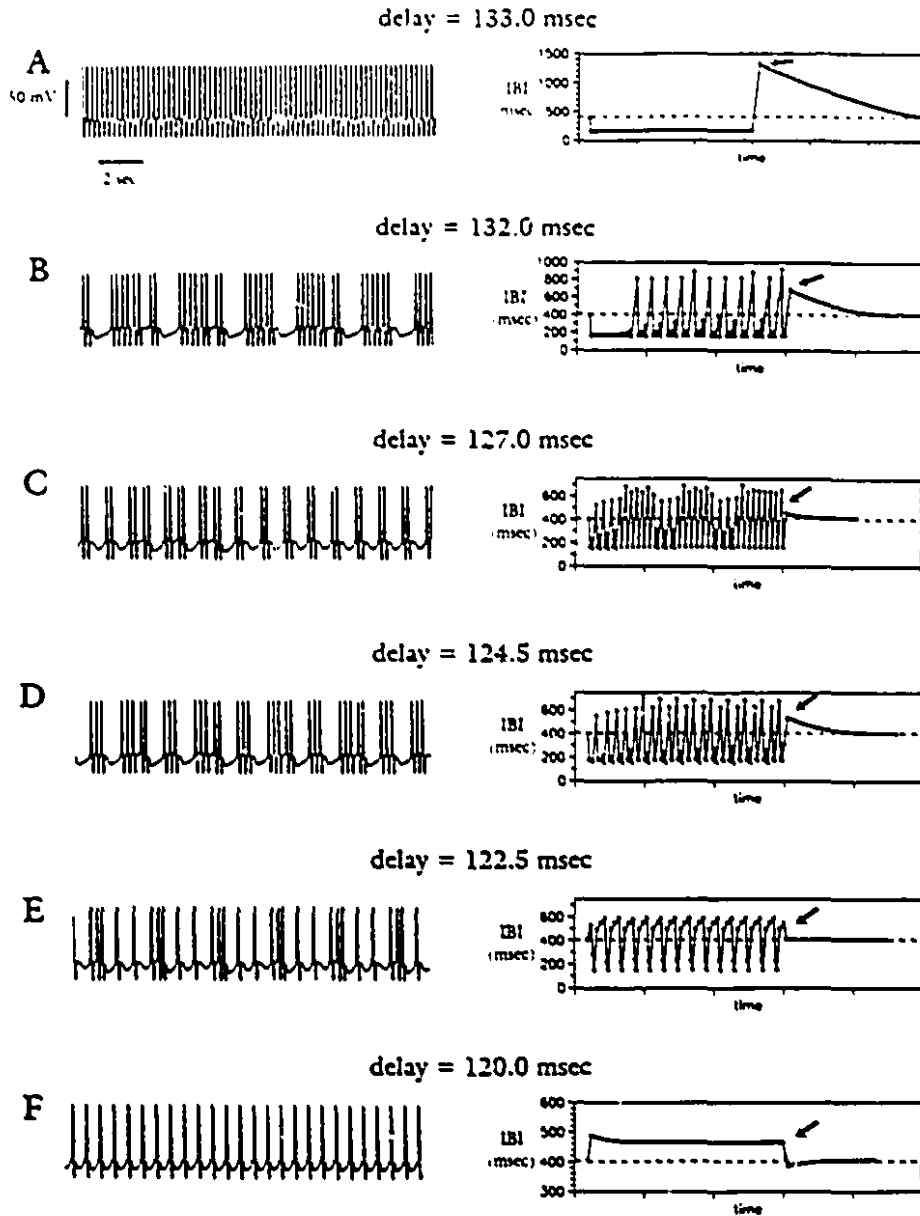


Figure 5.9: Numerical simulations of the modified Shrier-Clay ionic model during fixed delay stimulation for different delays. Left hand panels: simulated voltage traces (12 seconds). A graph of successive interbeat intervals appears on right. The dashed line shows the control cycle length. The arrow indicates the end of the protocol. Compare with Figures 5.2 and 5.7.

still poorly understood. The results presented in the current manuscript, obtained during fixed delay stimulation, indicate that the length of the pauses separating successive bursting sequences and the duration of the post-drive cycle length are almost identical. According to the assumptions of the previous model, a prolongation of 30% in the control PRC would result in a corresponding 30% difference (in terms of overdriven cycle length) between the lengths of the inter-burst and the post-drive pauses. Therefore, our data suggests that, although the phase of the PRC may effectively be scaled to the new cycle length, the length of the perturbed cycle length (in msec) is not scalable. Consequently, for long bursting sequences, overdrive suppression dominates the contributions from phase resetting to the length of the inter-burst pause.

The nonlinear model introduced in the present manuscript is an attempt to provide a simple way of understanding the qualitative nature of the interaction between the excitability of cardiac tissue and stimulation history and extends previous theoretical work [78, 70, 76] in which history dependent effects were not considered. Despite the relative simplicity of the mathematical formulation of these effects, the simulations of the nonlinear model fare well at reproducing the experimentally observed dynamics. Moreover, the nonlinear model is not preparation nor protocol specific and its results may therefore be applicable to a variety of experimental observations.

In the experimental context, very high action potential frequencies during prolonged rapid stimulation may cause the influx of sodium ions per unit time to exceed the maximum capacity of the sodium potassium pump (when saturated). Under such conditions, the first interbeat interval following the drive increases exponentially as a function of the duration of the stimulation protocol (unpublished observation); there is no saturation of overdrive suppression (provided that the original entrainment pattern can be maintained). Although this behaviour can be reproduced with the modified ionic model, the present mathematical description of history dependent effects in the nonlinear model necessarily implies an asymptotic approach to a steady state in terms of overdrive levels. This mandatory saturation of overdrive suppression is one of the limitations of the nonlinear model, especially during very long and rapid stimulation protocols.

The oscillations in interbeat intervals found in the numerical simulations are one

of the interesting results of this work. In general, the amplitude of these oscillations increased before loss of entrainment. The eventual break-up of entrainment generally occurred following a short interbeat interval. Since the oscillation was often (not always) of period 2, we may predict that, for some delays, alternations between sequences of  $N$  and  $N+2k$  ( $k$  integer) AP's per burst should be more common than mixing of odd and even numbers of AP's per burst. This seems to be the case in Panels B and E where sequences of 6, 8, 10 and 1 and 3 AP's per burst, respectively, are found. However, in the experimental context, there are spontaneous fluctuations in cycle length and action parameters (APD,  $V_{ov}$ ) that may interact with the mechanisms responsible for this phenomenon. As a result, although there is some tendency for analogous behavior, we have not found clear evidence for this oscillation in our experimental data.

Most of the experimental data presented in this chapter was obtained during stimulation of medium intensity. From the dynamical point of view, this range of stimulus amplitudes is particularly interesting due to the general shape of the phase resetting curve that allows the emergence of complex rhythms under various stimulation protocols [185, 26, 70, 105]. However, the qualitative results obtained with medium intensity stimulation are representative of other stimulus amplitudes as well. For example, fixed delay stimulation at lower amplitudes was characterized by increased stimulus to AP latencies, shorter interburst pauses (due to lower AP frequencies during stimulation) as well as a decrease in the range of delays where complex dynamics could be found. At high stimulus intensities, the range of delays where bursting behaviour could be found was also narrower, with typically more regular dynamics and very long interburst pauses (high AP frequencies).

### 5.6.1 Limitations of the ionic model

The development of the modified ionic model presented in the present manuscript was motivated by the need for a simple way of incorporating overdrive suppression. Previous studies in this preparation suggest that overdrive suppression is greatly reduced by ouabain, a blocker of the sodium pump [143]. Although the description of the sodium pump is crude, it is based on physiologically plausible assumptions and hence it may represent a useful step towards understanding the mechanisms of overdrive suppression. In its present formulation, the sodium pump term is insensitive

to changes in extracellular potassium concentrations. This assumption is justified by previous observations [164] that indicate that in contrast to other experimental preparations, accumulation of extracellular potassium during overdrive is minimal in embryonic chick heart cell aggregates.

In the present model, appreciable levels of overdrive are obtained at the cost of seemingly unrealistic increases in internal sodium levels (Figure 5.8). This is reminiscent of the notion of “fuzzy space” introduced to allow for significant changes in intracellular calcium concentrations in the context of developing models of the sodium-calcium exchanger [112, 22]. Although the existence of this hypothetical “fuzzy space” remains untested, it offers a possible explanation for our results.

In the ionic model, bursting behavior is found for a range of delays that is much more restricted than in experimental data, despite good quantitative agreement in terms of the magnitude of overdrive suppression. Therefore, in the present description of the ionic mechanisms underlying overdrive suppression, the modulation of excitability by time-dependent effects is weaker than in experimental data, and other subtle effects may also play a role in the complexity of the dynamics. In particular, the oscillations in the interbeat intervals prior to loss of entrainment that appear in Figure 5.9B and 5.9D are associated with noticeable changes in action potential overshoot and duration as well as changes to the balance of currents underlying phase resetting properties, which involves  $I_{K_r}$  and the fast sodium current  $I_{Na}$  [105]. In Figure 5.10, the top panel shows an enlarged portion of the voltage trace presented in Figure 5.9E. The action potential durations (APD, arbitrarily defined as the time interval between successive crossings of the  $-45$  mV threshold during the AP) and overshoot potentials ( $V_{ov}$ ) are presented in Panels b and c. The respective time courses of  $I_{K_r}$  and  $I_{Na}$  are shown in Panels d and e. In this figure, the delay corresponds approximately to the critical phase of the PRC (see Figure 5.5). As described previously [105], the advance (premature AP) or delay of excitation depends primarily on a delicate balance between  $I_{K_r}$  and  $I_{Na}$  at the time of stimulation. In the present case, the APD and action potential overshoot are modulated by the latency between the stimulus and the upstroke of the action potential. As a result, a stimulus applied at a fixed delay after a slightly longer action potential (second one in top trace) will fall closer relative to MDP, where a significant portion of  $I_{K_r}$  channels have not yet deactivated. Consequently,  $I_{K_r}$  dominates over  $I_{Na}$  resulting in a delayed AP. Because this AP has a lower overshoot and shorter APD (and because

of the longer interbeat interval), a larger fraction of  $I_{Kr}$  channels have deactivated at the time of stimulation, resulting in a shorter delay of the next AP. Since the subsequent AP's have increasingly shorter durations, the domination of  $I_{Na}$  over  $I_{Kr}$  increases progressively until a marked shortening in the prolongation is observed. Since this premature AP has the shortest duration,  $I_{Na}$  dominates strongly when the pulse is applied; the stimulus evokes an immediate action potential. Therefore, the bursting patterns observed in the ionic model are also partly due to an interaction between phase resetting and the modulation of action potential parameters by the prematurity of the stimulus relative to MDP, that could be described in terms of action potential restitution properties.

Rate-dependent changes in action potential characteristics have been studied in various preparations [17, 103]. As a result of this work, several mechanisms have been identified that underly the modulation of AP morphology by the prematurity of the stimulus. In many preparations, this phenomenon was attributed to an interplay between currents responsible for the plateau phase of the AP and the later repolarization phase [17, 103]. Because some of these currents also play a role in the time course of recovery from excitation (which is also described by the phase resetting curve), our results suggest that phenomena described in the current paper could also be found in other preparations. For example, an oscillation in the conduction time prior to loss of sustained reentrant rhythm is often found in experimental preparations [60, 163, 153, 166]. Because conduction time is a function of the recovery properties of the preparation (related to APD), changes in conduction time have often been modeled in terms of the evolution of APD during the drive [60, 26, 166, 93]. Since the underlying ionic mechanisms may be similar, we believe that our results may apply to a wider class of experimental phenomena.

### 5.6.2 Reentry

Previous studies have used an electronic circuit to model an accessory pathway in the analysis of atrioventricular reentry tachycardia [163, 153, 13, 166]. The current work extends these earlier studies by (1) delivering the stimulation directly to a spontaneous oscillator, and (2) developing theoretical models to describe the experimentally observed rhythms. Since the rhythms are similar to repetitive paroxysmal

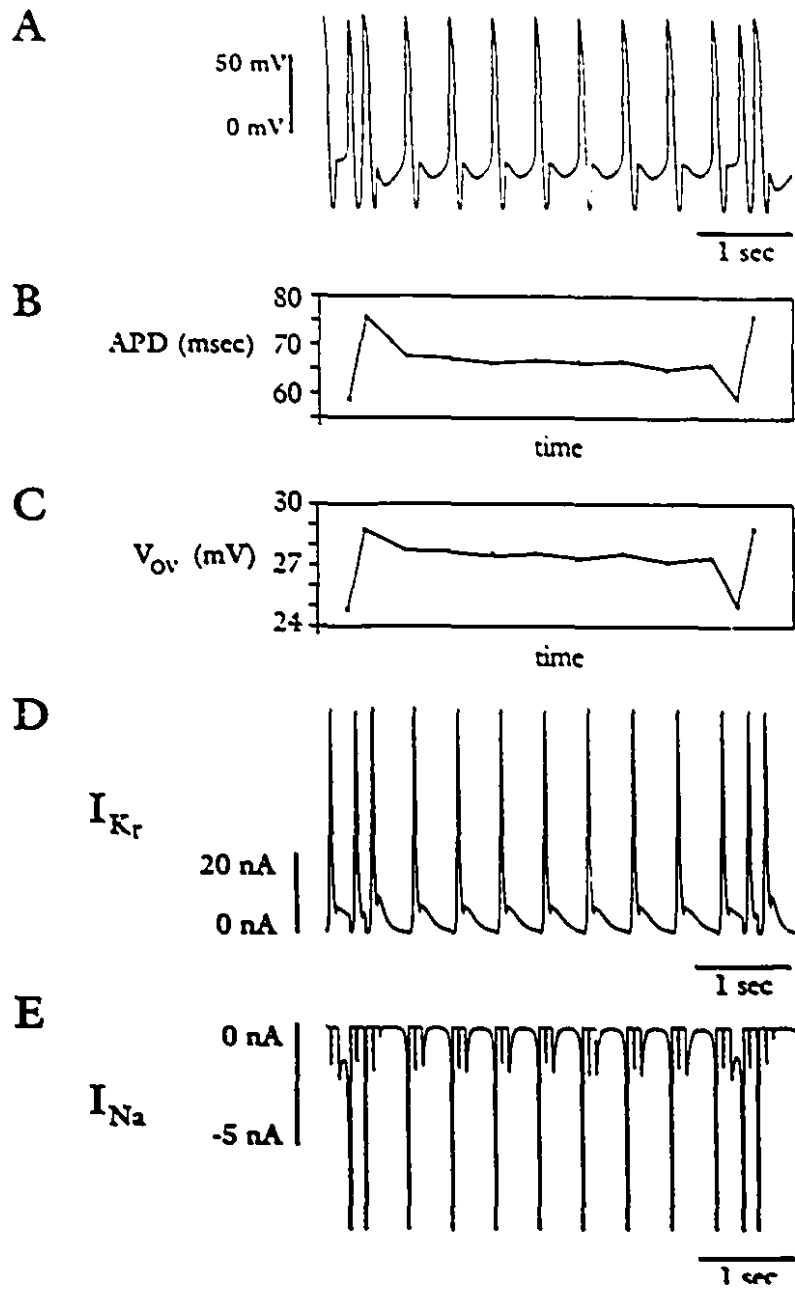


Figure 5.10: Ionic mechanisms contributing to the complex rhythms during fixed delay stimulation of the modified Shrier-Clay ionic model. In a: enlarged portion of voltage trace from Figure 5.9E. In Panels b and c, respectively: evolution of action potential duration (APD) and overshoot potential ( $V_{ov}$ ) versus time. In Panels d and e, respectively: time course of  $I_{Kr}$  and  $I_{Na}$  corresponding to the voltage trace in a. Note the changes in the magnitude of the currents as a function of the AP characteristics.

tachycardia, we believe that the current work forms a basis for understanding the dynamics of these arrhythmias. Prominent novel features in our analysis are the slow changes in the physiological rhythm associated with the buildup of overdrive suppression, and the delicate interactions between sodium and potassium currents that govern the excitability and refractoriness of the spontaneous oscillator.

Further work will be needed to determine the extent to which the features that we observe here can be applied in other circumstances. Even though we use a very simplified experimental model, certain characteristics of the dynamics can be found in other settings. For example, it is not unusual to observe a subtle alternation in cycle length prior to the cessation of supraventricular tachycardia [163, 153]. Since understanding the origin of this oscillation is key to understanding the factors that lead to the stabilization and destabilization of reentry tachycardia, it will be important to analyze in more detail the ionic mechanisms of this oscillation with particular emphasis on its sensitivity to drugs. In particular drugs that alter action potential duration and refractoriness are certain to play an important role in pharmacological management of reentry tachycardias [23, 84].

## 5.7 Appendix A: description of the modified ionic model

To incorporate an electrogenic sodium pump term ( $I_p$ ) into the Shrier-Clay ionic model we assume:

(1) The sodium pump term possesses 3:2 ( $\text{Na}^+:\text{K}^+$ ) stoichiometry. It is sensitive to the internal sodium concentration according to Michaelis-Menten kinetics and it is voltage independent.

(2) The magnitude of the fully activated hyperpolarizing sodium pump term ( $I_{p,max}$ ) is such that it equals the minimum value of the net inward current during diastolic depolarization. If fully activated, the slope of diastolic depolarization will equal zero. Under control conditions (steady state) we assume that, immediately after the upstroke phase of the action potential,  $I_p$  is about 60% of its maximal value [111].

(3) Three mechanisms contribute to beat to beat changes in internal sodium concentration: the entry of sodium ions during the upstroke phase of the action

potential (fast sodium current,  $I_{Na}$ ), the sodium pump, and the uptake of sodium ions *via* other mechanisms of unknown nature. The latter component may include mechanisms such as the sodium-calcium exchanger, the sodium-potassium-chloride cotransporter, the background current or other ionic flows of passive nature. It may also account for a hypothetical compartmentalization of the intracellular space available to sodium ions ("fuzzy space") [112, 22].

As a consequence of these assumptions, the equations describing the sodium pump term and the changes in internal sodium concentration are

$$I_p = I_{p,max} \frac{[Na_i]}{[Na_i] + k}, \quad (5.4)$$

where  $[Na_i]$  is the internal sodium concentration,  $k$  is the half-activation constant and  $I_{p,max}$  has been defined above; and

$$\frac{d([Na_i])}{dt} = -\alpha(I_{Na} + 3I_p) + \Delta([Na_i])\delta(t - t_{AP}) \quad (5.5)$$

where  $I_{Na}$  is the magnitude of the fast sodium current,  $\alpha$  is a conversion constant from charge to concentrations,  $\Delta([Na_i])$  is the instantaneous change in internal sodium concentration due to the third component described in Assumption 3,  $t_{AP}$  is the time of the upstroke of the action potential and  $\delta$  is the Dirac delta function. Finally, the value of  $\alpha$  can also be modified to account for a hypothetical compartmentalization of the intracellular space available to sodium ions.

During rapid drive, increased action potential frequency results in a build-up of intracellular levels of sodium. This, in turn, stimulates the sodium pump resulting in a decrease of the slope of diastolic depolarization and a corresponding increase in the cycle length. After cessation of stimulation, the sodium pump continues to function at a high rate while the action potential frequency is low (overdrive suppression). As a result, the internal sodium concentration gradually returns to control values and control electrical activity is resumed.

The method used to set the various parameters of the model is analogous to that described in Reference [111]. Briefly,  $I_{p,max}$  is set according to Assumption 2 (minimum slope of phase 4 equals zero). The total increase  $\Delta$  in internal sodium levels during the upstroke of the AP is dependent upon the experimentally measured magnitude of overdrive suppression. As in Reference [111],  $\Delta$  is determined from

$$\Delta = \left(\frac{T}{T_0} - 1\right) \left(\frac{[Na_i] + k}{1 - \phi}\right), \quad (5.6)$$

where  $T$  is the experimentally measured overdriven cycle length following a single premature AP elicited by a stimulus delivered at some phase  $\phi$ . Since control conditions are equivalent to a steady state in terms of beat to beat changes in internal sodium levels,  $\Delta([Na_i])$  is set to a value that compensates for the net loss of sodium ions due to the sum of the actions of  $I_p$  and  $I_{Na}$  during the cycle, for the value of  $\Delta$  determined from Equation 5.6. This steady state condition is also used to set  $\alpha$ , according to

$$\alpha = \frac{\Delta}{3I_p T_0},$$

which relates the net instantaneous change in  $[Na_i]$  (upstroke of AP) to the decrease in sodium levels during one cycle due to the electrogenic nature of the sodium pump.

The values of the parameters retained for the remainder of this work are:  $I_{p,max} = 5.7$  nA ;  $k=10.0$ ;  $[Na_i]=15.0$  immediately after the upstroke of the action potential;  $\alpha = 1.0$ ; and  $\Delta([Na_i])=1.0$ . Because the ionic model was originally designed to describe the electrical activity of small fast beating aggregates, the control cycle length was kept at 380 msec. Numerical simulations were carried out using a variable time step Euler iteration method [131] for the transmembrane potential and Rush and Larsen iteration technique for the gating parameters [155].

## 5.8 Appendix B: setting of parameters in nonlinear model

There are three parameters to be set in the nonlinear model. The control cycle length  $T_0$  is directly obtained from experimental data. The quantities  $\varepsilon$  and  $\tau$  are determined using the following procedure.

Let  $\phi_m$  be the smallest fixed phase of stimulation where 1:1 entrainment can be maintained (i.e. no bursting). From the description of the qualitative model, failure of excitation occurs when the initial phase rescaled by the overdriven cycle length is less than the critical phase  $\phi_c$ . Thus, we may consider stimulation at the phase  $\phi_m$  as the limit case where an infinite number of stimuli is necessary before the reentrant pattern terminates. Assuming that each stimulus of the train immediately evokes an AP (no latency), we have

$$IBI_i = \phi_m T_0, \quad \text{for all } i, \quad (5.7)$$

so that Equation 5.3 becomes an infinite geometrical sum and

$$S_{\infty} = \varepsilon(1 - \phi_m) \left( \frac{1}{1 - \exp(-\frac{\phi_m T_0}{\tau})} \right), \quad (5.8)$$

is the asymptotic value for the overdrive term following an infinite number of stimuli. This equation can be further simplified since, in general,  $\phi_m T_0 \ll \tau$  [186], so that

$$S_{\infty} \approx \varepsilon \left( \frac{\tau}{\phi_m T_0} \right) (1 - \phi_m), \quad (5.9)$$

which, combined with the condition for loss of 1:1 entrainment at infinity

$$\frac{\phi_m}{1 + S_{\infty}} = \phi_c, \quad (5.10)$$

can be solved for the product  $\varepsilon\tau$

$$\varepsilon\tau = \left( \frac{\phi_m}{\phi_c} - 1 \right) \left( \frac{\phi_m T_0}{1 - \phi_m} \right), \quad (5.11)$$

now expressed in terms of experimentally measurable quantities.

In a further step, we obtain the values of  $\varepsilon$  and  $\tau$  by deriving an approximate analytical expression for the number of action potentials contained in the initial sequence during fixed delay stimulation, as a function of the delay  $\delta$ . Let  $n$  denote the number of action potentials in the initial bursting sequence (for a given delay  $\delta$  and some stimulus intensity). If we assume again that each action potential of the sequence is evoked immediately after the stimulus is injected, Equation 5.3 yields an expression for the sum  $S_n$  after  $n$  action potentials

$$S_n = \varepsilon \left( 1 - \frac{\delta}{T_0} \right) \left( \frac{\exp(-(n+1)\delta/\tau) - 1}{\exp(-\delta/\tau) - 1} \right), \quad (5.12)$$

which is just the sum of a geometric series. Since the burst terminates when the effective phase is below the minimum phase at which a premature AP can be elicited (critical phase  $\phi_c$ , corresponds to refractory period), we find  $n$  by solving

$$\frac{\delta}{T_0(1 + S_n)} = \phi_c. \quad (5.13)$$

Because the above condition must be true at the time of the  $(n+1)$ th stimulus, we ought to find the smallest integer  $n$  such that

$$\frac{\delta}{T_0(1 + S_n)} \leq \phi_c,$$

where the first action potential in the bursting sequence is spontaneous and does not contribute to overdrive suppression. Thus,  $S$  is computed over  $(n - 1)$  iterates and 1 must be added to the solution to obtain the value of  $n$ . After some algebra, we have

$$n = 2 + INT \left[ \frac{-\tau}{\delta} \ln \left( \frac{\left(\frac{\delta}{T_0 \phi_c} - 1\right)(\exp(-\delta/\tau) - 1)}{\epsilon(1 - \delta/T_0)} + 1 \right) \right], \quad (5.14)$$

where  $INT$  is the integer function and all the quantities have been defined above.

Let's now suppose that the initial transient of  $n$  action potentials is followed by regular bursting activity with  $m$  AP's per burst. Since the level of overdrive suppression is the key factor in timing the termination of the burst, this assumption is equivalent to

$$S_n = S_{n+m}, \quad (5.15)$$

where  $S_n$  and  $S_{n+m}$  are the values of the overdrive sum after  $n$  and  $(n + m)$  AP's respectively. This equation is simply a steady state condition for overdrive. After the  $n$  initial AP's, overdrive is at a level  $S_n$ . The long pause which follows the first burst results in the decay of  $S_n$  by a certain amount  $\Delta S$ . When bursting activity resumes, the new sequence terminates after  $m$  action potentials when

$$S_n = (S_n - \Delta S) \exp(-m\delta/\tau) + \epsilon(1 - \delta/T_0) \frac{\exp(-m\delta/\tau - 1)}{\exp(-\delta/\tau - 1)} \quad (5.16)$$

where we must remember that the first AP of the burst does not contribute to the build-up of overdrive. In this equation,  $\Delta S$  is itself a function of  $S_n$  as well as of  $T_m$ , the maximum prolongation in the cycle length due to a premature stimulus. It is implicitly assumed that the maximum prolongation in the cycle length,  $T_m$ , is found exactly when  $\phi = \phi_c$ . This approximation is realistic for moderate to high stimulus intensities. Solving the above equation for  $m$  we obtain

$$m = 2 + INT \left[ 1 - \frac{\tau}{\delta} \left( \ln \left( \frac{A}{B} \right) + C \right) \right], \quad (5.17)$$

where

$$A = S_n \exp \left( -\frac{\delta}{\tau} - 1 \right) + \epsilon \left( 1 - \frac{\delta}{T_0} \right),$$

$$B = \left[ S_n \exp \left( \frac{-(1 + S_n)T_0 - (T_m - T_0)}{\tau} \right) + \epsilon \left( 1 - S_n - \frac{T_m}{T_0} \right) \right] \exp \left( -\frac{\delta}{\tau} \right),$$

and

$$C = \epsilon \left( 1 - \frac{\delta}{T_0} \right) \exp \left( -\frac{\delta}{\tau} \right).$$

After using Equation 5.11 to compute the product  $\varepsilon\tau$  from experimentally measured quantities, we calculate the quantities  $n$  and  $m$ , as a function of the delay  $\delta$ , for several choices of  $\varepsilon$  and  $\tau$ , subject to the condition  $\varepsilon\tau = \text{constant}$ . The resulting curves are compared with experimental data to yield the best set of parameters. This procedure is illustrated in Figure 5.11. The top panel shows the number of AP's in initial sequence,  $n$ , as a function of the delay  $\delta$  as determined experimentally (solid squares, see Figure 5.3), and by means of Equations 5.14- 5.17. In the simulations,  $\phi_c = 210$  msec,  $\phi_m = 460$  msec,  $T_0 = 760$  msec and  $T_m = 970$  msec, give  $\varepsilon\tau \approx 1.3$ . As indicated, the four curves correspond to different values of  $\tau$ . The staircase shape of the curves is a consequence of the integer function in Equation 5.14. The best fit to experimental data is achieved when  $\tau = 20$  sec. The corresponding values of  $m$  are shown in Panel B. In contrast with Panel A, the general shape of the curves does not depend strongly on the choice of  $\tau$ . The values  $\tau = 20$  sec and  $\varepsilon = .065$  were retained for the simulations.

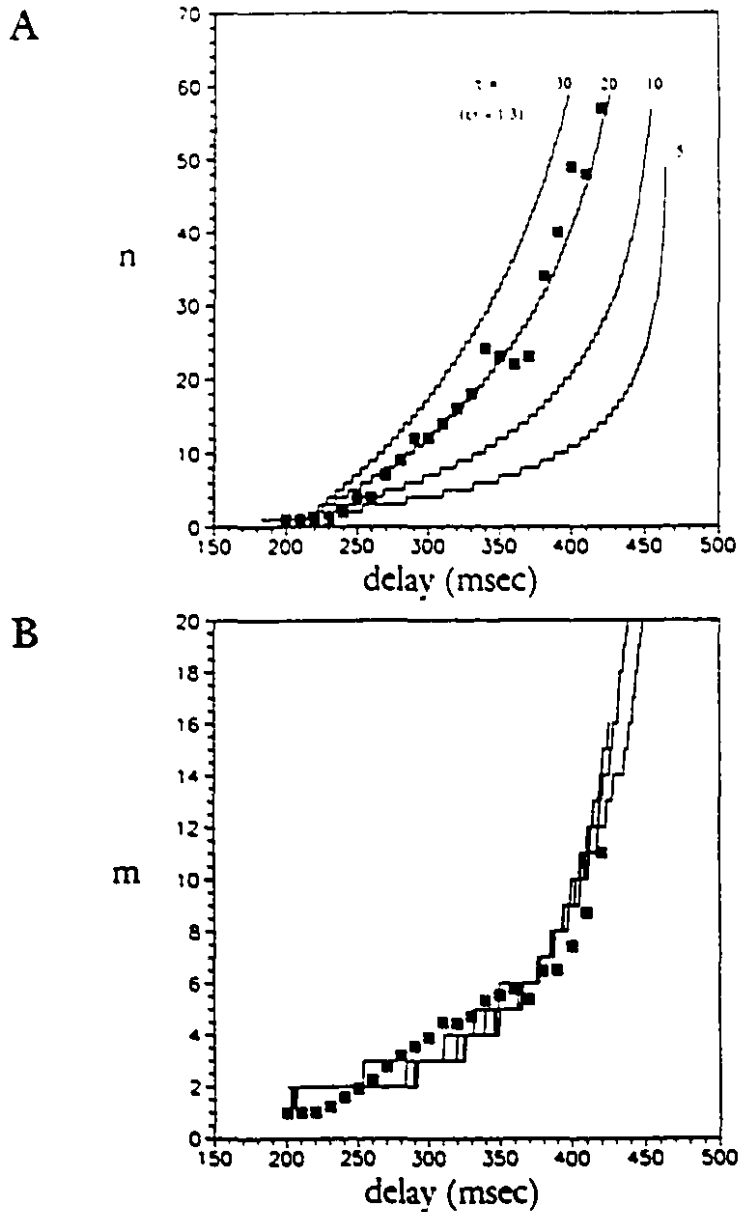


Figure 5.11: The parameters  $\epsilon$  and  $\tau$  are set by comparing the experimentally determined number of AP's in the initial sequence  $n$ , as a function of the delay, with numerical simulations of  $n$  (Equation 5.14) using different values of  $\epsilon$  and  $\tau$  subject to the condition  $\epsilon\tau = \text{constant}$ , as determined from Equation 5.11. In this figure,  $\epsilon\tau = 1.3$ . The best fit is obtained when  $\tau = 20$  seconds. Panel B: similar computation based on the steady state number of AP's per burst. The shape of the curves does not depend on the choice of  $\epsilon$  and  $\tau$ .

## Chapter 6

# Phase resetting and dynamics in isolated atrioventricular nodal cell clusters

### 6.1 Foreword

In the intact heart, the atrioventricular (AV) node is a small complex structure which plays a crucial role in regulating impulse conduction between the atria and the ventricles. AV nodal cells are in general characterized by slow action potential upstroke velocities (7 to 30 V/s, to compare with 100 to 200 V/s for neighbouring atrial or ventricular cells) which reflect the relatively slow kinetics of the ionic mechanism underlying electrical activity [12, 128, 162]. Under normal conditions, an electrical impulse generated by the primary pacemaker of the heart, the sinoatrial (SA) node, propagates across the atria and reaches the AV node which forms the only normal link between the atria and the ventricles. The functional aspects of the AV node may be summarized as follows: 1) conduction through the AV node is slow (and rate-dependent) therefore causing a delay in activation between the atria and the ventricles (coordination of activation), 2) the AV node is able to block impulses propagating from the atria to the ventricles hence protecting the latter from too rapid or complex atrial rhythms. (filtering), 3) under circumstances where the SA node fails in generating the heart rhythm, or when conduction is blocked between the atria and the ventricles, the AV node is capable of serving as a subsidiary pacemaker to the ventricles (pacemaking). In the clinical context, the AV node is therefore often the target of therapeutical or surgical interventions.

Since the pioneering work of Tawara [168], there has been substantial progress in our understanding of the excitability and conduction properties of the intact AV node. For example, periodic premature stimulation protocols are often used to evaluate nodal excitability and its rate-dependent properties [160, 167, 13, 14, 46]. In this procedure, a premature stimulus is introduced at various coupling intervals after sustained periodic pacing at a fixed frequency. The resulting recovery curve (conduction time  $SH$  versus recovery time  $HS$ ) is a representation of the excitability of the AV node. These recovery curves have been incorporated in an iterative mathematical procedure to predict the various rhythms of AV block in patients during atrial stimulation [160, 167].

In the last decade it has been shown that patterns similar to the rhythms of atrioventricular block can be seen *in vitro* in a virtually isopotential preparation of cardiac cells [78, 80]. These rhythms could largely be accounted for by analyzing the response of the preparation to single premature stimuli [80, 67]. Time-dependent effects (overdrive suppression) analogous to "fatigue" (rate-dependent prolongation in AV nodal conduction time) during periodic stimulation of the AV node [13, 14] were observed that could lead to an evolution of the entrainment pattern during the drive [186]. Such *in vitro* experiments may therefore provide an excellent basis for evaluating and modeling the dynamical response of AV nodal tissue to single or premature stimulation. In combination with electrophysiological studies carried out on single cellular preparations using the patch clamp technique, they can give us a better understanding of the spatial organization of the AV nodal tissue and of the ionic mechanisms underlying its functional properties.

In this study we characterize the response of AV nodal clusters to single and periodic stimulation. We investigate the consequences of changes in action potential morphology during periodic stimulation on the complexity of the experimentally observed rhythms. We also observe time-dependent effects which may be analogous to "fatigue" in the intact node.

## 6.2 Experimental protocols

The following experimental procedures were performed on both types of preparations. Typical aggregate size was  $180 \mu\text{m}$  with control cycle length between 470 and 650 msec. The control cycle length of the spontaneously active AV nodal cell clusters

was 300 to 520 msec.

### 6.2.1 Phase resetting

Single depolarizing current pulses of fixed amplitude were delivered every tenth spontaneous action potential at an increasing coupling interval through the entire spontaneous cycle. The duration of the pulse was typically of 20 msec. This protocol was repeated at several intensities of stimulation.

### 6.2.2 Overdrive suppression

The preparation was stimulated with increasing numbers of stimuli. Successive trains of 1,2,4,8,15,25,50,100,250 stimuli were delivered, separated by rest periods of approximately 30 seconds. All measured interbeat intervals were normalized to the control cycle length defined as the average of the 5 cycle lengths preceding the drive. The post drive cycle length was evaluated as a function of stimulation duration

### 6.2.3 Periodic stimulation

The preparation was stimulated with trains of 100 stimuli at different pacing frequencies and stimulus amplitudes. Successive episodes of pacing were separated by a 30 second rest period to allow for recovery from stimulation. The period of stimulation was automatically decremented. The entrainment rhythm during periodic stimulation was determined by visual inspection of the recorded voltage traces.

## 6.3 Iteration of phase resetting curves (PRC's)

The theory underlying the computation of phase locking based on the iteration of phase resetting curves is discussed at length elsewhere [181, 80, 67]. Briefly, the response of the preparation to periodic stimulation can be predicted from the corresponding PRC provided that the stimulation does not alter the intrinsic properties

of the oscillator. The main idea is that a single stimulus instantaneously resets the phase of the oscillation from one point of the cardiac cycle to another point on the cycle. For a given amplitude of stimulation, the phase resetting curve (PRC)  $\frac{T(\phi)}{T_0}$  (where  $T_0$  is the control cycle length and  $T(\phi)$  is the perturbed cycle length caused by a stimulus delivered at phase  $\phi$ ) describes the perturbation in the cycle length induced by a single stimulus delivered at phase  $\phi$ . Let now  $\phi_i$  be the phase of the  $i^{\text{th}}$  current pulse. We have,

$$\phi_i = f(\phi_{i-1}, \theta) = 1 + \phi_{i-1} - \frac{T(\phi_{i-1})}{T_0} + \theta \pmod{1}, \quad (6.1)$$

where  $\theta = T_s/T_0$  with  $T_s$  being the cycle length of the stimulus train, and  $\frac{T(\phi_{i-1})}{T_0}$  is obtained from the experimentally determined phase response curve  $PRC(\phi)$ . Under the assumption that  $\phi_0$  is the phase of the unperturbed spontaneous cycle at which the first stimulus of a train of periodic pulses is delivered, Equation (6.1) can be numerically iterated to determine the dynamics.

During periodic stimulation, 3 types of behavior are observed in Equation (6.1): quasiperiodicity, periodic orbits and chaotic dynamics. The Lyapunov number defined as:

$$\lambda = \lim_{N \rightarrow \infty} \frac{1}{N} \sum_{i=1}^N \ln |f'(\phi_i, \theta)|, \quad (6.2)$$

where  $N$  is the total number of iterations and  $f'(\phi_i, \theta)$  is the first derivative of the function  $f$  evaluated at successive phases  $\phi_i$ , can be used to discriminate between these 3 types of behavior [70]. The Lyapunov number is zero for quasiperiodicity, negative for periodic cycles and positive for chaos [87, 139].

Before carrying out the iteration procedures, the experimentally obtained phase resetting curves were fitted to analytical functions in order to reduce experimental noise (high local derivatives) due to fluctuations in cycle length. Based on our present understanding of the ionic mechanisms underlying electrical activity in cardiac preparations there is no *a priori* reason to choose a particular function to fit the PRC's. For the two highest amplitudes of stimulation, we used the functions:

$$\frac{T(\phi)}{T_0} = 1 + \frac{b}{\phi - \phi_0} + \frac{b}{\phi_0}, \quad (6.3)$$

when  $\phi \leq \phi_{crit}$ , and

$$\frac{T(\phi)}{T_0} = \phi \quad \text{otherwise (immediate premature action potential)}. \quad (6.4)$$

Since we assume that there is a rapid return to the limit cycle after the stimulus, the discontinuity in the PRC at  $\phi_{crit}$  (the phase of discontinuity) must be equal to 1 [67], and we have  $\phi_{crit} = \frac{\phi_0^2 + b}{\phi_0}$ . Because the lowest amplitude stimulus induced almost no changes in the cycle length of the preparation, we did not apply the iterative method for this stimulus intensity. The remaining PRC seems to violate the continuity assumption outlined above. This case is analogous to previous experimental observations reported in other cardiac preparations (see for example reference [70], pp. 113-116), or to phase resetting of integrate and fire models [68]. Although the presence of this apparent discontinuity may be attributable to insufficient experimental precision [70], we nonetheless used a simple piecewise linear function to fit the PRC. The theoretical implications of discontinuous phase resetting are further discussed elsewhere [70, 67, 181]. The PRC's were fitted using a graphics package (SigmaPlot) on an IBM compatible computer. The exact functions used to fit the experimental curves and the corresponding parameters are given in the legend of Figure 6.4.

## 6.4 Results

### 6.4.1 Phase resetting

The response of biological oscillators to a single stimulus depends on the amplitude of the stimulus and the phase of the oscillation where the stimulus is delivered [181, 80, 67] Figure 6.1A describes the phase-resetting protocol and defines the measurable quantities used throughout this part of the study. The control cycle length is denoted by  $T_0$ . The upstroke of the action potential is defined to have zero phase. A 20 msec depolarizing stimulus introduced every tenth action potential at increasing delay  $t_s$  (or phase  $\phi = \frac{t_s}{T_0}$ ) after the upstroke of the action potential induces a perturbed cycle length  $T_1$ . The time intervals from the last spontaneous AP to the  $j^{th}$  AP following the premature stimulus are denoted by  $T_j$ ,  $j=1$  to 5, as described in Figure 6.1A. In Panels B through D of Figure 6.1 we present superimposed voltage traces showing the response to stimulation in 3 different preparations. In all panels, the stimuli appear as the off-scale deflections and all the voltage traces are aligned on the upstroke of the last spontaneous action potential before stimulation. For

short coupling intervals, the stimulus fails to elicit a premature AP and the onset of the next spontaneous AP is generally delayed. For larger coupling intervals the stimulus evokes a premature action potential. In the atrial embryonic chick heart cell aggregate (Panel B), the phase of the stimulus does not significantly affect the size and shape of the premature AP. The traces presented in panels C and D were obtained from two different AV nodal clusters. The differences in spontaneous action potential morphologies may simply reflect the histological heterogeneity of the AV node [12, 128]. In both cases however, the premature action potential amplitudes, upstroke velocities and durations are strongly affected by the prematurity of the stimulus. This is in agreement with previous observations from the intact AV node [12] and may have important consequences on impulse conduction through the AV node. For example, during sustained periodic stimulation, the presence of graded responses may increase the complexity of the rhythms observed. Also, in the intact heart, a graded response to atrial stimulation may be insufficient to excite neighbouring cells therefore resulting in failed conduction.

The experimental protocol explained in Figure 6.1A can also be used to construct the phase resetting curve (PRC) for a given amplitude of the stimulus. The PRC describes the perturbation in the cycle length induced by a stimulus delivered at various phases of the cycle. The perturbed cycle length  $\frac{T_j}{T_0}$  is plotted as a function of the phase  $\phi$  of the premature stimulus. Under the assumption that the cardiac rhythm is a strongly attracting oscillation with rapid relaxation back to the cycle following the stimulation, the PRC can be used to predict the response of the preparation to sustained periodic stimulation [181, 67, 80]. In Figure 6.2 we present PRC's obtained from an AV nodal cell cluster for 4 different amplitudes of stimulation. In order to emphasize the general shapes of the curves and the presence of time-dependent effects, we chose to represent  $T_j$ ,  $j = 1$  to 5 (as defined in Figure 6.1A), normalized to control cycle length  $T_0$ , versus the phase  $\phi$ . For the same reason, the original data obtained for  $\phi$  between 0 and 1 is also repeated 3 times on the phase axis. For the lowest intensity of stimulation (24 nA, Panel A) a premature stimulus does not perturb the cycle length significantly. The predominance of horizontal lines in this panel is a hallmark of "weak" or "type 1" phase-resetting. In Panel B (48 nA, moderate intensity), as the phase of the stimulus increases, there is a sudden induction of premature AP's producing large gaps between the segments of the curves: we have an interesting example of an apparently discontinuous phase-resetting curve. In Panels

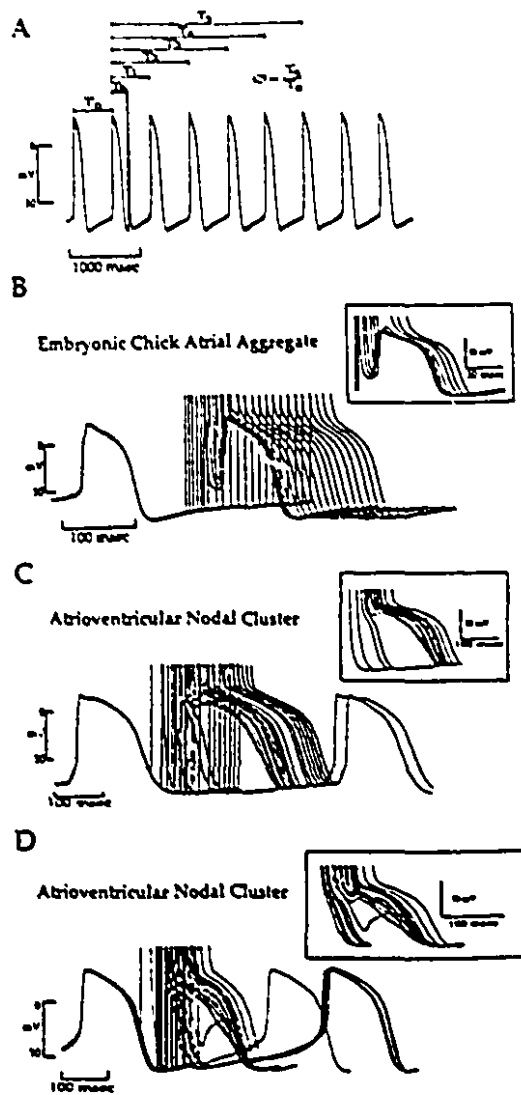


Figure 6.1: Description of the phase resetting protocol (Panel A) and traces showing response to premature stimulation for 2 different types of preparations (Panels B to D). Panel A: A 20 msec depolarizing stimulus of fixed amplitude is applied every 10 AP's at increasing phase  $\phi = \frac{t}{T_0}$ . Panels B through D: Superimposition of traces showing response to premature stimulation for 3 different preparations as the phase of the stimulus increases. The inserts show the premature AP's on a magnified scale. In Panel B (atrial embryonic chick heart cell aggregate),  $T_0 = 500$  msec, amplitude = 30 nA. In Panels C and D (AV nodal cell clusters), respectively,  $T_0 = 320$  msec, amplitude = 75 nA and  $T_0 = 550$  msec, amplitude = 120 nA. All the data presented in the remaining figures of this study was obtained for preparation C.

C and D (96 and 120 nA respectively), as the phase of the stimulus increases, there is first a delay in the onset of the next spontaneous AP. For larger stimulus phases, a premature AP is evoked. The predominance of diagonal lines in these panels indicates "strong" or "type 0" phase resetting. The relationship between "weak", "strong" or discontinuous phase resetting and the dynamics observed during periodic stimulation is discussed thoroughly in the literature [181, 67, 68].

Phase resetting normally implies that only the phase of the oscillation is affected by the premature stimulus. However, single stimuli may produce long lasting effects. For instance, in Panel C, a stimulus at phase  $\phi = .85$  first advances the phase of the oscillation ( $T_1 \approx .85$ ) but after 1 to 5 beats there is a net delay in the phase of the oscillation (for instance:  $T_3 \approx 5.2$ ). This effect is primarily due to a prolongation of the first interbeat interval following the premature AP ( $T_2 - T_1$ ) and is analogous to phenomena observed in the intact heart. In Figure 6.3 we summarize the relationship between the magnitude of this time-dependent effect and the phase of the stimulus as well as the number of stimuli applied. We also draw a comparison between our observations from AV nodal clusters (right hand panels) and atrial embryonic chick heart cell aggregates (left hand panels). In the top panels we show the two first normalized interbeat intervals ( $(T_2 - T_1)/T_0$  and  $(T_3 - T_2)/T_0$  respectively) after the premature AP, as a function of the phase of the stimulus. In both preparations, the initiation of a single premature AP is associated with a transient lengthening (up to 10 % in atrial embryonic chick heart cell aggregates, up to 40 % in clusters of AV nodal cells) of subsequent interbeat intervals. In atrial embryonic chick heart cell aggregates, there is a direct relationship between the amount of post-drive prolongation and the prematurity of the evoked AP (open symbols, first cycle length after premature AP, normalized to control). This time-dependent effect decays in time (filled symbols, second cycle length after premature AP, normalized to control). In clusters of AV nodal cells, there is a reverse relationship for the perturbation in the first cycle after the premature AP. However, there is no significant difference between the perturbation in the second cycle length as observed in embryonic chick heart atrial cell aggregates or AV nodal cell clusters (respectively, Panels A and B, filled symbols). This observation suggests that, in AV nodal clusters, two different mechanisms play a role in prolonging (or shortening) the cycle length after premature stimulation.

These changes in cycle length may have important effects on AV nodal excit-

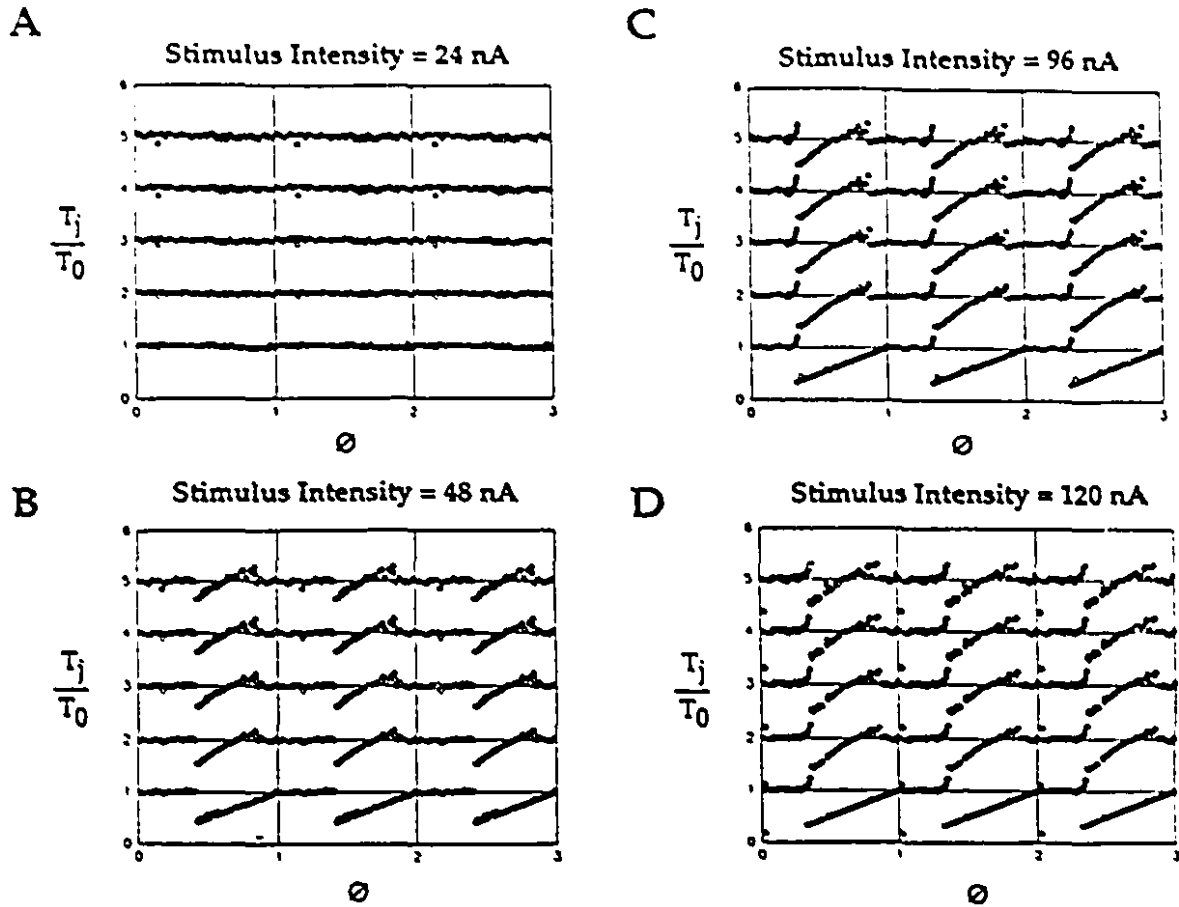


Figure 6.2: Phase resetting curves for AV nodal cell clusters using the protocol described in Figure 6.1A. Current pulses of 4 different intensities: 24 nA (Panel A), 48 nA (Panel B), 96 nA (Panel C), 120 nA (Panel D) were introduced every tenth spontaneous action potential. The normalized quantities  $\frac{T_j}{T_0}, i = 1$  to 5 are plotted as a function of the phase of the stimulus  $\phi = \frac{t}{T_0}$ .  $T_0$  is the average of five control cycle lengths before the stimulus. Panel A shows "weak" and Panels C and D show "strong" resetting. In Panel B, "discontinuous" resetting is observed. The lack of vertical translational symmetry may indicate the presence of a time-dependent process.

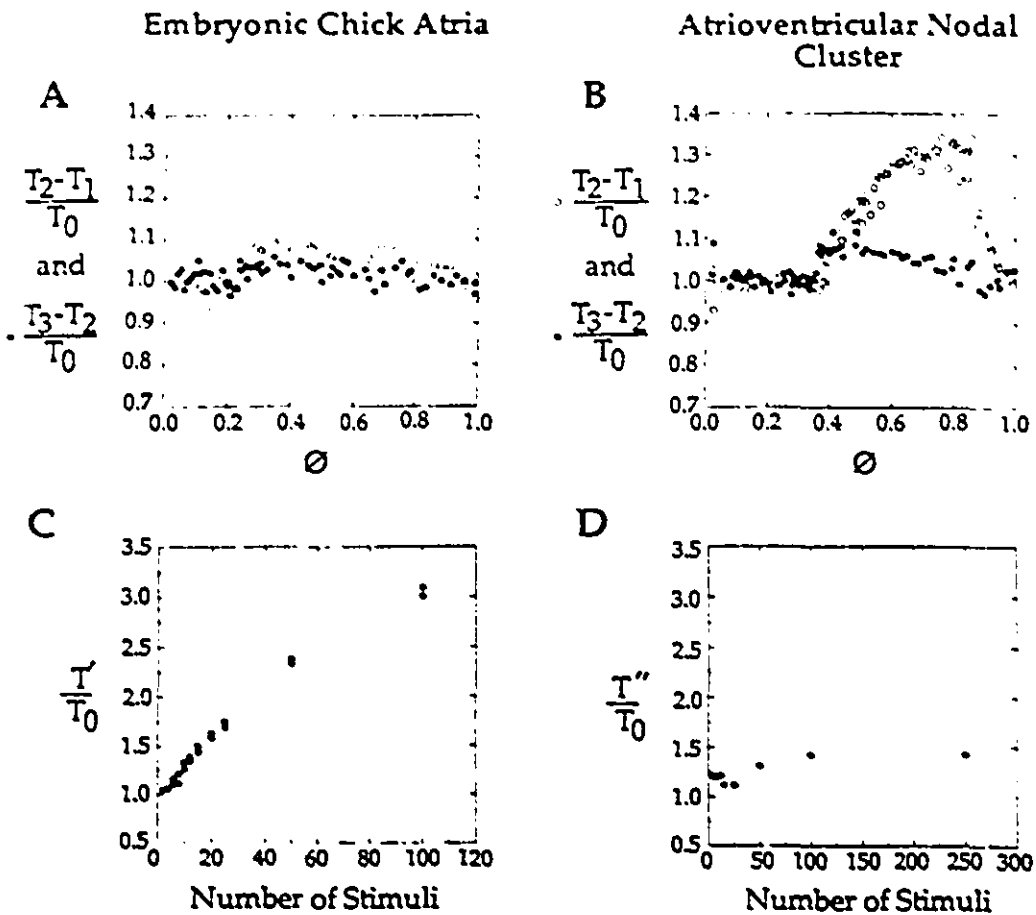


Figure 6.3: The effects of single or periodic stimulation on the interbeat interval (IBI) immediately following the pulse. Left hand panels: atrial embryonic chick aggregate. Right hand panels: AV node cell cluster. In Panels A and B: First and second interbeat intervals ( $T_2 - T_1$ , open symbols and  $T_3 - T_2$ , filled symbols), normalized to control cycle length, as a function of the phase  $\phi$  of the premature stimulus. The data in Panel B corresponds to the PRC shown in Figure 6.2D. In atrial chick heart aggregates, the perturbation in the first cycle length after the stimulus increases with the prematurity of the evoked action potential. In AV nodal clusters, a reverse relationship is observed for a wide range of stimulus phases. However, the perturbation in the second IBI following the stimulus is again an increasing function of the action potential prematurity. In Panels C and D: first IBI ( $T'$ ) after cessation of stimulation, normalized to control cycle length  $T_0$ , as a function of the number of stimuli applied. In both cases, the period of stimulation was  $0.6 T_0$  (1:1 entrainment). Note the striking differences in the magnitude of overdrive effects between the two preparations.

ability. For example, a prolonged interbeat interval may increase the refractoriness of the preparation to forthcoming excitation. Given the considerable magnitude of this effect (up to 40 %) and its rapid decay, we speculate that it may represent a protective and stabilizing mechanism against undesirable premature excitation.

#### 6.4.2 Overdrive suppression

Overdrive suppression can be defined as a transient suppression of automaticity following sustained periodic stimulation at a frequency faster than the intrinsic rate of the preparation and is the mechanism which ensures, in the intact heart, the domination of the SA node over subsidiary pacemakers [173] (including the AV node). Overdrive suppression has been studied extensively in a variety of preparations, including embryonic chick heart cell aggregates [186, 111]. There have been several theoretical attempts to model overdrive suppression in order to account for rate-dependent effects in the heart and for the evolution of rhythms during periodic stimulation [186, 111]. In some of these models, the change in the cycle length following a single stimulus was attributed to overdrive suppression. Following periodic stimulation in atrial embryonic chick heart cell aggregates the length of the post-drive pause increases with the number of stimuli and is directly proportional to the action potential frequency during the drive [111]. In Panels C and D of Figure 6.3 we show the length of the first interbeat interval after the drive normalized to control cycle length,  $\frac{T'}{T_0}$ , as a function of the number of stimuli applied. In all cases 1:1 entrainment was maintained between the stimulator and the preparation. In atrial aggregates, after 100 stimuli (pacing cycle length = .6 control cycle length), the spontaneous interbeat interval is 3 times control. Under similar conditions, in AV nodal cell clusters, we observe only 50 % of prolongation of the spontaneous cycle length (roughly equal to the amount of single stimulus overdrive). Since various cell parameters such as cell input impedance and the ionic basis of activity are different for AV nodal cells than for cells from the surrounding myocardium [162, 128], these results are not surprising. This finding may be consistent with the distinct and specialized functional properties of AV nodal tissue.

### 6.4.3 Periodic stimulation

In the healthy heart, the SA node normally entrains the AV node rhythm in a 1:1 fashion. However, in the clinical context, examples abound of other entrainment rhythms which often correspond to distinct pathological situations. Different mechanisms are generally believed to underly these various rhythms including Wenckebach, reverse or alternating Wenckebach and Mobitz type II atrioventricular block. Analogous rhythms can also be found in *in vitro* preparations [80, 78]. These rhythms can often be predicted using simple theoretical paradigms which suggests that they can be described in terms of dynamical properties of excitable cardiac tissue [80, 67]. In Figure 6.4 we identify some of the rhythms observed during periodic stimulation of AV nodal cell clusters with different stimulation frequencies for the 4 intensities corresponding to the PRC's in Figure 6.3. For the 3 highest amplitudes of stimulation, we draw a comparison between the experimentally observed rhythms (various symbols) and some of the entrainment patterns obtained by iterating the corresponding PRC's (horizontal bars: 1:1, 2:1, 3:1 phase locking; stippled: period doubling bifurcations and irregular dynamics). The experimentally observed patterns of entrainment were determined by visual inspection of the voltage traces. Since there was often an evolution of the rhythms during the drive, only stable rhythms were represented. For reasons of clarity only the most important patterns of entrainment are indicated. For example, at the lowest stimulus intensity, a plethora of quasiperiodic and Wenckebach rhythms can be found between 1:1 and 2:1 entrainment. In general the structure of the phase-locking zones (where the same type of N:M entrainment is found for different frequencies and amplitudes of stimulation) is similar to that observed in other *in vitro* preparations and to the theoretical predictions based on simple models of biological oscillators [78, 80, 67]. As the frequency of the stimulation increases, higher degrees of block are observed. The fact that we observe a 2:2 rhythm and 3:2 rhythm for the same amplitude of stimulation (96 nA) deserves special mention. A 2:2 rhythm corresponds to a period-2 oscillation in the phase of the stimulus. As the frequency of stimulation is increased, loss of entrainment will occur for one of the AP's in the period-2 cycle: we expect to have 2:1 entrainment (although a narrow band of 3:2 entrainment can sometimes be found). In view of this, our observation is interesting since it may suggest that a slow regenerative process is present that modulates AP duration. This is reminiscent of the

rate-dependent modulation of the action potential duration by the transient outward current in ventricular myocytes [103]. In some cases it is possible to drive the preparation in 1:1 fashion at a rate slower than control. Interestingly, there are very large zones where 2:2 and 4:2 entrainment is found. These entrainment patterns as well as the irregular rhythms correspond to situations where the action potential morphology is strongly modulated by stimulation (e.g. alternans). Because the PRC does not carry information related to changes in AP morphology induced by premature stimulation, the iteration of the PRC does not predict the existence of the wide regions where this type of complex action potential alternans and irregular dynamics are experimentally observed.

A simple description of the changes in action potential morphology during periodic stimulation can be obtained by calculating the area under the action potential with respect to some arbitrary threshold. In order to illustrate some of the observed rhythms, we show, in Figure 6.5, 9 voltage traces recorded during periodic stimulation. The rhythms that we chose are indicated in Figure 6.4 by capital letters referring to the panels of Figure 6.5. Under each trace, we show the corresponding AP area as computed using a trapezoidal integration rule of the voltage traces with respect to the  $-45$  mV threshold (as shown in the insert of Panel A). For presentation reasons, only 5 seconds traces are shown. Since a large stimulation artifact is present in our recordings, it may sometimes give rise to a small area. A sample of spontaneous activity is shown in Panel A. Under control conditions, there is no beat to beat changes in AP area. The same result holds for 1:1 stimulation as shown in Panels B. In Panel C, the preparation is underdriven (stimulus frequency lower than intrinsic rate) in a 1:1 fashion. In this case (and in subsequent panels too), the small area values are due to the stimulus artefact and ought to be ignored. Therefore, as in the previous case (Panel B), the area under the AP is constant during the drive. In Panels D and E, respectively, examples of 2:1 and 3:1 entrainment are shown. There are again no changes in AP area during the drive. The situation is more complicated in the remaining four panels (F through I). In Panel F, each stimulus evokes an AP but the shape of the AP changes, repeating itself every 4 stimuli (4:4 entrainment).

This alternation in AP parameters is nicely described by the plot of the AP area as a function of time. In a number of similar cases, visual inspection of rhythms can result in misleading interpretations. The measurement of the area under the AP therefore represents a useful complementary tool in characterizing the observed

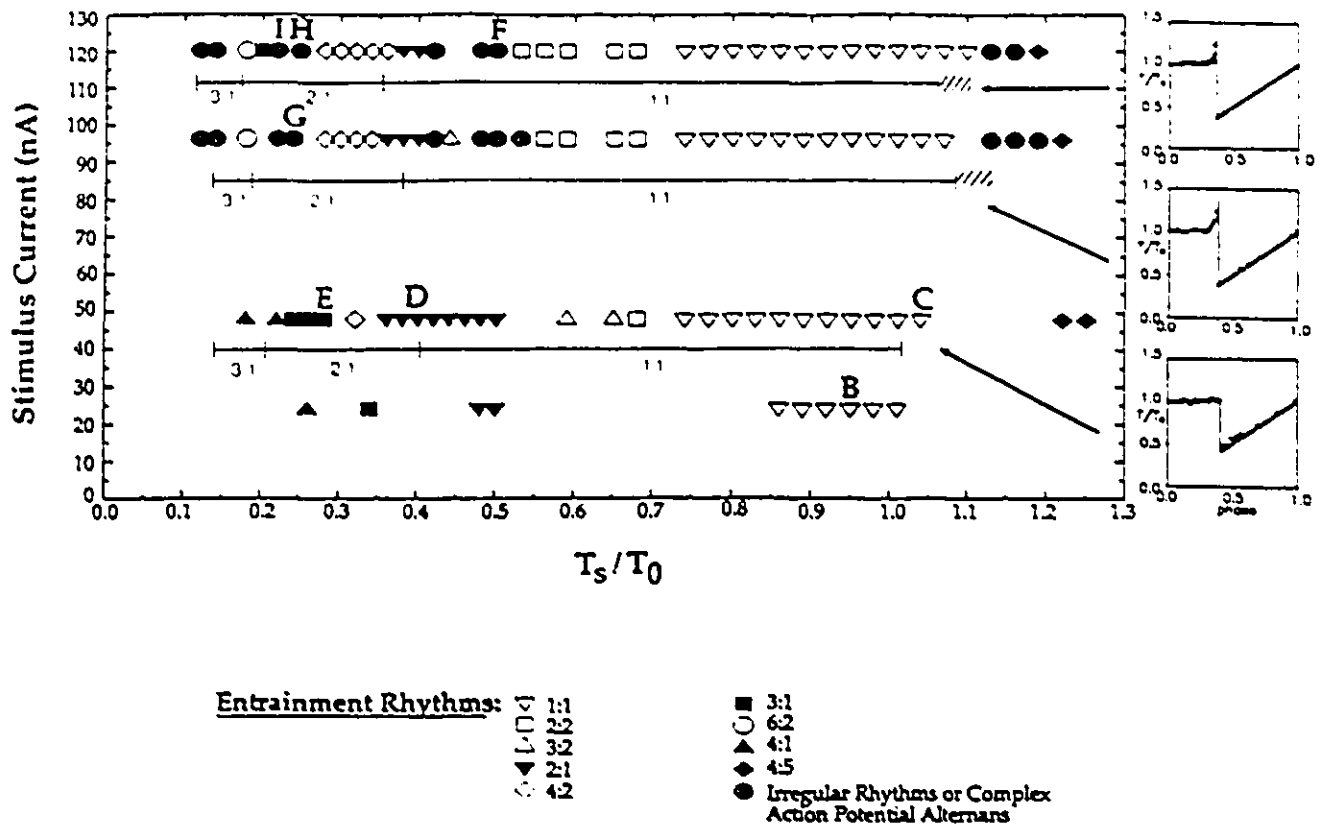


Figure 6.4: Phase locking zones. The various symbols illustrate different phase locked rhythms, as determined from visual inspection of experimental recordings obtained for 4 different amplitudes of stimulation, during sustained periodic stimulation for 100 stimuli at different frequencies. The horizontal bars indicate regions where 1:1, 2:1 and 3:1 entrainment was predicted based on the iteration of the PRC's (inserts). In the stippled regions, period doubling bifurcations and irregular dynamics were found. The abscissa is the period of stimulation normalized to control. The amplitude of the stimulus (in nA) is plotted on the vertical axis. The symbols represent 4:1 ( $\Delta$ ), 6:2 ( $\circ$ ), 3:1 ( $\square$ ), 4:2 ( $\diamond$ ), 2:1 ( $\nabla$ ), 3:2 ( $\triangle$ ), 2:2 ( $\square$ ), 1:1 ( $\nabla$ ), 4:5 ( $\diamond$ ), and irregular rhythms or long period action potential alternans ( $\bullet$ ). Note the prominence of the 2:2 zone and the large number of irregular looking rhythms. The letters B to I refer to the panels in Figure 6.4 where a few experimental traces during sustained periodic stimulation are shown together with information describing the evolution of action potential morphology during the drive. The experimentally measured phase resetting curves (points) superimposed on the fitted analytical functions (solid curves) used in iterative procedure are shown in the inserts. At the two highest amplitudes of stimulation (discontinuity = 1):  $\frac{T(\phi)}{T_0} = 1 + \frac{b}{\phi - \phi_0} + \frac{b}{\phi_0}$  when  $\phi \leq \phi_{crit}$  and  $\frac{T(\phi)}{T_0} = \phi$  otherwise. For 120 nA:  $b = -0.00179$ ,  $\phi_0 = 0.3705$ ,  $\phi_{crit} = 0.3656$ . For 96 nA:  $b = -0.00531$ ,  $\phi_0 = 0.3974$ ,  $\phi_{crit} = 0.3841$ . The PRC obtained with 48 nA stimuli was fitted using a piecewise linear function:  $\frac{T(\phi)}{T_0} = a\phi + b$  where  $a = 1.06$ ,  $b = 1$  when  $\phi \leq 0.408$  and  $a = 1$ ,  $b = 0$  otherwise.

dynamics. Other complicated rhythms can also be found. For example, in Panel G, there is a great deal a variability in the shapes of the action potentials, superimposed on a 2:1 rhythm. However, from the evolution of AP area as a function of time, a period-6 oscillation becomes transparent indicating that we have found 12:6 entrainment. Although the periodicity is not as clear in Panel H, this trace seems to correspond to 12:12 locking between the stimulator and the preparation. In Panel I, there are erratic changes in action potential morphology during stimulation. This recording is an example of an irregular rhythm. In all cases it is the changes in action potential morphology that account for the complexity of the dynamics. Although our measure of the area does not have a transparent physiological meaning, it is efficient at detecting general changes in AP morphology. In the clinical context, such changes may be important since they may influence impulse propagation through the AV node.

#### 6.4.4 Conclusions

In this study, we showed that the action potential characteristics of AV nodal cell clusters are modulated by the prematurity of the stimulus. These results are consistent with previous observations from the intact AV node [12] and single cellular preparations [162]. Moreover, single or sustained stimulation induces time-dependent effects that alter the spontaneous activity of the preparation and its excitation properties. During periodic stimulation, we find a variety of entrainment patterns which are analogous to the ventricular rhythms observed during atrial stimulation in the clinical setting. In many of these rhythms, there are large beat to beat changes in action potential morphology that increase the complexity of the observed dynamics and are not accounted for by the iteration of the phase resetting curves.

In electrocardiography, the term "concealed conduction" describes a situation where an atrial excitation fails to transverse the entire AV node [121, 2, 147]. Although active propagation is interrupted in this situation, remnant electrotonic currents will continue to propagate away from the site of block. The resulting sub-threshold activity at sites distal to the site of action potential failure is related to several phenomena that can affect the response of the AV node to subsequent activations (for review, see Pick et al. [147]). In view of this, concealed conduction is sometimes related to "electrotonic inhibition" as described by Antzelevitch and Moe

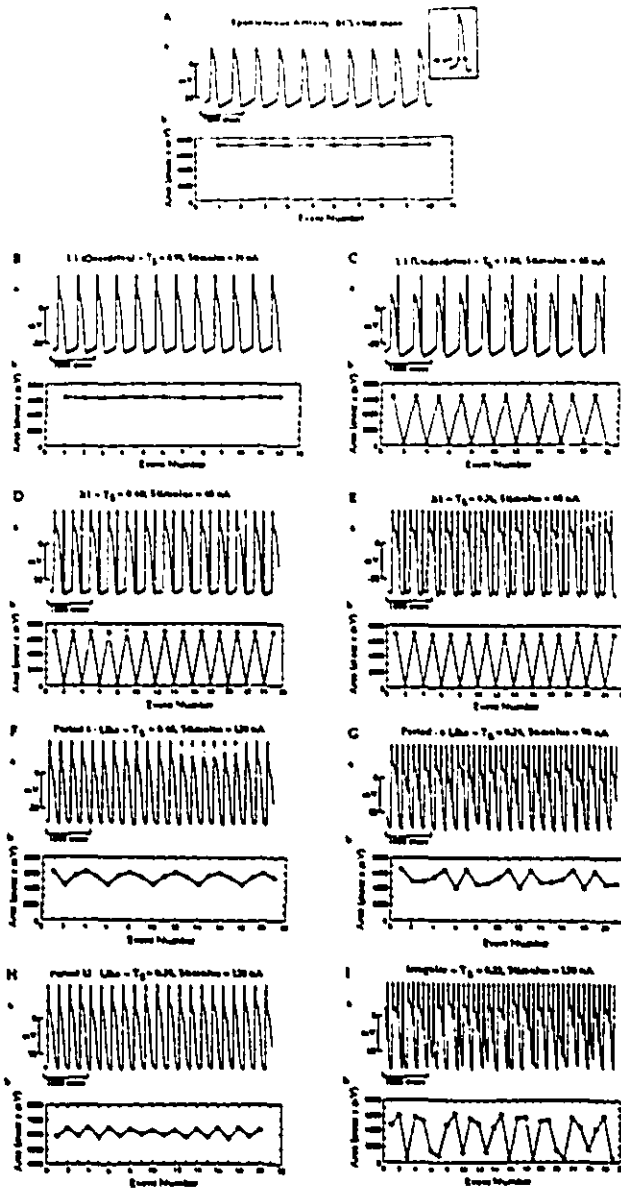


Figure 6.5: Experimental traces of recorded transmembrane potentials showing a few chosen entrainment rhythms (see corresponding letters in Figure 6.4) observed during sustained periodic stimulation (100 stimuli) at different frequencies and intensities of stimulation. For clarity, only 5 second traces are presented in each panel (Part a.). The stimulus artefacts appear as the off-scale vertical deflections. In Panel A, a sample of spontaneous activity is shown. The insert (right corner) describes the procedure for calculating the area under the action potential which corresponds to the area comprised between the experimental AP trace and the threshold fixed at  $-45$  mV. In each panel, the evolution of the area under the AP is shown in Part b. of the panel. In each panel, the strength, the period of stimulation (normalized to control) and the visually determined entrainment rhythm are indicated. Under certain circumstances, a failed action potential may result in a small but non-zero measured area. In some cases, very complex behavior is observed, associated with marked changes in AP characteristics.

[2]. The possible relationship between these two phenomena is further discussed by Liu et al. [121]. Our data collected during the phase-resetting protocol clearly shows that a single stimulus can modulate action potential morphology and produce phase dependent effects on intrinsic excitability cell. During periodic stimulation, we also observe great variability in action potential characteristics. Under *in vivo* conditions, graded responses may be insufficient to propagate through the entire AV node, and contribute to concealed conduction.

“Fatigue” is a rate-dependent prolongation in AV nodal conduction time that may be responsible for the evolution of rhythms often observed experimentally during sustained atrial pacing [13, 14]. For example, in healthy patients, atrial stimulation at rates faster than the sinus rate disturbs AV nodal conduction and causes an evolution of rhythms from 1:1 entrainment towards Wenkebach rhythms (periodic rhythms showing a progressive increase or decrease in action potential to stimulus latency before loss of entrainment) and higher degrees of AH block [24]. In our experimental study, we observe analogous effects. We have shown that a single premature AP can induce a significant change in the following interbeat interval (up to 40%). Periodic stimulation at a rate faster than control is followed by post-drive pause (up to 50%) that, for long episodes of pacing, is virtually independent of the duration of the drive, which is in agreement with previous studies carried out in nodal tissue [74]. This in contrast with overdrive suppression in atrial embryonic chick heart cell aggregates where the magnitude and the build-up of this effect are much more pronounced [186, 111]. The discrepancy in the magnitude of overdrive suppression measured in these two different preparations is likely to reflect the different nature of the underlying ionic mechanisms. Previous studies suggest that, although the sodium pump plays a major role in overdrive suppression in embryonic chick heart atrial cell aggregates [143], other factors, including increased internal calcium concentration and acetylcholine are determinant in overdrive suppression in nodal (SA) tissue [74]. Since there is a great deal of similarity between SA nodal and AV nodal cells, the same mechanisms may be involved in our experimental observations.

Under normal circumstances, there is 1:1 entrainment between the SA nodal and the AV nodal rhythms. By changing the frequency and the amplitude of the stimulation imposed on the AV nodal cell clusters, we investigated the response of AV nodal tissue to stimulation protocols which may simulate real pathological situations. The resulting rhythms, including Wenkebach and 2:1 block are analogous to experimental

or clinical observations. Recently, a number of simple iterative mathematical models were developed to account for the dynamics during periodic stimulation. For example, the structure of the phase-locking zones (different types of N:M entrainment) in an amplitude versus period of stimulation diagram (such as in Figure 4) can be predicted based on the topology of the experimentally determined PRC [181, 67, 68] (e.g. "type 1" or "type 0"). To date, most of the studies aimed at studying the dynamics during periodic stimulation were carried out in *in vitro* preparations which consisted of cells characterized by high AP upstroke velocities and hence almost ideal "one or none" responses to stimulation. However, in our preparation, the presence of graded responses plays an important role in increasing the complexity of the dynamics. As a consequence, mathematical models that incorporate both time-dependent effects in the cycle length and changes in action potential morphology must be developed. For example, two pulse protocols could be designed to study the relationship between the areas of successive premature action potentials, as well as the influence of single stimulus overdrive on the phase resetting properties of the preparation. Subsequently, a theoretical model, in the form of a pluri-dimensional difference equation, could be designed to encompass phase resetting, action potential area and overdrive, in an attempt to simulate the complex rhythms observed in the experimental context.

There is still a poor understanding of the ionic mechanisms that underly the electrical activity of AV nodal cells [162]. This task is made even more difficult by the diversity of cell profiles found in the AV node [12, 133, 162]. In the intact heart, a large number of hormonal, neural and mechanical inputs influence the properties of the AV node. All of these factors can influence the results of *in vivo* studies of the intact AV node, but can be more easily controlled by using our *in vitro* preparation. We hope that a combination of these different complementary approaches will give us a better understanding of how the AV node responds to sustained atrial pacing.

# Conclusions

This thesis studies the time dependent properties of excitable cardiac tissue, and their contribution to the dynamics during various stimulation protocols. Previous simplified models of the dynamics during sustained stimulation relied on the assumption that stimulation resets the phase of the cycle without changing the intrinsic properties of the oscillation. The experimental protocols performed in this study were specifically designed to examine situations where this assumption breaks down. The theoretical models presented in this thesis were developed to capture the contribution of time dependent effects to the experimentally observed dynamics, based on careful studies of the relationship between the excitability of the tissue and stimulation history, and to better understand the mechanisms underlying rhythmogenesis in the heart.

## Overdrive suppression

Overdrive suppression (underdrive acceleration) is the transient decrease (increase) in the intrinsic firing frequency following stimulation at a rate faster (slower) than control [173]. In embryonic chick heart cell aggregates, the sodium potassium pump is the major mechanism underlying overdrive suppression [143]. The qualitative study presented in Chapter 4 shows that the levels of overdrive suppression are an increasing function of drive duration and of action potential frequency. For a given stimulation frequency, overdrive suppression decreases with increasing degree of block. Since maximal overdrive suppression is associated with the fastest possible action potential frequency in a given entrainment regime, this finding may explain the peaking of overdrive suppression at intermediate frequencies often observed during the sinus node recovery test [101]. Overdrive suppression may also contribute to the evolution of rhythms reported experimentally and clinically under various stimu-

lation protocols [186]. The experimental study of Chapter 5 shows that, during fixed delay stimulation, overdrive suppression is responsible for the gradual increase in the interbeat intervals under conditions where the reentrant loop is maintained and may lead to the termination of reentrant activity. Similar time dependent phenomena (overdrive suppression, fatigue) may therefore play a crucial role in the sudden onset or termination of potentially lethal tachycardias.

## Theoretical modeling

The theoretical models of overdrive suppression described in this thesis were developed using a double strategy: (1) nonlinear models were constructed to provide a theoretical framework of relative transparency and simplicity, non preparation-specific and therefore applicable to a variety of systems; (2) the Shrier-Clay ionic model of electrical activity in embryonic chick heart cell aggregates was modified to include a simplified sodium pump term, thereby providing the means of understanding the experimentally observed dynamics in terms of the underlying ionic mechanisms.

The first of the nonlinear models is the classical iteration of the phase resetting curve used to predict and understand the mathematical structure of the dynamics arising during sustained periodic stimulation [78, 70]. Although this model is very successful at moderate stimulation frequencies, the lack of time dependent contributions limits its usefulness at rapid stimulation rates. A review of the results obtained by iteration of this model with phase resetting curves obtained experimentally or by numerical simulation of the Shrier-Clay equations was presented in Chapter 3. Since this class of models does not rely on preparation-specific ionic mechanisms, the results are applicable to a variety of oscillating or periodic systems [70, 181]. This model was modified in Chapter 5 to include a time dependent term that modifies the intrinsic beat rate by means of a weighted contribution of the preceding cycle lengths. The main assumption is that, provided that the phase of the stimulus is rescaled to the instantaneous cycle length of the preparation, the effects of a single stimulus on the rhythmic activity may be predicted based on the experimentally observed phase resetting curve. The success of this model lies partly in the fact that it combines the experimentally determined, and hence realistic phase resetting curves, with a reasonably efficient description of the overdrive-induced changes in the intrinsic cycle length.

Models based on iterative techniques necessarily imply a discretization of experimental time. Since overdrive suppression in embryonic chick heart cell aggregates is due to the increased activity of a hyperpolarizing current, a simplified model expressed in terms of ordinary differential equations was also developed. The theoretical model described in Chapter 4 is a simplified relaxation oscillator modified to include a time dependent term. The main assumption is that overdrive suppression is due to a hyperpolarizing current that is induced by action potentials. Despite good qualitative agreement with the experimentally obtained measurements of overdrive suppression following periodic stimulation at different frequencies, stimulation intensities and entrainment regimes, this theoretical model does not properly mimic the details of the experimentally determined phase resetting curves. Thus, the usefulness of the model is limited to experimental situations where the detailed shape of the phase resetting curve is not determinant to the rhythmic activity. However, the model is based on physiologically plausible assumptions and captures the dependence of overdrive suppression upon the duration of the drive and the stimulation frequency. More importantly, appreciable levels of overdrive suppression can be attained only by assuming large beat to beat changes in internal sodium levels. This may suggest a possible compartmentalization of the intracellular space available to sodium ions, as previously proposed [112, 22]. Finally, a close inspection of the equations shows that, for very fast stimulation frequencies and 1:1 entrainment, the beat to beat influx of sodium ions may exceed the maximal extrusion capacity of the postulated electrogenic mechanism. As a result, some stimulation frequency may exist above which the levels of overdrive suppression do not saturate following increasing long stimulation episodes. Although not tested, this prediction may have interesting implications in the experimental and clinical settings.

The results obtained by numerical simulation of the Shrier-Clay ionic model of electrical activity were presented in Chapter 3. In this study, the results of the Shrier-Clay ionic model were tested against experimental data obtained during phase resetting and phase locking protocols. Numerically simulated phase resetting curves were also iterated for comparison between this nonlinear iterative model of a cardiac oscillator and the results from the simulation of a fully developed ionic model. The success of the ionic model in mimicking the experimental phase resetting and phase locking behaviours lies primarily in the quality of the present description of  $I_{Kr}$  and  $I_{Na}$  whose interaction underlies the details of phase resetting in embryonic chick heart

cell aggregates. In Chapter 5, I have presented a modified version of this ionic model that incorporates a simplified sodium pump term. The description of the simplified sodium pump term is similar to that introduced in the above-mentioned modified relaxation oscillator model. In spite of appropriate phase resetting behaviour, the simulations of the modified ionic model under fixed delay stimulation conditions successfully mimic the experimental rhythms only for a relatively restricted range of delays. Nonetheless, overdrive suppression is properly reproduced and further modifications consisting of a model of the sodium calcium exchanger, a more elaborate description of the sodium potassium pump as well as a possible future dynamical description of all the important ion concentrations and of their effects on the individual ionic currents, are steps to be made in the future. Given the extent of testing against experimentally observed dynamics this model has undergone, it also comes to mind that such extensive numerical experiments are seldom attempted with the currently accepted ionic models of electrical activity. A careful examination of the results of numerical integration of ionic models using various stimulation protocols may therefore represent an important additional test for the validation of existing or new ionic models.

## Cardiac dynamics

The analysis and understanding of the dynamics observed during stimulation of embryonic chick heart cell aggregates may be relevant to the interpretation of cardiac arrhythmias. For example, the different degrees of block observed during sustained periodic stimulation of this preparation have direct analogs in the intact heart, including parasystole [95, 180] and atrioventricular block [160]. In Chapter 5, fixed delay stimulation of spontaneously beating chick heart cell aggregates is an experimental model of a reentrant loop involving a pacemaker. The paroxysmal starting and stopping of rapid activity observed during fixed delay stimulation may thus provide a novel mechanism for paroxysmal tachycardias observed clinically. In addition, the slight oscillation in cycle length prior to cessation of reentrant activity described in Chapter 5 is a relatively common observation in the context of supraventricular tachycardias [153, 163]. The identification of the key factors underlying such rhythms may therefore help design future treatments of this class of dysrhythmias. Finally, the experimental rhythms of Chapter 6 strongly resemble clinically observed atrioventricular dynamics.

The heart is a complex physiological system. This anatomical complexity is reflected by the variety of ionic mechanisms found in different cardiac cells. The modeling of cardiac dynamics, at the cellular level, is thus hindered by the considerable heterogeneity of the heart. An illustration of the differences in the dynamic properties of cell from distinct regions of the heart was given in Chapter 6. Atrioventricular tissue is characterized by slow action potential upstroke velocities that reflect the kinetics of the underlying ionic mechanisms [12, 128, 162]. In contrast to atrial cell which exhibit "one or none" responses to premature stimulation, phase resetting in spontaneously active AV nodal cell clusters often results in graded or incomplete activations following stimulation. During periodic stimulation, such changes in action potential morphology play an important role in complexifying the dynamics. Since models based on the phase resetting curve do not carry information related to action potential morphology, they are inadequate in describing the experimental rhythms. Therefore, new theoretical models must be developed that encompass phase resetting, time dependent phenomena and action potential changes in order to better understand atrioventricular dynamics. This type of approach, complemented by the development of ionic models of activity and the application of modern biomolecular techniques, is an important direction towards understanding and preventing cardiac arrhythmias.

# Bibliography

- [1] J. Alanis and D. Benitez. The decrease in the automatism of the Purkinje pacemaker fibres provoked by high frequencies of stimulation. *Jap. J. Physiol.*, **17**:556, 1967.
- [2] C. Antzelevitch and G. K. Moe. Electrotonic inhibition and summation of impulse conduction in mammalian Purkinje fibers. *Am. J. Physiol.*, **245**:H42, 1983.
- [3] J. M. B. Anumonwo, M. Delmar, A. Vinet, D. Michaels and J. Jalife. Phase resetting and entrainment of pacemaker activity in single sinus nodal cells. *Circ. Res.*, **68**:1138-1153, 1991.
- [4] V. I. Arnold. Small denominators. I. Mappings of the circumference onto itself. *Am. Math. Soc. Translations*. ser. 2, vol. 46. American Mathematics Society, Providence, 1965.
- [5] I. Atwater, C. M. Dawson, A. Scott, G. Eddlestone and E. Royas. The nature of oscillatory behaviour in electrical activity for pancreatic  $\beta$ -cells. In G. Thieme, editor, *Biochemistry and Biophysics of the Pancreatic  $\beta$ -Cell*. Verlag, Stuttgart, 1980.
- [6] P. Baconnier, G. Benchetrit, J. Demongeot and T. Pham Dinh. In M. Consard, J. Demongeot and A. Le Breton, editors, *Rhythms in Biology and Other Fields of Application, Lecture Notes in Biomechanics, vol. 49*. Springer-Verlag, Berlin, 1983.
- [7] J. R. Balsler, P. B. Bennett and D. M. Roden. Time dependent outward current in guinea pig ventricular myocytes. *J. Gen. Physiol.*, **96**:835-863, 1990.
- [8] B. Bean. Two kinds of calcium channels in canine atrial cells. *J. Gen. Physiol.*, **86**:1-30, 1985.

- [9] G. W. Beeler and H. Reuter. Reconstruction of the action potential of ventricular myocardial fibres. *J. Physiol. (Lond.)*, **268**:177, 1977.
- [10] B. P. Belousov. Periodically active reaction and its mechanism. In *Collection of Papers on Radiation Medicine for 1958*. Medgiz, Moscow, 1959.
- [11] B. P. Belousov. Periodically active reaction and its mechanism. In *Autowave Processes in Systems with Diffusion*. IPF AN SSSR, Gorki, 1981.
- [12] J. Billette. Atrioventricular nodal activation during periodic premature stimulation of the atrium. *Am. J. Physiol.*, **252**:H163, 1987.
- [13] J. Billette, R. Métayer and M. St-Vincent. Selective functional characteristics of rate-induced fatigue in the rabbit atrioventricular node. *Circ. Res.*, **62**:790-799, 1988.
- [14] J. Billette and S. Nattel. Dynamic behavior of the atrioventricular node: a functional model of interaction between recovery, facilitation, and fatigue. *J. Cardiovasc. Electrophysiol.*, **5**:90, 1994.
- [15] M. P. Blaustein and M. Lieberman. *Electrogenic Transport: Fundamental Principles and Physiological Implications*. Raven Press, New York, 1984.
- [16] W. K. Bleeker, A. J. C. Mackay, M. Masson-Pévet, L. N. Bouman and A. E. Becker. Functional and morphological organization of the rabbit sinus node. *Circ. Res.*, **46**:11, 1980.
- [17] M. R. Boyett and B. R. Jewell. A study of the factors responsible for rate-dependent shortening of the action potential in mammalian ventricular muscle. *J. Physiol.*, **285**:359-380, 1978.
- [18] B. A. Bradlow. Supraventricular paroxysmal tachycardia interrupted by repeated episodes of cardiac standstill with syncopal attacks. *Chest*, **58**:122-128, 1970.
- [19] R. M. Brochu, J. R. Clay and A. Shrier. Pacemaker current in single cells and in aggregates of cells dissociated from the embryonic chick heart. *J. Physiol.*, **454**:503-515, 1992.

- [20] A. M. Brown, K. S. Lee and T. Powell. Sodium ion current in single rat heart muscle cells. *J. Physiol.*, **318**:479-500, 1981.
- [21] J. O. Bustamante and T. F. McDonald. Sodium currents in segments of human heart cells. *Science*, **220**:320-321, 1983.
- [22] E. Carmeliet. A fuzzy subsarcolemmal space for intracellular Na<sup>+</sup> in cardiac cells? *Cardiovasc. Res.*, **26**:433-442, 1992.
- [23] E. Carmeliet. Use-dependent block of the delayed K<sup>+</sup> current in rabbit ventricular myocytes. *Cardiovasc. Drugs Therap.*, **7**(Suppl. 3):599-604, 1993.
- [24] A. Castellanos, A. Internian Jr. M. M. Cox and R. J. Myerburg. Alternating Wenckebach periods and allied arrhythmias. *Pace*, **16**:2285-2300, 1993.
- [25] T. R. Chay and J. Rinzel. Bursting, beating and chaos in an excitable membrane model. *Biophys. J.*, **47**:641, 1985.
- [26] D. R. Chialvo. Toward very simple generic models of excitable cells. Order and chaos in cardiac tissues. Facts and conjectures. *Ann. N.Y. Acad. Sci.*, **591**:351-366, 1990.
- [27] D. R. Chialvo, D. C. Michaels and J. Jalife. Supernormal excitability as a mechanism of chaotic dynamics of activation in cardiac Purkinje fibers. *Circ. Res.*, **66**:525-545, 1990.
- [28] F. J. Clark and C. von Euler. On the regulation of depth and rate of breathing. *J. Physiol.*, **222**:267-295, 1972.
- [29] J. R. Clay, L. J. DeFelice and R. L. DeHaan. Current noise parameters derived from voltage noise and impedance in embryonic heart cell aggregates. *Biophys. J.*, **28**(2):169-184, 1979.
- [30] J. R. Clay and R. L. DeHaan. Fluctuations in interbeat interval in rhythmic heart-cell clusters. Role of membrane voltage noise. *Biophys. J.*, **28**(3):377-89, 1979.
- [31] J. R. Clay and A. Shrier. Developmental changes in subthreshold pacemaker currents in chick embryonic heart cells. *J. Physiol.*, **312**:491-504, 1981.

- [32] J. R. Clay, M. R. Guevara and A. Shrier. Phase resetting of the rhythmic activity of embryonic heart cell aggregates: Experiment and theory. *Biophys. J.*, **45**:699-714, 1984.
- [33] J. R. Clay. Potassium current in the squid giant axon. *Intl. Rev. Neurobiol.*, **27**:363-384, 1985.
- [34] J. R. Clay, C. E. Hill, D. Roitman and A. Shrier. Repolarization current in embryonic chick atrial heart cells. *J. Physiol.*, **403**:525-537, 1988.
- [35] J. R. Clay, R. M. Brochu and A. Shrier. Phase resetting of embryonic atrial chick heart cell aggregates. Experiment and theory. *Biophys. J.*, **58**:609-621, 1990.
- [36] J. Cohen, H. Fozzard and S. S. Sheu. Increase in intracellular sodium ion activity during stimulation in mammalian cardiac muscle. *Circ. Res.*, **50**:651-662, 1982.
- [37] T. J. Colatsky. Voltage clamp measurements of sodium channel properties in rabbit cardiac Purkinje fibers. *J. Physiol.*, **305**:215-234, 1980.
- [38] K. S. Cole. Dynamical electrical characteristics of the squid axon membrane. *Archs. Sci. Physiol.*, **3**:253, 1949.
- [39] P. Coumel, P. Attuel, R. Slama, et al. 'Incessant' tachycardias in Wolff-Parkinson-White syndrome. II: Role of atypical cycle length dependency and nodal-His escape beats in initiating reciprocating tachycardias. *Brit. Heart. J.*, **38**:897-905, 1976.
- [40] P. Coumel, J.-F. Leclercq, R. Slama. Repetitive monomorphic idiopathic ventricular tachycardia. In D. P. Zipes, J. Jalife, editors: *Cardiac Electrophysiology and Arrhythmias*. Grune and Stratton, pp. 457-468, 1985.
- [41] K. R. Courtney and P. G. Sokolove. Importance of electrogenic sodium pump in normal and overdriven sinoatrial pacemaker. *J. Molec. Cell. Cardiol.*, **11**: 787, 1979.
- [42] A. R. Cushny. Stimulation of the isolated ventricle, with special reference to the development of the spontaneous rhythm. *Heart*, **3**:257, 1911.

- [43] R. L. DeHaan. Regulation of spontaneous activity and growth of embryonic chick heart cells in tissue culture. *Dev. Biol.*, **16**:216-249, 1967.
- [44] R. L. DeHaan. The potassium sensitivity of isolated embryonic heart cells increases with development. *Dev. Biol.*, **23**:226-240, 1970.
- [45] R. L. DeHaan and H. A. Fozzard. Membrane response to current pulses in spheroidal aggregates of embryonic heart cells. *J. Gen. Physiol.*, **65**:207-222, 1975.
- [46] M. Delmar and J. Jalife. Analysis of rate-dependent activation in single atrioventricular nodal cells. *Ann. N. Y. Acad. Sci.*, **591**:23-37, 1990.
- [47] R. L. Devaney. *An Introduction to Chaotic Systems*. Benjamin/Cummings, Menlo Park, 1986.
- [48] D. DiFrancesco and D. Noble. A model of cardiac electrical activity incorporating ionic pumps and concentration changes. *Phil. Trans. R. Soc. Lond.*, **B307**:353, 1985.
- [49] D. DiFrancesco. The cardiac hyperpolarization activated current  $i_f$ . Origins and developments. *Prog. Biophys. Mol. Biol.*, **46**:163-183, 1985..
- [50] L. Ebihara, N. Shigeto, M. Lieberman and E. A. Johnson. The initial inward current in spherical clusters of chick embryonic heart cells. *J. Gen. Physiol.*, **75**:437-456, 1980.
- [51] L. Ebihara and E. A. Johnson. Fast sodium current in cardiac muscle. A quantitative description. *Biophys. J.*, **32**:779-790, 1980.
- [52] J.-P. Eckmann. Roads to turbulence in dissipative dynamical systems. *Rev. Mod. Phys.*, **57**:643, 1981.
- [53] J. Erlanger and A. D. Hirschfelder. Further studies on the physiology of heart-block in mammals. *Am. J. Physiol.*, **15**:153, 1905-1906.
- [54] B. G. Farley and W. A. Clark. Activity in networks of neuronal elements. In C. Cherry, editor, *Information Theory*, 4th London Symposium, Butterworths, London, 1961.

- [55] R. Fischmeister, L. J. DeFelice, R. K. Ayer, R. Levi and R. L. DeHaan. Channel currents during spontaneous action potentials in embryonic chick heart cells. The action potential clamp. *Biophys. J.*, **46**:267-272, 1984.
- [56] R. FitzHugh. Mathematical models of threshold phenomena in the nerve membrane. *Bull. Math. Biophys.*, **17**:257-278, 1955.
- [57] R. FitzHugh. Pulses and physiological states in theoretical models of nerve membrane. *Biophys. J.*, **1**:445, 1961.
- [58] R. FitzHugh. Mathematical models of excitation and propagation in nerve. In H. P. Schwan, editor, *Biological Engineering*. McGraw-Hill, New York, 1969.
- [59] C. H. Follmer and T. J. Colatsky. Block of delayed rectifier potassium current,  $I_K$ , by flecanide and E-4031 in cat ventricular myocytes. *Circ.*, **82**:289-293, 1990.
- [60] L. H. Frame and M. B. Simson. Oscillations of conduction, action potential duration, and refractoriness: a mechanism for spontaneous termination of reentrant tachycardias. *Circ.*, **78**:1277-1287, 1988.
- [61] D. C. Gadsby, J. Kimura and A. Noma. Voltage dependence of Na/K pump current in isolated heart cells. *Nature*, **315**:63-65, 1985.
- [62] W. H. Gaskell. On the rhythm of the heart of the frog, and on the nature of the action of the vagus nerve. *Phil. Trans. Roy. Soc. Lond.*, **173**:993, 1882.
- [63] W. H. Gaskell. On the innervation of the heart, with especial reference to the heart of the tortoise. *J. Physiol. (Lond.)*, **4**:43-127, 1884.
- [64] W. H. Gaskell. The contraction of cardiac muscle. In E. A. Schafer, editor, *Textbook of Physiology*. vol. 2. Pentland, Edinburgh, 1900.
- [65] W. R. Giles and A. C. G. van Ginneken. A transient outward current in isolated cells from the crista terminalis of rabbit heart. *J. Physiol.*, **368**:243-264, 1985.
- [66] R. F. Gilmour, J. R. Davis and D. P. Zipes. Overdrive suppression of conduction at the canine Purkinje-muscle junction. *Circulation*, **76**:1388-1396, 1987.

- [67] L. Glass, M. R. Guevara, J. Bélair and A. Shrier. Global bifurcations of a periodically forced biological oscillator. *Phys. Rev. A.*, **29**:1348-1357, 1984.
- [68] L. Glass and A. T. Winfree. Discontinuities in phase-resetting experiments. *Am. J. Physiol.*, **246**:R251-258, 1984.
- [69] L. Glass, A. Shrier and J. Bélair. Chaotic cardiac dynamics. In A. Holden, editor: *Chaos*, pp. 235-256, Princeton University Press, Princeton, NJ, 1986.
- [70] L. Glass and M. Mackey. *From Clocks to Chaos: The Rhythms of Life*. Princeton University Press, Princeton, NJ, 1988.
- [71] D. E. Goldman. Potential, impedance and rectification in membranes. *J. Gen Physiol.*, **27**:37, 1943.
- [72] P. Grassberger. Do climatic attractors exist? *Nature*, **323**:609, 1986.
- [73] C. Grebogi, E. Ott and J. A. Yorke. Crises, sudden changes in chaotic attractors, and transient chaos. *Physica*, **7D**:181, 1983
- [74] Y. J. Greenberg and M. Vassalle. On the mechanism of suppression of automaticity in the guinea pig sinoatrial node. *J. Electrocardiol.*, **23**:53-67, 1990.
- [75] M. R. Guevara, L. Glass and A. Shrier. Phase locking, period-doubling bifurcations, and irregular dynamics in periodically stimulated cardiac cells. *Science*, **214**:1350, 1981.
- [76] M. R. Guevara and L. Glass. Phase-locking, period doubling bifurcations and chaos in mathematical model of a periodically driven oscillator: A theory for the entrainment of biological oscillators and the generation of cardiac dysrhythmias. *J. Math. Biol.*, **14**:1-23, 1982.
- [77] M. R. Guevara, L. Glass, M. Mackey and A. Shrier. Chaos in neurobiology. *IEEE Trans. Syst. Man Cybern.*, **13**:790-798, 1983.
- [78] M. R. Guevara. *Chaotic Cardiac Dynamics (PhD thesis)*. McGill University, Montreal, Canada, 1984.
- [79] M. R. Guevara, L. Glass and A. Shrier. Phase resetting of spontaneously beating embryonic ventricular heart cell aggregates. *Am J. Physiol.*, **251**:H1298-H1305, 1986.

- [80] M. R. Guevara, A. Shrier and L. Glass. Phase locked rhythms in periodically stimulated heart cell aggregates. *Am. J. Physiol.*, 254:H1-H10, 1988.
- [81] M. R. Guevara, A. Shrier and L. Glass. Chaotic and complex cardiac rhythms. In D. P. Zipes and J. Jalife, editors: *Cardiac electrophysiology: From Cell to Bedside*, pp. 192-201, W. B. Saunders, Philadelphia, 1990.
- [82] M. R. Guevara. Iteration of the human atrioventricular (AV) recovery curve predicts many rhythms of AV block. In L. Glass, P. Hunter and A. McCulloch editors, *Theory of Heart. Biomechanics, Biophysics, and Nonlinear Dynamics of Cardiac Function*. Springer, New York, 1991.
- [83] F. B. Gul'ko and A. A. Petrov. On a mathematical model of excitation processes in Purkinje fiber. *Biofizika*, 15(3), 1970.
- [84] T. Gumbrielle, R. W. Campbell. Pharmacological therapy of arrhythmias complicating dilated cardiomyopathy – implications of the arrhythmogenic substrate. *Eur. Heart J.*, 14:103-106, 1993.
- [85] N. Hagiwara, H. Irisawa, H. Kasanuki and S. Hosoda. Background current in sino-atrial node cells of the rabbit heart. *J. Physiol.*, 48:53-72, 1992.
- [86] J. Hale and H. Koçak. *Dynamics and Bifurcations*. Springer-Verlag, New York, 1991.
- [87] B. L. Hao. *Elementary Symbolic Dynamics and Chaos in Dissipative Systems*. World Scientific, Singapore, 1989.
- [88] B. Hille. *Ionic Channels of Excitable Membranes, 2nd edition*. Sinauer Associates Inc., Sunderland, MA, 1992.
- [89] A. L. Hodgkin and B. Katz. The effect of sodium ions on the electrical activity of the giant axon of the squid. *J. Physiol. (Lond.)*, 108:37, 1949.
- [90] A. L. Hodgkin and A. F. Huxley. A quantitative description of membrane currents and its application to conduction and excitation in nerve. *J. Physiol. (Lond.)*, 117:500-544, 1952.
- [91] H. E. Hoff. History of the refractory period. A neglected contribution of Felice Fontana. *Yale J. Biol. Med.*, 14:635, 1941-1942.

- [92] A. V. Holden. The mathematics of excitation. In L. M. Ricciardi and A. C. Scott, editors. *Biomathematics in 1980*. North-Holland Pub. Co., the Hague, 1982.
- [93] H. Ito and L. Glass. Theory of reentrant excitation in a ring of cardiac tissue. *Physica D*, **56**:84-106, 1991.
- [94] J. Jalife and G. K. Moe. Effect of electrotonic potentials on pacemaker activity of canine Purkinje fibers in relation to parasystole. *Cir. Res.*, **39**:801-808, 1976.
- [95] J. Jalife and G. K. Moe. Biologic model of parasystole. *Am. J. Cardiol.*, **43**:761-772, 1979.
- [96] J. Jalife. *Mathematical Approaches to Cardiac Arrhythmias*. *Ann. N.Y. Acad. Sci.*, **591**, 1990.
- [97] J. Zhao. *Functional Properties and Transient Responses in the Atrioventricular Node (PhD thesis)*. Université de Montréal, Montreal, Canada, 1992.
- [98] I. R. Josephson and N. Sperelakis. On the ionic mechanism underlying adrenergic-cholinergic antagonism in ventricular muscle. *J. Gen. Physiol.*, **79**:69-86, 1982.
- [99] I. R. Josephson, J. Sanchez-Chapula and A. M. Brown. A comparison of calcium currents in rat and guinea-pig single ventricular cells. *Circ. Res.*, **54**:144-156, 1984.
- [100] M. E. Josephson and C. D. Gottlieb. Ventricular tachycardias associated with coronary artery disease. In D. P. Zipes and J. Jalife, editors: *Cardiac electrophysiology. From Cell to Bedside*, pp. 571-580, W. B. Saunders, Philadelphia, PA, 1990.
- [101] M. E. Josephson. *Clinical Cardiac Electrophysiology, Techniques and Interpretations, 2nd edition*. Lea and Febiger, Philadelphia, 1993.
- [102] R. S. Kass and M. C. Sanguinetti. Inactivation of calcium channel current in the calf cardiac Purkinje fiber. *J. Gen. Physiol.*, **84**:705-726, 1984.
- [103] S. Kawano and M. Hiraoka. Transient outward currents and action potential alterations in rabbit ventricular myocytes. *J. Mol. Cell. Cardiol.*, **23**:681, 1991.

- [104] T. Killip, S. Yormak, E. Ettinger, B. Levitt and J. Roberts. Depression of ventricular automaticity by electrical stimulation (abstract). *Pharmacologist*, 8:203, 1966.
- [105] V. Kowtha, A. Kunysz, J. R. Clay, L. Glass and A. Shrier. Ionic mechanisms and nonlinear dynamics of embryonic chick heart cell aggregates. *Prog. Biophys. Molec. Bio.*, 61(3):255-281, 1994.
- [106] D. J. Krellenstein, M. B. Pliam, C. M. Brooks and M. Vassalle. On the mechanism of idioventricular pacemaker suppression by fast drive. *Circ. Res.*, 35:923, 1974.
- [107] D. Krikler, P. Curry, P. Attuel, et al. 'Incessant' tachycardias in Wolff-Parkinson-White syndrome. I: Initiation without antecedent extrasystoles or PR lengthening, with reference to reciprocation after shortening of cycle length. *Brit. Heart. J.*, 38:885-896, 1976.
- [108] V. I. Krinsky, A. M. Pertsov and A. N. Reshetilov. Investigation of the mechanism of the occurrence of an ectopic focus of excitation on modified Hodgkin-Huxley equations. *Biofizika*, 17(2), 1972.
- [109] V. I. Krinsky and Yu. M. Kokoz. Analysis of equations of excitable membranes. I. Reduction of the Hodgkin-Huxley equations to a second order system. *Biofizika*, 18(3), 1973.
- [110] A. S. Kristof, A. Shrier and J. R. Clay.  $I_L$  is the dominant  $I_{Ca}$  component in embryonic chick ventricular heart cells. *Biophys. J.*, 57:526a, 1990.
- [111] A. M. Kunysz, L. Glass and A. Shrier. Overdrive suppression of spontaneously beating chick heart cell aggregates: experiment and theory. *Am. J. Physiol.*, 269:H1153-H1164, 1995.
- [112] W. J. Lederer, E. Niggli and R. W. Hadley. Sodium-calcium exchange in excitable cells: fuzzy space. *Science*, 248:283, 1990.
- [113] K. S. Lee, E. Marban and R. W. Tsien. Inactivation of calcium channels in mammalian heart cells: Joint dependence on membrane potential and intracellular calcium. *J. Physiol.*, 364:395-411, 1985.

- [114] R. Lemery, P. Brugada, P. Della Bella, et al. Nonischemic ventricular tachycardia. Clinical course and long-term follow-up in patients without clinically overt heart disease. *Circulation*, **79**:990-999, 1989.
- [115] M. Levi. Qualitative analysis of the periodically forced relaxation oscillators. *Memoirs of the American Mathematical Society*, **32**(244), 1981.
- [116] N. Levinson. A second order differential equation with singular solutions. *Ann. Math.*, **50**(1):127-153, 1949.
- [117] T. Lewis. Notes upon alteration of the heart. *Quart. J. Med.*, **4**:141, 1910-1911.
- [118] M. Lieberman, C. R. Horres, J. F. Aiton, N. Shigetou and D. M. Wheeler. Developmental aspects of cardiac excitation: active transport. In *Normal and Abnormal Conduction in the Heart: Biophysics, Physiology, Pharmacology, and Ultrastructure*. Futura Pub. Co., New York, pp. 313-326, 1982.
- [119] L. S. Liebovitch and T. I. Toth. A model of ion channel kinetics using deterministic chaotic rather than stochastic processes. *J. Theor. Bio.*, **148**(2):243-267, 1991.
- [120] L. S. Liebovitch and F. P. Czegledy. A model of ion channel kinetics based on deterministic, chaotic motion in a potential with 2 local minima. *Ann. Biomed. Eng.*, **20**(5):517-531, 1992.
- [121] Y. Liu, W. Zeng, M. Delmar and J. Jalife. Ionic mechanisms of electronic inhibition and concealed conduction in rabbit atrioventricular nodal myocytes. *Circ.*, **88**(1):1634-1646, 1993.
- [122] R. E. McAllister, D. Noble and R. W. Tsien. Reconstruction of the electrical activity of Purkinje fibers. *J. Physiol. (Lond.)*, **251**:1-59, 1975.
- [123] B. Mandelbrot. *The Fractal Geometry of Nature*. W. H. Freeman and Co., New York, 1982.
- [124] G. Marmont. Studies on the axon membrane. I. A new method. *J. Cell. Comp. Physiol.*, **34**:351, 1949.

- [125] R. T. Mathias, L. Ebihara, M. Lieberman and E. A. Johnson. Linear electrical properties of passive and active currents in spherical heart cell clusters. *Biophys. J.*, **36**:221-242, 1981.
- [126] H. Matsuura, T. Ehara and Y. Imoto. An analysis of the delayed outward current in single ventricular cells of the guinea-pig. *Pflugers Archiv.*, **410**:596-603, 1987.
- [127] M. Mazzanti and L. J. DeFelice. K channel kinetics during the spontaneous heart beat in embryonic chick ventricle cells. *Biophys. J.*, **54**:1139-48, 1988.
- [128] F. L. Meijler and M. J. Janse. Morphology and electrophysiology of the mammalian atrioventricular node. *Physiol. Rev.*, **68** (2):608, 1988.
- [129] F. L. Meijler and C. Fisch. Does the atrioventricular node conduct? *Br. Heart J.*, **61**:309-315, 1989.
- [130] G. K. Moe, W. C. Rheinboldt and J. A. Abildskov. A computer model of atrial fibrillation. *Am. Heart. J.*, **58**:59, 1964.
- [131] J. W. Moore and F. Ramon. On numerical integration of the Hodgkin and Huxley equations for a membrane action potential. *J. Theor. Biol.*, **45**:249-273, 1974.
- [132] M. Morad and W. Trautwein. The effect of duration of the action potential on contraction in the mammalian heart tissue. *Pflugers Arch. ges. Physiol.*, **299**:257, 1968.
- [133] A. A. Munk, R. A. Adjemian, J. Zhao , A. Ogbaghebriel and A. Shrier. *J. Physiol. (Lond.)*, In Press.
- [134] E. Musso and M. Vassalle. The role of calcium in overdrive suppression of canine cardiac Purkinje fibers. *Circ. Res.*, **51**:167, 1982.
- [135] J. Nagumo, R. Suzuki and S. Sato. Electrochemical Active Network. Notes of professional group on nonlinear theory of IECE (Japan), 1963.
- [136] W. Nernst. Zur Kinetik der in Losung befindlichen Korper: Theorie der Diffusion. *Z. Phys. Chem.*, :613, 1888.

- [137] C. Nicolis and G. Nicolis. Is there a climatic attractor? *Nature*, **311**:529, 1983.
- [138] D. Noble. *The initiation of the heartbeat*. Clarendon Press, Oxford, 1975.
- [139] T. S. Parker and L. O. Chua. *Practical Numerical Algorithms for Chaotic Systems*. Springer-Verlag, New York, 1989.
- [140] J. Parkinson and C. Papp. Repetitive paroxysmal tachycardia. *Brit. Heart J.*, **9**:241-262, 1947.
- [141] T. Pavlidis. *Biological oscillators: Their mathematical analysis*. Academic Press, New York, NY, 1973.
- [142] D. Paydarfar and F. L. Eldridge. Phase resetting and dysrhythmic responses of the respiratory oscillator. *Am. J. Physiol.*, **252**:R55-62, 1987.
- [143] A. Pelleg, S. Vogel, L. Belardinelli and N. Sperlakis. Overdrive suppression of automaticity in cultured chick myocardial cells. *Am. J. Physiol.*, **238**:H24-H30, 1980.
- [144] D. H. Perkel, J. H. Schulman, T. H. Bullock, G. P. Moore and J. P. Segundo. Pacemaker neurons. Effects of regularly spaced synaptic input. *Science*, **145**:61-63, 1964.
- [145] G. A. Petrillo, L. Glass and T. Trippenbach. Phase locking of the respiratory rhythm in cats to a mechanical ventilator. *Can. J. Physiol. Pharmacol.*, **61**:599-607, 1983.
- [146] G. A. Petrillo and L. Glass. A theory for phase locking respiration in cats to a mechanical ventilator. *Am. J. Physiol.*, **246**:R311, 1984.
- [147] A. Pick and R. Langerdorf. In *Interpretation of Complex Arrhythmias*, Lee & Febiger, Philadelphia, Pa, pp. 471-541, 1979.
- [148] C. S. Pittendrigh. On the mechanism of entrainment of a circadian rhythm by light cycles. In J. Aschoff, editor: *Circadian Clocks*, pp. 277-297, Martinus, Nijhoff, Amsterdam, North Holland, 1965.
- [149] F. J. Prinsze and L. N. Bouman. The cellular basis of intrinsic sinus node recovery time. *Cardiovasc. Res.*, **25**:546-557, 1991.

- [150] F. J. Prinsze. Cellular aspects of overdrive suppression in the sinoatrial node. Feboedruk, Enschede, Netherlands, 1993.
- [151] N. G. Publicover and K. M. Sander. Are relaxation oscillators an appropriate model of gastrointestinal electrical activity? *Am J. Physiol.*, 256:G265, 1989.
- [152] J. V. O. Reid. The cardiac pacemaker effects of regularly spaced nervous input. *Am. Heart. J.*, 78:58-64, 1969.
- [153] D. L. Ross, W. R. M. Dassen, E. J. Vanagt. Cycle length alternation in circus movement tachycardia using an atrioventricular accessory pathway. *Circulation*, 65:862-868, 1982.
- [154] D. Ruelle. Where can one hope to profitably apply the ideas of chaos?. *Physics Today*, 47:24-30, July 1994.
- [155] S. Rush and H. Larsen. A practical algorithm for solving dynamic membrane equations. *IEEE (Inst. Electr. Electron. Eng.) Trans. Biomed. Eng.*, 25:389-392, 1975.
- [156] M. C. Sanguinetti and N. K. Jurkiewicz. Two components of cardiac delayed rectifier  $K^+$  current. *J. Gen. Physiol.*, 96:195-215, 1990.
- [157] A. Shrier and J. R. Clay. Pacemaker currents in chick embryonic heart cells change with development. *Nature*, 283:670-671, 1980.
- [158] A. Shrier and J. R. Clay. Comparison of the pacemaker properties of chick embryonic atrial and ventricular heart cells. *J. Memb. Biol.*, 69:49-56, 1982.
- [159] A. Shrier and J. R. Clay. Repolarization currents in embryonic chick atrial heart cell aggregates. *Biophys. J.*, 50:861-874, 1986.
- [160] A. Shrier, H. Dubarsky, M. Rosengarten, M. R. Guevara, S. Nattel and L. Glass. Prediction of complex atrioventricular conduction rhythms in humans with use of the atrioventricular nodal recovery curve. *Circulation*, 76:1196-1205, 1987.
- [161] A. Shrier, J. R. Clay and R. M. Brochu. Effects of tetrodotoxin on heart cell aggregates. Phase resetting and annihilation of activity. *Biophys. J.*, 58:623-629, 1990.

- [162] A. Shrier, R. A. Adjemian and A. A. Munk. In D. P. Zipes and J. Jalife, editors: *Cardiac Electrophysiology: From Cell to Bedside, 2nd edition.*
- [163] M. B. Simson, J. F. Spear, E. N. Moore. Stability of an experimental atrioventricular reentrant tachycardia in dogs. *Am. J. Physiol.*, **240**:H947-H953, 1981.
- [164] J. R. Stimers, N. Shigeto and M. Lieberman. Na/K pump current in aggregates of cultured chick cardiac myocytes. *J. Gen. Physiol.*, **95**:61-76, 1990.
- [165] *The Sodium Pump: Structure, Mechanism and Regulation.*, The Rockefeller University Press, New York, 1991.
- [166] M. Talajic, C. Villemaire, D. Papadatos. Cycle length alternation during supraventricular tachycardia: Occurrence and mechanism in a canine model of AV reentrant tachycardia. *PACE*, **13**:314, 1990.
- [167] M. Talajic, D. Papadatos, C. Villemaire, L. Glass and S. Nattel. A unified model of AV node conduction explains dynamic changes in Wenckebach periodicity. *Circ. Res.*, **68**:1280-1293, 1991.
- [168] S. Tawara, *Das Reizleitungssystem Des Herzens*, Fisher, Jena, Germany, pp. 563-584, 1906.
- [169] C. A. Vanderberg. Inward rectification of a potassium channel in cardiac ventricular cells depends on internal magnesium ions. *Proc. Natl. Acad. Sci. U.S.A.*, **85**:2560-2564, 1987.
- [170] B. van der Pol and J. van der Mark. The heartbeat considered as a relaxation oscillation, and an electrical model of the heart. *Arch. Neerl. Physiol.*, **14**: 418, 1929.
- [171] L. H. Van der Tweel, F. L. Meijler and F. J. L. Van Capelle. Synchronization of the heart. *J. Appl. Physiol.*, **34**:283-287, 1973.
- [172] M. Vassalle. Electrogenic suppression of automaticity in sheep and dog Purkinje fibers. *Circ. Res.*, **27**:361-377, 1970.
- [173] M. Vassalle. The relationship among cardiac pacemakers: Overdrive suppression. *Circ. Res.*, **41**:269, 1977.

- [174] R. L. Vick. Suppression of latent cardiac pacemaker: relation to slow diastolic depolarization. *Am. J. Physiol.*, **217**: 451, 1969.
- [175] F. F. Vincenzi and T. C. West. Release of autonomic mediators in cardiac tissues by direct subthreshold electrical stimulation. *J. Pharmacol. Exp. Ther.*, **141**:185, 1963.
- [176] A. Vinet, D. R. Chialvo, D. C. Michaels and J. Jalife. Nonlinear dynamics of rate-dependent activation in models of single cardiac cells *Circ. Res.*, **67**:1522-1524, 1990.
- [177] A. L. Waldo, R. W. Hewthorn, V. J. Plumb and W. A. H. Maclean. Demonstration of the mechanism of transient entrainment and interruption of ventricular tachycardia with rapid atrial pacing. *J. Am. Coll. Cardiol.*, **3**:422-430, 1984.
- [178] R. Wilders, H. J. Jongasma and A. O. G. van Ginneken. Pacemaker activity of the rabbit sinoatrial node. A comparison of mathematical models. *Biophys. J.*, **60**:1202-1216, 1991.
- [179] A. T. Winfree. Spiral waves of chemical activity. *Science*, **175**:634, 1972.
- [180] A. T. Winfree. Scroll-shaped waves of chemical activity in three dimensions. *Science*, **181**:937, 1973.
- [181] A. T. Winfree. *The Geometry of Biological Time*. Springer-Verlag, New York, 1980.
- [182] A. T. Winfree. *When Time Breaks Down*. Princeton University Press, Princeton, NJ, 1987.
- [183] A. Wolfe, J. B. Swift, H. L. Swinney and J. A. Vastano. Determining Lyapunov numbers from a time series. *Physica D*, **16**:285-317, 1985.
- [184] W. Z. Zeng, M. Courtemanche, L. Sehn, A. Shrier and L. Glass. Theoretical computation of phase locking in embryonic atrial heart cell aggregates. *J. Theor. Biol.*, **145**:225, 1990.
- [185] W. Z. Zeng, J. Morissette, R. Brochu, et al. Complex rhythms resulting from overdrive suppression in electrically stimulated heart cell aggregates. *PACE*, **13**:1678-1685, 1990.

- [186] W. Z. Zeng, L. Glass, and A. Shrier. Evolution of rhythms during periodic stimulation of embryonic chick heart cell aggregates. *Circ. Res.*, **69**:1022, 1991.
- [187] A. M. Zhabotinsky and A. N. Zaikin. Spatial effects in auto-oscillatory system. In *Oscillatory Processes in Biological and Chemical Systems*, vol. II. IBF AN SSSR, Pushchino-na-Oke, 1971.
- [188] V. S. Zykov. *Simulation of wave processes in excitable media*. Manchester University Press, New York, 1987.